Human Standing and Sitting Stability: Instrumented Objective Balance Evaluation and Quantification of Postural Control

by

Alireza Noamani

A thesis submitted in partial fulfillment of the requirements for the degree of

Doctor of Philosophy

Department of Mechanical Engineering
University of Alberta

Abstract

Falls are one of the most frequent causes of injury in the elderly and ambulatory individuals with neuromuscular impairments. Standing balance impairment is among the most consistent predictors of future falls. Furthermore, many individuals with neuromusculoskeletal conditions use a wheelchair for daily ambulation and often exhibit degraded trunk control during dynamic tasks, requiring assistance in seated stability. Therefore, implementing outcome measures that identify static balance difficulties may lead to more effective rehabilitation, and reduced future fall risk and fall severity in affected individuals. Characterizing the dynamic balance and neuromuscular control mechanisms are essential for identifying underlying impairments, implementing targeted rehabilitation, and developing assistive technologies. The overall goal of this thesis is to contribute toward developing methodologies for instrumented static and dynamic balance assessment with high sensitivity and responsiveness, allowing for a better understanding of the mechanisms of postural control. This thesis aimed to (1) develop and validate algorithms for reliable assessment of static balance using wearable technology, with the capability of being integrated into clinical tests for individuals with neuromuscular impairments; and (2) characterize the relationship between dynamic balance and risk of loss of balance and identify the roles of neuromuscular mechanisms involved in seated stability.

First, we validated an algorithm for characterizing static balance using wearable technology against measurements of gold-standard in-lab equipment. We showed that our proposed method could provide accurate kinematics and kinetics measures and could be recommended for monitoring standing balance.

Second, we used the validated algorithm to perform a static balance evaluation using wearable technology for ambulatory individuals with incomplete spinal cord injury (iSCI) with mild balance deficits during standing under various conditions. Our method enabled characterizing standing balance in this group compared to able-bodied participants with sufficient resolution and discriminatory ability for objective balance evaluation.

Third, we used the validated algorithm to compare the postural control strategy between the same iSCI and able-bodied participants by characterizing their trunk-leg movement coordination under different sensory conditions. We observed trunk-leg movement coordination showed high sensitivity, discriminatory ability, and excellent test-retest reliability to identify changes in postural control strategy post-iSCI.

Fourth, we investigated, in a clinical setting, the use of the validated algorithm above and the integration of wearable technology into a clinical scale test for objective outcome evaluation of balance rehabilitation in elderly with moderate-to-severe balance impairments. Our method enabled identifying and characterizing underlying causes of impaired balance pre- and post-rehabilitation with high sensitivity to subtle changes in balance.

Fifth, we determined the limit of dynamic seated stability as a function of the trunk kinematics relative to the base of support. We experimentally validated the predicted limit of stability using traditional motion capture cameras. We then validated an algorithm to use wearable technology for assessing dynamic seated stability and risk of loss of balance against a gold-standard system.

Sixth, we characterized the neuromuscular mechanisms involved in human sitting by identifying a nonlinear physiologically-meaningful neuromechanical model of seated stability. The model predicted the trunk sway behaviour during perturbed sitting with high accuracy. Our

method accounted for physiological uncertainties while allowing for real-time tracking and correction of parameters' variations due to external disturbances and muscle fatigue.

Seventh, we identified the high-level task goals of the neural control for regulating dynamic seated stability using nonlinear control theory. We observed the neural control might use trunk angular kinematics, primarily angular acceleration, as the input to achieve near-minimum muscle activation while keeping the deviations of the trunk angular position and acceleration sufficiently small.

The practical outcome of this research toward static balance assessment is the development of algorithms used with wearable sensors for clinical objective balance assessment and characterization of complex balance mechanisms during static quiet stance. Such algorithms may provide a significant increase in the sensitivity of diagnosis of impaired balance for ambulatory individuals with iSCI with mild balance deficits and elderly with moderate-to-severe balance impairments. The practical outcomes of this research toward dynamic balance assessment are: (a) obtaining dynamic limits of stability for sitting; (b) the development of an algorithm for assessing the risk of loss of balance using wearable technology; (c) the development of a novel methodologies for a mechanistic understanding of the several neuromuscular stabilization mechanisms and high-level task goals of the neural control for maintaining dynamic stability.

Preface

This thesis is an original work by Alireza Noamani. The research projects, of which this thesis is a part, received research ethics approval from the Health Research Ethics Board of the University of Alberta:

Project Name "Accuracy assessment of wearable technologies for objective clinical outcome evaluation," study ID Pro00065804.

Project Name "Using body-worn sensors to identify individuals with SCI at risk of falling," study ID Pro00069759.

Project Name "Clinical validity of a wearable biomedical device for balance assessment," study ID Pro00069565.

Project Name "Assessment of Dynamic Balance and Fall Risk in Sitting," study ID Pro00063998.

Chapter 3 of this thesis has been *published* as: A. Noamani, M. Nazarahari, J. Lewicke, A. H. Vette, H. Rouhani, "Validity of Using Wearable Inertial Sensors for Assessing the Dynamics of Standing Balance," Medical Engineering and Physics, 2020, Vol. 77, pp 53-59. I was responsible for conceptualization, study design, methodology, data collection, software implementation, investigation, writing the original draft, and visualization. M. Nazarahari assisted with the data collection and contributed to manuscript edits. A. H. Vette and H. Rouhani were the supervisory authors and were involved with conceptualization and study design, methodology, interpretation of the results, and reviewing and editing the manuscript.

Chapter 4 of this thesis has been *published* as: A. Noamani, J. F. Lemay, K. E. Musselman, H. Rouhani, "Characterization of Standing Balance after Incomplete Spinal Cord Injury: Alteration in Integration of Sensory Information in Ambulatory Individuals," Gait & Posture, 2021, Vol. 83, pp 152-159. I was responsible for conceptualization, study design, methodology, data collection, software implementation, investigation, writing the original draft, and visualization. J. F. Lemay and K. E. Musselman assisted with the data collection and contributed to manuscript edits. H. Rouhani was the supervisory author and was involved with conceptualization and study design, methodology, interpretation of the results, and reviewing and editing the manuscript.

Chapter 5 of this thesis has been *published* as: A. Noamani, J. F. Lemay, K. E. Musselman, H. Rouhani, "Postural Control Strategy after Incomplete Spinal Cord Injury: Effect of Sensory Inputs on Trunk-Leg Movement Coordination," Journal of Neuroengineering and Rehabilitation, 2020, Vol. 17(1), pp 1-12. I was responsible for conceptualization, study design, methodology, data collection, software implementation, investigation, writing the original draft, and visualization. J. F. Lemay, K. E. Musselman assisted with the data collection and contributed to manuscript edits. H. Rouhani was the supervisory author and was involved with conceptualization and study design, methodology, interpretation of the results, and reviewing and editing the manuscript.

Chapter 6 of this thesis has been *published* as: A. Noamani, A. H. Vette, H. Rouhani, "Instrumented Functional Test for Objective Outcome Evaluation of Balance Rehabilitation in Elderly Fallers: A Clinical Study," Gerontology 2022. I was responsible for conceptualization, study design, methodology, data collection, software implementation, investigation, writing the original draft, and visualization. A. H. Vette and H. Rouhani were the supervisory authors and were involved with conceptualization and study design, methodology, interpretation of the results, and reviewing and editing the manuscript.

Chapter 7 of this thesis has been *published* as: A. Noamani, K. Agarwal, A. H. Vette, H. Rouhani, "Predicted Threshold for Seated Stability: Estimation of Margin of Stability Using Wearable Inertial Sensors," IEEE Journal of Biomedical and Health Informatics, 2021, Vol 25(9), pp 3361-3372. I was responsible for conceptualization, study design, methodology, data collection, software implementation, investigation, writing the original draft, and visualization. K. Agarwal assisted with the data collection and contributed to manuscript edits. A. H. Vette and H. Rouhani were the supervisory authors and were involved with conceptualization and study design, methodology, interpretation of the results, and reviewing and editing the manuscript.

Chapter 8 of this thesis has been *published* as an article: A. Noamani, A. H. Vette, H. Rouhani, "Nonlinear Response of Human Trunk Musculature Explains Neuromuscular Stabilization Mechanisms in Sitting Posture," Journal of Neural Engineering, 2022, Vol 19, 026045. I was responsible for conceptualization, study design, methodology, data collection, software implementation, investigation, writing the original draft, and visualization. A. H. Vette and H. Rouhani were the supervisory authors and were involved with conceptualization and study design, methodology, interpretation of the results, and reviewing and editing the manuscript.

Chapter 9 of this thesis is *ready for submission* as an article: A. Noamani, A. H. Vette, H. Rouhani, "Nonlinear Neural Feedback Explains Task Goals of Central Nervous System for Trunk Stability in Sitting Posture," 2022. I was responsible for conceptualization, study design, methodology, data collection, software implementation, investigation, writing the original draft, and visualization. A. H. Vette and H. Rouhani were the supervisory authors and were involved with conceptualization and study design, methodology, interpretation of the results, and reviewing and editing the manuscript.

Dedicated to

My parents

Sadaf, my twin sister,

And

Shiva, my wife.

Acknowledgments

I would like to express my sincere gratitude to my supervisors, Dr. Hossein Rouhani and Dr. Albert H. Vette, for their encouragement, patience, motivation, and immense knowledge. Their guidance helped me tremendously in all the time of research and writing this thesis.

I would like to thank Dr. Mahdi Tavakoli for his invaluable insights as a member of my supervisory committee. Also, I would like to thank Dr. Vivian Mushahwar and Dr. Ronald Triolo for serving on my Ph.D. thesis exam committee and Dr. Rafiq Ahmad as my Ph.D. thesis exam chair.

I would like to thank Drs. Kristin E. Musselman and Jean-François Lemay for their help and guidance during my Ph.D. studies. I am extremely grateful to thank Kshitij Agarwal, Sarah-Beth Riske, Janelle Unger, and David J. Houston for their help during the experiments and data collection. I would also like to thank Justin Lewicke and Darrell Goertzen for lending their expertise and answering many questions. I would like to thank all members of the Geriatrics Clinic at the Glenrose Rehabilitation Hospital. Special thanks go to Karen Tiedemann, Leanne Trieu, and Michael Wadowski for their help with participant recruitment. Also, I had the privilege of working with researchers at the Neuromuscular Control & Biomechanics Laboratory. I could always count on Milad Nazarahari, Rezvan Nasiri, Amin Khandan, Hosein Bahari, Ramin Fathian, Ahmed Humadi, Karla Beltran Martínez, and Nasim Rahmanifar to help me whenever I needed assistance.

I would like to thank my mother, Nasrin Masoudi Nejad, my father, Behrouz Noamani, and my sister, Sadaf Noamani, who have been extremely supportive throughout the process, without any doubt, this journey would not have been possible without them. And finally, I would like to thank my wife, Shiva Zamani, for her love, patience, and endurance; none of this could have been possible without her support.

This project was made possible through the generous support of the Faculty of Engineering of the University of Alberta, the Faculty of Graduate Studies and Research, and the Natural Sciences and Engineering Research Council of Canada. Also, the generous financial support of the Alberta Innovates Graduate Student Scholarship, BMO Financial Group Graduate Scholarship, Alberta Graduate Excellence Scholarship, Sadler Graduate Scholarship, and other awards provided by the University of Alberta helped me through this journey.

Table of Contents

List of Tables

List of Figures

Abbreviations

3D	:	Three-Dimensional
AF	:	Anatomical Frame
AIS	:	American Spinal Injury Association Impairment Scale
ANOVA	:	Analysis of Variance
AP	:	Anteroposterior
Area-CE	:	95% Confidence Ellipse Area
Area-SW	:	Sway Area
AUKF	:	Adaptive Unscented Kalman Filter
BBS	:	Berg Balance Scale
BOS	:	Base of Support
CAREN	:	Computer-Assisted Rehabilitation Environment
CF-ACC	:	Centroid Frequency
CFREQ	:	Centroid Frequency
COM	:	Center of Mass
COP	:	Center of Pressure
EC	:	Eyes Closed
EKF	:	Extended Kalman Filter
EMG	:	Electromyography
EO	:	Eyes Open
FES	:	Functional Electrical Stimulation
FREQD	:	Frequency Dispersion
FS	:	Foam Surface
FSEC	:	Foam Surface Eyes Closed
FSEO	:	Foam Surface Eyes Open

FSR	:	Feasible Stability Region
GF	:	Global Frame
GRF	:	Ground Reaction Force
HAT	:	Head-Arms-Trunk
HS	:	Hard Surface
HSEC	:	Hard Surface Eyes Closed
HSEO	:	Hard Surface Eyes Open
ICC	:	Intraclass Correlation Coefficient
IMU	:	Inertial Measurement Unit
iSCI	:	Incomplete Spinal Cord Injury
JCR	:	Joint Center of Rotation
JERK	:	Sway jerkiness
LEMS	:	Lower Extremity Motor Score
MDIST	:	Mean Distance
MEDFREQ	:	Median Frequency
MFREQ	:	Mean Frequency
Mini-BEST	:	Mini Balance Evaluation System Test
ML	:	Mediolateral
MSC	:	Mean Magnitude-Squared Coherence
MVC	:	Maximum Voluntary Contraction
MVELO	:	Mean Velocity
PCA	:	Principal Component Analysis
PD	:	Proportional-Derivative
PID	:	Proportional-Integral-Derivative
RD	:	Resultant Distance
RDIST	:	Root-Mean-Square Distance
RMS-ACC	:	Root-Mean-Square Acceleration

RMSE	:	Root-Mean-Square Error
SCI	:	Spinal Cord Injury
SEM	:	Standard Error of Measurement
TOTEX	:	Total Excursion
TUG	:	Timed Up and GO
UKF	:	Unscented Kalman Filter

Chapter 1

Chapter 1 presents the motivations, objectives, and outline of this thesis.

1 Introduction

1.1 Motivation and Problem Statement

Falls are among the most frequent causes of injury in individuals with neuromuscular impairments and the elderly [1], [2]. Previous studies showed that impairment of gait or balance is the most consistent predictor of falls [3]. Hence, individuals with impaired balance are at high risk of falling, and therefore, the ability to maintain balance during gait, standing, and postural transitions has been used to evaluate fall risk in individuals and the effectiveness of rehabilitative interventions [4], [5]. Up to one-third of seniors fall at least once a year [6], with over 50% of fallers reporting multiple falls [7]. The fall rate among the elderly grows with age [8], making falls the fifth leading cause of death in older adults [9]. In addition, the literature has reported a high occurrence of falling incidences among individuals with spinal cord injury (SCI), with up to 78% of these individuals experiencing at least one fall post-rehabilitation [10]–[12]. Falls can lead to injuries and hospitalization [10], restriction in community participation [11], [13], [14], and the development of a fear of falling [15]. In addition, up to 30% of individuals with a recent SCI and most individuals with an incomplete spinal cord injury (iSCI) are able to regain partial balance and walking ability after the first year post-injury [16]. However, a significant challenge for individuals with iSCI is to maintain postural stability while recovering walking function [17]. iSCI affects the ability to safely stand and perform functional activities in this position [18]. The future level of ambulation in this population is associated with the initial level of balance and the amount of motor function below the level of the lesion [19]. Recovery of balance ability during standing and regaining the ability to walk are the top priorities for individuals with iSCI [16], [20], [21]. One of the major factors contributing to falls in this population is the loss of balance [14], [18], highlighting the lack of effective postural control in individuals with iSCI. Furthermore, greater postural control in this population is highly related to a more normal gait pattern, higher stride speed, less reliance on supervision or physical assistance, and more functional ambulatory status [16]. The development of fall prevention strategies is associated with effective postural control.

Hence, the implementation of outcome measures that identify the balance and walking abilities of individuals with neuromuscular impairments, such as iSCI, can lead to more effective rehabilitation [16]. Therefore, understanding the underlying mechanisms of how postural control is regulated post-impairment is of significant importance.

Many individuals with neuromusculoskeletal conditions, including more than 60% of individuals with SCI, use a wheelchair or scooter for daily ambulation [22] and often show degraded trunk control, which requires assistance in seated stability during activities of daily living [23]. Affected individuals commonly suffer from an inability to maintain an upright seated posture due to the impaired neuromuscular function of the trunk and pelvic musculature [24]. For instance, most lesions located above the first lumbar vertebra will lead to full or partial paralysis of the lumbar trunk muscles [25]. Consequently, the lumbar muscles cannot produce sufficient torques to maintain trunk stability [25]. Moreover, any lesion between the head and the tenth thoracic vertebra leads to further trunk impairment by also affecting sensorimotor transmission [26]. Thus, these individuals are at high risk of falling when exposed to sitting perturbations, making tips and falls the leading cause of injury in this population [27]. Up to 69% of wheelchair users experience at least one fall each year [28], and falls are the leading cause of injury in this population [27], often requiring hospitalization [29]. Trunk instability can also result in reduced functional independence during activities of daily living [26], [30], and respiratory dysfunction [31], [32]. Furthermore, these individuals use compensatory strategies such as the posterior pelvic tilt [33] and one-arm support while reaching [26], causing reduced work volume, asymmetric trunk configuration, and inadequate distribution of upper body weight, which can lead to secondary health complications such as kyphosis and pressure sores [4]. Consequently, individuals with impaired trunk stability (e.g., individuals with SCI) view sitting stability during daily activities as one of their most essential needs, even outweighing their desire to walk again [34]. In this light, an assessment methodology that can evaluate their sitting stability during daily life would dramatically increase their quality of life while wheeling in a wheelchair.

Physical therapists oftentimes use standard observational rating scales to evaluate balance. The concurrent validity of observational balance scales, e.g., Berg Balance Scale (BBS) or Mini Balance Evaluation System Test (Mini-BEST), among the elderly and individuals with iSCI has been studied in the past. However, previous studies reported an inability to predict future falls for such methodologies. Moreover, they tend to be subjective and may provide limited information

for understanding the potential underlying mechanisms for the balance difficulties [16], [35], [36], highlighting the requirement of a quantitative approach to evaluate standing balance. Hence, the instrumented version of such tests can provide a more precise impairment-level evaluation of balance by measuring how and why functional performance is impaired with increased sensitivity in the identification of mild changes [37]. Therapists may use such objective measures to track subtle changes in postural control over time and precisely focus the therapy on underlying causes [37].

Many studies have used stationary laboratory equipment, including motion capture systems and force plates, to derive measures for characterizing the control mechanisms of balance [38]–[42]. Such measures can quantify balance during both static and dynamic conditions [43]. On the one hand, measures obtained during static conditions corresponding to spontaneous body sway have been extensively used to assess postural control during quiet stance [42]. A commonly applied technique for assessing postural control and stability during quiet standing is utilizing measures of postural steadiness known as posturography [43]. On the other hand, applying external perturbations (e.g., platform translation or external forces) and sensory disturbances (e.g., visual, proprioceptive, and/or vestibular disturbances) have been used to characterize postural responses and underlying stabilization mechanisms during dynamic conditions [44]–[46].

1.1.1 Static Balance Assessment

Objective assessment of balance has been investigated based on the reaction forces from the ground, and body segments' motions (e.g., joint angles) measured via force plates and motion capture systems during standing, respectively [47], [48]. Nevertheless, the implementation of in-lab equipment for clinical research and practice has not become practical due to the requirement of expensive equipment and dedicated lab space. Body-worn inertial measurement units (IMUs) have been used as a reliable alternative for obtaining accurate and sensitive measures of balance in populations with neuromuscular impairments such as individuals with Parkinson's disease [49], traumatic brain injury [37], and SCI [50]. IMUs can be used to provide impairment-level measures that characterize the functional performance of balance with increased sensitivity to movement disorders, rehabilitation, and mild changes in postural stability [37], [49]. Moreover, IMUs are light-weight, relatively inexpensive, and can be easily integrated into functional tests, which makes them an ideal alternative to stationary laboratory equipment with a higher level of clinical utility [37], [51]. Despite recent developments, there is a need to (a) develop algorithms to characterize

the dynamics of standing balance using the wearable IMUs; (b) experimentally validate the accuracy of the wearable device against gold standard motion capture and force plate systems; (c) assess the sensitivity of the developed system for identifying impairment-related changes in standing balance, and (d) conduct a clinical study to evaluate the responsiveness and validity of the wearable device for clinical outcome evaluation of rehabilitation interventions.

1.1.2 Dynamic Balance Assessment

The literature has introduced several biomechanical criteria for defining the limits of dynamic stability during standing and walking based on the kinematics of the human body [52]–[58]. In addition, many studies have characterized postural responses and underlying stabilization mechanisms by applying external physical or sensory disturbances [45], [46], [59]–[65]. The literature has shown that characterizing neuromuscular control in able-bodied individuals is beneficial for identifying and restoring impaired balance in individuals with neuromuscular impairments [23], [59], [66]. Hence, characterizing neuromuscular control not only explains a fundamental question in human motor control but also contributes to objective balance evaluation and developing targeted rehabilitative interventions for improving impaired balance [60], [67]. The neuromuscular mechanisms of sitting and standing stability have been identified using closed-loop system identification techniques applied to body motion and muscle activation data recorded when the body was perturbed via external stimuli (e.g., external forces, moving support surface, or moving visual surround) [46], [65]. Nevertheless, previous work assumed a time-invariant linear behaviour for the neuromuscular control that maintains sitting or standing stability and neglected time-variant or nonlinear dynamics as well as physiological uncertainties in real-world conditions [68]–[71]. In this light, there is a need for a nonlinear neuromechanical model of dynamic stability that explains the roles of stabilization mechanisms while accounting for uncertainties associated with the complex neuromuscular system.

Yet, the literature has mostly focused on dynamic stability during standing to characterize underlying stabilization mechanisms. However, dynamic stability during sitting has not been fully investigated due to complexities associated with the human trunk structure and the number of muscles and the variety of stabilization mechanisms involved. Moreover, despite the significance of the dynamic balance assessment methodology, there is no standard biomechanical criterion that particularly quantifies the limits of dynamic balance during sitting. Consequently, the focus of this research on dynamic balance assessment was given to sitting balance. Therefore, this research

addresses the following gaps of knowledge: (a) biomechanical characterization and quantification of the relationship between the dynamic posture of the trunk and sitting balance; (b) a validated biomedical device for assessing dynamic sitting posture and fall risk; and (c) mechanistic understanding of the non-impaired neuromuscular control mechanisms and their roles in achieving seated stability [25], [60], [72].

1.2 Thesis Objectives

The overall goal of this thesis research is to contribute toward developing methodologies for comprehensive instrumented static and dynamic balance assessment with high sensitivity and responsiveness, allowing for a better understanding of the mechanisms of postural control. To achieve this goal, this research aimed to address two major gaps in the literature:

(1) Static balance: instrumented assessment of static balance, understanding the underlying mechanisms of how postural control is regulated in individuals with mild balance deficits (e.g., a group of ambulatory individuals with iSCI), and how rehabilitative interventions affect postural control in individuals with moderate-to-severe balance impairments.

(2) Dynamic balance: characterization of dynamic balance as well as gaining a mechanistic understanding of the neuromuscular mechanisms involved in dynamic seated stability in able-bodied individuals.

To address the first gap, this research aimed to develop and validate an algorithm for reliable assessment of static standing balance using wearable technology, with the capability of being integrated into clinical tests for individuals with neuromuscular impairments such as ambulatory individuals with iSCI with mild balance deficits as well as the elderly with moderate-to-severe balance impairments. For this purpose, we developed an algorithm to assess kinematic and kinetic parameters that characterize standing balance using the measurements of wearable IMUs. We achieved this objective by completing the following steps:

- We investigated the validity of an algorithm for estimating conventional balance biomarkers using wearable technology for the reliable assessment of the dynamics of standing balance.
- We used the validated algorithm above for using wearable IMUs to characterize changes in standing balance in a group of individuals with iSCI (with mild balance deficits and at least

partially preserved motor function below the lesion level) due to alteration in the integration of sensory information.

- We used the validated algorithm above for using wearable IMUs to identify changes to the postural control strategy by quantifying the trunk-leg movement coordination in the same group of individuals with iSCI.
- We investigated the feasibility of integrating the wearable technology above into the BBS test, in a clinical setting, to identify the effect of rehabilitative interventions on balance biomarkers in comparison to BBS scores in a group of the elderly with moderate-to-severe balance impairments.

To address the second gap, this research aimed to characterize the relationship between the dynamic posture of the trunk and dynamic balance and identify the roles of neuromuscular mechanisms involved in non-impaired dynamic stability. Note, since the literature has not fully investigated dynamic stability during sitting due to complexities associated with the structure of the human trunk, the focus in this thesis research was given to dynamic sitting balance. We achieved this objective by completing the following steps:

- We quantified the relationship between the dynamic posture of the trunk and fall risk during sitting by obtaining the limits of dynamic stability as a feasible stability region (FSR).
- We developed an algorithm for assessing seated stability using wearable technology.
- We identified the roles of the passive and active neuromuscular control mechanisms involved in seated stability using a nonlinear neuromechanical model to represent how the underlying stabilization mechanisms appear to operate.
- We identified the high-level task goals of the central nervous system (CNS) for achieving trunk stability in sitting posture based on nonlinear control and optimal control.

1.3 Thesis Impact and Significance

Each year, about 4,500 new cases of SCI are reported in Canada: about 1,800 cases as a consequence of traumatic injury and the rest as a result of diseases and other non-traumatic causes, and the total number of individuals with SCI living in Canada is estimated at 85,500 [73]. In addition, the annual incidences of new traumatic SCI in the United States are estimated as high as 17,800, and the current number of people living with SCI in this country is approximately 294,000

[74]. 32.6% of individuals with SCI in the United States had neurologically incomplete tetraplegia, 24.0% complete paraplegia, 18.5% complete tetraplegia, and 18.5% incomplete paraplegia [22]. Falls are among the leading causes of injury in the SCI population. Each year, about 180,000 injurious fall incidents are reported in Canada. More than 100,000 wheelchair-related injuries need emergency treatments. Rehabilitation due to bone fracture in individuals with SCI needs four to eight weeks of hospitalization. This results in reduced strength and an increased risk of developing blood clots. In addition, access to hospital care during the COVID-19 pandemic has been a challenge for high-risk individuals with other underlying health conditions. The annual direct-care costs of fall-related injuries in Canada are estimated as high as $2 billion [75]. Due to the impacts of falls on the quality of life of many Canadians and on the Canadian healthcare system and economy, the development of technologies that contribute to reducing the risk of falling is of significant interest to the Canadian healthcare system.

The overall contributions of this thesis toward developing instrumented static and dynamic balance assessment methodology are algorithms validated against gold-standard references to obtain sensitive and responsive measures of static and dynamic stability using wearable technology for understanding the underlying mechanisms of postural control. The practical outcome of this research toward static balance assessment is the development of algorithms for clinical objective balance assessment during static quiet stance using wearable technology for ambulatory individuals with iSCI and mild balance deficits and elderly with moderate-to-severe balance impairment. The advantages of this technology will be: (a) characterization of complex balance mechanisms without a dedicated laboratory; (b) capability of integration into conventional clinical tests; and (c) a significant increase in the sensitivity of diagnosis of impaired balance. The practical outcomes of this research toward dynamic balance assessment are: (a) obtaining and validating dynamic limits of stability for sitting; (b) the development and validation of an algorithm for assessing the risk of loss of balance in dynamic conditions using wearable technology; (c) the development of a novel methodology for a mechanistic understanding of the contribution of several underlying neuromuscular stabilization mechanisms to achieving dynamic stability; and (d) the development of a methodology to obtain a high-level understanding of the task goals of the neural control for maintaining dynamic stability, all tested among able-bodied individuals.

1.4 Thesis Outline

The remainder of this thesis explains the steps toward achieving the objectives and is organized as follows:

- Chapter 2 provides an overview of the literature relevant to this thesis research. First, it provides an overview of standing balance, including objective assessment methodologies using motion tracking systems, standing balance assessment post-iSCI, and standing balance assessment of the elderly in clinical research and practice. Second, it highlights an overview of sitting balance assessment, including trunk stability, the limit of stability, and neuromuscular control identification.
- Chapter 3 presents a novel algorithm for deriving reliable standing balance biomarkers using the recording of three body-mounted IMUs as well as its validity against a gold-standard optoelectronic motion capture system and a force plate. This chapter is based on a journal publication [76].
- Chapter 4 presents the characterization of standing balance in ambulatory individuals with iSCI with mild balance deficits under different sensory conditions using the balance biomarkers derived based on the measurements of our novel wearable device validated in Chapter 3. This chapter is based on a journal publication [77].
- Chapter 5 investigates the alteration of postural control strategy in ambulatory individuals with iSCI with mild balance deficits by characterizing trunk-leg movement coordination under different sensory conditions based on the measurements of our novel wearable device validated in Chapter 3. This study introduces a new balance biomarker capable of identifying impaired postural control strategies with high reliability. This chapter is based on a journal publication [78].
- Chapter 6 investigates, in a clinical setting, the use of IMUs integrated into the BBS test for objective outcome evaluation of balance rehabilitation compared to conventional BBS scores in elderly with moderate-to-severe balance impairment. This chapter is based on a journal publication [79].
- Chapter 7 presents a mathematical approach to obtaining the limit of dynamic seated stability as a function of the trunk motion, experimentally validates the predicted limit of stability using gold-standard motion capture, compares the predicted limit of stability with that predicted in

the literature for standing and walking, and validates an algorithm using a wearable device for assessing dynamic seated stability and risk of loss of balance. This chapter is based on a journal publication [80].

- Chapter 8 presents the characterization of the roles of passive and active stabilization mechanisms involved in human dynamic sitting stability by experimentally identifying nonlinear trunk dynamics in able-bodied individuals. This study uses an Adaptive Unscented Kalman Filter (AUKF) for identifying the parameters of a nonlinear model while accounting for the time-varying process and measurement noise. This chapter is based on a journal publication [81].
- Chapter 9 explains the task goals used by the neural control to regulate seated stability. This study uses a nonlinear neuromechanical model of the seated human along with a full-state feedback linearization approach and optimal control theory for identifying neural dynamics. This chapter is based on a submitted journal publication.
- Chapter 10 provides the conclusions and future perspectives.

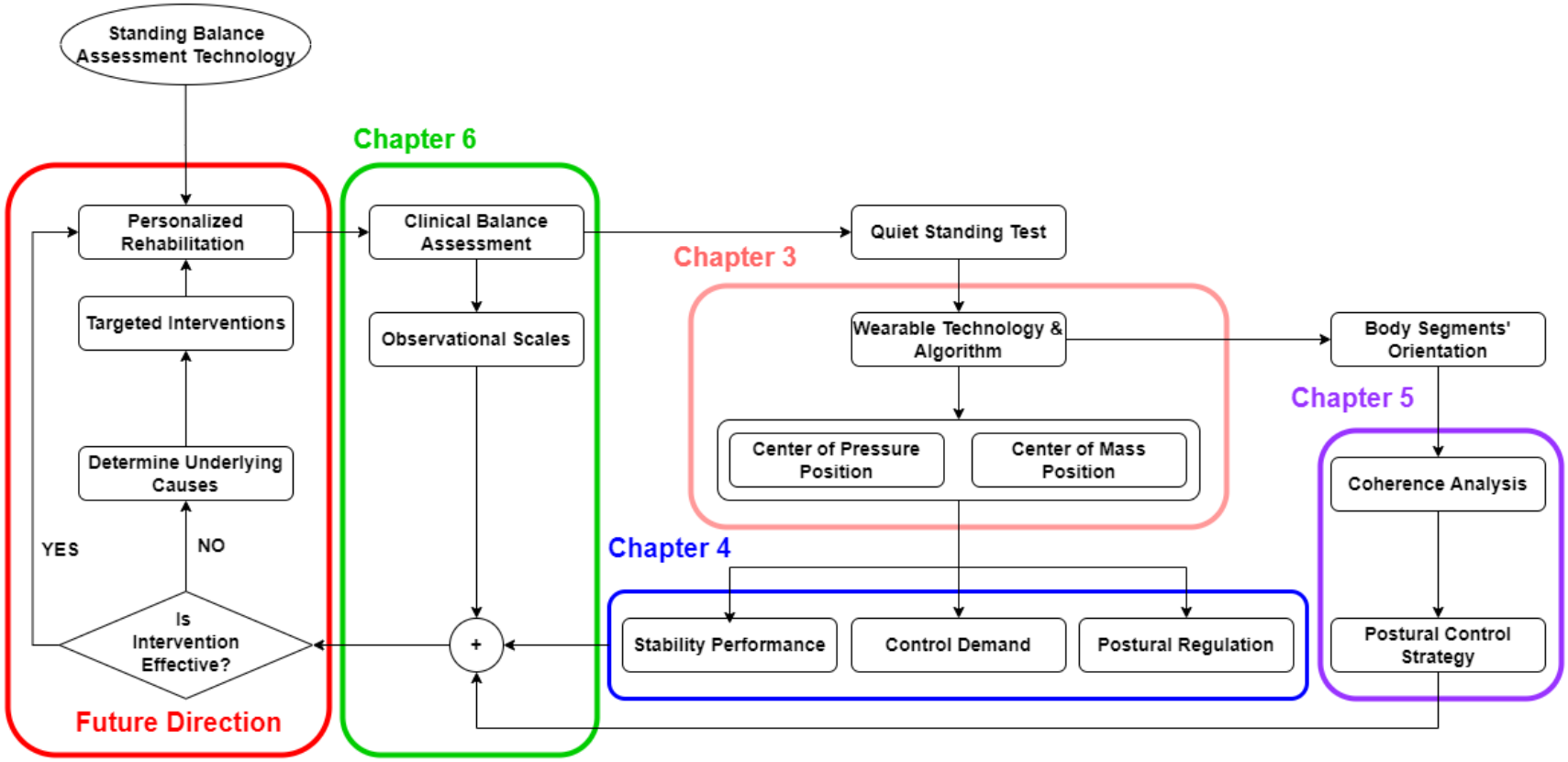

Figure 1-1. Elements of the proposed algorithm for objective standing balance assessment using wearable technology and their relation.

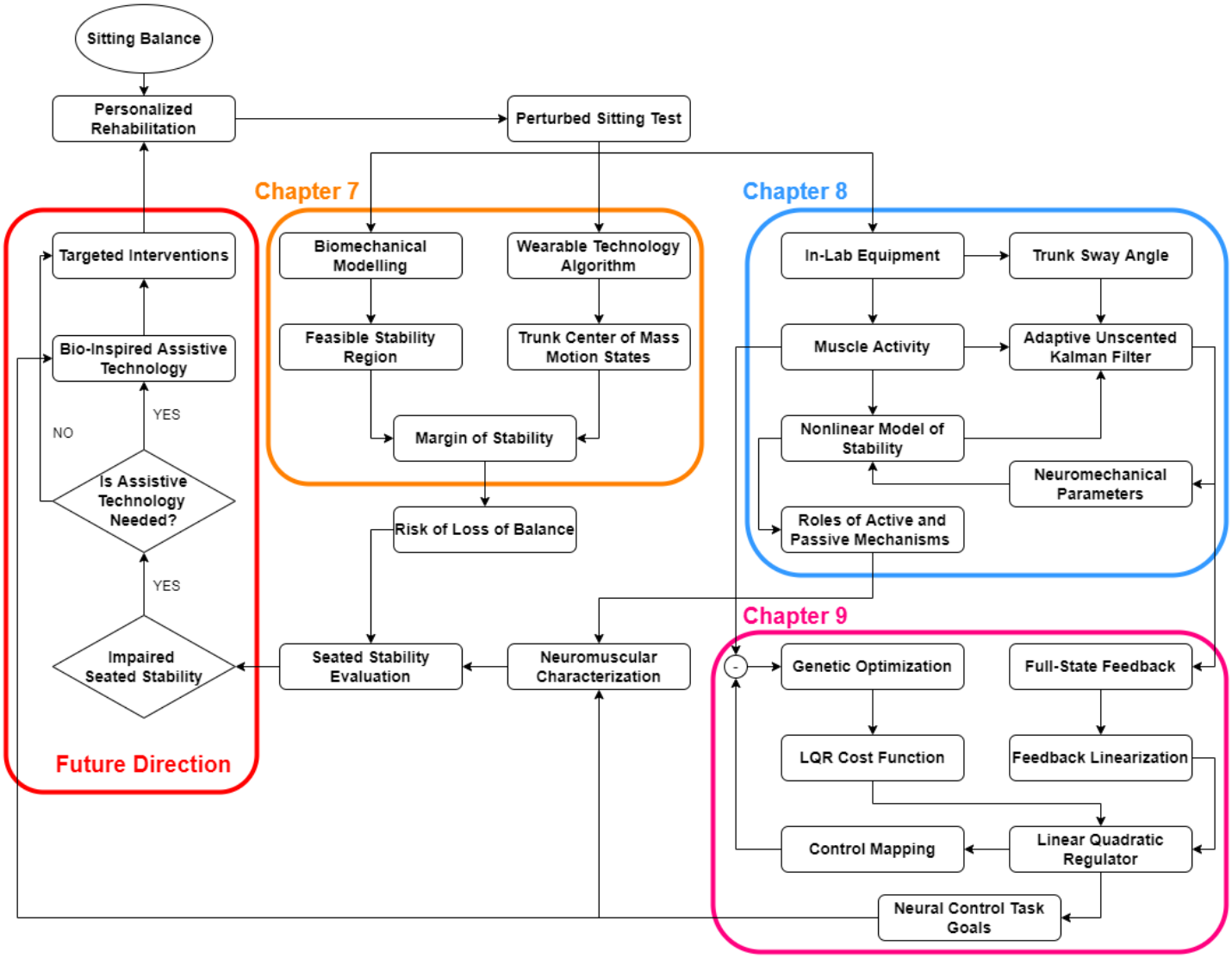

Figure 1-2. Elements of the proposed methodology for sitting balance assessment and neuromuscular characterization.

Chapter 2

Chapter 2 presents an overview of the literature relevant to this thesis research.

2 Literature Review

2.1 Static Balance Assessment

2.1.1 Quantification of Standing Balance

Bipedal human standing, from a mechanical point of view, is inherently unstable [82] since its stability needs a large mass consisting of many flexible segments to remain in an erect posture with the center of mass (COM) located within a relatively small base of support (BOS) [83]. Successful stabilization of the body posture requires coordination among different components of the body's neuro-musculoskeletal system, including joints and muscles [84]. Studying the mechanisms responsible for postural control is of significant interest to many researchers. Spontaneous sway during quiet standing has been widely used to investigate human postural control by analyzing the trajectory of the center of pressure (COP) [40], [41], the body COM [85], [86], or the ankle and hip joint motions [82], [87].

Standing balance represents an individual's ability to maintain the COM of the body and the COP within the boundaries of an established BOS [88]–[90]. The COM (also known as the center of gravity) represents the centroid of all mass of the body, while the COP represents the point of application of the ground reaction forces (GRFs) [89]. Researchers have extensively used both COM and COP to evaluate standing balance performance, identify impaired balance due to underlying health conditions, track retrospective falls, and predict prospective falls [89].

Traditionally, stationary laboratory equipment, including motion capture systems and force plates, has been used to derive COM- and COP-based balance biomarkers, respectively, for quantifying the dynamics of standing balance. Stationary equipment provides gold-standard reference measurements of COM- and COP-based balance biomarkers for both able-bodied individuals and those with neuromuscular impairment. However, the use of stationary equipment for clinical research and practice can be cumbersome due to the requirement of costly equipment in a dedicated lab space, which is not accessible at many locations such as hospitals and

rehabilitation clinics [89]. This results in the reduced utility of the stationary equipment outside the laboratory environment, limiting the ability of in-home monitoring, performing point-of-care clinical tests [37], [91], and routine objective outcome evaluation in clinical research and practice [92]. Body-worn IMUs, composed of a tri-axial accelerometer, gyroscope, and magnetometer, have been used as a reliable alternative for obtaining accurate and sensitive measures of standing balance in different populations such as able-bodied individuals [93], populations with Parkinson's disease [49], traumatic brain injury [37], and SCI [50]. IMUs are lightweight, unobtrusive, and relatively inexpensive. They can be easily integrated into functional tests, making them an ideal alternative to stationary laboratory equipment with a higher level of clinical utility [37], [51].

Increased use of COM- and COP-derived measures for assessing standing balance performance requires understanding what aspect of postural control these measures quantify and how they can be interpreted. COM- and COP-based measures quantify distinct aspects of postural control. Previous studies have shown that COM motion is controlled by the CNS via synergistically activating muscles in response to the COM movements [44], [45], [89], [94], implying that any movements of the COM lead to the initiation of the postural response. Therefore, COM motions indicate challenges in maintaining balance as well as the success of the neural response generated by the CNS to regulate stability [89]. On the other hand, COP provides information about the CNS response to COM imbalance, reflecting neuromuscular attempts to respond to instability [89]. Therefore, COP not only contains valuable information about the COM fluctuations but also about the utilized balance control strategy [43], [95]. Although COM- and COP-based measures may provide overlapping information about postural stability, there is a subtle distinction in what aspects of postural control COM and COP quantify. Mancini et al. [85] showed a moderate-to-weak correlation between COP and COM measures highlighting the distinction between these measures in quantifying postural control. Therefore, understanding such differences can help researchers and clinicians interpret changes in the balance performance of patients and evaluate the outcome of rehabilitation interventions.

Utilizing measures of postural steadiness based on COP and COM time series during quiet standing is known as posturography. Common posturographic measures introduced by the literature based on the measurements of in-lab equipment and wearable IMUs are discussed in sections 2.1.1.1 and 2.1.1.2, respectively.

2.1.1.1 Posturography

Many studies have used COP-based measures to characterize the control mechanisms of quiet standing [38]–[42]. The COP displacement can quantify standing balance during both dynamic and static conditions [43]. On the one hand, applying external perturbations (e.g., platform translation or external forces) and sensory disturbances (e.g., visual and/or proprioceptive) have been used to characterize postural responses and underlying stabilization mechanisms during dynamic conditions [44]–[46]. On the other hand, COP displacement during static conditions corresponds to spontaneous body sway and postural control during a quiet stance [42]. A commonly applied technique for assessing postural control and stability during quiet standing is utilizing measures of postural steadiness known as posturography [43]. The most common posturographic measures used to characterize quiet standing include time- and frequency-domain measures, which quantify displacement, velocity, area, and frequency properties of the COP (or COM) time series in the anteroposterior (AP) and mediolateral (ML) directions [41]. Other measures are Stabilogram Diffusion Function [38]–[40], Detrended Fluctuation Analysis [96], Approximate Entropy and Sample Entropy [97]–[99], and Lyapunov Exponent [100].

Collins and Luca [40] introduced a new concept for studying human postural control. They assumed maintaining an erect posture during an upright stance can be viewed as, in part, a stochastic process, and the COP can be analyzed as one- and two-dimensional random walks. They modelled COP trajectories as Brownian motion and assumed two short- and long-term mechanisms regulate quiet standing. They introduced averaged stabilogram diffusion plots as mean-square displacement of the COP vs. time interval. They estimated short- and long-term Hurst exponents as the slopes of the lines fitted to the short- and long-term regions of the log-log stabilogram diffusion plots, respectively. The short- and long-term regions ranged from 0 to 0.5 and 2 to 10 seconds, respectively. They suggested that the Hurst exponent of the short-term interval represents the open-loop mechanism of postural control while the long-term interval represents the closed-loop mechanism associated with neural feedback over a longer time. Note that the Hurst exponent is a number between 0 and 1, representing how the past increments of the displacement are correlated with the future increments. A Hurst exponent of 0.5 corresponds to zero correlation representing random walk behaviour, while a Hurst exponent larger (smaller) than 0.5 corresponds to positively (negatively) correlated stochastic process representing persistent (anti-persistent) behaviour.

Collins and Luca [38] also investigated the effect of visual input on standing balance using the same approach. They showed that visual inputs affect postural controls in two ways: a decrease in the stochastic process of the open-loop mechanism or an increase in the stochastic activity of the closed-loop mechanism. They suggested that in both scenarios, the visual input led to reduced stiffness of the musculoskeletal system. They attributed this hypothesis to reduced muscular activity at lower joints for the open-loop mechanism or to reduced gains of proprioceptive and vestibular components of the neural feedback for the closed-loop mechanism.

Prieto et al. [41] introduced a wide range of measures of postural steadiness based on the planar trajectory of the COP throughout the test called stabilogram. These measures were time-domain distance and area measures, frequency-domain measures, and hybrid measures (e.g., fractal dimension). Time-domain measures are associated with the displacement or the velocity of the COP trajectory as well as the area of the stabilogram. Frequency-domain measures characterize the area or the shape of the power spectral density of the COP trace. Hybrid measures model the stabilogram with a combination of time-domain distance measures. They concluded that among many COP-based measures introduced in this study, the use of (a) one time-domain distance or area measures (e.g., root-mean-square distance), (b) mean velocity, (c) one hybrid measure (e.g., mean frequency), and (d) one frequency-domain measure (e.g., centroid frequency) are recommended and together they can quantify different aspects of postural control during quiet standing.

COP-based measures characterize postural stability in three domains: stability performance, control demand, and postural regulation. Time-domain distance and area measures are related to stability performance, while the velocity measure was related to the control demand [101]–[104]. An increase in control demand can be attributed to increased visual contribution for postural stability [105]–[107] and an increased risk of falling [41]. Postural instability can be inferred from decreased stability performance shown by increased distance and area measures, as well as increased control demand shown by increased velocity measures. Hybrid measures combine the distance and velocity measures characterizing the relationship between stability performance and control demand [101]. The frequency measures are oftentimes calculated for the range of 0 to 5 Hz. The power frequency measures show alteration in preferential postural regulation [108], [109]. The centroid frequency indicates the inertia of an inverted pendulum model [43] and the time required for a system to return to its initial position [101]. Frequency

dispersion is a measure of variability in frequency content and is associated with active and passive stiffness or rigidity of the inverted pendulum [42].

Popovic et al. [90] introduced a new stability criterion based on the relationship between the COP position and the individual's stability. They identified four stability zones: a high preference zone as the area where the COP is located 99% of the time during quiet standing; a low preference zone as the area where the COP is located 1% of the time during quiet standing; an undesirable zone as the COP area where the individual needs to change their posture to maintain stability; and an unstable zone as the COP area where the individual needs to take a step to maintain stability. Their measure of stability ranges from zero to one. It is equal to zero in the high preference zone, linearly increases in the low preference zone, and is equal to one in undesirable and unstable zones.

Rocchi et al. [110] identified the features of the COP trajectory that are most sensitive to postural stability performance to eliminate redundancy. They applied thirty-seven posturographic measures used by Prieto et al. [41] to COP time series in both the AP and ML directions as well as COP resultant distance (RD). They conducted a feature selection process using Principal Component Analysis (PCA). They suggested that the COP RD time series can be characterized by four measures: (a) the size of the path travelled by the COP (e.g., root-mean-square distance); (b) a frequency characteristic (e.g., centroid frequency); (c) principal sway direction showing the relative weight of AP and ML components of the COP trajectory; and (d) frequency dispersion. They also recommended six measures for quantifying COP AP and ML time series: (a, b) dispersion in AP and ML directions using root-mean-square and their contrast; (c, d) mean velocity in AP and ML direction; (e) centroid frequency in AP direction; and (f) frequency dispersion in AP direction.

Human quiet standing is oftentimes modelled as a single inverted pendulum rotating about the ankle joint, stabilized primarily by active control of the ankle joint along with passive musculoskeletal stiffness and damping properties [111], [112]. Gage et al. [112] investigated the validity of the inverted pendulum model by examining the relationship between COM and COP during a 120-second quiet standing in able-bodied individuals. The 3D kinematics of 14 body segments were recorded using optoelectronic motion capture cameras while a force plate measured the COP trajectory and GRFs. Their results validated the inverted pendulum model of quiet standing, showing that the difference between COP and COM trajectories was significantly

correlated with the COM acceleration. They observed temporal and spatial synchronization between each segment COM and the whole-body COM, with the segmental COM increasing linearly with the height above the ankle joint. In addition, they showed that ankle joint angular displacement could track the COM motion.

Fok et al. [113] examined the error of the inverted pendulum model associated with the distance between the body COM and the ankle joint during natural unrestricted unperturbed standing as well as the error of having the ankle joint angular motion represent the COM angle. They used an optoelectronic motion capture system, and their experimental procedure included quiet standing with EO or EC, voluntary forward/backward sway, and freely moving. The distance change of the COM during EO and EC quiet standing was very small, i.e., close to the accuracy of their motion capture system. The distance change tended to be larger during forward and back voluntary sway, but it was not significant. Thus, they suggested that the inverted pendulum model is valid for quiet standing and voluntary sway if the inter-joint contribution, i.e., hip or knee joint torques, is not of interest. The COM sway angle and ankle joint angle had a moderate positive correlation during EO and EC quiet standing and voluntary sway, but a significant offset was observed. This implies that the ankle joint angle moderately represented the temporal features of the COM sway angle, and it may not provide an accurate estimate of COM spatial features.

Aramaki et al. [82] pointed out that hip joint motion also plays a significant role in efficient maintenance of the COM above the BOS since literature had suggested that restricted hip joint led to considerably higher ankle sway in able-bodied individuals [114]. They investigated how the coordination between the ankle and hip joints is controlled during a 30-second quiet standing with eyes open (EO) and eyes closed (EC). The angular motion of the ankle and hip joints was measured via laser displacement sensors. They observed a significantly higher magnitude of angular position, velocity, and acceleration for the hip joint compared to the ankle joint, confirming that the hip joint motion cannot be ignored during quiet standing. Furthermore, they discovered a reciprocal relationship between the angular accelerations of the hip and ankle joints, demonstrating that the ankle angular acceleration was compensated for by hip angular acceleration in the opposite direction. Such a consistent relationship was not observed for the angular displacement. Thus, they suggested that the angular motions of the ankle and hip are not supposed to minimize the COM displacement but, rather, to minimize the COM acceleration.

The ankle and hip strategies, along with stepping, are considered three coordinative patterns employed by the CNS to maintain stability during quiet standing [115], [116]. It is a common assumption that a quiet stance can be modelled by an inverted pendulum representing the ankle strategy and the hip joint only contributes during larger perturbations. The ankle strategy predominates during low-amplitude, low-velocity perturbations, while the hip strategy predominates during higher perturbation frequencies [115]. However, Creath et al. [116] demonstrated that a single segment model of quiet standing could be inadequate, and both ankle and hip strategies could be observable even during a quiet stance. They examined trunk-leg coordination of able-bodied individuals while standing on a hard surface (HS), foam surface (FS), and a sway-referenced surface with EC. During the sway-referenced trial, the platform was rotated in the AP direction equal to the hip angular displacement measured via a rod potentiometer. They used spectral analysis on trunk and leg angular displacement under different sensory conditions and observed the angular displacement of the trunk and leg were in-phase at sway frequencies below 1 Hz and anti-phase at sway frequencies above 1 Hz representing ankle and hip strategies, respectively. The transition from the ankle strategy to hip strategy was abrupt for the HS and FS conditions while a gradual transition was observed for the sway-referenced condition. They suggested that ankle and hip strategies are "simultaneously co-existing excitable modes" which are both present; however, the predomination of one strategy depends on the sensory information, and the characteristics of the task or perturbation. Similar results were observed by Zhang et al. [117] in both the AP and ML sway directions, further highlighting the utility of a double-linked inverted pendulum model of the dynamics of quiet standing.

Hsu et al. [84] also proposed that postural control during quiet standing depends on the coordination of multiple joints. They hypothesized that all major joints are equally active along the longitudinal axis of the body and coordinate to stabilize the spatial positions of the head and body COM. They examined this hypothesis by recording the motion of a multi-segment body model of able-bodied individuals during a five-minute quiet stance with EO or EC. They showed that the CNS minimizes the sway of the body COM and the head during quiet standing by coordinating the variance of joint motions in a way that the temporal variability of the joints has a minor effect on either the head or the COM position whereas, in an inverted pendulum model, the variability of the ankle joint motion would directly lead to variability in the COM and head positions. Depriving vision led to increased joint configuration variance compared to EO, while

its effect was insignificant on the variation of COM position, further highlighting the importance of multi-joint coordination to postural control during quiet standing.

Sasagawa et al. [118] investigated the effect of hip joint motion on the body kinematics in the sagittal plane during quiet standing of able-bodied individuals. They derived the actual COM acceleration by dividing the shear force measured by the force plate by the body mass. They estimated the COM acceleration using the angular motion data measured via laser sensors. They observed an anti-phase modulation between the ankle and hip angular acceleration. They showed that the COM acceleration could be precisely estimated only when the hip joint motion was considered in addition to the ankle joint motion.

Hay et al. [119] used magnitude squared coherence (MSC) to investigate the relationship between the free moment and COP in the AP and ML directions measured by a force plate during quiet standing with EO or EC. Regardless of vision condition, they observed a strong (weak) coherence between the free moment and AP (ML) COP at frequencies below 0.5 Hz, while the coherence decreased (increased) from 0.5 Hz to 1 Hz. The authors compared their results with previous studies that investigated multi-joint coordination [116] as well as ankle joint and muscle activation coherence [120]. They concluded that these observations resulted from ankle strategy at lower sway frequencies and hip strategy at higher sway frequencies.

2.1.1.2 IMU-Based Posturography

Posturographic measures using gold-standard force platforms and motion capture systems have shown high sensitivity and reliability for characterizing postural control. However, their cost and portability issues have hindered their utilization in clinics. Clinical rating scales are the most common approach for evaluating postural control in clinics; however, they are affected by clinicians' bias, low sensitivity to mild impairments, and poor reliability [85], [121]. Such limitations directly impact the ability of clinicians and researchers to identify individuals with mild balance impairment, monitor the progression of the disease, and evaluate the outcomes of interventions [37]. Mancini et al. [85] argued that there is a need for a more practical, objective balance assessment methodology for clinical applications that demonstrates high sensitivity to mild neurological impairments and good test-retest reliability with experimental and clinical validity. Many studies have proposed IMUs, particularly accelerometers, as a low-cost portable alternative [122]–[125]. A waist-mounted accelerometer has been suggested for the approximate

estimation of COM motion. Winter suggested that COM horizontal acceleration is proportional to the difference between COP and COM and, therefore, could potentially be a better postural sway measure representing the error signal within the postural control system [88].

Whitney et al. [123] investigated the test-retest reliability of three posturographic measures obtained from a waist-mounted accelerometer compared to COP during quiet standing with different sensory conditions. COM acceleration-based measures showed similar test-retest reliability as COP-based measures. Acceleration- and COP-based measures were significantly correlated under all test conditions. They suggested that the use of an accelerometer for balance evaluation may be useful to reduce clinical evaluation time.

Mancini et al. [85] investigated the sensitivity and experimental concurrent validity of using a waist-mounted accelerometer compared to a force plate for measuring postural sway. They also examined test-retest reliability and concurrent validity of acceleration-based measures compared to clinical scores (postural instability and gait disability sub-score of the Unified Parkinson's Disease Rating Scale). They used the common posturographic time- and frequency-domain measures with both COM acceleration and COP time series. They also introduced an acceleration based-measure called JERK [126]. They observed the capability of acceleration-based measures in distinguishing postural sway characteristics of able-bodied individuals compared to individuals with untreated Parkinson's disease. JERK and time-domain measures showed high test-retest reliability. They observed a significant correlation between acceleration-based measures and clinical scores. Hence, they suggested that the use of COM acceleration-based measures, including JERK, root-mean-square amplitude, mean velocity, and centroid frequency, are valid, sensitive, and reliable measures of postural stability.

Alberts et al. [127] used the IMU composed of accelerometers and gyroscopes of an iPad attached to the sacrum to approximate the COM and quantify postural stability compared to a force platform in able-bodied individuals. Participants completed a Sensory Organization Test. They calculated the COM sway angle using both IMU reading and COP measured by the force plate. They demonstrated that using IMUs could quantify postural stability with sufficient precision and accuracy. They suggested that using IMUs, at the time, did not replace biomechanical analysis; however, they can translate complex in-lab biomechanical analyses to a broader field such as clinical evaluations and athletic training.

Heebner et al. [128] also investigated the capability and reliability of accelerometry measures compared to COP-based measures to characterize postural stability in healthy athletic individuals during tasks with varying difficulty, including four static tasks with EO or EC and two dynamic tasks. The COM acceleration-based measures showed high reliability with the ability to differentiate tasks with varying difficulties. Moderate-to-weak correlation between the acceleration- and COP-based measures, proposed by Heebner et al., was observed, highlighting the fact that the two methods do not represent the same component of postural stability. However, both methods showed similar patterns of postural stability scores across different tasks.

Hansson and Tornberg [129] examined the correlation between a waist-mounted IMU and a force plate, as well as the reliability of the IMU for quantifying standing balance with EO or EC. A strong correlation was observed between two measuring devices in both the AP and ML directions with EO and EC. They observed moderate to good intra- and inter-trial reliability for the IMU. They suggested that the two assessment devices were not interchangeable, and there is a significant need for a reliable algorithm with the ability to move the balance assessment using wearable technology out into real life.

In a 2019 survey, Ghislieri et al. [130] reviewed the use of wearable IMUs for assessing standing balance. They investigated the application of IMUs for quantifying balance in different populations, sensor placement, common IMU-derived parameters, and validation against gold-standard. Many studies utilized IMUs to assess balance in healthy, young, and/or older adults and patients with Parkinson's disease [131]–[134] and multiple sclerosis [135], [136]. Regarding sensor placement, the most common place was the lower back (e.g., sacral region) as a representation of the body COM. Other studies have placed the IMU on areas of the lower limb, such as the thigh or shank, sternum, upper back, i.e., thoracic region, wrist, and forehead. Placing sensors on both the lower back and lower limb enables assessing postural control strategies (e.g., ankle or hip strategies) [131], [132]. The most common parameters were acceleration-based measures, including root-mean-square of the acceleration, JERK, range of acceleration, and centroid frequency. Few studies used gyroscope readings. Generally, there was a lack of sensor calibration procedures prior to calculating parameters assuming sensor misalignment was negligible. Many studies investigated the sensitivity and experimental validity of acceleration-based measures compared to COP-based measures and clinical scores. IMU-derived acceleration-based measures and COP-based measures quantify different aspects of postural control, hindering

direct comparison between the two methods. Nevertheless, the authors stated a lack of information about the sensitivity of wearable systems compared to traditional force plate posturography, particularly in the clinical field, for detecting mild changes in balance performance. They highlighted that IMUs have not become a practical tool of posturography for balance assessment due to a lack of accuracy validation of IMU-based measures compared to gold-standard force platforms. Thus, an innovative wearable balance assessment technology can be highly beneficial to both healthy and pathological populations.

In a 2021 review article, Baker et al. [137] investigated the concurrent and discriminant validity as well as the inter-sensor and test-retest reliability of wearable IMUs for assessing standing balance in healthy adults. Concurrent validity was investigated by comparing IMU-based measures with those of force plate [85], [128], and a combination of motion capture and force plate [138]–[140], showing moderate to strong correlation in both the AP and ML directions. The authors observed consistent moderate to excellent test-retest reliability for static balance assessment using wearable sensors across different studies. Moreover, discriminant validity was assessed across different studies, highlighting the capability of wearable sensors to distinguish the balance performance of young from older adults and fallers from non-fallers [141]. Furthermore, a single sensor placed near the body COM was as reliable as multiple sensors, showing moderate to good validity and test-retest reliability [137]. Using a single waist-mount accelerometer (over the lumbar region L3-L5) provides simplicity, encouraging clinicians to integrate wearable sensors into practice. This is especially important during telehealth interactions when healthcare is provided remotely. Such a simple wearable device would increase flexibility for clinical treatment when physical distancing is practiced, such as during the COVID-19 pandemic [137].

Richmond et al. [89] explored the current and future applications of COM- and COP-based measures for assessing standing balance. The authors pointed out that traditional posturography using motion capture cameras and force platforms for measuring the COM motion and COP, respectively, could be costly with reduced utility outside of the laboratory. Recent developments of wearable IMUs and innovative algorithms which can extract useful measures for quantifying standing balance look promising. However, such portable devices are not without their limitations, including sub-optimal noise minimization due to poor design of internal components and synchronization between sensors [142]. The authors believed that such limitations are being eliminated by the recent advancements in the field and the emerging concern is how the outcome

of wearable technologies can relate to gold-standard laboratory equipment in practice. Since IMU-based measures have different units compared to measures obtained from laboratory equipment, the direct comparison of outcome measures across the literature is cumbersome. Such difficulty can affect the translatability of IMU-based measures to clinical applications. Moreover, the accuracy of IMU-based measures significantly depends on sensor placement and post-processing algorithms. Similar to Ghislieri et al. [130], the authors of this study also believed there is a major need for a validation study between IMUs and motion capture cameras for measuring the COM kinematics during quiet standing. Given the differences between COM- and COP-based measures, additional investigation is needed to understand the clinical applicability of IMU-derived COM measures compared to traditional COP measures.

In sections 2.1.2 and 2.1.3, we discuss how the literature has benefited from traditional posturography using motion capture and force platform and recent advancements in wearable IMUs to characterize postural control during quiet standing based on the body COM and COP in two groups with degraded standing balance: (a) individuals with iSCI, and (b) the elderly, respectively.

2.1.2 Balance Assessment in Individuals with iSCI

The literature has reported that regaining the ability to maintain postural stability and walking function is among the top priorities for individuals with iSCI [16], [20], [21]. Up to one-third of all individuals with recent SCI are able to regain partial balance and walking ability after the first year post-injury [16], [143]. However, their prospective level of ambulation is related to the initial amount of motor function below the level of the lesion [19]. For instance, 80-100% of individuals with iSCI rated D on the American Spinal Injury Association Impairment Scale (AIS) are able to partially recover walking function, indicating some preservation of motor and sensory function below the level of lesion a year post-injury [16], [144]. This shows the necessity of implementing outcome measures that allow for the identification of the balance and walking capacities of individuals with iSCI to guide the delivery of more effective rehabilitative interventions [16].

Integration of sensory information from the somatosensory, visual, proprioceptive, and vestibular systems plays a predominant role in effective postural control [10], [17]. While iSCI results in motor impairment below the level of the injury [18], it may also change sensory

reweighting due to, e.g., reduced somatosensation. Developing compensatory strategies to maintain postural stability post-iSCI leads to alteration in reweighting of sensory information [20], [35]. As a result, alteration of sensory information such as visual [17] and somatosensory [145] inputs can further challenge postural control in individuals with iSCI. Hence, the implementation of methodologies for identifying changes in postural control and underlying impaired balance mechanisms allows for targeted and guided rehabilitation after iSCI [35]. Such interventions can have a positive impact on the improvement of postural control and movement coordination [20].

Sayenko et al. [20] used COP-based measures from a force plate to investigate the effect of the visual feedback on standing balance in individuals with iSCI. They also determined whether static and dynamic stability could be improved during training-irrelevant tasks after balance training. Participants attended twelve training sessions over four weeks. During each training session, they stood on a force plate and were instructed to look at a monitor placed at their eye level in front of the force plate. COP planar position was used as an input for the game-based exercises. In addition, static and dynamic stability was evaluated before and after training. Static balance was evaluated using COP distance, area, and velocity measures obtained during quiet standing with EO or EC. Dynamic balance was evaluated based on the maximum voluntary displacement of COP toward eight targets placed 45 degrees apart around the center without losing balance. The displacements of COP in eight directions formed an octagon, and its area was calculated as a measure of dynamic stability. They observed a significant improvement of static and dynamic stability measures post-training showing the effectiveness of visual feedback on postural control of individuals with iSCI. This could be attributed to the improvement of existing motor strategies as well as the development of new strategies and integration of the sensorimotor system.

Grangeon et al. [101] determined the minimum COP-based measures required for characterizing seated stability in individuals with SCI compared to able-bodied individuals by comparing 39 COP-based posturographic measures. Two sitting positions were performed by each participant: first with both hands on the thighs and second with both upper extremities flexed and abducted at 70 degrees and 45 degrees, respectively. COP-based measures were able to distinguish the balance of individuals with SCI compared to able-bodied participants irrespective of sitting positions. Bilateral hand support led to reduced AP sway in individuals with SCI and was suggested as a compensatory strategy. COP time-domain distance and area measures were highly

correlated, while frequency-domain measures were discriminative and uncorrelated. They suggested that posturographic measures for characterizing balance post-SCI should include mean distance, mean velocity, centroid frequency, median frequency, and frequency dispersion in both the AP and ML directions.

Lemay et al. [17] compared individuals with iSCI and able-bodied individuals in terms of the use of visual information to maintain standing balance. They also quantified the relationship between the contribution of visual inputs to postural stability and a clinical balance scale. All participants performed two 45-second quiet standing on a force plate with EO or EC. They used root-mean-square distance, mean velocity, and sway area as posturographic measures. Individuals with iSCI were also assessed with Mini-BEST as a clinical balance scale. They observed worse postural stability in individuals with iSCI compared to able-bodied individuals in both conditions. Moreover, the Romberg ratios (i.e., measure in EO / measure in EC) of mean velocity and sway area were significantly larger for individuals with iSCI compared to able-bodied individuals implying a higher contribution of visual inputs to postural steadiness post-iSCI. Romberg ratios of root-mean-square distance and sway area were significantly correlated with Mini-BEST. Since SCI causes somatosensory impairments following a lesion, the contribution of visual information during standing may be increased post-iSCI in comparison with a healthy population due to altered sensory reweighting.

Maintaining balance is an essential component of safe standing and walking; however, it is a major challenge for individuals with iSCI as they regain the ability to walk [17]. A more normal walking pattern, higher stride speed, less reliance on supervision or physical assistance, and more functional ambulatory status are highly correlated with greater postural control in individuals with iSCI [16]. The literature has demonstrated that clinical measures of standing balance, such as Berg Balance Scale scores, for individuals with iSCI correlate well with various walking outcome measures such as speed, endurance, and reliance on mobility-related assistive devices [16], [36]. However, the major bottlenecks of the BBS are its ceiling effect, its inability to predict future falls, and the inability to determine the underlying cause of balance difficulty [16]. As a complementary approach, Lemay et al. [36] investigated the concurrent validity of Smart Balance Master tests in individuals with iSCI compared to observational BBS. Smart Balance Master consisted of two force platforms used to determine the COM position with an eye-level screen showing the participant's COM and the evaluation task. In addition to BBS, participants

performed a static task, including standing on the force platform with EO and then EC with sway area as the measure. Then, a limit of stability task was performed where participants were asked to reach eight equally spaced targets as fast as possible. Sway path length and time were averaged over eight directions. Finally, participants performed a weight shifting task in the AP and ML directions by following a target with their COM shown on the screen with the absolute error expressed as a percentage of the limit of stability being reported. They observed no stability performance difference between tetraplegic and paraplegic individuals using posturographic measures. The limit of stability test showed the highest correlation with BBS and other Smart Balance Master tests. Therefore, the limit of stability test was suggested as a complementary method to BBS for assessing the dynamics of standing balance in individuals with iSCI.

In another study, Lemay et al. [18] characterized dynamic postural balance during standing among individuals with iSCI compared to able-bodied individuals using the comfortable multi-directional limit of stability and investigated its association with quiet standing posturography. Participants were asked to lean toward eight targets placed 45 degrees apart while standing on a force plate, and COP visual feedback was provided. The absolute maximal distance and the path length of COP were calculated for each direction. Furthermore, quiet standing was performed with EC, and time-domain COP measures were computed. The observed COP path length was significantly greater for individuals with iSCI compared to able-bodied individuals in all directions except for the AP direction. The maximum position reached in the AP direction was significantly smaller in individuals with iSCI. They observed little correlation between quiet standing time-domain measures and the limit of dynamic stability. They suggested that a comprehensive assessment of postural stability should also include outcome measures evaluating both static and dynamic stability.

Tamburella et al. [146] analyzed the reliability, validity, and responsiveness of COP-based measures to assess standing balance under different conditions in individuals with iSCI. They examined twenty-three individuals in 111 sessions over one year. Each session included clinical scale tests such as BBS and stabilogram analysis on a force platform. Test conditions comprised of open feet and closed feet with EO and EC. COP-based measures were path length, mean velocity in the AP, ML, and RD directions, ellipse area, x-axis, and y-axis of the ellipse area. Among all COP-based measures, mean velocity was the most repeatable measure with the lowest coefficient of variation and highest intraclass correlation coefficient (ICC). Path length and mean velocity in

the ML and RD directions had the lowest percentage change due to the measurement error quantified by Minimal Detectable Change. Path length and mean velocity in the AP, ML, and RD directions were also the most valid measures with the highest correlation with BBS. Among the test conditions, the open-feet test with EO was the most valid, while the open-feet test with EC was the most reliable with the highest ICC. In terms of responsiveness, BBS was the most sensitive clinical scale, while all COP-based measures were shown to be more sensitive than all clinical scales.

In a systematic review, Arora et al. [10] explored the balance measures used to evaluate the balance performance of individuals with iSCI and compared them in terms of their clinical utility, psychometric properties, and comprehensiveness. They identified 31 balance measures, including eleven biomechanical measures and twenty balance scales. Balance scales have shown higher clinical utility compared to biomechanical measures (e.g., COM- and COP-based measures), limiting the use of biomechanical measures in a clinical environment. Therefore, developing biomechanical measures with high clinical utility is of significance. Among balance scales, the BBS and Functional Reach Test had higher validity [16], [147]–[149], reliability [146], [149], [150], and responsiveness [147], [151]. Although BBS was the most common test, it was not able to predict future falls in individuals with iSCI [150], [152]. The comprehensiveness of the clinical measures was based on how many domains of postural control they could evaluate, including static stability, underlying motor systems, functional stability limit, verticality, reactive postural control, anticipatory postural control, dynamic stability, sensory integration, and cognitive influences. The Mini-BEST was the most comprehensive among clinical scales. The authors believed there was no single test/measure that concurrently demonstrated high clinical utility, strong psychometric properties, and comprehensiveness. Three gaps were identified by the authors. First, the measures should be further investigated for their psychometric properties in individuals with sub-acute and chronic SCI, with the focus on identifying cut-off scores indicating a high risk of falling. Second, the responsiveness of the measures to changes in postural control in individuals with SCI should be further studied. Third, comprehensive balance measures during transferring in wheel-chair users should be further investigated.

Chan et al. [35] evaluated the test-retest reliability of Mini-BEST via ICC and assessed the concurrent validity of mini-BEST by examining its Pearson's correlation with COP-based measures. COP-based measures have shown high reliability and validity as the gold standard in

the literature [146]. The Mini-BEST evaluates balance via 14 standing and walking tasks scored on a three-point ordinal scale. Participants performed Mini-BEST twice two weeks apart. They also performed a quiet standing test on a force plate with EO or EC. They observed excellent test-retest reliability of the Mini-BEST. They observed a negative correlation between the Mini-BEST score and COP mean velocity during the EO condition. In terms of convergent validity, they observed a strong correlation between Mini-BEST total score and lower extremity strength.

In a prospective cohort study, Musselman et al. [153] investigated the performance of COP-based measures and clinical scores for distinguishing fallers and non-fallers in ambulatory individuals with iSCI. Participants completed two test sessions. In the first session, participants performed quiet standing with EO or EC on a force plate. The mean velocity of COP was calculated in the AP and ML directions. In the second session, a physical therapist performed a clinical assessment, including lower extremity strength, proprioception, cutaneous sensation, walking speed, and balance self-efficacy. Participants then self-reported their falls for one year after test sessions. Participants were classified as fallers if their number of falls exceeded the median number of falls among all participants. Outcome measures of lower extremity strength, cutaneous pressure sensitivity, walking speed, and the COP mean velocity in the ML direction could distinguish fallers from non-fallers. The authors suggested that COP mean velocity, along with the above-mentioned clinical scores, could be useful for the clinician to identify ambulatory individuals with iSCI with a high risk of future falls.

2.1.2.1 Summary and the Gaps

In summary, many studies mentioned above have taken advantage of in-lab equipment such as motion capture cameras and force plates along with clinical scales to obtain objective measures of standing balance in ambulatory individuals with iSCI. However, the use of body-worn IMUs to obtain clinically meaningful measures of standing balance in individuals with iSCI has not been fully investigated. There is a significant need for a comprehensive balance evaluation using wearable sensors in individuals with iSCI compared to able-bodied individuals during a variety of challenging standing conditions affecting sensory inputs. Furthermore, since individuals with iSCI suffer from impaired sensorimotor function and dysfunctional postural control, they may adapt postural movement strategies compared to able-bodied individuals to compensate for reduced postural control. Although COP- and COM-based measures are strong indicators of impaired postural control, they do not directly reflect all aspects of the adaptive postural movement

strategies employed during impaired standing [136]. Therefore, identifying alteration of postural control strategies post-iSCI compared to able-bodied individuals under different sensory conditions using wearable technologies remains a significant need.

2.1.3 Balance Assessment in Elderly

Up to one-third of senior adults fall at least once a year [6], and over half of these individuals report multiple falling incidences [7]. Therefore, it is not surprising that falls are among the most common causes of injuries in senior adults [1], [2]. Poor postural stability is a key contributor to falls in seniors, and balance evaluation is an effective measure for introducing targeted rehabilitative interventions [154], with effective interventions preventing more than 50% of potential falls in seniors [155]. Targeted rehabilitative interventions are carried out to not only prevent future falls but also reduce fall severity [8]. In this light, to reduce future fall incidences and their adverse consequences among senior adults, it is essential to (1) implement effective balance assessment methodologies; (2) introduce targeted patient-specific rehabilitative interventions; and (3) evaluate the effectiveness of such interventions [1], [8], [156].

The BBS test is also commonly used in geriatrics clinics for assessing the balance performance of the elderly and for clinical outcome evaluation of rehabilitative interventions. It was previously discussed that although BBS is relatively fast and reliable, it tends to be, in part, subjective in nature due to the involvement of human decision-making [157], low construct validity, and may not always result in reliable and sensitive outcomes [49]. In addition, clinical scales provide little information for understanding potential underlying causes of balance difficulties and for evaluating the effect of therapy on balance performance [16], [35], [36]. Hence, there is a need for a more quantitative, objective methodology to evaluate balance when choosing targeted rehabilitative interventions and when performing their objective outcome evaluation [85], [121]. The literature has shown that quantitative balance biomarkers such as COM- and COP-based measures allow for identifying age-related changes in balance and, thus, the risk of falling in the elderly population with high sensitivity and reliability [41], [91], [158]–[160].

Collins et al. [39] used the Stabilogram Diffusion Function to investigate the age-related changes in characteristics of open- and closed-loop control mechanisms of balance. They measured the COP trajectories using a force platform during quiet standing in the young and senior adults. They obtained short- and long-term diffusion coefficients and Hurst exponents as the slopes of the

lines fitted to the short- and long-term regions of the linear-linear and the log-log stabilogram diffusion plots, respectively. They observed that the steady-state behaviour of the open-loop postural control in senior adults was more positively correlated and, thus, more unstable compared to young adults. On the other hand, they observed that the steady-state of the closed-loop postural control was more negatively correlated in senior adults, implying a more stable closed-loop mechanism over the long term. Interestingly, seniors used the open-loop control mechanism for longer time intervals which could be associated with larger COP displacement in this population. This suggests a longer delay in utilizing the closed-loop control mechanism in senior adults.

Panzer et al. [161] performed a biomechanical assessment of quiet standing to investigate age-related changes in postural stability. They used the mean, variability, and total path length of the body COM, individual body segments, and COP. They observed a significant association between aging and increased variability of COM, head, and hip motions. They observed an altered postural control strategy in the elderly compared to young adults as a compensatory strategy for primary balance deficits. The elderly showed reduced small continuous movements while exhibiting larger adjustments involving the trunk and hip motions. They also observed increased AP COP path length during the EC condition without any significant change in the COM. Based on this result, the authors believed there was no evidence of reduced postural stability concurrent with aging since balance maintains the COM over the BOS, and therefore, the assessment of balance must be based on the COM. However, they stated that postural adjustments due to aging could be less effective when the balance is challenged.

Prieto et al. [41] compared a variety of COP-based time- and frequency-domain measures to investigate age-related changes in postural steadiness during quiet standing with EO or EC. They observed that different measures could distinguish EO and EC conditions in young and senior adults. The mean velocity of COP was the only measure that could concurrently identify age-related changes and eye conditions in balance. They suggested that multiple measures are required to adequately characterize changes in the balance due to aging as well as eyes condition within each age group. They recommended the use of COP mean velocity, one time-domain distance measure, such as root-mean-square distance, one time-domain hybrid measure such as mean frequency, and one frequency-domain measure, such as centroid frequency, as they may characterize different aspects of postural stability.

Freitas et al. [162] investigated the effect of aging on human postural control during prolonged standing. Young and senior adults performed 30-minute and 60-second quiet standing trials on a force plate. Both groups showed increased COP root-mean-square distance and velocity during prolonged standing. However, the elderly group exhibited smaller changes in postural sway during prolonged standing. The authors attributed this to the lack of mobility in the elderly, which may contribute to an increased risk of falling in this population.

Raymakers et al. [163] investigated the choice of COP-based measures for assessing standing balance with EO or EC on both HS and FS with or without cognitive tasks for able-bodied young and elderly and elderly with balance impairments. They used COP-based measures, including mean velocity, maximal AP and ML range of movement, area, deviation, and stabilogram diffusion function. Mean velocity was the most consistent measure, showing differences between test conditions, health conditions, and age; however, it was not discriminative when the cognitive task was introduced to able-bodied older individuals. Maximal ML movement range was discriminative among groups and test conditions but not the cognitive task in able-bodied young and elderly individuals. The critical time derived from the stabilogram diffusion plot exhibited no association with other measures while distinguishing the effect of the cognitive task in older individuals standing on HS. They concluded that the mean velocity seemed to be the most informative measure of balance in all groups and conditions.

Amoud et al. [96] used fractal time series analysis to quantify the postural stability of the elderly compared to able-bodied young adults. They employed two methods for computing Hurst exponent for fractal and nonlinear time series analysis using COP time series: Detrended Fluctuation Analysis and Stabilogram Diffusion Analysis. They used three different sizes of sliding windows (2.5, 5, and 10 seconds) and investigated the effect of age, time, and computation method on the Hurst exponent while ICC was used as a reliability measure. Both methods were able to identify age-related differences in postural stability with the time of five seconds with good to excellent ICC for the Detrended Fluctuation Analysis method showing more robustness.

When using the inverted-pendulum model of standing balance, the distance between the COP and vertical projection of COM (COP-COM) shows the relationship between the controlling and controlled variables of postural control. The COM acceleration is proportional to COP-COM. Masani et al. [164] claimed that, since aging affects postural control, these two variables could be affected. They compared the COP-COM and COM acceleration between a group of able-bodied

young adults and a group of elderly during quiet standing with EO or EC. They observed higher COP-COM variability and larger COM acceleration in the elderly compared to young adults, irrespective of vision condition. They observed that COM acceleration was proportional to COP-COM in both groups, implying the validity of using the inverted pendulum model in the elderly. They suggested that the increase in variability in COP-COM due to aging resulted from changes in postural control strategy and, consequently, COM acceleration became larger.

Lin et al. [165] investigated the within-day and between-day reliability of COP-based measures for identifying age-related differences. COP was recorded during quiet standing on four different days. The COP-based measures included root-mean-square distance, mean velocity, median frequency, sway area, and detrended fluctuation analysis. ICC and standard error of measurement (SEM) were used to quantify reliability. Within-day reliability was higher than between-day reliability. Consistent with previous studies, mean velocity was the most reliable measure. Older participants, compared to younger individuals, exhibited better ICC for all COP-based measures and comparable SEM except for mean velocity and sway area.

Tucker et al. [166] investigated age-related differences in postural reaction time and coordination during voluntary sway in the AP and ML directions in response to an auditory cue initiated from a static quiet stance or dynamic switching of sway between two directions. Participants stood on a force plate while wearing tri-axial accelerometers mounted on the head and lower trunk. Reaction time was defined as the difference between cue onset and the first observable change in COP or acceleration. Measures included reaction time, the difference between reaction time of COP, head and trunk acceleration, and COP-head-trunk coupling. The elderly group exhibited a slower reaction time during both static and dynamic tasks. They observed a smaller difference between reaction time and phase between COP, trunk acceleration, and head acceleration. They suggested that the elderly group adopted a more rigid coordination strategy compared to younger adults. This could be a compensatory strategy in response to balance difficulty in the elderly compared to younger adults.

O'Sullivan et al. [157] argued that measurement of COM acceleration with a relatively inexpensive, light-weight body-worn accelerometer could be a potential solution to the subjectivity of clinical scales and a potential alternative to expensive in-lab equipment. They investigated the correlation of accelerometry with BBS and TUG and characterized the accelerometer response to challenging balance conditions in fallers and non-fallers. Elderly patients of a hospital identified

as fallers and non-fallers participated in the study. COM acceleration was measured using a waist-mounted accelerometer during standing EO or EC on both HS and FS. The root-mean-square of COM acceleration increased with task complexity. The accelerometry could distinguish fallers and non-fallers under the FSEO condition. A high inverse correlation between the accelerometry and BBS and a positive correlation between the accelerometry and the TUG was observed for the FSEO condition. Therefore, they demonstrated that accelerometry could be an efficient quantitative approach for assessing balance in older adults.

Singh et al. [167] investigated the effect of age, vision, and surface compliance on the spectral content of COP time series. Able-bodied young and elderly individuals stood on a force plate with EO or EC on HS or FS. The mean power spectral density of COP over discretized bands was calculated. The effects of vision, surface, and age were distinguishable using this measure in the AP and ML directions. They observed a significant change in the spectral content of the COP in both AP and MLwith task difficulty (EO vs. EC and HS vs. FS) and in older adults. They suggested that vision and surface condition were predominantly related to the musculature responses associated with the body sway in AP and ML directions. The authors suggested that using the spectral content of COP to distinguish the contribution of different sensory inputs to postural control could be useful for identifying elderly individuals with impaired balance. Similar results were observed by Fujimoto et al. [168].

The literature has shown that the anti-phase action between the leg and trunk reduces the COM acceleration during quiet standing, playing a major role in postural stability [82], [116]. Kato et al. [169] investigated the effect of aging on trunk-leg movement coordination during standing. They measured trunk and leg motion in the AP direction using laser displacement sensors in young and elderly participants. They observed significantly higher COM velocity and acceleration in the elderly compared to young individuals. They also observed increased angular acceleration of the trunk and leg segments as well as reduced trunk-leg anti-phase action. They concluded that reduced trunk-leg anti-phase action due to aging is the major contributor to increased COM acceleration and, thus, is responsible for reduced postural stability in the elderly.

Li et al. [170] assessed the reliability and validity of COP-based measures for balance assessment in older adults. Participants were evaluated using both BBS and a force plate two times a week apart. They used ICC and Pearson correlation to assess the reliability and validity of COP-based measures, respectively. Good to excellent reliability was observed for twelve COP-based

measures. Moderate to good negative correlation was observed between the measures and the BBS. Therefore, the authors recommended the use of COP-based measures as reliable, valid measures for balance evaluation in older adults.

Ghahramani et al. [171] analyzed the postural sway of senior adults categorized as non-fallers, once-fallers, and multiple-fallers using clustering techniques. They performed quiet standing with EO, EC, and feet together as well as single-leg and tandem standing. Trunk angular position and velocity in the frontal and sagittal planes were measured using an IMU attached to the lower back. Data clustering techniques were applied to the recorded data in the form of unsupervised learning to identify meaningful patterns between groups and test conditions. A sway index was defined as the ratio of the difference between the number of all data samples and the number of data in the common cluster over the number of all data samples. The sway index of standing on one foot and with one foot in front of the other could distinguish older fallers from non-fallers with comparable sensitivity and specificity with BBS. Therefore, they suggested that such a protocol could be an alternative or a complementary approach to BBS for identifying older fallers.

A similar study was conducted by Johansson et al. [172]. They investigated how postural sway measures could predict fall incidences in 1900 community-dwelling older adults. Postural sway was measured during quiet standing with EO or EC using a force platform. The COP path length was used as a measure. A TUG test was also carried out to assess lower leg muscle strength, gait performance, and functional mobility. A hydraulic hand dynamometer was used to measure the maximum grip strength of the non-dominant hand. Participants reported incidents of falls six and 12 months after the examination. COP path length was significantly greater among fallers than that of non-fallers during both EO and EC conditions, with a strong correlation between the two trials. The authors obtained a nonlinear distribution of falls and COP path length during EO by dividing the path lengths into quintiles with significantly increased fall frequency in the 5^{th} quintile. Independent predictors of falls were explored using two logistic regression models. The first classification model used only the COP path length as an independent predictor of falls, while the second model included other measures (e.g., sex, weight, grip strength, TUG). They observed that postural sway quantified by COP path length could independently predict fall incidents in community-dwelling older adults, highlighting the importance of posturographic measures as predictors of future falls in the elderly population.

In a comprehensive study, Pizzigalli et al. [160] reviewed the postural characteristics of older adults with a high risk of falling based on static and dynamic balance assessments. They observed that COP path length, mean velocity, and sway in the AP and ML directions are the main measures capable of distinguishing fallers and non-fallers in the elderly population. COP-COM was found to be a reliable measure of postural stability in healthy older adults, and it can potentially be used to track clinical changes in this population. Common COP-based time- and frequency-domain measures exhibited better ICC and SEM with aging except for sway area and mean velocity. Older adults have shown weaker muscle strength and resistant torque in dynamic conditions compared to younger adults, affecting their ability to restore postural stability. Furthermore, older adults require higher muscle activity compared to younger adults to produce resistant torque leading to premature fatigue and increased fall risk. Balance indicators in the ML direction, including COP-based mean velocity, mean amplitude, and root-mean-square displacement during EO and EC, are the best indicators for identifying postural stability differences between future fallers and non-fallers among older adults. Tandem standing and standing with feet placed together have shown to be effective tests for distinguishing fallers from non-fallers. Standing with EC could also be effective since fallers had lower proprioception and more reliance on visual inputs. Standing on FS has shown a higher increase in COP path length in non-fallers compared to fallers, implying that faller older adults seemed to be less affected by the reduction in somatosensory input. Older adults exhibited a reduced cutaneous sensation causing an inability to detect the COP movement under their feet which would delay compensatory reactions when a fall happens, making reaction time one of the best identifiers of fallers. Older adults, compared to younger adults, had more antagonist muscle activation adopting a hip strategy to restore postural stability in dynamic conditions. During voluntary sway, older adults have shown slower, less reliable, and less responsive postural reflexes, suggesting issues with hierarchical movement organization. In addition, reduced muscle strength (e.g., ankle dorsiflexion weakness) due to atrophy, deterioration of mechanical properties, and loss of motor units are responsible for reduced postural stability in older adults. Moreover, greater postural sway and higher muscle activations correlated with lower clinical scores and increased fall risk in older adults. The authors concluded that objective balance evaluation in older adults is essential for fall risk prediction and evaluation of the effectiveness of balance training programs aimed at preventing future falls.

Montesinos et al. [173] reviewed the application of wearable IMUs for fall risk evaluation in older adults. They identified the optimal combination of sensor placement, task, and feature categories. Their results showed that (1) angular velocity during walking measured via an IMU attached to the shin and (2) linear acceleration during quiet standing, sit-to-stand, and stand-to-sit measured via an IMU attached to the lower back are the best combination. The measures that were significantly higher in elderly fallers were: (1) the root-mean-square acceleration in the ML direction during quiet standing with EC; (2) the number of steps and total time to complete a TUG test; (3) step time during walking.

Roman-Liu [158] performed a systematic review and meta-analysis of available data to investigate age-related changes in COP range and velocity in the AP and ML directions. They formed a numerical database with the mean and standard deviation of selected COP-based measures classified with eye condition (EO or EC) and age group (younger or older adults). Their results showed that body sway range and velocity increased with age, with the velocity measure exhibiting larger age-related changes. COP measures were higher for the EC condition and for older adults and, thus, quiet standing with EC could provide clearer results for identifying age-related changes. They concluded that such quantitative measures of stability with cut-off scores could be used for generating standards and recommendations for balance evaluations.

Sun and Sosnoff [174] reviewed the sensing technologies used to provide objective fall risk assessment in older adults. Four major sensing technologies were IMUs, video/depth cameras, pressure sensing platforms, and displacement laser sensing. Assessment tasks included walking, static/dynamic balance, and functional mobility. The authors believed the variation in outcome measures, sensor location, task, assessment tools, and modelling techniques hinders any conclusion on the capability of such technology in predicting future falls in older adults. There is a need for appropriate model construction/validation before using such technologies for fall risk assessment in everyday life. In addition, most previous studies have used retrospective fall history along with clinical scales such as BBS and TUG as the reference for identifying fall risk, which may not be accurate. The authors suggested the use of prospective fall occurrence six-month post-examination as a better alternative. Nevertheless, future work is needed to identify clinically meaningful and easy-to-interpret outcome measures for identifying fall risk in the elderly based on evident research.

Patel et al. [141] investigated gait and posture differences between older adult fallers and non-fallers based on the measurements of wearable IMUs. They identified 149 gait and posture characteristic differences. Spatiotemporal measures, including slower walking speed, shorter step, and stride lengths, as well as acceleration-based measures such as reduced root-mean-square acceleration, were the measures highly attributed to the risk of falling when performing dynamic tasks. On the other hand, increased root-mean-square acceleration of the trunk was an indicator of fall risk during static tasks. A single waist-mounted IMU was a successful choice for determining various gait and posture characteristics. There was a lack of studies conducted outside laboratories such as clinics. IMUs are promising tools to be integrated into current clinical fall risk evaluation methods, and they are even more effective for continuous unsupervised monitoring. Due to the portable, lightweight nature of IMUs, they can be used outside a laboratory environment which has not been widely investigated. The authors suggested that the use of IMUs allows clinicians to make a more objective, informed assessment of fall risk and, therefore, their application in a clinical setting should be further investigated in the future.

2.1.3.1 Summary and Gaps

In summary, there is a growing need for an objective balance assessment of the elderly and those with neuromuscular impairments. Particularly, objective balance assessment methodologies using wearable IMUs have not been employed in a clinical setting to obtain an objective outcome evaluation of rehabilitative interventions. There is a need to investigate the feasibility of using IMUs integrated into the functional scale tests for identifying, in a clinical setting, the effect of rehabilitative interventions on objective balance measures and clinical scores. Therefore, it is essential to develop and validate an algorithm for reliable assessment of standing balance using wearable technology integrated into clinical functional tests. For this purpose, research studies should: (1) develop algorithms to assess kinematic and kinetic parameters characterizing standing balance using the measurement of wearable IMUs and experimentally validate the accuracy of these parameters against gold standard motion capture and force plate systems; (2) investigate the feasibility of using a validated algorithm for identifying changes of balance biomarkers measured by wearable technology in the elderly fallers or those with neuromuscular impairment at rehabilitation hospitals/clinics compared to able-bodied young adults; (3) investigate the capability of the validated algorithm for identifying the effect of rehabilitative interventions on the balance

measures; and (4) compare the obtained objective balance measures from the validated algorithm with the clinical scores recorded by certified clinicians.

2.2 Dynamic Balance Assessment

Previous studies have suggested that an understanding of healthy neuromuscular control can be useful for identifying impaired balance and restoring functional abilities in individuals with neuromuscular impairments [23], [59], [66]. Therefore, characterizing the underlying mechanisms of neuromuscular control in able-bodied individuals can potentially pave the way for objective balance evaluation and the development of targeted rehabilitative interventions for improving impaired sitting balance [60], [67]. Furthermore, assistive technologies based on neuromodulation, such as FES, could be useful for restoring dynamic stability by stimulating impaired muscles via both open- [175] and closed-loop [27], [176]–[180] control strategies. It has been observed that closed-loop control of stimulation using kinematic feedback can reduce muscle fatigue, ensure smoother muscle contractions, and improve joint trajectory tracking [181]. Therefore, motion states (i.e., position and velocity) of the body COM during dynamic conditions can be significant in utilizing closed-loop control of assistive technologies. Furthermore, several biomechanical criteria have been introduced by the literature to quantify the dynamic stability during standing and walking based on the motion states of the body COM [52]–[58]. However, there is no standard biomechanical criterion that quantifies the relationship between the motion states of the trunk COM and sitting balance during dynamic tasks. In addition, designing bio-inspired controllers for assistive technologies (e.g., closed-loop FES systems) is challenging [25], [60], [72] since such complex technologies must provide physiological actions similar to those of motor commands (e.g., muscle activation) produced by the healthy neural control system [25]. Therefore, characterizing the neural control of non-impaired seated stability is a prerequisite for bio-inspired closed-loop neuromodulation technology [60].

In sections 2.2.1 and 2.2.2, we discuss how the literature has quantified the concept of dynamic stability and characterized the neuromuscular control mechanisms involved in postural stability, respectively.

2.2.1 Extrapolated COM and Feasible Stability Region

Previous studies have characterized dynamic standing and gait stability based on the motion states of the body's COM with respect to the BOS using biomechanical models of bipedal

human standing and walking [52]–[58]. However, to the best of the author's knowledge, dynamic seated stability has not been comprehensively investigated in the past based on the concepts of extrapolated COM and Feasible Stability Region (FSR). The relationship between the COM motion states and dynamic stability during gait and standing has been quantified using two concepts: the extrapolated COM [182] and FSR [57], [183]. In static conditions, as long as the vertical projection of the body's COM remains within the boundaries of the BOS, stability is achieved. However, in dynamic conditions, the COM velocity plays an important role in stability, and it must be taken into account [52]. In dynamic conditions, when the COM position is within the boundaries of the BOS, a COM velocity directed outward may lead to an unstable condition. On the other hand, when the COM position is not within the BOS, a COM velocity toward the BOS may lead to a stable condition [52].

The abovementioned concept of dynamic stability was first introduced by Hof et al. [52] as extrapolated COM. They suggested that the position of the COM plus its velocity, multiplied by a factor, should remain within the BOS for dynamic stability. This factor is identified based on a simple one-segment inverted pendulum biomechanical model and is equal to the inverse of the natural frequency of the pendulum as $\omega_0 = \sqrt{l/g}$ where l is the pendulum length and g is the gravitational acceleration. They also introduced two measures of stability defined as 'margin of stability' and 'temporal stability margin.' The margin of stability is defined as the minimum distance from the extrapolated COM to the boundary of the BOS. The temporal stability margin is defined as the time that the COM would reach the boundary of the BOS without any interventions.

Later, Hof [182] expanded the concept of extrapolated COM to the dynamic stability of walking. They stated that, in a simplified gait model, the extrapolated COM trajectory succeeds a straight line directed in the line from the COP to the extrapolated COM at the time of foot contact with COM following the extrapolated COM in a sinusoidal trajectory. They proposed that a sufficient rule for achieving dynamic gait stability is the COP should be placed at a specific distance outward and behind the extrapolated COM at the time of foot placement. They showed that a disturbance causing a change in the COM velocity (Δv) could be compensated by a change in COP position by $\Delta v/\omega_0$ in the same direction.

On the other hand, the concept of FSR was first introduced by Pai et al. [54]. FSR is a region of the COM motion state space in which the body can maintain a stable posture without

loss of balance. More specifically, the FSR is defined as the range of feasible COM velocities for an initial COM position that would bring the COM to the edge of the BOS with a velocity of zero. Hence, the FSR is a subspace of the COM motion states with boundaries that determine the limits of dynamic stability. Note that there is a distinction between loss of balance and fall. Loss of balance during standing or walking does not always result in falling but requires action for recovery, such as taking a step forward or backward. Falls commonly happen after the loss of balance; however, not all loss of balance incidents lead to falling. Therefore, the FSR is a subspace of the COM motion state space with boundaries that determine the limits of dynamic stability. Dynamic stability is achieved if the COM motion states remain within the boundaries of the FSR. If the COM states during a gait cycle or standing remain within the FSR limits, the occurrence of loss of balance is unlikely. However, COM states falling outside of the FSR boundaries indicate a high possibility of a loss of balance.

The initial FSR introduced by Pai and Patton [54] was based on a two-segment model of standing predicting the dynamic stability of the body as a single-segment inverted pendulum rotating about the ankle joint with the area under the foot segment representing the BOS. They used dynamic optimization to obtain thresholds against forward and backward loss of balance based on the maximum and minimum feasible COM velocities, respectively, for a set of pre-determined COM positions for which dynamic stability could be achieved. They claimed that forward (backward) loss of balance would occur if COM motion states exceeded the upper (lower) boundary. The proposed FSR was then tested in a later study by Pai et al. [184] to predict stepping as compensatory recovery action in participants of different ages and fall history when forward waist pulls were applied. The dynamic model of stability was significantly better in predicting stepping initiations compared to traditional static stability models.

Patton et al. [185] investigated the validity of the limits of dynamic stability proposed by Pai and Patton [54] as the FSR in terms of COM state boundaries and torque boundaries against empirical data. Participants recovered their balance after voluntarily pulling on a handle. They observed the empirical trajectories fell within the boundaries of the COM state and torque, showing the validity of the obtained limits of dynamic stability. They also observed the margins of stability on the torque boundaries were highly correlated with the COP safety margin, defined as the COP's nearest distance to the edge of the feet. In a later study, Patton et al. [186] investigated the effect of learning on relative stability as the participants practiced the dynamic pulling task. They

observed COP safety margin means and standard deviations increased and decreased, respectively, with practice, indicating better postural control in task execution. They suggested that the safety margin is used by the CNS in both feedback and feedforward control.

Pai and Iqbal [55] obtained the FSR for a slipping scenario modelled with BOS translation. The FSR obtained for slipping differed from the non-slipping condition, with a 30% overlap in the stability region. Their finding supported the idea that movement strategies could be used following an unexpected slip to restore stability. They also found out that forced sliding using a moving platform can have similar effects on stability to those of slipping, as indicated by the 50% overlap between the region of stability of the two conditions.

Pai et al. [183] investigated the capability of the dynamic model of stability in predicting the need to step in response to moving platform perturbation compared to the static model of stability. The COM motion state trajectories were measured for able-bodied participants while external perturbations in the form of AP translation of the supporting platform with three different acceleration levels were applied. The measured COM motion states were then compared to the thresholds for stepping predicted by the static and dynamic COM stability models. The FSR associated with the dynamic stability boundaries was obtained using an optimization routine for an inverted pendulum biomechanical model with the measured platform acceleration as the input. Moreover, based on the static model, the step initiation was reached if the COM position fell beyond the limits of the BOS. The dynamic stability model showed significantly better performance in predicting step initiation compared to the static model. This highlights the importance of incorporating the COM velocity for determining stability in dynamic conditions.

Iqbal and Pai [53] used a four-segment biomechanical model to see the effect of knee motion on the predicted FSR for balance recovery. The FSR was obtained for three conditions: unrestricted knee motion, restricted knee motion, and unrestricted knee motion, with an initial posture matching the restricted knee motion condition. Their results indicated that the knee motion had a considerable impact on the termination of the forward movement of the COM in the FSR. They concluded that incorporating knee motion when estimating FSR for balance recovery could be important.

Yang et al. [187] determined the minimum required forward COM velocity with respect to its initial position to avoid backward loss of balance during gait. They used a seven-segment biomechanical model along with dynamic optimization to obtain the FSR in two conditions: initial

posture at the time of toe-off during gait and symmetrical bipedal standing. The FSR against backward loss of balance during gait had a similar trend compared to that of the standing. However, the minimum required COM velocity to avoid backward loss of balance during gait was greater than that of standing.

In a later study, Yang et al. [188] used a seven-segment biomechanical model to predict the FSR at lift-off of the trailing foot in gait based on the threshold of the required forward COM velocity relative to the BOS to avoid backward loss of balance under slip and non-slip conditions. The required forward COM velocity was approximately two times greater under slip conditions compared to non-slip conditions. The predicted threshold agreed with the experimental data. They showed that the predicted threshold obtained using the seven-segment biomechanical model was more accurate than the threshold obtained using the two-segment model. Yang et al. [57] also obtained the FSR in the frontal plane based on the two-segment biomechanical model during gait and compared the results with experimental data. The FSR lower boundary was obtained as the minimum rightward COM velocity at lift-off of the left foot that brings the COM into the BOS. The FSR upper boundary was obtained as the maximum rightward COM velocity beyond which the left foot must land to the right of the BOS (crossover step) for balance recovery.

2.2.1.1 Summary and Gaps

In summary, the FSR boundaries in the COM state space can be obtained as nonlinear functions representing the complex body motion and posture and external perturbations [58], unlike the extrapolated COM, which obtains the limits of dynamic stability as a linear function of the COM position and velocity. Additionally, the FSR concept allows for using complex biomechanical models for characterizing dynamic stability during various tasks and postures. The abovementioned studies have shown the validity of using the FSR to determine the limits of dynamic stability during standing [54], [189] and walking [56], [57], [187], as well as during gait following a slip [188] and BOS perturbations [58]. However, to the best of our knowledge, FSR has not been identified and validated against experimental data for quantifying the relationship between the trunk COM states and seated stability following BOS perturbations. Furthermore, the margin of stability is obtained as the nearest distance between the stability limit and the motion trajectory of the COM. Hence, measuring the motion states of the body's COM during real-world perturbed conditions and comparing them with the previously obtained FSR boundaries in the state-space plane is needed to characterize the risk of loss of balance. Stationary equipment such

as motion capture cameras has been used in the past to obtain the margin of stability based on the extrapolated COM or the FSR stability during standing [54], [189], and walking [58]. However, measuring the margin of stability during activities of daily living requires a portable device. Wearable IMUs offer a feasible alternative for this purpose and can be a low-cost, user-friendly tool for out-of-lab assessment of dynamic stability. Nonetheless, their accuracy for measuring the COM motion states must first be validated against motion capture cameras as a gold-standard reference.

2.2.2 Neuromuscular Control Characterization

Several components of the sensorimotor system interact to maintain an upright seated posture by stabilizing the inherently unstable trunk. Characterizing the roles of underlying neuromuscular mechanisms involved in stabilizing the human trunk has been a long-term challenge in human motor control research [23]. Moreover, determining the task goals of the CNS for given motor behaviour, such as seated stability, and how the CNS accomplishes these goals has been a challenge. The complex interrelation between neuromuscular mechanisms and their contribution to the closed-loop postural control system hinders our mechanistic understanding of the roles carried out by these mechanisms toward maintaining seated stability [44]. The literature has shown that such a mechanistic understanding of neuromuscular control in able-bodied individuals contributes to identifying and improving impaired balance and developing assistive technologies for restoring trunk stability during impaired sitting [59]. Characterizing neuromuscular control contributes to objective balance evaluation and developing targeted rehabilitative interventions for improving impaired balance [60], [67]. Furthermore, recent advancements in developing assistive technologies, such as FES, have shown promising outcomes for restoring seated stability. However, a lack of knowledge about the non-impaired neuromuscular control of seated stability challenges designing such a complex technology [25], [60], [72]. Therefore, characterizing neuromuscular control of non-impaired seated stability would facilitate bio-inspired designs of assistive technologies [60] that can provide physiological action similar to intact motor commands in able-bodied individuals [25].

Seated stability is a complex motor behaviour involving contributions of the CNS, sensorimotor system, muscles, and mechanical properties of the human body. Mechanical properties (i.e., stiffness and damping) of the muscles, ligaments and surrounding tissues provide a delay-free resistive stabilization moment known as passive control [46]. The passive mechanism

is complemented by delayed phasic joint moments generated by muscle activations, especially in response to external perturbations [25], [60]. This complementary stabilization mechanism, known as an active control, is generated by the sensorimotor system and involves feedforward and feedback dynamics [46], [60], [62].

Active feedback control involves multiple steps. First, the kinematics of the body are perceived by sensory receptors, including the proprioception, vestibular, somatosensory, auditory, and visual systems [46], [61]. Second, perceived information is fed back to the CNS, where it is converted to a motor command [46]. Third, the motor command activates relevant muscles producing joint moments for stabilizing the trunk [44], [46]. These three steps are known as sensory, neural, and muscular dynamics, respectively. The process of feedback dynamics is delayed due to sensorimotor time delay, including three components: (a) feedback time delay caused by the transmission of sensory information to the CNS; (b) motor command time delay caused by the processing of sensory information in the CNS and transmitting neuro-electrical signals to the relevant muscles; and (c) electromechanical time delay caused by the calcium release dynamics, muscle fibre conduction velocities, and time delay associated with the chemical reactions to produce a muscle force and eventually joint moment [44], [46], [61]. The feedforward dynamics involve a similar active control mechanism to the feedback dynamics. However, instead of sensory feedback, the CNS anticipates the body kinematics and predictable perturbations based on past experience and generates motor commands to activate relevant muscles [190], [191] to counteract the effect of disturbances on the body's posture [192]. For instance, previous work reported the immediate co-activation of the antagonist's muscles to increase the overall stiffness of the trunk during sitting [190]. Although the feedforward mechanism assists the feedback mechanism, it does not provide enough support when unpredictable disturbances are imposed [193].

Previous studies have used descriptive measures and closed-loop system identification techniques to characterize different components of postural control. Descriptive measures are oftentimes obtained from the body segments' kinematics, COM- and COP-based posturography, GRFs, or muscle activities recorded during quiet standing or sitting [43], [62] as discussed in detail in previous sections. Closed-loop system identification techniques, along with applying external perturbations (e.g., platform translation or external forces) and sensory disturbances (e.g., visual and/or proprioceptive), have been used to characterize postural responses and underlying

stabilization mechanisms during dynamic conditions [44]–[46]. Van der Kooij et al. [46] stated that the latter approach provides a more accurate estimate of postural control since posturographic measures do not isolate the contribution of different components of the underlying postural control system.

Linear closed-loop system identification techniques described in the literature to identify postural control mechanisms include the direct approach, the indirect approach, and the joint input-output approach [46], [194]. The direct approach models the underlying system as an open-loop system, with the output of the plant and controller being independent of their input. Such an assumption for a closed-loop system leads to an erroneous identification [46]. The indirect approach estimates the sensitivity function of the input and output to the applied external perturbation. For a closed-loop system, such sensitivity function will depend on both the controller and the plant dynamics. Therefore, for identifying either the controller or the plant, prior knowledge of the plant or the controller is required [46]. The joint input-out approach allows for separately identifying the controller and the plant without requiring prior knowledge of the controller of the plant. The controller can be identified as the ratio of the sensitivity function of the plant output and the applied physical disturbance over the sensitivity function of the plant input and the applied physical disturbance. The plant can be identified as the ratio of the sensitivity function of the controller input and the applied sensory disturbance and the sensitivity function of the controller output and the applied sensory disturbance [46].

Linear closed-loop system identification techniques have been widely used to identify postural control mechanisms responsible for maintaining standing stability in able-bodied individuals [67]. The direct approach [63], the indirect approach [59], [61], [66], [195], and the joint input-output approach [44], [45] have been used to identify human body dynamics [45], [59], [196], [197], the sensorimotor time delay [44], [59], passive and active controls [44], [59], the muscular dynamics [44], [59], and the sensory dynamics [61], [198]–[200]. The indirect approach has been used by Goodworth and Peterka [199] to identify the contribution of sensorimotor integration to seated stability in humans. In addition, Audu et al. [60] identified the active and passive control mechanisms of seated stability; however, they did not account for the muscular dynamics. Agarwal [67] used the joint input-output approach to identify seated stability components, including human body dynamics, active and passive controls, muscular dynamics, and sensorimotor time delay.

2.2.2.1 Sensory Dynamics

The information from somatosensory, visual, vestibular, and proprioception systems enables the CNS to maintain postural stability. The somatosensory system provides information on touch, vibration, and temperature, helping with maintaining stability [61]. The visual system is believed to play a significant role in maintaining standing [61] and sitting [199] balance even with higher contribution than proprioception and vestibular systems [201]. The literature has reported that alteration in the visual inputs (e.g., physical or virtual motion of a screen) can lead to reduced stability [45], [59], [61]. The vestibular system provides information on spatial orientation by detecting the linear and rotational motions of the head [61], capturing the deviations from the gravity direction. Galvanic vestibular stimulation has been used to alter vestibular information to investigate its effect on postural stability [202], [203]. The proprioception system senses the 3D movements of the joints via proprioceptors. The information from the proprioception and vestibular systems is combined by the CNS and is used along with other sensory inputs to obtain a complete sense of the body's motion states [61]. The effect of alteration in proprioception on postural stability can be investigated by applying rotation to the base of support [204].

Research studies have used system identification techniques to identify the sensory dynamics by simultaneously stimulating sensory receptors and measuring body kinematics, muscle activities, and GRFs [46], [61]. Stimulation methods included motion stimuli such as rotating visual surround and/or the BOS [45], [59], [61], [198], [199], muscle-tendon vibration [205], and galvanic vestibular stimulation [206]. Peterka [61] provided a concept that each sensory input has an individual weight, with the sum of all sensory weights being equal to one. Furthermore, the CNS can dynamically alter the weight associated with each sensory system, known as sensory reweighting or dynamic regulation of sensory dynamics [67]. The sensory reweighting becomes essential when sensory information from one or more sensory receptors becomes unavailable or altered. Previous studies have assumed the sensory dynamics as unity when all sensory inputs are present [61], [198].

2.2.2.2 Neural Dynamics

Information on postural stability sensed by the sensory receptors is converted to neuro-electrical signals sent to the CNS for processing. The process of converting sensory information into motor commands through active feedback control by the CNS is called neural dynamics.

Previous studies identified the neural dynamics along with the passive and active controls of standing and seated stability using linear closed-loop system identification techniques applied to body kinematics and muscle activation data recorded when the body was perturbed via external stimuli (e.g., moving support surface, external forces, or perturbed visual surround) [46], [65]. To identify the neural dynamics as the controller, they have used multi-sinusoidal signals or filtered white noise as the external disturbance noise dominating the intrinsic output noise [44], [46], [59], [60]. The literature suggests that the neural dynamic generates motor commands based on minimizing the angular position and velocity [44], [59], [62], [94] as well as angular acceleration [44], [59] with respect to the static upright posture. Minimizing the angular kinematics could be inferred as the task goals of the CNS for given motor behaviour, such as maintaining stability [44]. Thus, angular kinematics of the body modelled as an inverted pendulum have been used as the input of neural dynamics.

The literature has reported on the use of linear closed-loop system identification to provide non-parametric estimates of the neural dynamics in both standing and sitting postures [44], [59], [60], [197]. In addition, parametric estimates of the neural dynamics have been proposed based on linear controllers such as proportional-integral-derivative (PID) control [60], [61], [198], [199], proportional-derivative (PD) control [62], [65], and PD control with acceleration feedback [59], [207] to model the behavior of the CNS. Furthermore, linear optimal control theory has been used to infer CNS task goals associated with postural stability [44]. This approach assumes that the CNS acts as an optimal controller minimizing a cost function that penalizes the motor commands (e.g., muscle activations) and motion states (e.g., body angular kinematics). Inferring cost function structure allows for characterizing the task goals for postural stability [44]. For a given neuromechanical model of the body as the plant, there is optimal neural feedback that minimizes the cost function. Hence, identifying such a neuromechanical model and the neural feedback for a given motor task (e.g., seated stability) would allow us to interpret the cost function and, therefore, obtain a high-level understanding of the task goals used by the CNS [44].

2.2.2.3 Muscular Dynamics

Muscular dynamics have been characterized to quantify the relationship between muscle activations and produced joint moments [44], [45], [59], [62]. The literature has emphasized the usefulness of identification of muscular dynamics for developing assistive and rehabilitative technologies aimed at restoring/improving postural stability [176], [208], [209]. Previous studies

have identified the muscular dynamics by applying external disturbances and measuring body kinematics, joint moments, and muscle activations. Muscular dynamics consists of muscle activation, contraction dynamics, and musculoskeletal dynamics [210]. Either a first-order transfer function or a critically-damped second-order transfer function has been used to model muscular dynamics [45], [59], [209]. This transfer function is characterized by a natural frequency, a damping coefficient, and a gain representing the dynamic behaviour of the muscle activation due to calcium release dynamics, muscle fibre conduction velocities, and the time delay associated with chemical reactions [69], [211].

2.2.2.4 Sensorimotor Time Delay

The sensorimotor time delay is the delay involved in transmitting sensory information to the CNS, processing sensory information in the CNS, transmitting motor commands to the muscles, and producing a response in the muscles. The sensorimotor time delay includes three components: (a) feedback time delay, (b) motor command time delay, and (c) electromechanical time delay. The feedback time delay is due to the transmission of sensory information from the sensory receptors to the CNS. The motor command time delay is due to the processing of sensory information in the CNS and transmitting neuro-electrical signals to the relevant muscles. The electromechanical time delay is due to the calcium release dynamics, muscle fibre conduction velocities, and time delay associated with the chemical reactions to produce a muscle force and eventually joint moment [44], [46], [61].

2.2.2.5 Mechanical Dynamics

The intrinsic properties (e.g., inertial and viscoelastic properties) of the materials comprising the body (e.g., bones, muscles, ligaments, and tissues) and intra-abdominal pressure provide a delay-free resistive moment when the body is exposed to an external disturbance [44]–[46], [59], [60], [62], [198]. This resistive moment would not suffice to prevent the deviation of the body from an upright posture due to the gravitational force. Previous studies have commonly used the mass-spring-damper system to model the mechanical dynamics [44], [59], [60]. Vette et al. identified the stiffness and damping of the trunk during sitting by applying a pulling force in eight different directions [212]. Moreover, system identification techniques along with physical/sensory perturbations have been employed to obtain non-parametric estimates of the

mechanical dynamics. Non-parametric estimates were then parameterized using first-order differential equations of a mass-spring-damper system [44], [59], [60].

2.2.2.6 Feedback Control Model of Human Stability

Many studies have used feedback control models of postural stability to identify different components of underlying neuromuscular stabilization mechanisms using system identification techniques [45], [46], [59]–[65]. The feedback control model generally comprises a plant, active and passive controls, and feedback. The plant represents the human body dynamics as an inverted pendulum that receives stabilizing joint moments from the active and passive control mechanisms as the input. The plant's output is the angular kinematics of the inverted pendulum representing the body's COM motion. The feedback branch represents the sensory dynamics modelled as unity when all sensory inputs are present. The active control mechanism involves neural dynamics, muscular dynamics, and sensorimotor time delay, while the passive control mechanism involves mechanical dynamics.

Masani et al. [63] investigated the contribution of body sway velocity on controlling ankle extensor activities during quiet standing. Experimental and simulation studies were carried out. Able-bodied participants performed quiet standing with EO or EC. The COP and COM positions and velocities were recorded. EMG electrodes measured the activity of relevant muscles modulating the ankle joint. Their simulation involved modelling the human body during standing as an inverted pendulum, with the output being the AP sway of the COM with respect to the vertical line. A feedback time delay and a neuromechanical time delay were assumed. They assumed the COM displacement is controlled by a PD controller generating a stabilizing moment once with high and once with low derivative gains. Cross-correlation analysis was used to investigate the relationship between the ankle joint moment and the COM displacement/velocity. They observed cross-correlation results of the simulation with high derivative gain closely matched the cross-correlation results of the experimental study. They concluded that the postural control system relies considerably on the velocity information of the COM, and such a feedback controller, despite sensorimotor time delay, can modulate muscle activity without using a feedforward mechanism.

Vette et al. [62] identified the contribution of the active and passive control mechanisms to the total ankle joint moment during standing. Experimental data, including body sway angle and the activity of relevant muscles, were collected from able-bodied participants while standing still

on a force plate. The parameters of the neuromechanical model were obtained via optimization to achieve matching between the measured and predicted ankle joint moment. The plant was modelled as an inverted pendulum rotating about the ankle joint with the COM sway angle as the output. The input of the plant was the sum of stabilizing moments from the active and passive mechanisms; both modelled as PD controllers. The muscular dynamics were modelled as a critically-damped second-order transfer function. The sensorimotor time delay was modelled with three components of feedback, motor command, and electromechanical time delays. Their results showed the significant contribution of both active and passive control mechanisms to total ankle joint moment. Their proposed neuromechanical control scheme could successfully model the physiological behaviour of underlying stabilization mechanisms during a quiet stance, despite long sensorimotor time delays.

In a review article, Pasma et al. [213] argued that current clinical balance assessment methodologies do not allow for differentiating between cause and effect in the closed-loop postural control system. Thus, there is an essential need for novel techniques to identify underlying impairments and compensatory strategies based on the application of external sensory and physical disturbances along with system identification techniques. They proposed that a neuromechanical control scheme based on a two-segment inverted pendulum model could be helpful. Sensory and physical disturbances should be applied while the biomechanical and electrophysiological responses are recorded. The visual, vestibular, and proprioceptive systems could be perturbed by the screen movement, galvanic stimulation, and BOS rotation, respectively. Physical disturbances should be imposed by external independent forces pushing the upper and lower body segments. The measurements should include the body segments' kinematics and GRFs, and the activity of relevant muscles via motion capture system, force plate, and EMG electrodes, respectively. Based on the measured data, the sensory dynamics, the active and passive control mechanisms, the sensorimotor time delay, and the muscular dynamics could be mathematically characterized using closed-loop system identification techniques.

In a later study, Pasma et al. [197] employed a multi-input multi-output closed-loop system identification technique to identify different components of the closed-loop postural control associated with standing balance. They applied both sensory and mechanical disturbances, perturbing the visual and proprioception systems as well as the ankle and hip joints simultaneously. Their results demonstrated that system identification along with sensory/physical perturbations

enables characterizing the underlying mechanisms involved in standing stability. They concluded that such promising results could pave the way for implementing more tools for diagnosing the underlying cause of impaired balance in the future.

Audu and Triolo [60] examined the contribution of passive and active control mechanisms to seated stability in the sagittal and frontal planes in able-bodied participants and individuals with SCI. Participants sat on a moving platform that applied BOS perturbations in the form of BOS translations in the AP and ML directions. Trunk sway angle was measured. They used a linear parametric model to relate the platform displacement to the trunk angle in the time domain. The active control was characterized by a PID controller followed by a long-latency time delay. The passive controller was characterized by a PD controller representing the stiffness and damping, with the damping component being delayed with a short-latency stretch-reflex pathway. The trunk was modelled as an inverted pendulum. Their parametric identification could distinguish the SCI group from the control (able-bodied) group. Their results indicated that SCI led to a systematic reduction of active control parameters while most passive control characteristics remained unchanged. In both groups, the passive control was not sufficient to maintain seated stability. Passive stiffness was significantly larger in the ML direction compared to the AP direction implying that the contribution of the active control in the AP direction was essential for maintaining stability. The proportional and derivative terms of the active control were significantly larger than the integral term implying that a PD controller could model the active control. Their study demonstrated the application of system identification to diagnose impaired aspects of balance in individuals with neuromuscular impairments. However, they did not consider the role of muscular dynamics in their study.

Pasma et al. [59] examined the additional value of identifying muscular dynamics and electromyography in system identification. They investigated whether considering lower leg muscle activation, as well as an acceleration feedback controller, could improve the accuracy and reliability of estimated parameters associated with the underlying systems. Able-bodied participants stood on a platform while the BOS rotation was applied to disturb proprioceptive information. The kinematics of the body and activity of lower leg muscles were collected using motion capture and EMG electrodes, respectively. The human body dynamic was modelled as an inverted pendulum rotation about the ankle joint. The neural dynamics were modelled as a PD controller with acceleration feedback. The mechanical dynamics were modelled as a PD controller.

A single time delay component representing sensorimotor time delay was used. The muscular dynamics were modelled as a critically-damped second-order transfer function. They observed that adding acceleration feedback and muscular dynamics led to higher reliability and accuracy of the closed-loop identification. They concluded that measuring muscle activation along with incorporating muscular dynamics and acceleration feedback improves the accuracy and reliability of estimated parameters and allows for separating the intrinsic dynamics from reflexive dynamics and the muscle activation from the neural time delay.

2.2.2.7 Summary and Gaps

In summary, all the abovementioned studies ignored the time-variant or nonlinear dynamics of the underlying neuromuscular mechanisms and assumed linear time-invariant behaviour for the neuromuscular control that maintains sitting or standing stability. They used offline optimization techniques to estimate parameters of their postural control models that require time-consuming post-processing of acquired data. This limits the applicability of such models for fast identification of impaired balance or when designing assistive technologies that are robust against time-varying nonlinear neuromuscular dynamics of the body (e.g., due to disturbances and muscle fatigue) and physiological uncertainties in real-world conditions [68]–[71]. In addition, the assumption of a linear time-invariant system could lead to erroneous estimates of the neural dynamics, consequently affecting our understanding of the task goals used by the CNS to regulate postural stability. Recent work has proposed the use of Extended Kalman filters (EKF) [69], [214] and adaptive fuzzy modelling [71], [215] for online identification of nonlinear time-varying neuromechanical models associated with the human shoulder and knee. Such models can be used to define robust muscle stimulation patterns and enable online adaptation of the stimulation by estimating relevant neuromuscular information [69]. However, despite their potential, these approaches have not been exploited for identifying nonlinear trunk dynamics and characterizing mechanisms of seated stability. In this light, there is a paramount need for a nonlinear neuromechanical model of seated stability that explains the roles of passive and active stabilization mechanisms while accounting for time-varying properties of the neuromuscular system. Utilizing a nonlinear neuromechanical model along with the nonlinear control theory for identification would lead to a better mechanistic understanding of the postural control system.

2.3 Conclusion

2.3.1 Static Balance

In Chapter 2, section 2.1, a review of the literature on static balance that is relevant to this thesis was presented. The review revealed that many research studies utilized in-lab equipment such as motion capture cameras and force platforms, in addition to conventional clinical scales, to obtain objective balance measures in ambulatory individuals with iSCI and the elderly. However, the use of wearable IMUs has not been fully investigated in these populations to obtain clinically meaningful measures of standing balance as well as objective outcome evaluation of rehabilitative interventions. There is an increasing need to: (1) develop algorithms to characterize standing balance using the measurement of wearable IMUs and experimentally validate the accuracy of these measures against gold standard equipment (Chapter 3); (2) investigate the feasibility of using the validated algorithm for identifying changes of balance biomarkers using wearable technology (Chapter 4) and postural control strategies (Chapter 5) in ambulatory individuals with iSCI with mild balance deficits compared to age-matched able-bodied individuals and; (3) investigate the capability of the validated algorithm for identifying age-related changes in the elderly fallers compared to young adults at rehabilitation hospitals/clinics (Chapter 6); and (4) compare the obtained objective balance measures with clinical scales for evaluating the effectiveness of rehabilitative interventions on the standing balance (Chapter 6).

2.3.2 Dynamic Balance

In Chapter 2, section 2.2, a review of the literature on dynamic balance that is relevant to this thesis was presented. The review revealed that characterizing neuromuscular control in able-bodied individuals is beneficial for identifying and restoring impaired sitting balance in individuals with neuromuscular impairments via objective balance evaluation, targeted rehabilitative interventions, and assistive technologies such neuromodulation. However, the development of objective assessment methodologies and assistive technologies has been challenging due to the lack of (1) standard biomechanical criterion that quantifies sitting balance; and (2) mechanistic understanding of the roles of underlying mechanisms involved in stabilizing the human trunk and their complex interrelations. Therefore, there is a significant need for (1) biomechanical characterization and quantification of the relationship between the dynamic posture of the trunk and sitting balance, along with a validated biomedical device for assessing dynamic sitting posture

and fall risk (Chapter 7); (2) a mechanistic understanding of the non-impaired passive and active neuromuscular mechanisms and their roles in achieving seated stability (Chapter 8); and (3) mechanistic understanding of the task goals of the neural control for regulating seated stability (Chapter 9).

Chapter 3

This chapter provides the details of validating an algorithm for assessing the dynamics of standing balance using wearable technology. This chapter has been adopted and/or edited from:

A. Noamani, M. Nazarahari, J. Lewicke, A. H. Vette, and H. Rouhani, "Validity of using wearable inertial sensors for assessing the dynamics of standing balance," Med. Eng. Phys., vol. 77, pp. 53–59, 2020, doi: 10.1016/j.medengphy.2019.10.018.

3 Wearable Technology for Balance Assessment

3.1 Introduction

Falls are one of the most frequent causes of injury in individuals with neuromuscular impairments and elderly individuals. Previous studies showed that impairment of gait or balance is the most consistent predictor of future falls [3]. Hence, individuals with impaired balance are at high risk of falling and therefore, the ability to maintain balance during gait, standing, and postural transitions have been used to evaluate fall risk in individuals and the effectiveness of rehabilitative interventions [4], [5]. Observational balance tests such as the Berg Balance Scale (BBS), which includes standing balance trials, are commonly used for this purpose [216]. However, they tend to be subjective [157] and may not always yield reliable and sensitive outcomes [49]. Hence, a quantitative balance assessment methodology is needed for developing rehabilitative strategies and for objective outcome evaluation of treatments [85], [121].

Objective assessment of balance has been investigated by quantifying body sway during quiet standing using the trajectory of the center of pressure (COP) measured via a force plate [47], [48]. Such studies assume the human body to behave like an inverted pendulum swaying about the ankle joint [83], [112]. However, the surprisingly complex neuromuscular mechanisms of standing balance cannot be captured via a single-segment model of the body. Consequently, other studies investigated the contribution of the ankle, hip, and other body joints to standing balance using the kinematics of a multi-segment body model measured via in-lab equipment [84], [118].

In addition, joint moments have been used to objectively evaluate the outcome of rehabilitation treatments, evaluate muscle strength associated with balance recovery [217], and for

clinical evaluation of Parkinson's disease [218], cerebral palsy [219], and ankle osteoarthritis [220], [221]. Generally, joint moments are estimated via a bottom-up inverse dynamics approach using data measured by a three-dimensional (3D) motion-capture system and force plate.

Despite this work, the implementation of in-lab equipment for clinical research and practice is not practical due to the requirement of expensive equipment in a dedicated lab space, which is not accessible at many hospitals. Moreover, patients are restricted to the lab space, which limits the ability of in-home monitoring [92]. The advantage of wearable technologies over in-lab equipment is the feasibility of using them in spaces other than an equipped lab space (i.e., home). Nonetheless, such an advantage does not eliminate the necessity of training prior to using the equipment, which is essential for any kind of assessment tool. Although wearable sensors provide a low-cost alternative that enables out-of-lab balance assessment, their accuracy and reliability for clinical research and practice, especially for kinematics and kinetics assessment of standing balance, have not been validated [222].

The objective of this research is to investigate the validity of an algorithm for a reliable assessment of the dynamics of standing balance using wearable technology. We developed algorithms to assess kinematic and kinetic parameters of a four-segment body model that characterize standing balance using the measurement of: (1) accelerometers; and (2) accelerometers plus gyroscopes. Subsequently, we experimentally validated the accuracy of the measured parameters against motion-capture cameras as a gold-standard reference to compare these two solutions.

3.2 Methods

3.2.1 Experimental procedures

Ten able-bodied male individuals (age: 24.8±2.8 years, body mass: 77.1±6.3 kg) with no history of musculoskeletal impairments or any neurological, vestibular, or other balance-related disorders participated in data collection. All participants provided written consent prior to participation. The Research Ethics Board of the University of Alberta approved the study protocol (Pro00065804). Each participant was asked to stand still on a force plate for one two-minute quiet standing test. Participants were asked to maintain a natural, relaxed posture and stance width during the trial, with the arms crossed over the chest.

3.2.2 Data acquisition

Four inertial measurement units (IMUs) (MTws, XSENS Technologies, NL) were used to measure the kinematics of a four-segment body model at a sampling rate of 100 Hz. Each IMU was composed of a tri-axial gyroscope (range: ±2000 deg/s) and a tri-axial accelerometer (range: ±16g). Each IMU was mounted on a rigid plate equipped with a cluster of four retro-reflective markers. The plates were placed over the foot, tibia, sacrum, and sternum, representing the foot, leg, pelvis, and head-arms-trunk (HAT) segments, respectively. The raw acceleration and gyroscope data were low-pass filtered via a dual-pass 8th-order Butterworth filter ($f_{cut\text{-}off}$ = 30 Hz).

Sixteen retro-reflective markers were placed on anatomical landmarks of the torso (C7, incisuria jugularis, and xiphoid), pelvis (left and right ASISs and PSISs), shank (tibial tuberosity, head of the fibula, medial and lateral malleolus), and foot (calcaneus, 1st, 2nd, and 5th metatarsal heads). Eight motion-capture cameras (VICON, Oxford Metrics Group, UK) measured the trajectories of the markers, and a force plate (AMTI, Watertown, MA, USA) recorded the ground reaction forces (GRFs) and COP position as a reference. The cameras and the force plate recorded synchronously with the IMUs at sampling rates of 100 Hz and 1000 Hz, respectively. The synchronous recording was conducted by sending an analog trigger from IMUs to the motion capture system and the force plate at the beginning and end of each trial. Therefore, all three sets of equipment synchronously recorded. The time series were low-pass filtered via a dual-pass 8th-order Butterworth filter ($f_{cut\text{-}off}$ = 20 Hz).

3.2.3 Multi-segment model of the body

The human body was modelled with four rigid segments (Figure 3-1) connected to each other by 3D revolute joints. Moreover, it was assumed that the segments were bilaterally symmetric with respect to the sagittal plane, and that the feet were motionless during the standing trial.

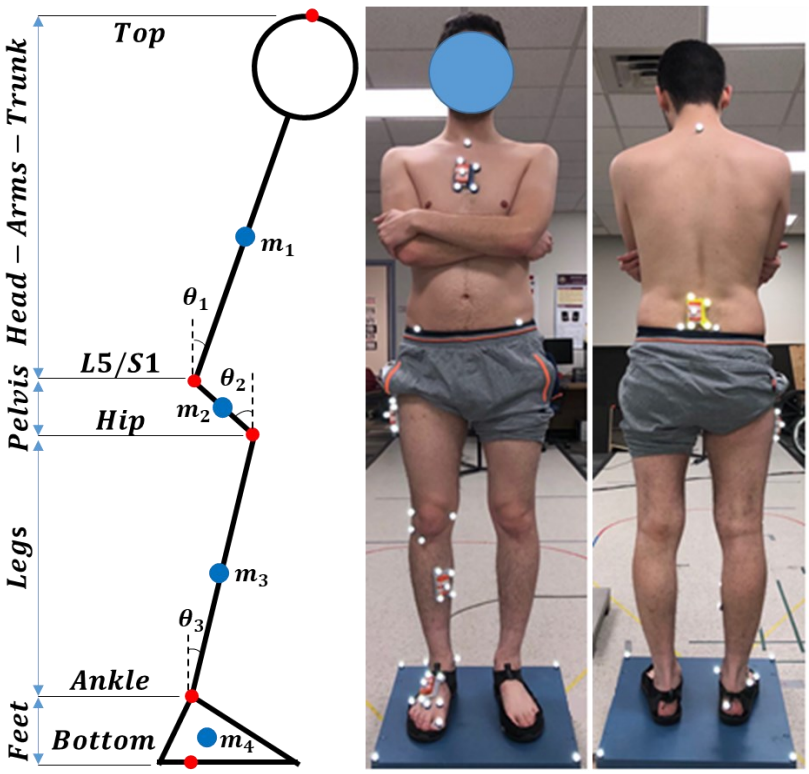

Figure 3-1. Simultaneous kinematics and kinetics assessment of a four-segment model of the human body using a motion-capture system (cameras and force plate) and IMUs. Retro-reflective markers were placed on the anatomical landmarks of each segment. IMUs were mounted on rigid plates equipped with a cluster of markers attached to the body.

Anthropometric parameters of each segment, including the mass, center of mass (COM), joint centers of rotation (JCRs), and moments of inertia were estimated based on the individual's body mass and height according to [223]. The instantaneous location of the JCRs of each segment was calculated from the position of the anatomical landmarks. The length of each segment was then obtained as the distance between the proximal and distal JCRs. Subsequently, the location of the COM for each segment was determined as a portion of the segment length from the distal joint. Note that when IMUs are used, the length of the segments and the location of JCRs can be measured by estimating the length of each segment as a portion of the body height based on [223].

The masses of the markers, plates, and IMUs were incorporated as additional weights to each segment. Nevertheless, the moments of inertia associated with the rigid plates were neglected in comparison to the moments of inertia of body segments.

The anatomical frame (AF) of each segment was defined based on [224]; however, the sequence of the axes was modified such that the X-, Y-, and Z- axes represented lateral-bending, flexion-extension, and axial rotation, respectively. For each participant, the lab-fixed frame was defined based on the median of the pelvic landmarks during a ten-second time interval at the beginning of each trial, with the origin at the mid-point between the right and left ASIS, and the X-, Y-, and Z- axes pointing anteriorly, to the right, and downward, respectively. The COM, JCRs, moments of inertia, GRFs, COP, and orientation of the segments were obtained with respect to this lab-fixed frame during the quiet standing trial.

3.2.4 Inverse Dynamics

We implemented the Newton-Euler formulation for joint moment calculation in a custom-built MATLAB program (MathWorks, Natick, MA, USA):

$$\vec{F}_i = m_{s_{i-1}}\left(\vec{a}_{s_{i-1}} - \vec{g}\right) + \vec{F}_{i-1} \quad (1)$$

$$\vec{M}_{s_{i-1}} = {}^{GF}_{AF}R_{s_{i-1}}\left(I_{s_{i-1}}\vec{\alpha}_{s_{i-1}} + \vec{\omega}_{s_{i-1}} \times I_{s_{i-1}}\vec{\omega}_{s_{i-1}}\right) \quad (2)$$

$$\vec{M}_i = \vec{M}_{i-1} + \vec{M}_{s_{i-1}} + \left(\vec{P}_{COM_{s_{i-1}}} - \vec{P}_{JCR_i}\right) \times \vec{F}_i + \left(\vec{P}_{JCR_{i-1}} - \vec{P}_{COM_{s_{i-1}}}\right) \times \vec{F}_{i-1} \quad (3)$$

where i and s_i represent joint and segment indexes, respectively; $\vec{M}_i$ and $\vec{F}_i$ represent moment and force vectors acting on joint i, respectively; $\vec{a}_{s_i}$represents a segment's linear acceleration; $\vec{P}_{COM_{s_i}}$ and $\vec{P}_{JCR_i}$ represent the position of a segment's COM and JCRs. Moreover, $I_{s_{i-1}}$, $\vec{\alpha}_{s_i}$, and $\vec{\omega}_{s_i}$ represent individual-specific moments of inertia, angular acceleration and velocity of the segment expressed in the segment-fixed frame, respectively, and ${}^{GF}_{AF}R$ is the rotation matrix from the segment-fixed frame to the lab-fixed frame.

We used four different approaches to estimate the joint moments:

Approach 1) Camera-based bottom-up approach: We used the measurement of the cameras and the force plate to estimate the joint moments in the proposed four-segment model. The instantaneous orientation of each segment (${}^{GF}_{AF}R_{s_i}$) was obtained according to section 3.2.3, $\vec{a}_{s_i}$ was obtained as the 2nd-order differential of $\vec{P}_{COM_{s_i}}$, and $\vec{\alpha}_{s_i}$ and $\vec{\omega}_{s_i}$were calculated from ${}^{GF}_{AF}R_{s_i}$. Joint moments were then calculated using Eq. 1 to Eq. 3 using a bottom-up inverse dynamics approach. This approach started from the most inferior segment by assuming the force plate measurements as the boundary condition of the bottom-most segment and then proceeded upwards.

Approach 2) Camera-based top-down approach: We used the same kinematic data obtained from the cameras as described above. However, in this approach, the inverse dynamics calculation started from the top-most segment, assuming an unloaded condition at the top-most JCR as the boundary condition, and proceeded downwards.

Approach 3) IMU-based (only accelerometer) top-down approach: We used the kinematic data recorded by the IMUs to estimate the joint moments. The instantaneous orientation of the segments (${}^{GF}_{AF}R_{s_i}$) was estimated based on the segment's inclination angle. The rotation matrix which mapped the sensor-fixed frame to the lab-fixed frame was determined by aligning the accelerometer's vertical axis with gravity during quiet standing as follows [225], [226]:

$$x_{GF} = [ACC_x, ACC_y, ACC_z], \;\; x_{GF} = x_{GF}/\|x_{GF}\| \tag{4}$$

$$y_{GF} = [0\ 0\ 1]^T \times x_{GF}, \qquad y_{GF} = y_{GF}/\|y_{GF}\| \tag{5}$$

$$z_{GF} = x_{GF} \times y_{GF}, \; z_{GF} = z_{GF}/\|z_{GF}\| \tag{6}$$

$${}^{GF}_{SF}R_{s_i} = [x_{GF}\ y_{GF}\ z_{GF}]^T \tag{7}$$

where $[ACC_x, ACC_y, ACC_z]$ is the accelerometer readout, and ${}^{GF}_{SF}R_{s_i}$ is the vertical alignment matrix. To obtain ${}^{GF}_{AF}R_{s_i}$, a sensor-to-body calibration procedure [227] was used based on the markers on the anatomical landmarks and rigid plates.

Assuming the segments as rigid links, the instantaneous $\vec{P}_{COM_{s_i}}$ and $\vec{P}_{JCR_i}$ of each segment were calculated using their values initially recorded in the segment's anatomical frame and the instantaneous ${}^{GF}_{AF}R_{s_i}$ associated with each segment. The instantaneous $\vec{a}_{s_i}$, $\vec{\alpha}_{s_i}$ and $\vec{\omega}_{s_i}$ of each segment were then obtained based on the calculated $\vec{P}_{COM_{s_i}}$ and ${}^{GF}_{AF}R_{s_i}$. Finally, the joint moments ($\vec{M}_i$) were estimated using the top-down approach.

Approach 4) IMU-based (accelerometer and gyroscope) top-down approach: We used the data recorded by the IMUs and the same approach as described above. However, this time the orientation of each segment (${}^{GF}_{AF}R_{s_i}$) was obtained from the IMU's built-in Kalman filter, which provides the sensor's instantaneous orientation based on the readout of both accelerometers and gyroscopes.

The joint moments and forces acting on the ankle and the bottom-most joints (a hypothetical joint between the foot and ground defined as the projection of the ankle joint on the

ground [228]) were obtained from Approaches 2 to 4. The anterior-posterior and medial-lateral position of the COP was estimated using the dynamic equilibrium of the foot segment.

Finally, to validate the results obtained from the IMU-based approaches (Approach 3 and 4) against those obtained from the gold-standard reference system (Approach 1), we used the marker clusters mounted on the rigid plate to calculate instantaneous transformation matrices from the sensor-fixed frames to the lab-fixed frame. Using the obtained transformation matrices, all results are expressed in the lab-fixed frame ($^{GF}_{SF}R_{s_i}$). Notably, results obtained from Approach 2 were already expressed in the lab-fixed frame since the camera-based data were used.

3.2.5 Data Analysis

To assess the validity of Approaches 2 to 4, the root-mean-square error (RMSE) of the segments' orientation (expressed as Euler angles), GRFs, COP position, and joint moments between the estimations of Approaches 2 to 4 and those of Approach 1 were calculated. Moreover, the correlation coefficients between the estimated COP positions and ankle joint moment via Approaches 2 to 4 and those measured via the force plate in Approach 1 were calculated.

We also performed a statistical analysis on the aforementioned results to detect any significant differences between the approaches in terms of the RMSE and correlation coefficient values. For each case, the Jarque-Bera test was used to confirm that the data followed a normal distribution, followed by Levene's test to determine the equality of variance. We performed a one-way Analysis of Variance (ANOVA) with its significance level set at 0.05, followed by a multiple comparison post-hoc test.

3.3 Results

The RMSE of the Euler angles representing flexion-extension for the HAT, pelvis and leg segments were 0.11°, 0.26°, 0.13° and 0.12°, 0.26°, 0.14° (average across participants) estimated via Approach 3 and Approach 4, respectively (Figure 3-2). For the lateral-bending angles, these values were 0.16°, 0.09°, 0.08° and 0.21°, 0.12°, 0.09° for Approach 3 and Approach 4, respectively. Differences between approaches were not significant.

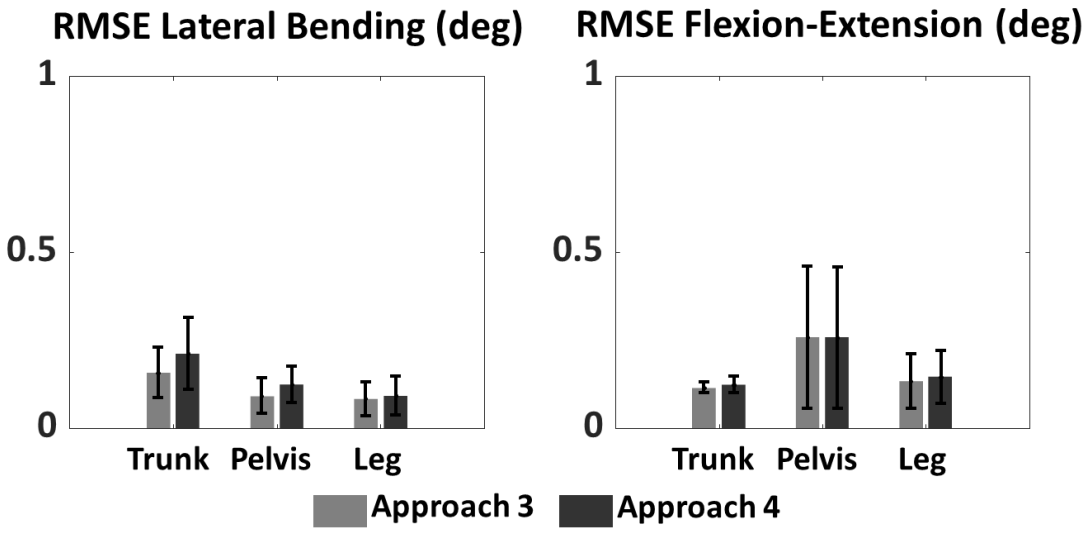

Figure 3-2. Root-mean-square error (RMSE) of the segments' orientation (expressed with Euler angles for lateral bending and flexion-extension), estimated via IMU. Results of Approach 3 (accelerometer only) and Approach 4 (accelerometer and gyroscope) are presented. No significant difference was observed between the approaches for all segments (p-values > 0.05).

The mean RMSE of the joint moments was smaller than 0.016 N.m/kg (average across participants) for the coronal and sagittal components. The ankle joint moment in the sagittal plane had significantly smaller RMSE when estimated via Approach 2 compared to Approaches 3 and 4. No significant differences were observed between the RMSE of other joint moments estimated via Approach 2 to 4 (Figure 3-3).

Figure 3-4 shows the time series of the anterior-posterior and medial-lateral COP positions as measured by the force plate and estimated by Approaches 2 to 4 for one participant. The average correlation coefficient between the estimated and measured COP was greater than 0.93 and 0.81 (average across participants) for the anterior-posterior and medial-lateral directions, respectively, for Approaches 2 to 4 (Figure 3-5). The RMSEs of the anterior-posterior and medial-lateral COP positions were smaller than 1.4 mm. Approach 2 had significantly smaller RMSE of the anterior-posterior position of the COP compared to Approaches 3 and 4. There was no other significant difference between the RMSEs and correlation coefficients of the COP position in both directions obtained via Approaches 2 to 4. The RMSE of GRFs estimated via Approaches 2 to 4 was smaller than 0.2 N/kg. Approach 2 obtained significantly smaller RMSE of the vertical GRF and anterior-posterior GRF compared to Approaches 3 and 4; however, no significant differences were observed in the RMSE of the medial-lateral GRF between the approaches (Figure 3-5).

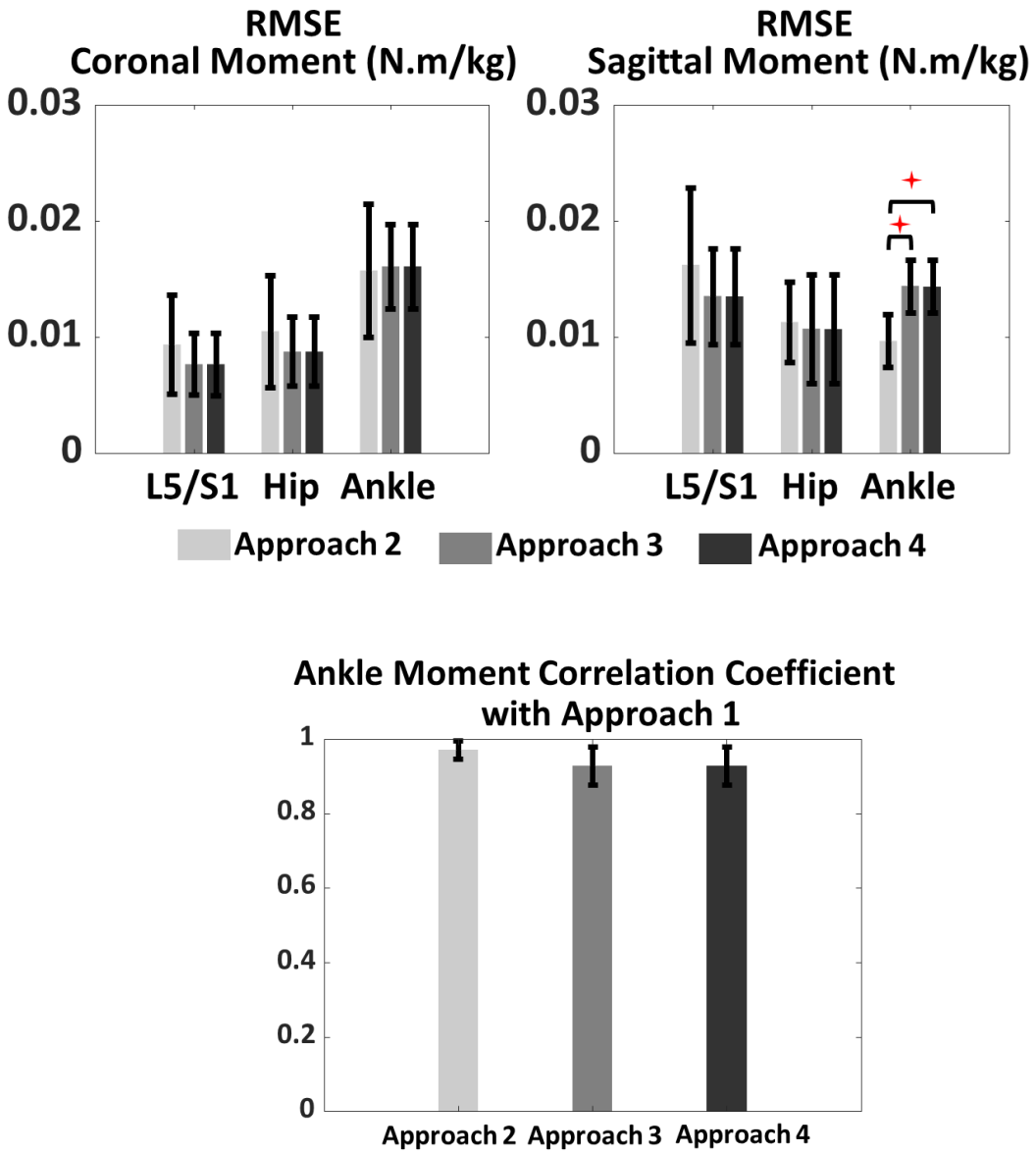

Figure 3-3. (a) Root-mean-square error (RMSE) of the joint moment as estimated via the camera-based top-down approach (Approach 2), the IMU-based (only accelerometer) top-down approach (Approach 3), and the IMU-based (accelerometer) top-down approach (Approach 4). (b) The correlation coefficient of the ankle moment as estimated via Approaches 2 to 4, with Approach 1. The red sign indicates p-value < 0.05.

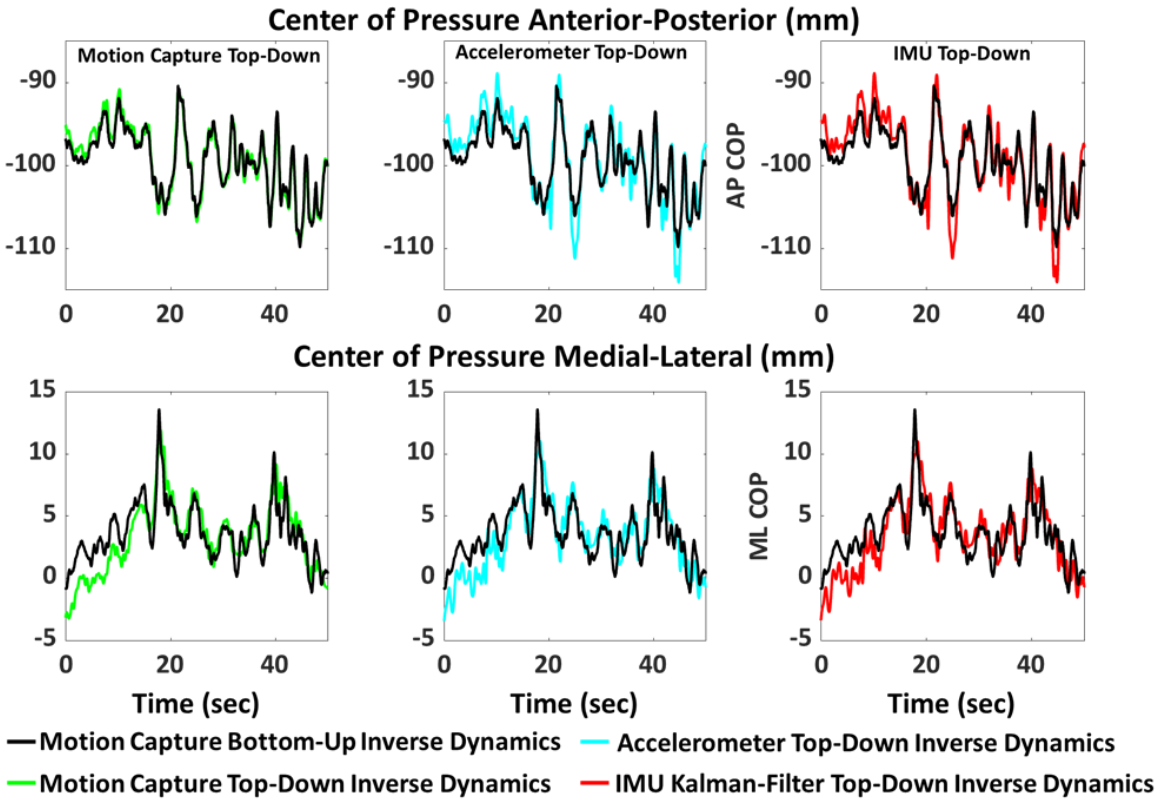

Figure 3-4. Time-series of the center of pressure position as measured with the force plate (Approach 1), estimated via the camera-based top-down approach (Approach 2), and estimated via the IMU-based approaches (Approaches 3 and 4) for one of the participants.

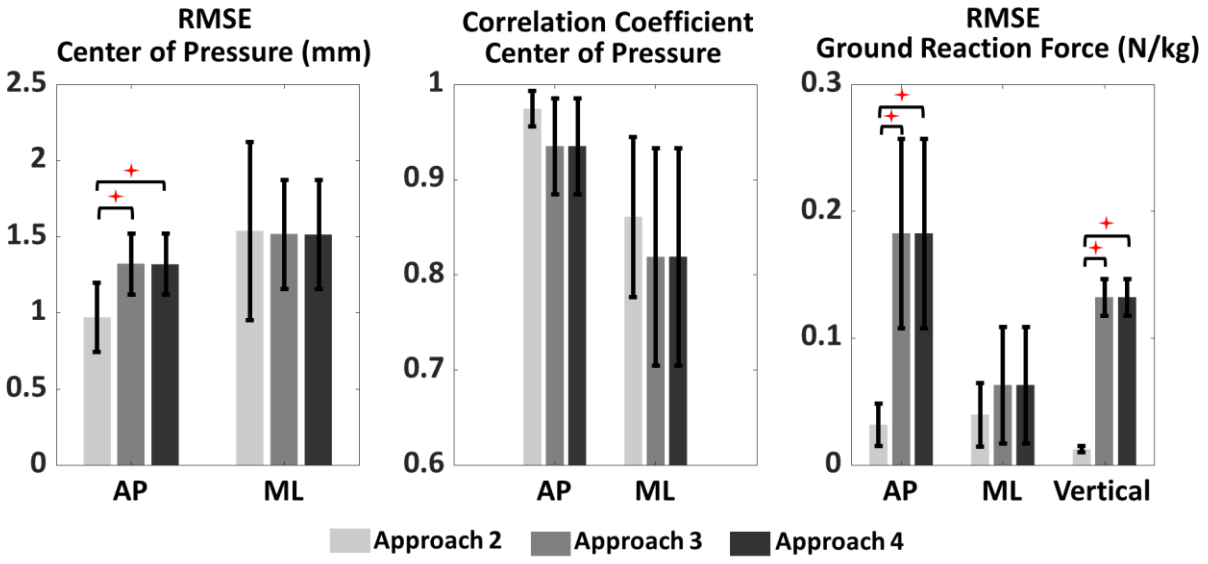

Figure 3-5.Root-mean-square error (RMSE) and correlation coefficient of the center of pressure (COP) positions and ground reaction forces (GRFs) as estimated via the camera-based top-down approach (Approach 2), IMU-based (accelerometer only) top-down approach (Approach 3), and IMU-based (accelerometer and gyroscope) top-down approach (Approach 4). The red sign indicates p-value < 0.05.

3.4 Discussion

This study presents a comprehensive validation of the accuracy of assessing the dynamics of standing balance via wearable IMUs against gold-standard in-lab equipment. The obtained results were in good agreement with previously published studies [229]–[231]. We also investigated the necessity of using the recordings of accelerometers and gyroscopes, together with sensor fusion algorithms (Approach 4), in comparison to using only the recordings of accelerometers (Approach 3).

3.4.1 Estimation of the Euler Angles

Both Approach 3 (using only accelerometers) and Approach 4 (using both accelerometers and gyroscopes) showed high accuracy (small RMSE values in Figure 3-2) in estimating both flexion-extension and lateral-bending angles. For all segments, their difference was not significant. This implies that measuring body sway kinematics during quiet standing using only accelerometers is sufficiently accurate to estimate body segment orientation.

3.4.2 Estimation of the Joint Moments

The obtained RMSE of the joint moments agreed with previously reported values [230], [231]. The RMSE of the estimated joint moments tended to increase from the proximal joints to the distal joints. Previous studies have demonstrated the propagation of experimental errors in estimating joint moments using inverse dynamics [232], [233]. The inaccuracies in estimating individual-specific anthropometric parameters and systematic COP offset errors in the force plate recording could cause a difference in the results of the bottom-up and top-down inverse dynamics approaches. Because of the small inter-segmental upper body motions during quiet standing, we expect that the effect of the HAT segmentation on the estimation of the distal joint moment (e.g., ankle joint) using top-down inverse dynamics is negligible.

Furthermore, both the inevitable inaccuracies of IMUs and motion capture could induce differences between the joint angle estimation via those two systems. This effect could propagate into the joint moment estimation. Joint moments estimated via Approaches 2 to 4 showed high correlation coefficients with Approach 1 at the ankle joint (greater than 0.93) (Figure 3-3b). Due to the small variation of the moments at the hip and L5/S1 joints during quiet standing, the correlation coefficient is not a proper metric for the agreement of Approaches 2 to 4 with Approach 1. Nevertheless, the RMSE of the hip and L5/S1 moments was smaller than 0.01 N.m/kg (average

across participants), implying a high accuracy of Approaches 2 to 4 in estimating joint moments. Although Approach 2 had a significantly smaller RMSE of sagittal ankle moment compared to Approaches 3 and 4, the IMU-based approaches showed a high correlation with Approach 1 in the joint moment estimation (Figure 3-3b). Considering the joint moments estimated by the camera-based bottom-up approach (Approach 1) as a reference, both IMU-based approaches obtained the joint moment estimation with small RMSE (smaller than 0.016 N.m/kg) (Figure 3-3 and Figure 3-5). Since no significant differences were observed between Approach 3 and Approach 4, the use of only accelerometers is sufficient for assessing the dynamics of standing balance during static unperturbed quiet standing.

3.4.3 Estimation of COP and GRFs

Although the camera-based top-down approach (Approach 2) tended to obtain greater correlation coefficients than IMU-based approaches (Approaches 3 and 4), the differences were not significant. The small differences in the accuracy of the camera-based and IMU-based approaches were due to the inaccuracy of estimating the segments' orientation using IMUs. Nonetheless, the IMU-based approaches obtained accurate COP positions that were highly correlated with the force plate measurements during quiet standing. The RMSE of the COP positions obtained in this study showed an improvement compared to the reported RMSE (around 3 cm) in previous studies [230]. Note that, during the quiet standing test, the excursion of the COP is smaller compared to other tasks such as sit-to-stand and lifting. Hence, a higher resolution and accuracy are required in estimating the COP position during quiet standing.

Approaches 3 and 4 obtained significantly larger RMSE in estimating the vertical GRF and anterior-posterior GRF compared to Approach 2. Although no significant difference was observed for the medial-lateral GRFs, Approach 2 tended to obtain smaller RMSE. These results showed RMSE of GRFs smaller than 15 N for our static quiet standing test, which was in agreement with Faber et al. [229], who reported the RMSE of the GRFs in a range of 20 N during trunk-bending.

3.4.4 Motion capture system versus IMU

The optoelectronic motion capture system is the most widely used device for accurate measurement of human body kinematics [223], [234]. Therefore, it has been frequently used as a gold-standard reference to investigate the accuracy of orientation estimation using IMU [235]–[237]. We compared the joint angles obtained by IMUs with those obtained by a motion capture

system, and the differences were, in general, less than 0.5° (Figure 3-2). Therefore, the accuracy of both systems in body joint angle measurement was similar. Nevertheless, the motion capture system is not error-free and cannot assess the absolute error of IMUs.

In addition, previous studies suggested the use of a force plate along with a motion capture system to estimate kinetic parameters via bottom-up inverse dynamics. They used the results of the bottom-up inverse dynamics as a reference to investigate the accuracy of the top-down inverse dynamics in estimating kinetic parameters [229]. Moreover, the literature [229], [233] suggests that due to the propagation of experimental errors, top-down inverse dynamics may result in an erroneous estimation of joint moments and forces in the distal joint. Hence, estimating kinematic and kinetic parameters using the measurements of a motion capture system and a force plate along with bottom-up inverse dynamics (Approach 1) has been recommended as a reference by literature despite its inherent errors.

3.4.5 Sufficiency of using accelerometers for assessing static balance

The use of a gyroscope in addition to an accelerometer may improve the orientation estimation accuracy in the short term but may deteriorate the accuracy over time due to the drift associated with the gyroscope output. Complex sensor fusion algorithms (e.g., Kalman filter) can reduce this risk and are integrated into some commercially available IMUs for estimating orientation. However, the addition of gyroscopes and sensor fusion algorithms increases the cost of IMU and requires unnecessary complex computation and parameter tuning. Moreover, the gyroscope has significantly higher power consumption than an accelerometer, and its addition reduces battery durability, which may be important for clinical applications. Our study showed that the use of accelerometers alone (Approach 3) could be sufficient to obtain joint moments, GRFs, and COP during standing with similar accuracy compared to the camera-based top-down inverse dynamics approach (Approach 2). Also, the addition of gyroscopes, magnetometers, and sensor fusion (Approach 4) does not significantly improve measurement accuracy.

3.4.6 Limitations

We used measurements of the motion capture system in Approach 1 as the gold-standard reference for orientation estimation. Since this approach requires marker placement on anatomical landmarks, its accuracy could be affected due to experimental errors such as soft tissue artifacts [238]. Nevertheless, in the current study, the effect of soft-tissue artifacts on estimating the

orientation of each body segment using a motion capture system would not be significant due to the absence of large movement during quiet standing.

We previously showed that inaccuracies in estimating anthropometric parameters of body segments induced uncertainties in the net joint moment and, consequently, in estimating COP position [233]. In the present study, anthropometric parameters were estimated by the participant's body height and weight, which could be a source of inaccuracies in Approaches 2 to 4 when estimating COP. Although the errors in the joint moment and COP estimation using IMUs were small, the sensitivity of the obtained kinetic parameters to the inaccuracies in the estimation of the anthropometric parameters should be further investigated.

We used a 3D four-segment model of the human body to estimate joint moments in the sagittal and frontal plane, and COP positions in both anteroposterior and mediolateral directions. However, bilateral symmetry was assumed for the model in this study, which ignores any asymmetric motion patterns and joint moments between the left and right legs. Our four-segment model of the body incorporated the ankle, hip, and L5/S1 joints since these joints were reported to play a significant role in maintaining standing balance and may be independently affected by pathological conditions [84], [87], [116], [239]. We assumed the shank and thigh as a single rigid segment, which neglects the relative angle at the knee joint that has a minor contribution to standing balance compared to the joints considered in our study [118]. Moreover, we expect that the addition of the knee joint to the model, which requires the addition of an IMU on the thigh, has a minor effect on the validity of IMUs for assessing the dynamics of standing balance. Yet, the inclusion of the knee joint in the model should be investigated for various muscle tension scenarios.

Based on data collected from able-bodied individuals, this study showed that the proposed use of IMUs could provide an accurate and suitable means of performing balance assessment out-of-laboratory. We expect this system to be accurate and suitable for standing balance assessment of those with balance impairment as long as they can stand still for a minute or more. Yet, the techniques validated in the current study should be further studied in different groups of affected individuals with a high risk of falling prior to coming to any clinical conclusion. Nevertheless, accelerometers have been used as a reliable alternative for obtaining sensitive measures of standing balance in able-bodied individuals [93] and populations with Parkinson's disease [49], elderly [157], and SCI [50]. Finally, the proposed methodology is expected to assess the risk of falling

associated with the neuromuscular mechanisms that affect standing balance. Assessing other risk factors should be studied in the future.

3.5 Conclusion

This study presents a comparison between camera-based, and IMU-based inverse dynamics approaches for assessing the 3D dynamics of standing balance during unperturbed static stance in able-bodied young adults. Accelerometers with or without gyroscopes estimated the leg, pelvis and trunk segment orientation accurately. The estimations of ankle, hip and L5/S1 joint moments, 3D GRF, and COP position were accurate when top-down inverse dynamics were implemented without force plate measurements. These accuracies were in general comparable (no statistical difference; $p > 0.05$) when motion data was obtained using cameras, accelerometers, or a combination of accelerometers and gyroscopes. Therefore, it could be suggested that in Internet-of-Thing-based clinical research and practice, when power-saving is important, the use of accelerometers only has sufficient accuracy and could be recommended for body kinematics and kinetics monitoring during standing balance assessment. Nevertheless, the validity of the proposed technology for different groups of individuals with impaired neuromuscular functions is yet to be further investigated prior to any clinical application. Such an application, with further investigation and research in the future, can enable in-field clinical evaluations and the development of injury prevention and rehabilitation strategies for those with balance impairment with the ability to stand still.

3.5.1 What is next?

In this chapter, an algorithm was validated for assessing static balance during standing using wearable technology in able-bodied individuals. However, the sensitivity and responsiveness of the developed algorithm to identify the subtle changes in balance in individuals with balance impairments are yet to be investigated. In the next chapter, this technology will be employed to investigate its sensitivity to characterize postural control and subtle differences in balance mechanisms in individuals with mild balance deficits (i.e., ambulatory individuals with iSCI with mild balance deficits and with walking ability) under different sensory conditions.

Chapter 4

This chapter shows how the validated algorithm can be used to characterize standing balance in ambulatory individuals with iSCI with mild balance deficits *under different sensory manipulations using wearable technology. This chapter has been adopted and/or edited from:*

A. Noamani, J. F. Lemay, K. E. Musselman, and H. Rouhani, "Characterization of standing balance after incomplete spinal cord injury: Alteration in integration of sensory information in ambulatory individuals," Gait Posture, vol. 83, no. October 2020, pp. 152–159, 2021, doi: 10.1016/j.gaitpost.2020.10.027.

4 Characterization of Standing Balance after iSCI

4.1 Introduction

Recovery of balance ability during standing and regaining the ability to walk are the top priorities for individuals with iSCI [16], [20], [21]. Up to 30% of individuals with a recent SCI and most individuals with an incomplete lesion are able to regain partial balance and walking ability after the first year post-injury [16]. However, the future level of ambulation in this population is associated with the initial level of balance and the amount of motor function below the level of the lesion [19]. Hence, the implementation of outcome measures that identify the balance and walking abilities of individuals with SCI can lead to more effective rehabilitation [16].

Literature showed that ambulatory individuals with iSCI are at a greater risk of falling than those who use a wheelchair for mobility [12]. Moreover, previous studies have shown that standing balance evaluation, such as Berg Balance Scale scores, for individuals with SCI is significantly correlated with various walking outcome measures and with their reliance on mobility-related assistive devices [16], [36]. Greater postural control in this population is highly associated with a more normal walking pattern, higher stride speed, less reliance on supervision or physical assistance, and more functional ambulatory status [16].

However, maintaining postural stability is a major challenge for individuals with SCI as they regain the ability to walk [17]. Up to 75% of individuals with iSCI experience injurious falls while standing and frequent losses of balance post-rehabilitation [10], [11]. This can result in

physical injuries, decreased social involvement [11], [13], [14], and developing a fear of falling [15]. These individuals identified loss of balance as the most significant contributor to their falls [14], [18], implying that effective control of balance is required for developing fall prevention strategies.

Control of balance during quiet standing depends on the integration of sensory information from the somatosensory, visual, and vestibular systems [17] and the interaction of the body with the changing environment [10]. Hence, understanding the underlying mechanisms of how postural control is regulated post-SCI is of significant importance. iSCI causes sensory and/or motor impairments at and below the level of the lesion [18], and sensory reweighting may be affected because of impaired somatosensory information. This alteration in reweighting of sensory information post-SCI results from the development of compensatory strategies to maintain balance [20], [35]. Therefore, postural stability can be further challenged in this population by altering the availability of visual [17] and somatosensory [145] inputs, highlighting the fact that many contributors to balance control are affected following an SCI. Identifying the underlying impairments and changes to postural control is necessary for targeted and guided rehabilitation post-SCI [35] since such training can have a positive effect on postural control and coordination improvement [20]. For instance, the literature suggests that the over-reliance on visual cues post-iSCI during walking and standing is due to somatosensory impairment [17], [145]. In addition, previous studies have shown the positive effect of sensorimotor integration, such as visual feedback [20] and haptic input [240], on balance rehabilitation post-iSCI. However, the effect of concurrent restricted visual and somatosensory inputs on standing balance post-iSCI has yet to be investigated. Hence, a comprehensive balance evaluation for ambulatory individuals with iSCI with mild balance deficits during a variety of challenging standing conditions remains a significant need.

Physical therapists oftentimes use standard observational rating scales to evaluate balance. The concurrent validity of observational balance scales (e.g., Berg Balance Scale or mini-BESTest) among individuals with SCI has been validated. However, previous studies reported an inability to predict future falls post-SCI for such methodologies. Moreover, they are subjective and provide minor information for understanding the potential underlying mechanisms for the balance difficulties [16], [35], [36], highlighting the requirement of a quantitative approach to evaluate standing balance. The instrumented version of such tests can provide a precise “impairment-level”

evaluation of balance by measuring how and why functional performance is impaired with increased sensitivity to the identification of mild changes [37]. Therapists can use such objective measures to characterize specific impairments and identify where the problem is occurring. These measures can then be employed to precisely focus the therapy on underlying causes and track subtle changes in postural control over time [37]. Body-worn inertial measurement units (IMUs) have been used as a reliable alternative for obtaining accurate and sensitive measures of standing balance in able-bodied individuals [93], and populations with Parkinson's disease [49], traumatic brain injury [37], and SCI [50]. IMUs can provide impairment-level measures that characterize the functional performance of balance with increased sensitivity to movement disorders, rehabilitation, and mild changes in postural stability [37], [49]. Moreover, IMUs are light-weight, relatively inexpensive, and can be easily integrated into functional tests, which makes them an ideal alternative to stationary laboratory equipment with a higher level of clinical utility [37], [51]. Therefore, the aim of this study was to characterize the impact of a variety of challenging conditions on the standing balance of a small group of ambulatory individuals with iSCI with walking ability using a waist-mounted IMU. We compared balance biomarkers derived from IMU readouts under conditions that challenge balance by affecting somatosensory (i.e., standing on hard and foam surfaces) and visual (i.e., eyes open and closed) inputs. In addition, we compared balance biomarkers between the participants with iSCI (AIS level D) and able-bodied participants to characterize changes in postural control post-iSCI based on reliance on somatosensory and visual information. We hypothesize that ambulatory individuals with iSCI have a reduced stability performance, increased control demand, and a less effective active correction post-iSCI in standing conditions considered in this study. We assume that ambulatory individuals with iSCI have a lower reliance on somatosensory information compared to able-bodied individuals, and they rely more on visual information for maintaining standing balance.

4.2 Methods

4.2.1 Participants

Eight individuals with a traumatic or a non-traumatic iSCI AIS level D (hereafter iSCI group) and twelve age-matched able-bodied individuals volunteered to participate in this study (Table 4-1). Participants with iSCI were recruited from the outpatient population of the CIUSSS

du Centre-Sud-de-l'Île-de-Montréal (Installation Gingras-Lindsay) and the Lyndhurst Centre, Toronto Rehabilitation Institute-University Health Network.

Table 4-1. (a) Demographic information of participants with incomplete spinal cord injury; (b) Demographic information of able-bodied participants; and (C) Level of injury and American Spinal Injury Association Impairment Scale (AIS) for individuals with incomplete spinal cord injury participated in this study.

Participants with incomplete spinal cord injury

Variable	Mean (Standard Deviation)	Range
Age (years)	47.5 (19.3)	20-70
Height (cm)	174.9 (9.4)	161-187.9
Weight (kg)	80.0 (19.3)	57-113.4
Time post lesion (months)	74.1 (87.9)	29-289
Lower Extremity Motor Score (/50)	46.1 (2.4)	43-49
Variable	**Number**	
Sex (Male/Female)	Male = 8, Female = 0	
Level of lesion	Paraplegia: 4, Tetraplegia: 4	
Type of lesion	Traumatic: 7, Non-traumatic: 1	

Able-bodied participants

Variable	Mean (Standard Deviation)	Range
Age (years)	43.0 (20.1)	18-84
Height (cm)	169.2 (9.2)	156-181
Weight (kg)	66.8 (13.1)	47.5-92.2
Variable	**Number**	
Sex (Male/Female)	Male = 6, Female = 6	

Participants with incomplete spinal cord injury: level of injury and AIS

Participant	Injury Level	AIS
1	C6	D
2	L1	D
3	C5	D
4	T12	D
5	C6	D
6	T8	D
7	C5	D
8	T1	D

Inclusion criteria were the following: (a) adults with traumatic and non-traumatic motor and sensory iSCI with American Spinal Injury Association Impairment Scale (AIS) C or D; (b) at least 5 months post-injury; and (c) able to walk for six minutes without assistive devices or assistance of another person to ensure that intrinsic balance ability could be studied. Furthermore, exclusion criteria were as follows: (a) presence of other neurological disorders; (b) visual impairments not corrected with glasses; and (c) vestibular deficits. Ethics approval was obtained from the local ethics committees. Each participant provided written informed consent prior to participation.

4.2.2 Data acquisition and human body modelling

One IMU (Physilog®5, GaitUp, Switzerland) was placed over the sacrum of each participant to measure the kinematics of the body at a sampling rate of 256 Hz. The IMU readouts were low-pass filtered via a dual-pass 8^{th}-order Butterworth filter with a cut-off frequency of 20 Hz.

The human body (above the ankle) was modelled as a one-segment inverted pendulum, connected to the ankle joint by a 3D revolute joint, the feet were motionless during the standing trial, and the center-of-mass (COM) of the body was located at the level of the sacrum where the IMU was placed. Anthropometric parameters of the body segment, including the mass, COM, ankle joint center of rotation, and moments of inertia were estimated based on the body mass and height, according to Winter [223]. The instantaneous orientation of the body segment was determined by aligning the accelerometer's vertical axis with gravity during quiet standing [225], [227]. Assuming the body segment as a rigid link, the instantaneous position of the COM, linear acceleration, and angular velocity of the body were calculated using its instantaneous orientation. Subsequently, we employed an IMU-based top-down inverse dynamics method to estimate the ankle joint moment and center-of-pressure (COP) position based on our previous study [93] using a custom-built MATLAB program (MathWorks, USA).

4.2.3 Outcome measures and data analysis

To identify changes in the standing balance due to iSCI (AIS level D) and to investigate the effect of altered visual and somatosensory inputs, a total of ten COP-based measures [241] and three COM acceleration-based measures [85] were calculated for each trial (Table 4-2). COP-based measures were categorized into the time-domain (i.e., distance, area, and hybrid) measures,

and frequency-domain measures, according to Prieto et al. [241]. In the following sections, these measures are used to study postural stability for (a) stability performance, (b) control demand, and (c) postural regulations [242].

Table 4-2. A total of ten center-of-pressure (COP) measures were calculated according to [241]. Different types of COP-based measures were used to characterize stability performance, control demand, and postural regulation. In addition, three center-of-mass (COM) acceleration-based measures were used based on [85].

Outcome Measure	**Nomenclature**	**Definition**	**Type**
Root-Mean-Square Distance	RDIST	RMS distance of COP	COP Time-domain distance measures
Mean Distance	MDIST	Average distance from mean COP	
Total Excursion	TOTEX	Total length of COP path	
Mean Velocity	MVELO	Average velocity of COP	
95% Ellipse Area	Area-CE	Ellipse area that encloses 95% of the points on the COP path	COP area measure
Sway Area	Area-SW	Area enclosed by the COP path per unit of time	COP Time-domain hybrid measures
Mean Frequency	MFREQ	Revolution per second if the COP travelled the total excursion around a circle with a radius of the mean distance	
Median Frequency	MEDFREQ	Frequency below which 50% of the total power is found	COP Frequency-domain measures
Centroid Frequency	CFREQ	Frequency at which the spectral mass is concentrated	
Frequency Dispersion	FREQD	A unit-less measure of variability in the frequency content of the power spectral density	
Sway jerkiness	JERK	Time derivative of acceleration	COM acceleration-based measures
Root-Mean-Square Acceleration	RMS-ACC	RMS of Acceleration time series	
Centroid Frequency	CF-ACC	Centroid frequency of acceleration time series	

We performed statistical analyses on each outcome measure to identify the main and interaction effects of health condition (able-bodied vs. iSCI), vision condition (EO vs. EC), and surface condition (HS vs. FS) on standing balance. For each measure, the Kolmogorov-Smirnov

test was used to check that the data were normally distributed, followed by Levene's test to determine the equality of variance. Subsequently, we performed either a three-way Analysis of Variance (ANOVA) or a Kruskal-Wallis test (significance level = 0.05) with Bonferroni correction followed by multiple comparison post-hoc tests (MATLAB 2019b, MathWorks, USA). A significant difference implies a p-value smaller than 0.05. To investigate the effect of altered visual and somatosensory inputs on each group, Cohen's d effect size was calculated, which is defined as the difference between two means divided by a standard deviation for the data.

4.3 Results

4.3.1 COP time-domain distance and area measures

Table 4-3. Effect size and p-value of challenging surface (foam surface vs. hard surface) and impaired vision (eyes open and eyes closed) on balance parameters for both able-bodied participants and individuals with incomplete spinal cord injury (iSCI).

	Effect of Challenging Surface				**Effect of Impaired Vision**			
	Able-bodied		**iSCI**		**Able-bodied**		**iSCI**	
	Effect Size	**p-values**	**Effect Size**	**p-value**	**Effect Size**	**p-value**	**Effect Size**	**p-value**
RDIST	0.82	0.047	0.50	0.743	0.22	0.757	0.48	0.457
MDIST	0.80	0.047	0.48	0.810	0.18	0.817	0.44	0.572
TOTEX	1.39	0.003	0.90	0.434	0.92	0.080	0.98	0.139
MVELO	1.36	0.003	0.85	0.567	0.92	0.078	1.05	0.126
Area-CE	0.93	0.011	0.85	0.359	0.17	0.952	0.26	0.810
Area-SW	1.12	0.003	0.82	0.480	0.48	0.520	0.67	0.462
MFREQ	0.23	0.886	0.26	0.802	0.28	0.532	0.43	0.669
MEDFREQ	0.25	0.742	0.02	1.000	0.43	0.524	0.48	0.592
CFREQ	0.20	0.996	0.49	0.553	0.30	0.824	0.50	0.504
FREQD	0.35	0.917	0.18	0.606	0.20	0.992	0.01	0.987
JERK	1.14	0.007	0.82	0.562	0.85	0.125	0.86	0.161
RMS-ACC	0.57	0.220	0.14	0.945	0.01	1.000	0.35	0.611
CF-ACC	0.24	0.833	0.10	1.000	0.66	0.179	0.39	0.790

All COP time-domain distance measures were significantly larger for the iSCI group compared to able-bodied participants for all conditions (p-values = 0.000, see Figure 4-1A and Table 4-4A). Standing on FS compared to HS increased all COP time-domain distance measures. The impaired vision caused larger TOTEX and MVELO, while it did not reflect any effect on RDIST and MDIST (Table 4-4A). Able-bodied participants had larger time-domain distance

measures while standing on FS compared to HS; however, its effect was insignificant for the iSCI group (all p-values < 0.047, see Table 4-4B). Nevertheless, the iSCI group had larger distance measures even during standing on HS compared to able-bodied participants standing on FS (Figure 4-1A). Although the effect of impaired vision on the distance measures was not significant for both groups (Table 4-4C), a general comparison between the effect sizes of impaired vision on distance measures shows relatively larger effect sizes for the iSCI group compared to able-bodied individuals (Table 4-3). The iSCI group had larger distance measures even with eyes open (EO) compared to able-bodied individuals standing with eyes closed (EC) (Figure 4-1A).

Able-bodied participants had smaller Area-CE compared to the iSCI group (p-value = 0.000, see Figure 4-1B and Table 4-1A). Standing on FS led to larger Area-CE for able-bodied participants (p-value = 0.011), whereas its effect was not significant for the iSCI group (Table 4-4B). Despite this, Area-CE for the iSCI group was larger even during standing on HS compared to able-bodied participants standing on FS (Figure 4-1B). Although standing with EC showed no significant effect on the Area-CE for both groups (Table 4-4C), its effect size was relatively larger for the iSCI group (Table 4-3).

(A) Time-domain distance measures

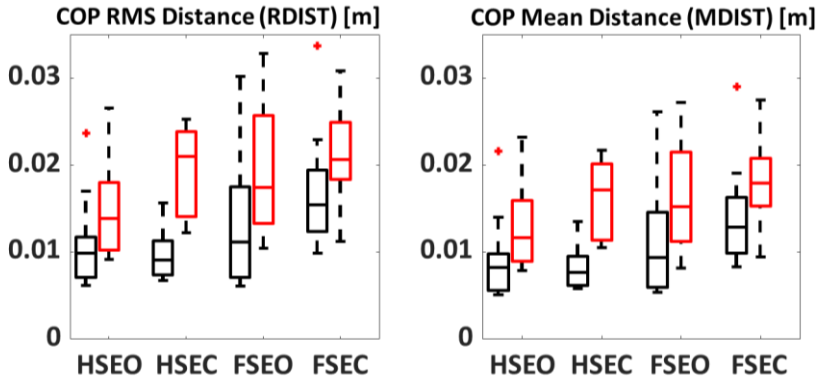

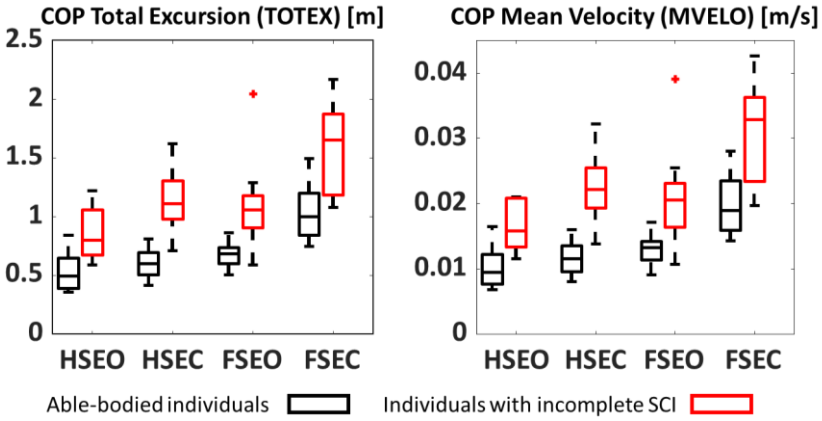

(B) Time-domain area measure

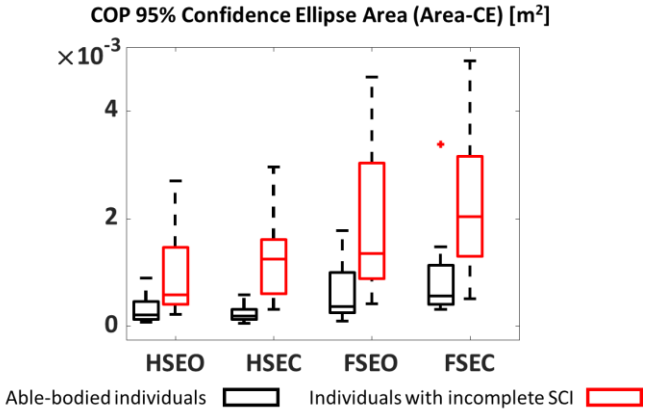

(C) Time-domain hybrid measures

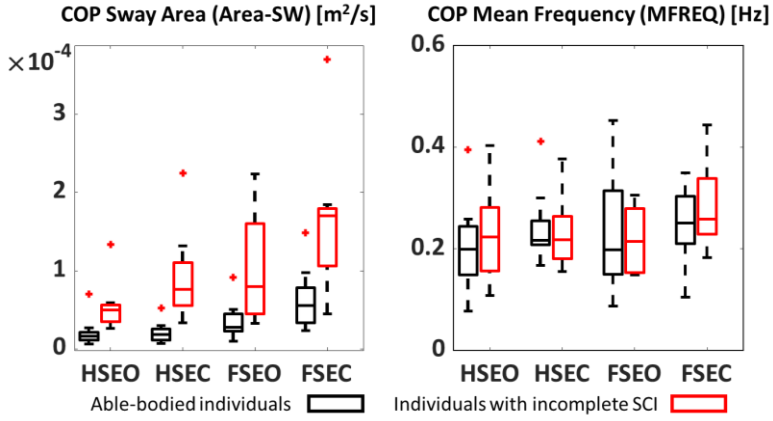

Figure 4-1. Center-of-pressure balance biomarkers: (A) time-domain distance measures, including COP RMS distance, mean distance, total excursion, and mean velocity. (B) time-domain area measure as determined by 95% confidence ellipse area. (C) time-domain hybrid measures, including COP sway area and COP mean frequency. Biomarkers were measured during four standing conditions on a hard surface (HS) and foam surface (FS) with eyes open (EO) and eyes closed (EC) for able-bodied participants (black) and ambulatory individuals with iSCI AIS level D (red). The red crosses show outliers.

Table 4-4. **(A)** P-values from statistical analysis on balance parameters for the main effects of health condition (able-bodied (AB) vs. iSCI groups), surface condition (Hard Surface (HS) vs. Foam Surface (FS)), and vision condition (Eyes Open (EO) vs. Eyes Closed (EC)). **(B)** P-values from statistical analysis on balance parameters for the interaction effect of health condition (AB vs. iSCI) and surface condition (HS vs. FS). **(C)** P-values from statistical analysis on balance parameters for the interaction effect of health condition (AB vs. iSCI) and vision condition (EO vs. EC).

(A)	**P-value**		
	iSCI vs. AB	**FS vs. HS**	**EC vs. EO**
RDIST	**0.000**	**0.008**	0.090
MDIST	**0.000**	**0.010**	0.136
TOTEX	**0.000**	**0.000**	**0.001**
MVELO	**0.000**	**0.000**	**0.001**
Area-CE	**0.000**	**0.001**	0.331
Area-SW	**0.000**	**0.000**	**0.047**
MFREQ	0.473	0.256	0.078
MEDFREQ	0.746	0.453	0.065
CFREQ	0.536	0.317	0.121
FREQD	0.387	0.201	0.992
JERK	**0.000**	**0.001**	**0.003**
RMS-ACC	**0.000**	0.066	0.408
CF-ACC	0.169	0.532	**0.031**

(B)	**P-value**					
	AB-HS vs. AB-FS	**AB-HS vs. iSCI-HS**	**AB-HS vs. iSCI-FS**	**AB-FS vs. iSCI-HS**	**AB-FS vs. iSCI-FS**	**iSCI-HS vs. iSCI-FS**
RDIST	**0.047**	**0.002**	**0.000**	0.593	0.085	0.743
MDIST	**0.047**	**0.001**	**0.000**	0.498	0.081	0.810
TOTEX	**0.003**	**0.000**	**0.000**	0.550	**0.016**	0.434
MVELO	**0.003**	**0.000**	**0.000**	0.470	**0.022**	0.567
Area-CE	**0.011**	**0.000**	**0.000**	0.524	**0.009**	0.359
Area-SW	**0.003**	**0.000**	**0.000**	0.366	**0.008**	0.480
MFREQ	0.886	0.987	0.545	0.989	0.906	0.802
MEDFREQ	0.742	0.893	0.915	0.997	0.994	1.000
CFREQ	0.996	0.713	0.981	0.591	0.998	0.553
FREQD	0.917	0.751	0.985	0.393	0.996	0.606
JERK	**0.007**	**0.000**	**0.000**	0.401	**0.015**	0.562
RMS-ACC	0.220	**0.009**	**0.001**	0.482	0.175	0.945
CF-ACC	0.833	0.515	0.547	0.926	0.941	1.000

(C)	P-value					
	AB-EO vs. AB-EC	AB-EO vs. iSCI-EO	AB-EO vs. iSCI-EC	AB-EC vs. iSCI-EO	AB-EC vs. iSCI-EC	iSCI-EO vs. iSCI-EC
RDIST	0.757	**0.046**	**0.000**	0.313	**0.005**	0.457
MDIST	0.817	**0.032**	**0.000**	0.206	**0.004**	0.572
TOTEX	0.080	**0.002**	**0.000**	0.466	**0.001**	0.139
MVELO	0.078	**0.002**	**0.000**	0.485	**0.001**	0.126
Area-CE	0.952	**0.004**	**0.000**	**0.019**	**0.001**	0.810
Area-SW	0.520	**0.001**	**0.000**	**0.055**	**0.000**	0.462
MFREQ	0.532	0.962	0.308	0.891	0.953	0.669
MEDFREQ	0.524	0.990	0.710	0.422	0.999	0.592
CFREQ	0.824	0.848	0.893	0.387	1.000	0.504
FREQD	0.992	0.793	0.945	0.910	0.991	0.987
JERK	0.125	**0.002**	**0.000**	0.380	**0.001**	0.161
RMS-ACC	1.000	0.207	**0.006**	0.233	**0.007**	0.611
CF-ACC	0.179	0.940	0.971	0.080	0.519	0.790

4.3.2 COP hybrid and frequency measures

The iSCI group had a larger Area-SW (p-value = 0.000); however, no differences were observed between groups for MFREQ (Figure 4-1C and Table 4-4A). We observed a larger Area-SW for able-bodied individuals while standing on FS compared to HS (p-value = 0.003), whereas the effect of surface condition was insignificant for the iSCI group (Table 4-4B). However, able-bodied participants had smaller Area-SW even during standing on FS compared to the iSCI group standing on HS (Figure 4-1C). Surface conditions did not affect MFREQ for both groups (Table 4-3). Moreover, the effect of impaired vision (EC) on the hybrid measures was not significant, but it tended to increase these measures (Table 4-4A). Nevertheless, larger Area-SW was observed for the iSCI group even during standing with EO compared to able-bodied participants standing with EC (p-values < 0.05 Table 4-4C). Regarding the impaired vision, the effect size was relatively larger for the iSCI group.

The effect of health condition (able-bodied vs. iSCI), surface (HS vs. FS), and vision (EO vs. EC) conditions, as well as their interaction effects, were insignificant for frequency-domain measures (Figure 4-2).

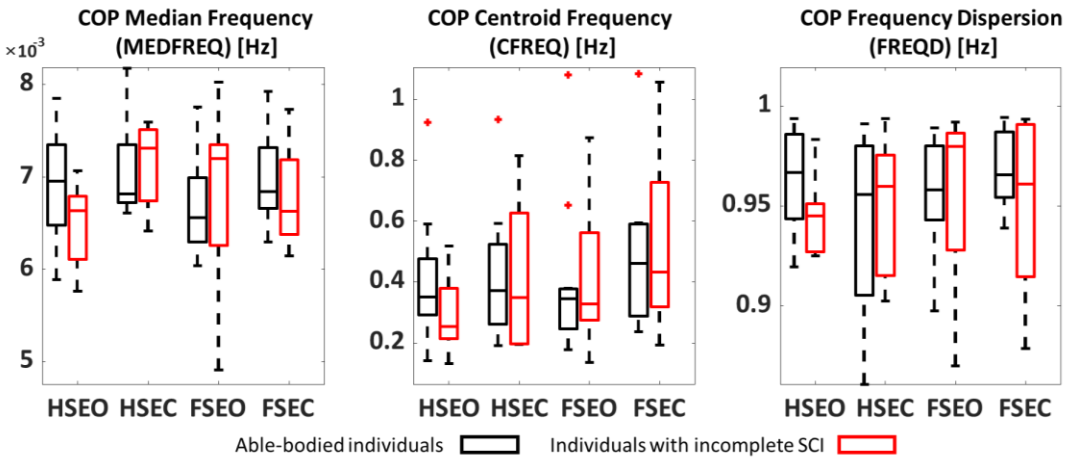

Figure 4-2. Center-of-pressure balance biomarkers: frequency-domain measures including median frequency, centroid frequency, and frequency dispersion during four standing conditions on a hard surface (HS) and foam surface (FS) with eyes open (EO) and eyes closed (EC) for able-bodied participants (black) and ambulatory individuals with iSCI (AIS level D) (red). The red crosses show outliers.

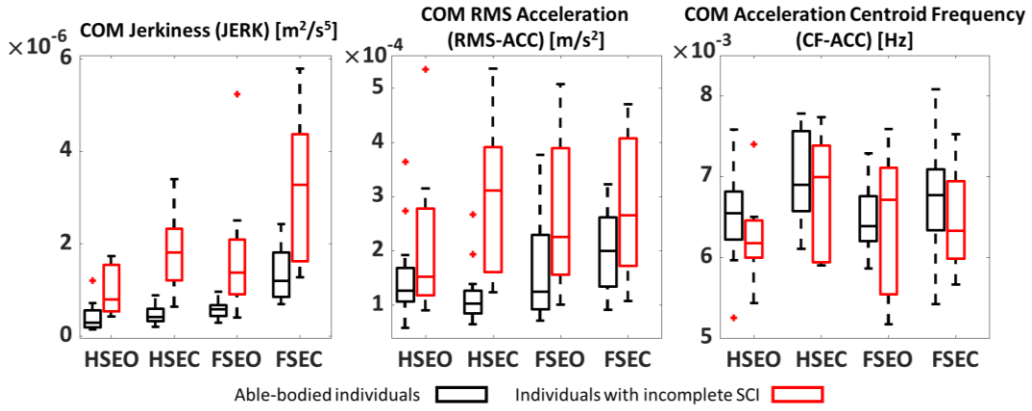

Figure 4-3. Center-of-mass (COM) acceleration-based measures including COM JERK, RMS acceleration, and centroid frequency during four standing conditions on a hard surface (HS) and foam surface (FS) with eyes open (EO) and eyes closed (EC) for able-bodied participants (black) and ambulatory individuals with iSCI (AIS level D) (red). The red crosses show outliers.

4.3.3 COM acceleration-based measures

The iSCI group had larger COM JERK, and RMS-ACC compared to able-bodied participants (Figure 4-3). JERK increased when able-bodied participants stood on FS compared to HS; however, the effect of the surface was insignificant for the iSCI group. Although standing with EC did not significantly increase JERK and RMS-ACC, it led to larger effect size for the RMS-ACC of the iSCI group (Table 4-3). No significant effect was observed in CF-ACC.

Table 4-4 (A), (B), and (C) present the p-value for the main effects of the health (able-bodied vs. iSCI), surface (HS vs. FS), and vision (EO vs. EC) conditions and their interaction effects for each outcome measure used in this study.

4.4 Discussion

The present study provides a static balance evaluation for a group of ambulatory individuals with iSCI (AIS level D) compared to age-matched able-bodied individuals during a variety of challenging standing conditions that affected somatosensory and visual inputs. To this end, we obtained COP-based and COM-based balance biomarkers using a waist-mounted IMU. We compared these biomarkers between the two groups in different challenging conditions to characterize changes in postural control after iSCI (AIS level D) based on reliance on somatosensory and visual information.

4.4.1 Postural stability

Postural stability can be characterized by three aspects: (a) stability performance, (b) control demand, and (c) postural regulations [101]. Stability performance is an indicator of an individual's ability to maintain balance within the stability limit. Attentional resources needed to maintain stability are indicated by control demand [101], [242]. Previous studies [102], [242] suggested that COP time-domain distance measures quantify stability performance while the velocity of COP is an indicator of control demand. Therefore, reduced stability performance and increased control demand imply poorer postural stability that leads to an increased risk of falling. In addition, previous studies [43], [109], [243] suggested that COP frequency-domain measures can be used as an indication of postural regulations by providing insight into postural disturbances due to neurological impairments. More specifically, centroid frequency shows the inertia of an inverted pendulum and the time required for returning to its initial position [43]; frequency dispersion indicates the rigidity and stiffness of the system [242], and power frequency indicates changes in preferential postural regulation and is sensitive to the contribution of sensory information [101], [242].

Our results indicate that the iSCI group had larger COP time-domain distance measures compared to able-bodied individuals in all standing conditions, which implies poor stability performance. In line with previous studies, larger COP RDIST post-iSCI may be associated with less effectiveness of the mechanisms that regulate postural stability due to neurological

impairment. Moreover, higher COP MVELO observed post-iSCI may suggest a less effective correction made by the nervous system as well as higher control demand. Poorer stability performance and higher control demand post-iSCI led to a larger COP area and hybrid measures in the iSCI group implying a potentially higher risk of falling in this group. Moreover, increased postural sway quantified by time-domain distance, area, and hybrid measures in the iSCI group may reflect impaired somatosensory feedback, muscle proprioceptors, and joint receptors in their postural control. Such impaired postural control may be due to inaccurate sensory information regarding the position of the body in space and incorrect perception of limits of stability [126]. In addition, larger COM JERK and RMS-ACC post-iSCI may be an indication of frequent corrections of postural sway direction. Previous studies [85], [126] interpreted JERK as a measure of dynamic stability that shows the amount of active postural corrections. Therefore, higher values of COM JERK and RMS-ACC post-iSCI may be associated with increased control demand and poorer active postural corrections in the iSCI group.

4.4.2 Integration of sensory information

Control of balance during quiet standing depends on the integration of sensory information from the somatosensory, visual, and vestibular systems. However, individuals with iSCI exhibit sensory and motor impairments at and below the lesion level, causing an alteration in the integration of sensory inputs to maintain balance. In the present study, we investigated the balance performance of a group of ambulatory individuals with iSCI (AIS level D) compared to able-bodied participants by challenging somatosensory (standing on HS and FS) and visual (EO and EC) inputs.

Standing on FS introduced altered somatosensory information during standing compared to standing on HS. Our results revealed that able-bodied participants had larger COP time-domain distance measures, the area measure, hybrid sway area, COM JERK, and RMS-ACC when standing on FS compared to HS. In contrast, although standing on FS tended to increase these parameters in the iSCI group, its effect was insignificant. Literature suggests that somatosensory information is the main input used by able-bodied individuals for maintaining postural stability [17]. This may justify the significant effect of altering somatosensory inputs on balance parameters for able-bodied participants. On the other hand, iSCI caused changes in the somatosensory tracts located in the dorsal column, which reduces the relative contribution of somatosensory inputs to postural stability [17]. Therefore, the iSCI group could compensate for the FS using the same

sensory information (visual) as when they were standing on HS. This may explain the insignificant effect of altering surface conditions on the balance parameters in the iSCI group. Individuals with iSCI have impaired somatosensory feedback from the foot sole in the postural control loop resulting in inaccurate sensory information and an abnormal internal map of stability limits [126]. Therefore, due to impaired somatosensation, they may use visual information to partially compensate for FS compared to HS. On the other hand, the somatosensory feedback in able-bodied individuals was intact and is the primary input for maintaining postural stability [17]. Thus, their balance was significantly challenged during standing on FS compared to HS. Nevertheless, the iSCI group showed poorer postural stability even during standing on HS compared to able-bodied individuals standing on FS. This could be due to reduced postural performance and increased control demand, as discussed in the previous section. Our results also showed an increase in COP TOTEX and MVELO due to impaired vision, while it did not affect RDIST and MDIST (p-value > 0.05) (Table 4-4). This may imply an increase in control demand in the absence of visual information.

Moreover, a general comparison between standing trials with EO and EC for both groups revealed a relatively larger effect size in COP time-domain distance measures, area measure, hybrid sway area, and COM RMS-ACC for the iSCI group compared to able-bodied participants. This may imply that, in general, the iSCI group could be more dependent on visual inputs compared to able-bodied participants. Indeed, since somatosensory information is impaired in the iSCI group, it is possible that the contribution of the visual information is increased to compensate for the lack of sensory information (i.e., somatosensory input) as a more reliable source of information to achieve stability, in contrast to able-bodied individuals. Nevertheless, the iSCI group showed worse postural stability even during standing with EO compared to able-bodied participants standing with EC due to impaired sensory information, poorer postural performance, and higher control demand.

In summary, our results may reflect that because of the contribution of visual inputs toward maintaining postural stability post-iSCI, alteration of somatosensory input did not reflect significant changes in balance biomarkers. This may suggest the presence of over-reliance on visual information to maintain balance post-iSCI. Therefore, two approaches may be pursued by future studies as rehabilitative intervention: (1) have the affected individuals maximize their remaining somatosensory information for maintaining balance; and (2) compensate for the

impaired somatosensory information using visual information such as visual feedback training that incorporates learning from visual cues might be of significant benefit for balance rehabilitation.

4.4.3 Limitation

The data used in the current study were collected from a relatively small and homogeneous group of male individuals with iSCI with walking ability, which limits generalization. A larger population would be required to identify any clinically meaningful changes in postural control. We only recruited individuals with iSCI AIS level D. Recruiting participants with a greater level of motor and/or sensory impairments (AIS levels A, B, and C) is needed to assess the feasibility and sensitivity of detecting changes in standing balance under different standing conditions. Furthermore, we only challenged the use of visual and somatosensory information in the present study. Future studies should investigate the effect of other sensory information (e.g., vestibular information) on the standing balance of ambulatory individuals with iSCI. In the present study, the lack of significant differences in the effect of surface and vision for the iSCI group is associated with a lack of statistical power. Although using a single IMU increase clinical utility for balance evaluation, adding more IMUs would provide more information regarding the balance strategy used by this group. Moreover, we assumed a bilateral symmetry condition in this study, which neglects any asymmetric motion patterns between the left and right legs. The assumption of bilateral symmetry for participants with iSCI was based on our preliminary experimental examination that did not show a significantly weaker or stronger side. We observed that the Lower Extremity Motor Scores (LEMS) for the right and left sides were 22.6 ± 1.4 and 22.4 ± 3.6 out of 25, respectively. We did not observe a statistically significant difference between the sides (p-value = 0.8336). Finally, this study showed altered integration of sensory information for maintaining balance after iSCI AIS level D. A more complex methodology (i.e., system identification approach) would be required to quantify the changes to sensory dynamics and sensory reweighting post-iSCI.

4.5 Conclusion

We presented a balance evaluation for a group of ambulatory individuals with iSCI (AIS level D) compared to age-matched able-bodied individuals during standing on hard and foam surfaces with eyes open and closed. We observed a reduced stability performance, an increased control demand, and a less effective active correction in the iSCI group in all standing conditions.

Our result may suggest that, due to impaired somatosensory feedback, the iSCI group showed a higher and lower reliance on visual and somatosensory information, respectively, for maintaining balance. Using a single waist-mounted IMU, our method was able to characterize standing balance in the iSCI group compared to able-bodied participants. Having high clinical utility and sufficient resolution with discriminatory ability, this study suggests that it may be appropriate to use the proposed method in the future to objectively evaluate the effectiveness of rehabilitative interventions on the balance performance for individuals with ambulatory individuals with iSCI AIS level D.

4.5.1 What is next?

The validated algorithm showed sensitivity and responsiveness for characterizing postural control and subtle differences in balance mechanisms using wearable technology in ambulatory individuals with iSCI with mild balance deficits (AIS level D) under different sensory conditions. However, the COP- and COM-based measures used in this chapter do not directly reflect all aspects of the adaptive postural movement strategies employed during standing. Even though such balance biomarkers can reflect reduced postural control due to mild balance impairment, they are unable to reveal the alteration in balance control strategies due to mild balance deficit. The next chapter will use the developed algorithm and wearable technology to investigate the differences in postural control strategies during static standing in the same group of individuals with iSCI compared to able-bodied participants.

Chapter 5

This chapter shows how the validated algorithm can be used to characterize postural control strategy using wearable technology during standing in ambulatory individuals with iSCI with mild balance deficits *under different sensory manipulations. This chapter has been adopted and/or edited from:*

A. Noamani, J.-F. Lemay, K. E. Musselman, and H. Rouhani, "Postural control strategy after incomplete spinal cord injury: effect of sensory inputs on trunk–leg movement coordination," J. Neuroeng. Rehabil., vol. 17, no. 1, 2020, doi: 10.1186/s12984-020-00775-2.

5 Postural Control Strategy after iSCI

5.1 Introduction

Regaining walking function and maintaining a steady standing posture are listed as top priorities for individuals with iSCI [16], [20], [21]. Literature reported that, at one-year post-injury, up to one-third of individuals with recent iSCI would recover partial balance and walking ability [16], [143]. Future ambulatory status is related to the initial amount of motor function below the level of the lesion [19]. For instance, statistics indicate partial recovery of walking function among 80-100% of individuals with iSCI rated D on the American Spinal Injury Association Impairment Scale (AIS), indicating some preservation of motor and sensory function below the level of injury after the first year of injury [16], [144]. This highlights the importance of implementing outcome measures that identify the balance and walking capacities of individuals with iSCI to guide the delivery of more effective rehabilitative interventions.

A significant challenge for individuals with iSCI is to maintain postural stability while recovering walking function [17]. iSCI affects the ability to safely stand and perform functional activities in this position [18]. The literature has reported a high occurrence of falling among the SCI population, with up to 78% of these individuals experiencing at least one fall post-rehabilitation [10]–[12]. Falls can lead to injuries and hospitalization [10], restriction in community participation [11], [13], [14], and a fear of falling [15]. One of the major factors contributing to falls in this population is the loss of balance [14], [18], highlighting the lack of

effective postural control in individuals with iSCI. Furthermore, greater postural control in this population is highly related to a more normal gait pattern, higher stride speed, less reliance on supervision or physical assistance, and more functional ambulatory status [16]. Therefore, the development of fall prevention strategies is associated with effective postural control.

Effective postural control is obtained via the integration of sensory information [17] and the interaction of the body with the changing environment [10]. Due to the sensory and motor impairments at and below the level of the lesion post-SCI [18], sensory reweighting may be affected. This effect on sensory reweighting results from the development of compensatory strategies to maintain postural stability [20], [35]. Consequently, any alteration in the availability of sensory inputs [17], [145] can further challenge postural stability in this population and may lead to a variety of adaptive movement coordination patterns. Hence, identifying the underlying impairments and changes to movement coordination patterns is necessary for effective rehabilitation post-SCI [20], [35].

Observational balance assessment methodologies have been used for balance assessment post-SCI. Yet, they tend to be subjective and provide minor information for understanding the adaptive postural control strategies for compensating for balance difficulties [16], [35], [36], highlighting the necessity of a quantitative method to assess postural stability.

Quantitative evaluation of postural stability is usually performed using measures based on the displacement of the center-of-pressure (COP) on a force platform [18] or using measures based on center-of-mass (COM) acceleration from an inertial measurement unit (IMU) on the lower trunk [85], [244]. Previous studies have used COP-based measures to investigate the limits of stability [18] and the effect of sensory information on postural stability [17] post-SCI. The over-reliance on visual cues while walking and standing due to impaired somatosensation was highlighted [17], [145]. Recently, we characterized the effect of distorted visual and somatosensory inputs on postural control using a waist-mounted IMU and compared balance biomarkers between iSCI and able-bodied populations [245].

Due to impaired somatosensation and reduced muscle control, individuals with iSCI may adapt postural movement strategies compared to able-bodied individuals to compensate for reduced postural control. While COP- and COM-based measures are strong indicators of dysfunctional postural control, they do not directly reflect all aspects of the adaptive postural movement strategies employed during standing [136]. Therefore, although such balance

biomarkers can indicate reduced postural control post-iSCI, they are unable to reveal the underlying mechanism of how and why the postural control is altered. Measuring the kinematics between the body segments during standing allows us to capture not only the dysfunctional postural control but also how impaired balance is compensated post-iSCI by alteration of inter-segment motions. Kinematic assessment of body segments during standing enables a better understanding of how individuals with iSCI employ adaptive postural strategies to compensate for balance difficulties due to impaired somatosensory feedback. For example, the impaired control of the ankle joint motion for maintaining the body COM stability during standing might be compensated by the altered motion control of the hip joint. During quiet standing, the human body is modelled as single and double inverted pendulums to study what is known as ankle and hip strategies, respectively. The human body mainly pivots around the ankle joint with increasing contribution of hip motion with larger postural sways. Previous literature [116], [136] has shown that, at sway oscillations below 1 Hz, able-bodied individuals move their trunk and leg in an in-phase manner indicating an ankle strategy. However, at sway oscillations above 1 Hz, trunk and leg motion is anti-phase, indicating a hip or mixed ankle-hip strategy. This implies the domination of the ankle strategy during low-amplitude, low-velocity, or low-frequency motions, whereas the hip strategy dominates during larger sway perturbations [115], [116], [246]. Neurological impairments could alter the ankle and hip strategies in affected individuals at different sway frequencies [247]. The selection of segmental coordination pattern (in-phase or anti-phase) and between-patterns transition may be associated with a loss of stability and pre-selected movement strategy based on the task [116], [248]. Although the balance strategies of able-bodied individuals have been studied in the past, the segmental coordination patterns utilized by the iSCI group during quiet stance are yet to be investigated.

Our recent study [245] showed that ambulatory individuals with iSCI (AIS level D) can exhibit reduced stability performance, increased control demand, and a less effective active correction with a higher reliance on visual information and lower reliance on somatosensory information. In the present study, we aim to (1) compare the postural movement between the same group of ambulatory individuals with iSCI (AIS level D) and able-bodied individuals to quantify the inter-segment coordination of the trunk and the leg motions; (2) investigate the alteration of postural movement strategies under conditions that challenge balance by affecting somatosensory (standing on hard vs. foam surfaces) and visual (eyes open vs. closed) inputs; and (3) characterize

the test-retest reliability of inter-segment coordination quantification and compare it with that of conventional balance biomarkers for the iSCI group.

We expected that ambulatory individuals with iSCI (AIS level D) would have difficulties adapting trunk-leg movement patterns from the ankle strategy at lower frequencies to the mixed strategy at higher frequencies due to their sensory and motor impairment.

5.2 Methods

5.2.1 Participants

Table 5-1. Demographic information of participants with incomplete spinal cord injury (iSCI); and demographic information of able-bodied participants

Group	Variable	Mean (Standard Deviation)	Range
iSCI	Age (years)	52.4 (20.5)	20-87
	Height (cm)	174.7 (7.8)	161-188
	Weight (kg)	82.1 (18.3)	57-113.4
	Time post lesion (months)	62.2 (70.1)	27-289
	Lower Extremity Motor Score (/50)	44.8 (4.3)	32-49
Able-bodied	Age (years)	39.4 (19.3)	18-84
	Height (cm)	170.5 (8.4)	156-181
	Weight (kg)	69.8 (14.4)	47.5-96
	Variable	**Number**	
iSCI	Sex (Male/Female)	Male = 12, Female = 1	
	Level of lesion	Paraplegia: 8, Tetraplegia: 5	
	Type of lesion	Traumatic: 10, Non-traumatic: 3	
Able-bodied	Sex (Male/Female)	Male = 7, Female = 7	

Thirteen ambulatory individuals with a traumatic or a non-traumatic iSCI AIS level D (hereafter iSCI group) and fourteen aged-matched able-bodied individuals voluntarily participated in this study (Table 5-1). In the present study, we used ±3 years for age matching. There was no significant difference between the age of the able-bodied participants and individuals with iSCI (p-value = 0.1146). Participants with iSCI were recruited from the outpatient population of the CIUSSS du Centre-Sud-de-l'Île-de-Montréal (Installation Gingras-Lindsay) and the Lyndhurst Centre, Toronto Rehabilitation Institute-University Health Network. The inclusion criteria for the iSCI group were: (a) adults with traumatic and non-traumatic motor and sensory iSCI with American Spinal Injury Association Impairment Scale (AIS) C or D; (b) at least 5 months post-injury; and (c) able to walk for six minutes without assistive devices or assistance of another person to ensure that intrinsic balance ability could be studied. Exclusion criteria were: (a) presence of

other neurological disorders; (b) visual impairments not corrected with glasses; and (c) vestibular deficits. Ethics approval was obtained from the local ethics committees. Each participant provided written informed consent prior to participation.

5.2.2 Experimental procedure

Previous studies have suggested that assessing balance during quiet standing on hard or foam surfaces with eyes open or closed could provide useful information to evaluate the balance performance of individuals with iSCI [157], [163], [167]. Participants were asked to perform a one-minute quiet stance with their feet shoulder-width apart under four different sensory conditions: (1) hard surface with eyes open (HSEO), (2) hard surface with eyes closed (HSEC), (3) foam surface with eyes open (FSEO), and (4) foam surface with eyes closed (FSEC). The purpose of using a foam surface was to alter somatosensory information while standing. Foam pads with medium density and a thickness of 7.62 cm (3 inches) (Velva 60, Domfoam, Canada) were attached to the participants' shoes using Velcro straps. The EC condition was used to eliminate the effect of visual feedback on balance. Participants were asked to close their eyes for the duration of the EC condition. The standing conditions were performed in a randomized order using simple randomization, and rest breaks were taken between trials as needed. The length of the rest breaks was adjusted to eliminate the impact of fatigue on the performance of the participants. The iSCI group participated in two testing sessions (two weeks apart) to assess the test-retest reliability of the proposed outcome measures.

5.2.3 Data acquisition and human body modelling

To measure the kinematics of the trunk and leg, we used two IMUs (Physilog®5, GaitUp, Switzerland) placed over the sacrum and right tibia of each participant (Figure 5-1a and 1b). Each IMU contained a tri-axial accelerometer (range: ±16g) and a tri-axial gyroscope (range: ±2000 deg/s) and recorded the motion of the body segments at a sampling frequency of 256 Hz. The IMU recordings were low-pass filtered via a zero-lag 8^{th}-order Butterworth filter with a cut-off frequency of 5 Hz.

The human body was modelled as a double inverted pendulum with trunk, leg, and foot segments connected to each other by two 3D revolute joints representing hip and ankle joints. The feet were assumed motionless during the standing trials. The mass, length, COM, and moments of inertia of the segments were estimated based on the body mass and height, according to Winter

[223]. We obtained the instantaneous orientation of the trunk and leg segments by aligning the accelerometer's vertical axis with gravity during quiet stance [225], [227]. We assumed the segments as rigid links and calculated the instantaneous position of the COM, linear acceleration, and angular velocity of the body using the segments' orientation. We developed a custom-built MATLAB (MathWorks, USA) program for an IMU-based top-down inverse dynamics to estimate the ankle and hip joint moments and center-of-pressure (COP) position based on our previous study [93].

5.2.4 Outcome measures and data analysis

To identify changes in inter-segment movement coordination and control strategy in the iSCI group, we calculated the Magnitude-Squared Coherence (MSC) between the acceleration patterns of the trunk and leg segments in the anterior-posterior direction. MSC was then calculated as:

$$MSC = |C_{xy}(f)|^2 = \frac{|P_{xy}(f)|^2}{P_{xx}(f).P_{yy}(f)} \quad (1)$$

Where $C_{xy}(f)$ and $P_{xy}(f)$ are the complex coherence and cross-spectral density between two signals, $P_{xx}(f)$ and $P_{yy}(f)$ are the power spectral densities for the signals being compared, and f is frequency. We calculated the power spectral density and cross-power spectral density using Welch's averaged method. A Hanning window of 10 seconds with an overlap of 50% was used across frequencies of 0-5 Hz. The range of the frequency 0 to 5 Hz was selected based on the frequency content of the time series obtained via Fast Fourier Transform. Previous literature [116], [136] showed that, in able-bodied individuals, the trunk and leg have in-phase motions at sway oscillation below 1 Hz, indicating the domination of the ankle strategy during low-frequency motions. However, as the sway oscillation increases above 1 Hz, trunk and leg motions become anti-phase, indicating a hip or mixed ankle-hip strategy during larger sway perturbations [115], [116], [246]. Since the literature [116], [248] has shown that a frequency of 1 Hz is the cut-off between in-phase (ankle strategy) and anti-phase (ankle-hip strategy) movement coordination, we calculated the mean of MSC of all frequencies (1) below or equal to 1 Hz, and (2) above 1 Hz for each participant and each standing condition as an outcome measure for balance assessment. An MSC of 1 indicates an in-phase trunk-leg motion pattern, and the smaller the MSC, the lower the degree of in-phase action between trunk and leg segments [116].

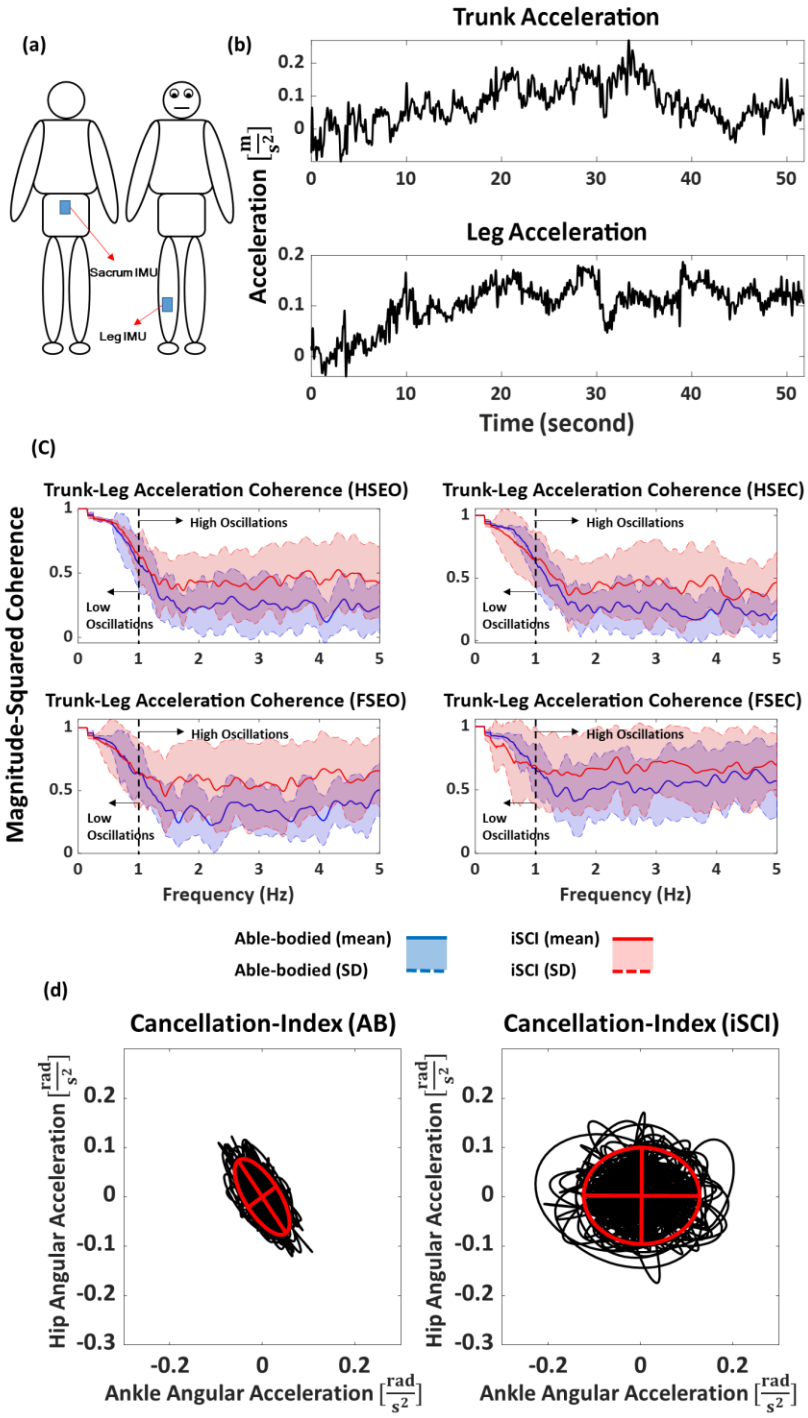

Figure 5-1. **(a)** Inertial measurement units (IMUs) were placed on the sacrum and the tibia of the right leg. **(b)** Acceleration signals in the time-domain for trunk and leg segments for one participant for standing on a hard surface with eyes open. **(c)** Trunk-leg Magnitude-Squared Coherence (MSC) for the iSCI group (red) and able-bodied (AB) individuals (blue) presented as an ensemble average (mean ± standard deviation) for both groups and each standing condition on a hard surface (HS) and foam surface (FS) with eyes open (EO) and eyes closed (EC). **(d)** Cancellation-index indicates the reciprocal action between the angular acceleration of the ankle and hip joints as presented for one participant from the AB and iSCI groups for standing on a hard surface with eyes open.

We also used the cancellation-index proposed by Kato et al. [87], in addition to MSC, to identify changes in reciprocal action between the ankle and hip joints (mixed strategy) during standing in the iSCI group as follows:

$$CI = \frac{\sqrt{k_1^2 var(\ddot{\theta}_{leg}) + k_2^2 var(\ddot{\theta}_{trunk})}}{\sqrt{k_1^2 var(\ddot{\theta}_{leg}) + k_2^2 var(\ddot{\theta}_{trunk}) + 2k_1 k_2 cov(\ddot{\theta}_{leg}, \ddot{\theta}_{trunk})}} \quad (2)$$

Where CI is cancellation-index, $\ddot{\theta}$ is angular acceleration; k_1 and k_2 are constants obtained based on the mass and length of the segments as explained by Kato et al. [87]; and $var(x)$ and $cov(x, y)$ represent the variance of x and the covariance of x and y, respectively. A cancellation-index of 1 indicates that there is no reciprocal action between ankle and hip joints, and the greater the cancellation-index, the greater the degree of reciprocal action.

Table 5-2. As conventional outcome measures, a total of ten center-of-pressure (COP) measures were calculated according to [241]. In addition, three center-of-mass (COM) acceleration-based measures were used based on [85]. For movement coordination, we used Cancellation Index based on [87] and Magnitude-Squared Coherence (MSC) between trunk and leg segments.

Outcome Measure	Nomenclature	Type
Root-Mean-Square Distance	**RDIST**	COP Time-domain distance measures
Mean Distance	**MDIST**	
Total Excursion	**TOTEX**	
Mean Velocity	**MVELO**	
95% Confidence Ellipse Area	**Area-CE**	COP area measure
Sway Area	**Area-SW**	COP Time-domain hybrid measures
Mean Frequency	**MFREQ**	
Median Frequency	**MEDFREQ**	COP Frequency-domain measures
Centroid Frequency	**CFREQ**	
Frequency Dispersion	**FREQD**	
Sway jerkiness	**JERK**	COM acceleration-based measures
Root-Mean-Square Acceleration	**RMS-ACC**	
Centroid Frequency	**CF-ACC**	
Cancellation-Index	**CI**	Trunk-leg acceleration pattern coordination
Magnitude-Squared Coherence	**MSC**	

To identify changes to movement coordination strategies due to impairment (iSCI vs. able-bodied) and altered sensory inputs (HS vs. FS and EO vs. EC), we performed statistical analyses

on MSC-based outcome measures at low and high frequencies. The Kolmogorov-Smirnov test was used to check that the data were normally distributed, followed by Levene's test to determine the equality of variance. Subsequently, we performed either a three-way Analysis of Variance (ANOVA) or a Kruskal-Wallis test (significance level = 0.05) with Bonferroni correction followed by a multiple comparison post-hoc test (MATLAB 2019b, MathWorks, USA). We also used Cohen's d effect size to compare the effect of altered sensory inputs on the adaptation of inter-segment coordination between iSCI and able-bodied groups.

Furthermore, we calculated COP-based and COM acceleration-based measures (Table 5-2), similar to our previous study [245], to compare the test-retest reliability of MSC-based measures with conventional balance biomarkers. We used the intra-class correlation coefficient (ICC) for the model (2, k) to evaluate the reliability of each outcome measure.

5.3 Results

5.3.1 Effect size between groups

At lower frequencies ($f \leq 1$ Hz), the mean MSC between the trunk and leg accelerations was high (above 0.88 medians across participants) for both able-bodied and the iSCI groups across all standing conditions (Table 5-3a). Moreover, the effect sizes between populations were small, ranging from 0.06 to 0.42. At higher frequencies ($f > 1$ Hz), mean MSC between trunk and leg accelerations were reduced for both groups. However, at higher frequencies, the iSCI group had significantly larger mean MSC between trunk and leg accelerations compared to able-bodied participants with large effect sizes between groups, ranging from 0.53 to 1.13 across all standing conditions.

5.3.2 Effect size between conditions

At lower frequencies, the pairwise comparison between mean MSC at different standing conditions revealed small effect sizes for both groups (Table 5-3b). However, at higher frequencies, medium and large effect sizes were observed for able-bodied participants ranging from 0.77 to 1.61 showing larger effect sizes with more challenging conditions (Table 5-3b). Similar patterns were observed for the iSCI group; however, the effect sizes were relatively smaller compared to able-bodied participants at higher frequencies.

Table 5-3. **(a)** Mean Magnitude-Squared Coherence (MSC) between trunk and leg accelerations presented as [25%, 50%, 75%] percentiles for able-bodied (AB) participants and ambulatory individuals iSCI AIS level D at lower and higher frequencies for different standing conditions as well as between-group Cohen's d effect size. **(b)** Between-conditions Cohen's d effect size for AB and iSCI groups at lower and higher frequencies. **(c)** Cancellation-index proposed by Kato et al. [87] as an indicator of trunk-leg reciprocal action presented as [25%, 50%, 75%] percentiles for AB and iSCI groups with the between-group effect size for each standing condition. Cohen's d effect size was defined as very small (d = 0.01), small (d = 0.20), medium (d = 0.50), large (d = 0.80), very large (d = 1.20), and huge (d = 2.00).

(a)	**Lower Frequencies (f ≤ 1 Hz)**		
	AB	**iSCI**	**Cohen's d**
HSEO	[0.87, 0.88, 0.89]	[0.86, 0.89, 0.89]	0.34
HSEC	[0.88, 0.89, 0.9]	[0.84, 0.88, 0.9]	0.36
FSEO	[0.84, 0.89, 0.9]	[0.85, 0.9, 0.91]	0.06
FSEC	[0.85, 0.89, 0.9]	[0.78, 0.9, 0.94]	0.42
	Higher Frequencies (f > 1 Hz)		
	AB	**iSCI**	**Cohen's d**
HSEO	[0.18, 0.21, 0.29]	[0.29, 0.44, 0.57]	1.13
HSEC	[0.19, 0.24, 0.33]	[0.27, 0.44, 0.57]	0.99
FSEO	[0.28, 0.34, 0.47]	[0.43, 0.49, 0.83]	1.11
FSEC	[0.38, 0.59, 0.72]	[0.52, 0.78, 0.87]	0.53

(b)	**Cohen's d effect size between conditions**			
	AB		**iSCI**	
	f ≤ 1 Hz	**f > 1 Hz**	**f ≤ 1 Hz**	**f > 1 Hz**
HSEO vs. HSEC	0.37	0.08	0.33	0.04
HSEO vs. FSEO	0.02	0.77	0.26	0.58
HSEO vs. FSEC	0.35	1.58	0.41	0.97
HSEC vs. FSEO	0.33	0.79	0.05	0.59
HSEC vs. FSEC	0.01	1.61	0.12	0.96
FSEO vs. FSEC	0.32	1.11	0.16	0.35

(c)	Cancellation Index		
	AB	iSCI	Cohen's d
HSEO	[1.012, 1.018, 1.02]	[1.013, 1.015, 1.018]	0.43
HSEC	[1.015, 1.017, 1.019]	[1.012, 1.014, 1.018]	0.58
FSEO	[1.013, 1.017, 1.019]	[1.013, 1.016, 1.018]	0.27
FSEC	[1.015, 1.016, 1.019]	[1.012, 1.015, 1.018]	0.49

5.3.3 Main effects

The main effect of the health condition (Table 5-4a) shows no significant differences between able-bodied and iSCI groups for mean MSC of trunk and leg accelerations at lower frequencies ($f \leq 1$ Hz). However, at higher frequencies ($f > 1$ Hz), the iSCI group had a significantly larger mean MSC between trunk and leg accelerations compared to able-bodied participants (Figure 5-1c). Moreover, the cancellation-index was significantly smaller for the iSCI group compared to able-bodied participants (Table 5-4a and Figure 5-1d).

The main effect of the surface condition (Table 5-4a) revealed a significantly larger mean MSC for standing on FS compared to HS at higher frequencies, while its effect was negligible on mean MSC at lower frequencies and on the cancellation-index. No main effect of vision (EO vs. EC) was observed on the mean MSC and on the cancellation-index.

Table 5-4. Statistical analysis on Mean Magnitude-Squared Coherence (MSC) between trunk and leg accelerations at lower and higher frequencies and on Cancellation-Index (CI): **(a)** the main effect of health (iSCI vs AB), surface (FS vs. HS), and vision (EC vs, EO) conditions; and interaction effect of **(b)** surface and vision conditions, **(c)** health and surface conditions, and **(d)** health and vision conditions. Bold numbers show significant difference (P-value < 0.05).

(a)	Main Effects (P-value)		
	iSCI vs. AB	FS vs. HS	EC vs. EO
MSC ($f \leq 1$ Hz)	0.756	0.218	0.564
MSC ($f > 1$ Hz)	**0.000**	**0.000**	0.189
CI	**0.042**	0.995	0.658

(b)	Interaction effect of surface and vision conditions (P-value)					
	HSEO vs. HSEC	HSEO vs. FSEO	HSEO vs. FSEC	HSEC vs. FSEO	HSEC vs. FSEC	FSEO vs. FSEC
MSC ($f \leq 1$ Hz)	0.939	0.727	0.576	0.967	0.896	0.995
MSC ($f > 1$ Hz)	1.000	0.190	**0.001**	0.214	**0.001**	0.274
CI	0.947	0.995	0.989	0.990	0.996	1.000

(c)	Interaction effect of health and surface conditions (P-value)					
	AB-HS vs. AB-FS	AB-HS vs. iSCI-HS	AB-HS vs. iSCI-FS	AB-FS vs. iSCI-HS	AB-FS vs. iSCI-FS	iSCI-HS vs. iSCI-FS
MSC (f ≤ 1 Hz)	0.956	0.999	0.687	0.910	0.932	0.600
MSC (f > 1 Hz)	**0.003**	**0.006**	**0.000**	0.999	0.134	0.110
CI	0.990	0.301	0.482	0.473	0.673	0.990

(d)	Interaction effect of health and vision conditions (P-value)					
	AB-EO vs. AB-EC	AB-EO vs. iSCI-EO	AB-EO vs. iSCI-EC	AB-EC vs. iSCI-EO	AB-EC vs. iSCI-EC	iSCI-EO vs. iSCI-EC
MSC (f ≤ 1 Hz)	0.920	0.970	0.926	0.998	1.000	0.998
MSC (f > 1 Hz)	0.416	**0.005**	**0.002**	0.270	0.149	0.991
CI	0.999	0.595	0.296	0.680	0.367	0.960

Table 5-5. Test-retest reliability of conventional balance biomarkers [245] and Mean Magnitude-Squared Coherence (MSC) between trunk and leg accelerations at lower and higher frequencies for ambulatory individuals with iSCI AIS level D as measured by Intra-class Correlation Coefficient (ICC) across different standing conditions on foam (FS) and hard surfaces (HS) with eyes open (EO) and closed (EC).

	Intra-class Correlation Coefficient (ICC)			
	HSEO	HSEC	FSEO	FSEC
RDIST	1.00	0.94	0.90	0.68
MDIST	1.00	0.93	0.92	0.70
TOTEX	1.00	0.87	0.78	0.88
MVELO	1.00	0.87	0.79	0.84
Area-CE	0.99	0.74	0.81	0.06
Area-SW	1.00	0.65	0.75	0.12
MFREQ	0.77	0.60	0.52	0.28
MEDFREQ	0.18	0.58	0.08	0.13
CFREQ	0.83	0.60	0.59	0.13
FREQD	0.80	0.24	0.70	0.33
JERK	1.00	0.64	0.41	0.99
RMS-ACC	1.00	1.00	1.00	1.00
CF-ACC	0.22	0.16	0.18	0.03
CI	0.50	0.80	0.76	0.41
MSC (f ≤ 1 Hz)	1.00	1.00	1.00	1.00
MSC (f > 1 Hz)	1.00	1.00	1.00	1.00
Poor	**Fair**	**Good**	**Excellent**	
0 - 0.40	0.40 - 0.6	0.6 - 0.74	0.75 - 1	

5.3.4 Interaction effects

The interaction effect of vision and surface conditions (Table 5-4b) showed that the FSEC condition significantly increased mean MSC compared to HSEO and HSEC at higher frequencies. In addition, at higher frequencies, the mean MSC of able-bodied participants increased while standing on FS compared to HS (Table 5-4c). Although a similar trend was observed for the iSCI group, its effect was not significant. The effect of EC on mean MSC was not significant for both groups. However, the iSCI group had a significantly larger mean MSC even with EO and EC compared to able-bodied standing with EO (Table 5-4d). At lower frequencies, all interaction effects were not significant for the cancellation-index and mean MSC. The between-group effect sizes for the cancellation-index were small to medium ranging from 0.27 to 0.58 for different standing conditions (Table 5-3c).

5.3.5 Test-retest reliability

Table 5-5 shows test-retest reliability as measured via ICC for conventional balance biomarkers, presented in our previous study [245], and mean MSC at lower and higher frequencies for the iSCI group. Among conventional balance biomarkers, only two COP time-domain measures (TOTALX and MVELO) and RMS-ACC showed excellent reliability across all standing conditions. The rest of these measures showed average or poor reliability for the FSEC or FSEO conditions. The highest reliability was observed for mean MSC with excellent reliability at all standing conditions.

5.4 Discussion

This study provides an evaluation of the balance control strategy and inter-segment movement coordination for a group of ambulatory individuals with iSCI (AIS level D) compared to age-matched able-bodied individuals during a variety of challenging standing conditions that affected somatosensory and visual inputs. Using IMUs placed on the trunk and leg, we obtained MSC between the trunk and leg acceleration patterns. We compared mean MSC at lower ($f \leq 1$ Hz) and higher ($f > 1$ Hz) frequencies between groups in different challenging conditions to characterize changes in movement coordination patterns after iSCI (AIS level D) based on reliance on somatosensory and visual information.

Previous studies [116], [136] showed that able-bodied individuals move their trunk and leg in an in-phase motion at sway frequencies below 1 Hz, indicating an ankle strategy. However, at

sway frequencies above 1 Hz, the movement of the trunk and leg segments is anti-phase, indicating a hip or mixed ankle-hip strategy. Creath et al. [116] demonstrated that able-bodied individuals have high trunk-leg coherence at lower frequencies, and low trunk-leg coherence at higher frequencies representing ankle (in-phase) and ankle-hip (anti-phase) balance control strategies, respectively. We observed that movement coordination patterns of the iSCI group were affected due to impaired sensory and motor function compared to able-bodied individuals. We also observed that the iSCI group had difficulties adapting trunk-leg movement patterns from the ankle strategy at lower frequencies to the mixed strategy at higher frequencies due to their impaired somatosensation.

5.4.1 Effect of iSCI on balance strategy

Our results indicate that mean MSC between the trunk and leg acceleration patterns at frequencies below 1 Hz were high (above 0.88 medians across participants) for both groups reflecting an ankle strategy at lower frequencies. No significant main effect of health condition (able-bodied vs. iSCI) was observed on mean MSC at lower frequencies, and we observed small effect sizes between the groups across all standing conditions. These findings may imply that the iSCI group considered in this study display a similar balance control strategy (i.e., ankle strategy) compared to able-bodied individuals at lower frequencies with moving their trunk and leg in an in-phase manner.

As we expected, the mean MSC between the trunk and leg acceleration patterns reduced as sway frequency increased from 1.0 to 5.0 Hz in both groups. This highlights the transition from the ankle strategy to the mixed ankle-hip strategy at higher frequencies and is in agreement with previous studies [116], [136]. However, our results revealed that the iSCI group showed significantly larger mean MSC at higher frequencies compared to able-bodied participants. Moreover, large effect sizes were observed between the groups in the mean MSC across all standing conditions at higher frequencies. These findings may confirm our hypothesis that inter-segment movement coordination is affected post-iSCI due to impaired sensory and motor function compared to able-bodied individuals.

Moreover, as sway frequency increased, able-bodied individuals reduced their trunk-leg acceleration coherence representing a switch from an ankle strategy to a hip or mixed strategy [116]. However, the iSCI group showed a significantly larger mean MSC between trunk and leg

accelerations. This indicates that they are less able to adapt their movement patterns from the ankle strategy to a mixed strategy at higher frequencies compared to able-bodied individuals. In addition, we used the cancellation-index from the literature [82], [87] to investigate reciprocal motions of the ankle and hip joints during quiet standing, highlighting the degree of mixed ankle-hip strategy. We observed a significantly smaller cancellation-index in the iSCI group compared to able-bodied individuals confirming reduced anti-phase motion between the ankle and hip joints post-iSCI. This also highlights an inability to utilize the mixed ankle-hip strategy for maintaining balance due to impairment in this group.

5.4.2 Effect of alteration of sensory information

We investigated the effect of altered sensory information on balance control strategy in able-bodied and iSCI groups. We compared mean MSC at lower and higher frequencies under conditions that challenge balance by affecting somatosensory (standing on HS vs. FS) and visual (EO vs. EC) inputs. The main effect of surface condition revealed a significantly larger mean MSC at higher frequencies for standing on FS compared to HS. However, the main effect of surface condition was insignificant on the cancellation-index and the mean MSC at lower frequencies. Larger mean MSC at higher frequencies may imply that when the somatosensory feedback is distorted due to standing on FS, utilizing the mixed ankle-hip strategy is challenged at higher sway frequencies. In contrast, depriving visual information did not reveal any significant effect on the mean MSC at lower and higher frequencies. This may imply the minor effect of vision on the transition from the ankle strategy to the ankle-hip strategy at higher frequencies. The interaction effect of surface and vision conditions (Table 5-4b) revealed a similar finding showing a significant increase in mean MSC at higher frequencies for FSEC compared to HSEO and HSEC conditions, while no significant effect of vision was observed.

At higher frequencies, mean MSC significantly increased for able-bodied participants when standing on FS compared to HS. This may imply that altered somatosensory information challenged the use of a mixed ankle-hip strategy at higher frequencies for able-bodied individuals. In contrast, the effect of FS compared to HS on mean MSC was insignificant for the iSCI group. This may be associated with impaired somatosensory feedback post-iSCI. iSCI alters somatosensory tracts located in the dorsal column decreasing the relative contribution of somatosensory information to maintaining balance [17], whereas able-bodied individuals primarily use somatosensory information for maintaining balance [17]. This may provide useful

information on why altering somatosensory information significantly affected the balance control strategy in able-bodied individuals while its effect was minor on the iSCI group. Moreover, it is suggested by the literature that individuals with iSCI mainly use visual information to maintain postural stability [245] and therefore, this may justify why altering the somatosensory information by using a foam surface had a lesser impact on the control strategy used by the iSCI group.

In agreement with the findings above, the pairwise comparison between mean MSC of different conditions showed small effect sizes at lower frequencies and medium to large effect sizes at higher frequencies for both groups due to alteration of sensory inputs. Between-condition effect sizes were relatively smaller for the iSCI group compared to able-bodied individuals confirming less adaptive movement coordination at higher frequencies post-iSCI.

Note that although the cancellation-index was able to distinguish movement coordination patterns of the iSCI group from able-bodied participants, it was incapable of identifying changes in balance strategies due to altered sensory information, in contrast to MSC. This is due to the fact that the cancellation-index is a time-domain measure that indicates the trunk-leg reciprocal action across the whole frequency spectrum and does not identify the transition from in-phase to anti-phase inter-segment coordination as sway frequency increases. Hence, using the cancellation-index to quantify trunk-leg anti-phase action may not be sensitive enough to identify changes to inter-segment coordination due to the alteration of sensory inputs. In contrast, mean MSC across different ranges of frequency showed sensitivity to alteration of sensory information. This highlights the power of using MSC between trunk and leg accelerations, compared to the cancellation-index, in identifying changes to balance control strategies not only due to neuromuscular impairments but also due to the alteration of sensory inputs.

5.4.3 Test-retest reliability

Although a majority of the conventional biomarkers of standing balance previously suggested in the literature showed excellent test-retest reliability in the least challenging condition (HSEO), only three of them (COP Total Excursion, COP Mean Velocity, and COM RMS Acceleration) had good to excellent test-retest reliability in all four conditions. The cancellation-index showed good to excellent test-retest reliability in only two conditions. However, MSC in both lower and higher frequencies showed excellent test-retest reliability for all conditions. As such, despite its complex mathematical definition, MSC in both lower and higher frequencies

provided repeatable, responsive and sensitive outcome measures with neurophysiological relevance for the evaluation of balance strategy in ambulatory individuals with iSCI AIS level D.

5.4.4 Limitations

The data used in the present study were obtained from a relatively small and homogeneous group of individuals with iSCI, which limited the generalization of the observations and reached conclusions. A larger population would be needed to identify any clinically meaningful changes in balance control. We only recruited individuals with iSCI AIS level D. Participants with a greater level of motor and/or sensory impairments (AIS levels A, B, and C) must be recruited to assess the postural control strategy using trunk-leg coordination measures under different standing conditions across a more diverse iSCI population. Moreover, bilateral symmetry was assumed in this study, which ignores any asymmetric motion patterns between the left and right legs. The assumption of bilateral symmetry for individuals with iSCI was based on our preliminary experimental investigations that did not reflect a significantly weaker (or stronger) side. Participants with iSCI showed relatively good motor recovery and had Lower Extremity Motor Scores (LEMS) of 44.8 ± 4.3 (mean ± standard deviation) out of 50 for both sides. In addition, the LEMS for the right and left sides were 22.6 ± 1.4 and 22.4 ± 3.6 out of 25, respectively, showing no statistically significant difference between the sides (p-value = 0.8336). Nevertheless, this assumption is a limitation of this study.

We assumed the shank and thigh as a single segment, which neglects the relative angle at the knee joint. Literature has shown a minor contribution of the knee joint to the standing balance of able-bodied individuals compared to the ankle and hip joints considered in this study [118]. Despite this, the effect of the knee joint on the movement coordination of individuals with iSCI during quiet standing should be investigated in the future.

5.4.5 Future directions

This study highlights how the integration of the sensory inputs and motor strategies are related and how they are impaired in a group of ambulatory individuals with iSCI (AIS level D). It shows the necessity of evaluating sensory integration in individuals with iSCI and observing how the motor control strategies are affected due to iSCI under different sensory conditions. Sensory integration can be evaluated with various devices (such as the Smart Balance Master™) and also with clinical scales such as the mini BESTest. However, most clinical evaluations do not

specifically characterize ankle and/or hip strategies. This study suggests that a more comprehensive evaluation of balance in individuals with iSCI should assess how motor control strategies are modified following iSCI. We do not know at this point whether these motor control strategies could be improved if therapists train individuals with iSCI under these various sensory conditions. Nevertheless, future studies may use such an objective method to characterize specific impairments and identify underlying causes. Obtained measures may then be used to precisely focus the therapy on underlying causes and track subtle changes in postural control over time. As a future direction, it could be investigated how trunk-leg movement coordination in the iSCI group would change following rehabilitative interventions. In addition, it could provide clinicians with an insight into how adaptive movement strategies affect postural control post-iSCI. Future studies should also investigate postural control strategies post-iSCI in the presence of internally generated or externally applied perturbations as well as during walking in ambulatory individuals with iSCI.

5.5 Conclusion

We presented an assessment of balance control strategy and inter-segment movement coordination for a group of ambulatory individuals with iSCI (AIS level D) compared to age-matched able-bodied participants during standing on hard and foam surfaces with eyes open and closed using only two IMUs. Our observations suggest a similar balance strategy at lower frequencies between iSCI and able-bodied groups. However, we observed a decreased ability post-iSCI in adapting inter-segment coordination between trunk and leg segments changing from ankle strategy to mixed ankle-hip strategy as the sway frequency increases. Using coherence between trunk and leg accelerations, we also showed that alteration of somatosensory inputs may affect trunk-leg movement coordination in both groups. Characterization of trunk-leg movement coordination based on coherence analysis provided a sufficient sensitivity with the discriminatory ability and excellent test-retest reliability to identify changes in balance control strategy in ambulatory individuals with iSCI (AIS level D). Conventional IMU-based balance biomarkers were not able to obtain a similar extent of responsiveness and repeatability. Future studies should investigate the use of our proposed method for objective outcome evaluation of rehabilitative interventions on postural control post-iSCI in a more diverse population.

5.5.1 What is next?

We validated a wearable technology algorithm (Chapter 3) and used it to characterize subtle differences in balance and postural control mechanisms in individuals with mild balance deficits under different sensory conditions (Chapters 4 and 5). However, there is a need for a clinical study to investigate the applicability of the developed algorithm along with the wearable sensors for objective outcome evaluation of balance rehabilitation compared to conventional clinical observational scales in individuals with moderate-to-severe balance impairment. In the next chapter, we used our developed algorithm along with wearable sensors integrated into a clinical functional test to assess its sensitivity and responsiveness for clinical outcome evaluation of balance rehabilitation in elderly individuals with moderate-to-severe balance impairment.

Chapter 6

This chapter shows how the validated algorithm can be integrated into a clinical functional test for the evaluation of rehabilitative interventions using wearable technology in a clinical setting. This chapter has been adopted and/or edited from:

A. Noamani, A. H. Vette, and H. Rouhani, "Instrumented Functional Test for Objective Outcome Evaluation of Balance Rehabilitation in Elderly Fallers: A Clinical Study," Gerontology 2022, doi: 10.1159/000521001.

6 Instrumented Clinical Balance Evaluation

6.1 Introduction

Falls are among the most frequent causes of fatal and non-fatal injuries in the elderly [1], [2]. Up to one-third of seniors fall at least once a year [6], with over 50% of fallers reporting multiple falls [7]. The fall rate among the elderly grows with age [8], making falls the fifth leading cause of death in older adults [9]. Falling is a common concern among community-dwelling elderly, with a prevalence rate of 30% to 85% [249]–[251], which may contribute to declined mental and physical health [156], [249]. Literature has shown that poor postural balance is one of the key indicators of falls in the elderly, and evaluation of balance can help prevent falls by introducing targeted rehabilitative interventions [154]. The ultimate goal of rehabilitative interventions is twofold: (1) preventing future falls and (2) reducing fall severity [8]. Effective interventions could prevent more than half of the potential falls in the elderly population [155]. In this light, it is crucial to not only implement balance assessment methodologies and introduce targeted rehabilitative interventions, but also to evaluate the effectiveness of such interventions to reduce future fall incidences and their adverse consequences among the elderly [1], [8], [156].

Clinicians such as physical therapists commonly use observational assessment methodologies and functional mobility assessment tools to examine static and dynamic stability. Many tests have been validated in clinical settings, such as the Berg Balance Scale (BBS). Although therapists assign a score between 1 to 4 for each BBS task to produce a quantitative measure of balancing ability, the assignment process involves human decision-making.

Accordingly, such human decision-making can introduce subjective error to assigned scores. Therefore, despite such tests being relatively fast and reliable, they tend to be, in part, subjective in nature [157], lack constructs validity, and may not always result in reliable and sensitive outcomes [49]. Moreover, these tests provide little information for understanding potential underlying causes of balance difficulties and for evaluating the effect of therapy on balance performance [16], [35], [36]. These facts highlight the paramount need for a more quantitative objective methodology to evaluate balance when choosing targeted rehabilitative interventions and when performing their objective outcome evaluation [85], [121].

Previous studies have shown a high inverse association between static standing balance and the risk of falling [158], [160]. Standing balance is quantitatively evaluated using balance biomarkers obtained from the displacement of the center-of-pressure (COP) measured by a force platform [241] or the COP estimated via inertial measurement units (IMUs) [76]. In addition, some balance biomarkers have been proposed based on the acceleration of the body's COM measured by an IMU placed on the lower trunk [85]. Previous studies have shown that such quantitative balance biomarkers enable identifying age-related changes in balance and, thus, the risk of falling in the elderly population with high sensitivity and reliability [91], [158]–[160], [241]. Furthermore, the accuracy and efficiency of using IMUs for obtaining such measures have been investigated in the past [76], [91]. However, the capability of IMU-based balance biomarkers compared to functional observational tests for identifying the effect of rehabilitative interventions in objective outcome evaluation is yet to be investigated in a clinical setting. If IMUs show such a capacity besides their user-friendliness and relatively low cost, they can be integrated into point-of-care clinical tests [37], [91] and utilized for routine objective outcome evaluation in clinical research and practice.

Instrumenting functional tests with IMUs, compared to functional observational tests, allows the identification of mild changes in balance by providing quantitative objective measures. Hence, instrumented tests have the potential to provide a precise and sensitive "impairment-level" balance evaluation of how and why functional performance is impaired compared to able-bodied individuals [37]. First, clinicians can use such objective measures to identify balance disorders and determine the underlying causes by comparing balance biomarkers of the patients with balance biomarkers of able-bodied individuals. Second, the therapy can be precisely focused on these underlying causes. Third, therapists can track subtle changes in a patient's balance and follow the

patient's progress over the course of the rehabilitation [37]. Fourth, therapists can objectively evaluate the effectiveness of the introduced interventions by comparing the balance biomarkers pre- and post-rehabilitation. Therefore, the improved and yet impaired aspects of balance can be identified post-rehabilitation. Hence, objective balance biomarkers allow the therapists to characterize and determine intrinsic risk factors post-rehabilitation, whereas functional observational tests only show changes in overall balance. In addition, despite the worldwide increase in the ageing population, there are insufficient healthcare professionals such as physical therapists to identify the elderly with mild balance impairments in a timely manner for implementing early targeted interventions [8]. Therefore, in contrast to the functional tests, the use of IMUs would allow balance evaluation of elderly cohorts in a timelier manner in the clinical settings or even remotely at patients' homes. This enables remote health assessments without requiring the physical presence of healthcare professionals, wherever professional resources are limited [8]. This would facilitate more sensitive outcome evaluation toward the identification of those individuals with higher fall risk, which would lead to more effective targeted rehabilitative interventions.

In this light, this study addresses the growing need for an objective balance assessment of the elderly and an objective outcome evaluation of rehabilitative interventions in clinical settings. Particularly this study aims to investigate the feasibility of using IMUs integrated into the BBS test for identifying, in a clinical setting, the effect of rehabilitative interventions on balance biomarkers in comparison to BBS scores. To achieve this goal, this study: (1) investigates the feasibility of using IMUs for identifying age-related changes of balance biomarkers in in-patient elderly fallers at their admission to the rehabilitation hospital compared to healthy young adults; (2) investigates the effect of rehabilitative interventions on the balance biomarkers by comparing them between admission and discharge test sessions; and (3) compares the objective balance biomarkers with the observational BBS scores recorded by certified physical therapists.

Note that balance biomarkers obtained from the balance test of healthy young adults allow therapists to have a baseline for each biomarker. Significant deviation from the baseline can identify balance difficulty/impairment and can be attributed to underlying causes that depend on the type of biomarker. Additionally, previous studies have used force-plates and IMUs to obtain, respectively, COP-based and acceleration-based balance biomarkers for clinically identifying age-related changes in balance. In the present study, we used IMUs to estimate COP using an algorithm

that we validated in our previous study [76] in a clinical setting. Therefore, we believe that investigating the capability of IMU-derived COP-based balance biomarkers, in addition to acceleration-based biomarkers, for identifying age-related changes is necessary.

We hypothesized that (1) IMU-based balance biomarkers can identify different aspects of impaired balance associated with reduced stability performance, increased control demand, less effective active correction, and reduced inter-segment coordination in senior adults; (2) IMU-based balance biomarkers are capable of identifying subtle changes in the abovementioned aspects of balance due to rehabilitative interventions in senior adults and can be used for objective outcome evaluation to identify the improved and yet impaired aspects of balance in senior adults post-rehabilitation; and (3) IMU-based balance biomarkers enable quantifying balance characteristics that the conventional BBS cannot identify.

6.2 Methods

Table 6-1. **(a)** Demographic information of senior adults, and **(b)** demographic information of young adults.

Senior Adults		
Variable	**Mean ± Standard Deviation**	**Range**
Age [years]	81± 7	67-93
Body mass [kg]	75.5 ± 23.8	46.6-150.0
Body height [cm]	163.4 ± 12.1	136.0-195.0
Falls [#]	3 ± 3	1-10
Sex	Male = 16, Female = 20	
Young adults		
Variable	**Mean ± Standard Deviation**	**Range**
Age [years]	24 ± 3	18-28
Body mass [kg]	69.9 ± 8.3	59.6-87.0
Body height [cm]	175.6 ± 7.0	160.0-184.0
Variable	**Number**	
Sex	Male = 11, Female = 0	

6.2.1 Participants

Thirty-six senior adults were recruited from the in-patient population of the Geriatrics Clinic at the Glenrose Rehabilitation Hospital, Edmonton, Canada (Table 6-1a). The number of participants was determined based on previous studies [141]. Participants with a six-month fall history of at least one fall prior to admission to the hospital were included. Participants were excluded if they had: (1) any neurological impairments (e.g., Parkinson's disease) that affected

their balance other than age-related decline of balance; (2) visual impairments not corrected with glasses; and/or (c) vestibular deficits. In addition, eleven young adults were recruited from the general student population at the University of Alberta, Edmonton, Canada, who participated in our study at the Syncrude Centre for Motion and Balance (SCMB) at the Glenrose Rehabilitation Hospital (Table 6-1b). Ethical approval was obtained from the health research ethics board of the university. Each participant provided written informed consent prior to participation in our study.

6.2.2 Data acquisition

Three IMUs (Physilog®, GaitUp, Switzerland) were placed over the sternum, sacrum, and tibia of the dominant leg of each participant to measure the motion of the trunk, pelvis, and leg, respectively. Each IMU was composed of a tri-axial accelerometer (range: ±11g) and a tri-axial gyroscope (range: ±1200 deg/s). IMUs were placed such that their x-, y-, and z-axes represented the anterior, vertical, and lateral directions, respectively. In cases where the orientation of an IMU did not meet this convention, a calibration function was employed to virtually rotate the channels of the IMU to be in accordance with the described representation. The IMUs recorded the sway of the body segments at a sampling rate of 500 Hz. The recordings were then low-pass filtered via a dual-pass, 8th-order Butterworth filter with a cut-off frequency of 5 Hz. The cut-off frequency of the low-pass filter was chosen based on inspecting the IMU time series' magnitude spectra, with the meaningful frequency content (i.e., the frequency content associated with the motion of the participant) found between 0 and 5 Hz. In agreement with this, previous studies have shown that sway oscillations of standing balance contain frequencies between 0 and 5 Hz [78], [116].

6.2.3 Experimental procedure

Senior adults: After placing the IMUs according to Section 2.2, participants were asked to sit on the edge of a bed with adjustable height. The bed height was adjusted to allow the participant's legs to hang vertically downward without the feet touching the ground. A passive knee flexion-extension task was performed with the help of the experimenter as a functional calibration task to align the IMU frame with the anatomical frame of the tibia (see [252] for details). This functional calibration task was not dependent on the bed height. This method is a calibration procedure that uses the IMU readouts to align the inertial frame of the IMUs with the anatomical frames. The IMUs were first virtually rotated by aligning the vertical axis of the accelerometer with gravity using the first 5 seconds of the IMU readouts during quiet stance. The

leg IMU was then virtually rotated about the vertical axis, such that the x- and z-axes of the IMUs represented the anatomical anterior and lateral directions, respectively. Principal Component Analysis (PCA) was applied to the IMU readouts of the knee flexion-extension task to obtain the rotation matrix that maximized the angular motion about the pitch axis while minimizing motion about the roll axis. Subsequently, participants were asked to perform, at their admission to the Geriatrics Clinic, a series of fourteen tasks according to the BBS test in the presence of a certified physical therapist. Subsequently, they completed a rehabilitation program as in-patients for two to four weeks at the Glenrose Rehabilitation Hospital. The type of rehabilitative intervention used for each patient depended on the underlying cause of impaired balance, as diagnosed by a team of physicians and therapists at the Geriatrics Clinic of the Glenrose Rehabilitation Hospital. Additionally, the length of the rehabilitation program varied between patients and was set by initial balance performance (as quantified by initial BBS scores) and was adjusted according to progress during the program (as determined by physical therapists via observational assessment). After completing their rehabilitation program, participants were asked to once again perform, prior to their discharge from the hospital, the BBS test with the IMUs in the presence of a certified physical therapist. Physical therapists performed their own assessment of each participant's balance in the form of the BBS scores for both admission and discharge test sessions. In addition, they recorded the age, weight, height, dominant leg, and six-month history of falls for each participant. Moreover, the length of the foot and the heights of the ankle, knee, hip, L5-S1 joints and shoulders were measured by a tape measure (from the ground up).

Young adults: The participants were asked to perform a two-minute quiet standing test after placing the IMUs on their body segments according to Section 2.2. They were instructed to maintain a natural standing posture with their feet comfortably apart (at shoulder width) while looking straight ahead, similar to task 2 of the BBS. Participants also performed a knee flexion-extension task while seated at the edge of a seat as a functional calibration task.

6.2.4 Human body modelling

We modelled the human body with four rigid links representing trunk, pelvis, legs, and feet segments, connected to each other by 3D revolute joints (Figure 6-1). The inter-segment joints represent the L5-S1, hip, and ankle joints. The feet were assumed stationary during quiet standing. We estimated the body segment parameters, including the length, mass, COM, joint centers of rotation, and moments of inertia of each segment using the participant's weight and height [223].

The lengths of the segments were directly measured for the senior adults, as explained in Section 2.3, to avoid any uncertainties associated with ageing.

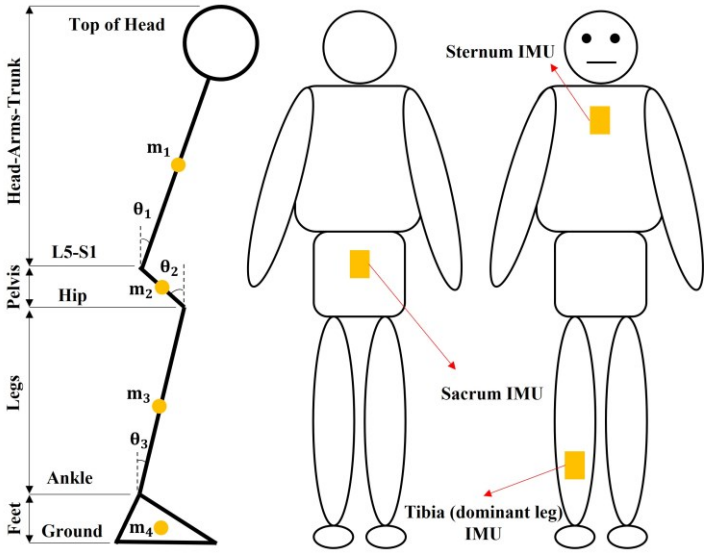

Figure 6-1. Location of the inertial measurement units (IMUs) on the body. The human body is modelled as a system with three rigid link segments connected to each other by 3D revolute joints representing trunk, pelvis, and leg segments. Feet were assumed to be motionless during quiet standing. IMUs were used to estimate the orientation of the trunk, pelvis, and leg segments.

We implemented a custom-built MATLAB (MathWorks, USA) program to estimate the joint moments at the L5-S1, hip, and ankle joints using a top-down inverse dynamics approach. Subsequently, we estimated the COP positions in the anterior-posterior (AP) and medial-lateral (ML) directions according to our previous study [76]. The segments' orientation was calculated by aligning the accelerometers' vertical axis with gravity during quiet standing [225], [227]. We obtained the instantaneous position of the COM, linear/angular velocity and acceleration of each segment based on its instantaneous orientation.

6.2.5 Outcome measures and statistical data analysis

For the senior adults, we extracted the IMUs' recording during the two-minute quiet standing task (task 2 of BBS) to calculate conventional balance biomarkers for both admission and discharge test sessions. We only used IMU recordings during the two-minute quiet standing task (i.e., task 2 of BBS) to calculate conventional balance biomarkers for the admission and discharge test sessions. Although balance biomarkers for the other BBS tasks could provide additional information on balance performance, the use of the IMU recordings for these tasks for calculating balance biomarkers might not be reliable due to the short task and thus recording duration (i.e.,

less than 30 seconds). Our preliminary investigation demonstrated that a minimum test duration of 30 seconds is required for reliable balance evaluation using most IMU-based biomarkers. Moreover, the minimum required test duration can increase to 120 seconds for some COM acceleration-based balance biomarkers. Therefore, calculating the balance biomarkers for other BBS tasks would require increasing the task duration, which would negatively impact the integration of IMUs into conventional BBS tests used in clinical settings.

We used conventional balance biomarkers to identify age-related changes and the effect of rehabilitation on the balance performance of senior adults compared to young adults. For each trial and each group of participants, we calculated a total of ten COP-based measures [241], thirteen COM acceleration-based measures [85], and two inter-segment coordination measures [78], [87] (see Table 6-2). COP- and COM acceleration-based measures were grouped into time-domain (i.e., distance, area, and hybrid) measures and frequency-domain measures [85], [241]. These measures are commonly used to study: (1) standing balance performance; (2) the control demand and active postural corrections during standing balance; and (3) postural regulations during standing balance [242]. Furthermore, we used the Magnitude-Squared Coherence (MSC) at lower ($f \leq 1$ Hz) and higher ($f > 1$ Hz) sway frequencies between the acceleration of the trunk-leg segments and the pelvis-leg segments to identify changes in inter-segment coordination [78]. Previous studies [78], [116], [136] demonstrated that, in healthy young adults, the trunk/pelvis and leg move in an in-phase manner at lower sway frequencies ($f \leq 1$ Hz), reflecting the domination of the ankle strategy during low sway oscillations. As the sway frequency increases above 1 Hz, the trunk/pelvis and leg movements show anti-phase coordination, reflecting a mixed ankle-hip strategy during larger sway oscillations [78], [116]. An MSC of 1 indicates a perfect in-phase inter-segment coordination, whereas a smaller MSC reflects a lower degree of in-phase inter-segment coordination [116].

First, we used the Wilcoxon rank-sum test to identify any age-related changes in the balance biomarkers of the senior adults compared to the young adults. Second, we used the Wilcoxon signed rank test to identify any differences between the balance biomarkers of the senior adults at their admission and discharge test sessions. This allowed us to identify the effect of rehabilitative interventions on the balance performance of senior adults. Third, we used Spearman's correlation test between the BBS total scores provided by the physical therapists and each balance biomarker. This allowed us to investigate any association between the BBS, as a

subjective functional test, and the objective balance biomarkers obtained by IMUs. Note that statistical comparisons between groups were conducted for each balance biomarker separately with a significance level of 0.05. We did not perform multiple comparisons and did not extend our conclusions to a group of biomarkers.

Table 6-2. List of balance biomarkers obtained using IMUs: center-of-pressure (COP) measures, center-of-mass (COM) acceleration-based measures, and inter-segment coordination measures.

Outcome Measure	Nomenclature	Type
Root-Mean-Square Distance	RDIST	Time-domain distance measures (calculated for both COP and COM-acceleration)
Mean Distance	MDIST	
Total Excursion	TOTEX	
Mean Velocity	MVELO	
95% Confidence Ellipse Area	Area-CE	Time-domain area measure (calculated for both COP and COM-acceleration)
Sway Area	Area-SW	Time-domain hybrid measures (calculated for both COP and COM-acceleration)
Mean Frequency	MFREQ	
Median Frequency	MEDFREQ	Frequency-domain measures (calculated for both COP and COM-acceleration)
Centroid Frequency	CFREQ	
Frequency Dispersion	FREQD	
ISway Sway jerkiness	JERK	Calculated for only COM-acceleration measures
ISway Root-Mean-Square Acceleration	RMS-ACC	
ISway Centroid Frequency	CF-ACC	
Mean Magnitude-Squared Coherence ($f \leq 1$ Hz)	MSC	Inter-segment coordination
Mean Magnitude-Squared Coherence ($f > 1$ Hz)		

6.3 Results

6.3.1 Senior adults versus young adults

All COP-based measures were able to distinguish the balance performance of senior adults from that of young adults (Table 6-3). Senior adults showed significantly higher COP time-domain distance, area, and hybrid measures in AP and ML directions ($P < 0.05$). This trend was also observed for the time-domain measures obtained based on the resultant distance (RD) of COP (Table 6-3). We also observed significant differences between the senior and young adults for the frequency-domain measures of COP in AP, ML, and RD directions (Table 6-3, $P < 0.05$).

Time-domain distance measures of COM acceleration in AP, ML, and RD directions were significantly higher for the senior adults compared to the young adults (Table 6-4, $P < 0.05$). COM acceleration Area-CE and Area-SW were significantly higher for the senior adults. Among the frequency-domain measures of COM acceleration, only AP-MEDFREQ and RD-MEDFREQ were significantly different between the two groups. We observed a significantly reduced degree of anti-

phase coordination between the body segments in senior adults compared to young adults (Table 6-5, $P < 0.05$). Particularly, we observed significant differences between the two groups for trunk-leg MSC at lower sway oscillations ($f \leq 1$ Hz) and pelvis-leg MSC and trunk-leg MSC at higher sway oscillations ($f > 1$ Hz).

Table 6-3. Center of pressure (COP) measures of standing balance presented as resultant distance (RD), in anterior-posterior (AP) direction, and in medial-lateral (ML) direction. Results are presented as [25% 50% 75%] percentiles for the senior adults at their admission and discharge test sessions and for the young adults. Bold numbers show significant differences ($P < 0.05$). P-values less than 0.0001 were equated to 0.

	COP Measures	Senior Adults (Admission)	Senior Adults (Discharge)	Young Adults	P (Admission vs. Discharge)	P (Senior Admission vs. Young Adults)
RD	**RDIST**	[0.014, 0.017, 0.022]	[0.013, 0.017, 0.023]	[0.007, 0.009, 0.011]	0.561	**0.0004**
	MDIST	[0.012, 0.015, 0.02]	[0.011, 0.014, 0.019]	[0.006, 0.008, 0.01]	0.6151	**0.0005**
	TOTEX	[8.043, 11.781, 16.889]	[8.072, 10.156, 13.577]	[5.257, 5.82, 7.252]	0.4699	**0.0004**
	MVELO	[0.08, 0.118, 0.164]	[0.08, 0.1, 0.138]	[0.029, 0.03, 0.036]	0.3459	**0**
	Area-CE	[0.001, 0.002, 0.005]	[0.001, 0.002, 0.003]	[0, 0.001, 0.001]	0.3223	**0.0008**
	Area-SW	[0, 0.001, 0.001]	[0, 0, 0.001]	[0, 0, 0]	0.4321	**0**
	MFREQ	[1.004, 1.259, 1.571]	[0.891, 1.168, 1.501]	[0.515, 0.673, 0.948]	0.162	**0.0002**
	MEDFREQ	[0.003, 0.004, 0.004]	[0.003, 0.003, 0.004]	[0.002, 0.002, 0.002]	0.4321	**0**
	CFREQ	[0.786, 1.137, 1.347]	[0.886, 1.063, 1.238]	[0.475, 0.595, 0.856]	0.4699	**0.0048**
	FREQD	[0.944, 0.953, 0.962]	[0.943, 0.952, 0.969]	[0.975, 0.985, 0.992]	0.561	**0.0001**
AP	**RDIST**	[0.012, 0.014, 0.019]	[0.011, 0.014, 0.02]	[0.005, 0.006, 0.01]	0.7534	**0.0005**
	MDIST	[0.009, 0.01, 0.014]	[0.009, 0.01, 0.015]	[0.004, 0.004, 0.008]	0.9124	**0.0009**
	TOTEX	[6.058, 8.682, 12.586]	[5.626, 7.984, 9.708]	[3.667, 3.983, 5.527]	0.9249	**0.0003**
	MVELO	[0.061, 0.088, 0.137]	[0.056, 0.08, 0.097]	[0.02, 0.02, 0.028]	0.4796	**0**
	MFREQ	[0.94, 1.327, 1.66]	[0.869, 1.107, 1.458]	[0.456, 0.729, 0.886]	0.0758	**0.0006**
	MEDFREQ	[0.081, 0.29, 0.667]	[0.089, 0.303, 0.415]	[0.011, 0.037, 0.077]	0.144	**0.0012**
	CFREQ	[1.251, 1.665, 2.071]	[1.299, 1.441, 1.817]	[0.828, 0.979, 1.262]	0.1869	**0.004**
	FREQD	[0.797, 0.846, 0.932]	[0.805, 0.857, 0.909]	[0.912, 0.968, 0.986]	0.6714	**0.0012**
ML	**RDIST**	[0.007, 0.009, 0.013]	[0.007, 0.008, 0.011]	[0.004, 0.005, 0.007]	0.3459	**0.0006**
	MDIST	[0.005, 0.007, 0.01]	[0.005, 0.007, 0.008]	[0.003, 0.003, 0.005]	0.414	**0.0006**
	TOTEX	[4.158, 5.214, 7.196]	[3.97, 4.902, 7.212]	[3.038, 3.407, 3.885]	0.4414	**0.0006**
	MVELO	[0.041, 0.053, 0.072]	[0.039, 0.049, 0.072]	[0.016, 0.018, 0.02]	0.3622	**0**
	MFREQ	[1.05, 1.257, 1.538]	[1.007, 1.312, 1.639]	[0.558, 0.711, 1.021]	0.5824	**0.0012**
	MEDFREQ	[0.092, 0.286, 0.58]	[0.117, 0.325, 0.619]	[0.012, 0.025, 0.149]	0.8015	**0.001**
	CFREQ	[1.209, 1.543, 1.876]	[1.249, 1.532, 1.884]	[0.785, 1.026, 1.326]	0.4321	**0.0036**
	FREQD	[0.811, 0.85, 0.897]	[0.784, 0.843, 0.913]	[0.906, 0.952, 0.977]	0.9374	**0.0004**

Table 6-4. Center of mass (COM) acceleration measures of balance presented as resultant distance (RD), in anterior-posterior (AP) direction, in medial-lateral (ML) direction, and ISway measures [85]. Results are presented as [25% 50% 75%] percentiles for the senior adults at their admission and discharge test sessions and for the young adults. Bold numbers show significant differences ($P < 0.05$). P-values less than 0.0001 were equated to 0.

	COM Measures	Senior Adults (Admission)	Senior Adults (Discharge)	Young Adults	P (Admission vs. Discharge)	P (Senior Admission vs. Young Adults)
RD	**RDIST**	[0.153, 0.187, 0.258]	[0.139, 0.202, 0.281]	[0.091, 0.098, 0.117]	0.8137	**0.0001**
	MDIST	[0.131, 0.156, 0.202]	[0.119, 0.168, 0.225]	[0.075, 0.087, 0.089]	0.9499	**0**
	TOTEX	[52.612, 60.822, 83.616]	[50.743, 59.056, 71.626]	[73.139, 76.55, 97.23]	0.0758	**0.013**
	MVELO	[0.537, 0.624, 0.851]	[0.495, 0.6, 0.685]	[0.386, 0.408, 0.489]	**0.0247**	**0.0001**
	Area-CE	[0.111, 0.177, 0.351]	[0.102, 0.155, 0.258]	[0.033, 0.049, 0.156]	0.3379	**0.0094**
	Area-SW	[0.025, 0.035, 0.051]	[0.023, 0.031, 0.048]	[0.01, 0.012, 0.014]	0.4321	**0.0003**
	MFREQ	[0.472, 0.652, 0.875]	[0.444, 0.599, 0.806]	[0.693, 0.881, 1.002]	0.0868	0.0716
	MEDFREQ	[0.003, 0.004, 0.004]	[0.003, 0.004, 0.004]	[0.002, 0.002, 0.002]	0.414	**0.0003**
	CFREQ	[0.484, 0.642, 0.818]	[0.437, 0.561, 0.795]	[0.52, 0.689, 0.806]	0.2204	0.5232
	FREQD	[0.963, 0.977, 0.985]	[0.97, 0.976, 0.985]	[0.968, 0.98, 0.983]	0.7296	0.8094
AP	**RDIST**	[0.131, 0.172, 0.206]	[0.125, 0.185, 0.261]	[0.08, 0.086, 0.102]	0.6714	**0**
	MDIST	[0.106, 0.126, 0.158]	[0.1, 0.152, 0.205]	[0.055, 0.068, 0.081]	0.3705	**0**
	TOTEX	[35.265, 38.08, 48.523]	[34.287, 38.044, 44.04]	[43.539, 46.838, 57.381]	0.3459	**0.0241**
	MVELO	[0.353, 0.385, 0.489]	[0.342, 0.374, 0.439]	[0.228, 0.249, 0.287]	0.0868	**0.0001**
	MFREQ	[0.357, 0.496, 0.667]	[0.306, 0.425, 0.596]	[0.522, 0.577, 0.774]	0.0615	0.1601
	MEDFREQ	[0.029, 0.078, 0.117]	[0.021, 0.045, 0.069]	[0.01, 0.015, 0.043]	0.0928	**0.013**
	CFREQ	[0.665, 0.933, 1.18]	[0.689, 1.07, 1.525]	[0.619, 0.811, 1.171]	0.3223	0.6601
	FREQD	[0.922, 0.953, 0.983]	[0.944, 0.971, 0.991]	[0.935, 0.969, 0.983]	0.1315	0.7875
ML	**RDIST**	[0.056, 0.073, 0.101]	[0.049, 0.063, 0.074]	[0.033, 0.038, 0.061]	**0.0353**	**0.0067**
	MDIST	[0.044, 0.057, 0.08]	[0.038, 0.05, 0.06]	[0.026, 0.029, 0.045]	**0.0278**	**0.0014**
	TOTEX	[34.384, 39.094, 47.191]	[30.727, 37.049, 42.201]	[48.36, 53.037, 62.246]	0.0553	**0.0048**
	MVELO	[0.344, 0.391, 0.482]	[0.306, 0.369, 0.42]	[0.254, 0.278, 0.318]	**0.0218**	**0.0009**
	MFREQ	[0.837, 1.055, 1.616]	[1.031, 1.224, 1.6]	[0.998, 1.461, 1.834]	0.4414	0.1967
	MEDFREQ	[0.035, 0.093, 0.34]	[0.086, 0.144, 0.282]	[0.031, 0.077, 0.49]	0.9124	0.6601
	CFREQ	[1.121, 1.528, 2.049]	[1.288, 1.635, 2.058]	[1.499, 1.765, 1.897]	0.5297	0.4869
	FREQD	[0.834, 0.9, 0.949]	[0.817, 0.871, 0.91]	[0.841, 0.865, 0.896]	0.3875	0.5049
ISway	**JERK**	[0.045, 0.06, 0.116]	[0.036, 0.054, 0.08]	[0.037, 0.043, 0.065]	0.1162	0.3003
	RMS-ACC	[0.201, 0.266, 0.366]	[0.189, 0.289, 0.421]	[0.112, 0.174, 0.188]	0.7894	**0.001**
	CF-ACC	[0.377, 0.497, 0.671]	[0.405, 0.502, 0.605]	[0.342, 0.508, 0.648]	0.8876	0.7875

6.3.2 Senior adults: admission versus discharge

The BBS total score significantly increased between admission and discharge test sessions (Figure 6-2A and Figure 6-21B). BBS scores for each BBS task and participant at both the admission and discharge test sessions are provided in Supp Table 3 in *Supplementary Material*.

Although the COP measures and inter-segment coordination improved after rehabilitation, their changes were not significant between the admission and discharge test sessions (Table 6-3

and Table 6-5). Nevertheless, COM acceleration RD-MVELO, ML-RDIST, ML-MDIST, and ML-MVELO were significantly improved after receiving therapy (Table 6-4).

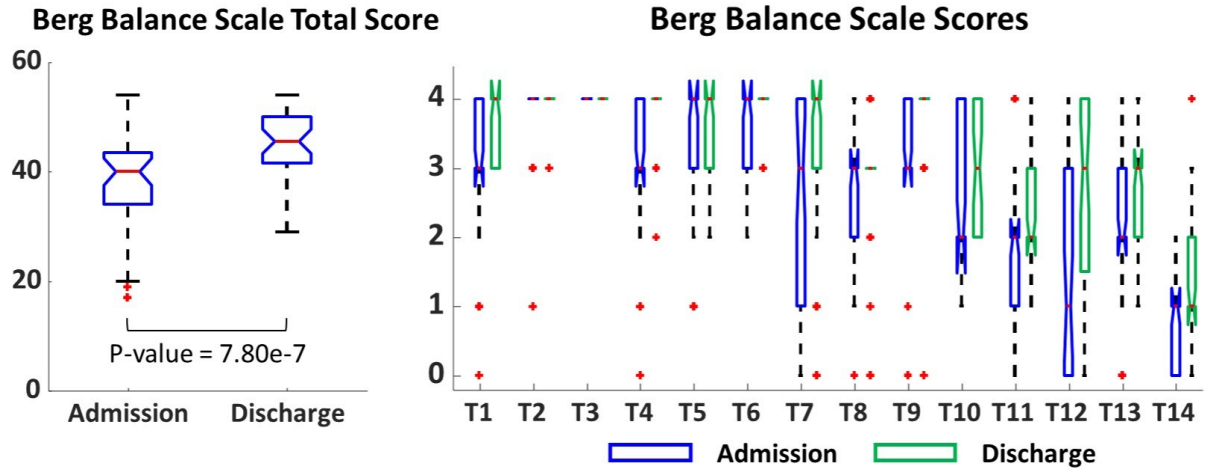

Figure 6-2. **(A)** The Berg Balance Scale total score (out of 56) was recorded by certified physical therapists for the senior adults at their admission and at their discharge test sessions. **(B)** The Berg Balance Scale scores (out of 4) for each task (T1 to T14) were reported by certified physical therapists for the senior adults at their admission (blue) and at their discharge (green) test sessions.

Table 6-5. Inter-segment coordination measures of standing balance are presented as mean Magnitude-Squared Coherence (MSC). Results are presented as [25% 50% 75%] percentiles for the senior adults at their admission and discharge test sessions and for the young adults. Bold numbers show significant differences ($P < 0.05$). P-values less than 0.0001 were equated to 0.

Inter-segment Coordination Measures	Senior Adults (Admission)	Senior Adults (Discharge)	Young Adults
Pelvis-Leg MSC (f ≤ 1 Hz)	[0.746, 0.777, 0.789]	[0.745, 0.775, 0.795]	[0.78, 0.791, 0.798]
Trunk-Leg MSC (f ≤ 1 Hz)	[0.649, 0.696, 0.726]	[0.64, 0.685, 0.711]	[0.706, 0.743, 0.768]
Pelvis-Leg MSC (f > 1 Hz)	[0.117, 0.23, 0.411]	[0.141, 0.218, 0.325]	[0.05, 0.059, 0.064]
Trunk-Leg MSC (f > 1 Hz)	[0.105, 0.186, 0.291]	[0.097, 0.15, 0.236]	[0.038, 0.04, 0.049]

P (Admission vs. Discharge)	P (Senior Admission vs. Young Adults)	[ρ, P] (IMUs vs. BBS Admission)	[ρ, P] (IMUs vs. BBS Discharge)
0.6096	0.0715	[-0.2, 0.2344]	[-0.01, 0.9359]
0.3944	**0.03**	[-0.08, 0.6388]	[0.25, 0.1395]
0.5824	**0**	**[-0.37, 0.0283]**	**[-0.55, 0.0005]**
0.2418	**0**	[-0.29, 0.0876]	**[-0.52, 0.001]**

6.3.3 Balance biomarkers obtained by IMUs versus BBS

We observed a significant Spearman's correlation between the BBS total score and the pelvis-leg MSC at high sway oscillations at both admission (ρ = -0.55, $P < 0.05$) and discharge (ρ

= -0.37, $P < 0.05$) test sessions: BBS total score was negatively correlated with pelvis-leg MSC at high sway oscillations. The correlations between the BBS total score and other balance biomarkers were not significant.

The Spearman's correlation between each IMU-based balance biomarker and each BBS task score, as well as BBS total score for both the admission and discharge test sessions, are provided in Supp Table 4, Supp Table 5, and Supp Table 6 of the *Supplementary Material*. Spearman's correlation test did not show a significant correlation between each BBS task score and each balance biomarker. The effect sizes between balance biomarkers at the admission and discharge test sessions are reported in Supp Table 7 of the *Supplementary Material*.

6.4 Discussion

This study shows the capability of an instrumented BBS test with IMUs for identifying several aspects of balance impairment in senior adults and for objective outcome evaluation of the rehabilitative interventions in geriatrics clinics. To this end, first, we used the balance biomarkers for identifying age-related changes in elderly fallers. Second, we evaluated the effect of rehabilitation on the balance biomarkers in senior adults by comparing them between the admission and discharge test sessions. Third, we investigated the association between the balance biomarkers obtained from the IMUs and the observational BBS scores recorded by certified physical therapists. Standing balance may be investigated for three different aspects: (1) balance performance; (2) control demand and active postural corrections; and (3) postural regulations [101]. Time-domain distance and area measures quantify balance performance [102], [242]. In addition, velocity measures quantify the attentional resources required to maintain balance, which indicates the control demand and degree of active postural corrections [101], [242]. Finally, frequency-domain measures provide information about postural regulation and any disturbances caused by neurological deficits [43], [109], [243]. Hence, impaired balance can be diagnosed via reduced balance performance, increased control demand, and reduced postural regulation.

6.4.1 Senior adults versus young adults: age-related changes

We observed significantly higher COP and COM acceleration time-domain distance and area measures in seniors compared to young adults. Poor balance performance in senior adults

highlights declined static balance and, thus, may imply a higher risk of falling [158], [160]. This may indicate the lower effectiveness of the postural regulatory mechanisms associated with ageing. We also observed increased AP-, ML-, and RD-MVELO of both COP and COM acceleration measures in senior adults. A higher MVELO could be associated with a higher control demand. The literature has shown that slow and less reliable postural reflexes in senior adults could not appropriately respond to voluntary sway demands [160]. Moreover, increased COP hybrid measures in all directions and increased COM acceleration hybrid sway area may highlight reduced stability and a greater need for attentional resources.

We observed that frequency-domain measures obtained using COP are more sensitive to detecting age-related changes compared to those obtained using COM acceleration. MEDFREQ has been shown to be an indicator of the contribution of the sensory inputs to balance and preferential postural regulation [101], [242]. This could suggest difficulty in integrating sensory information in closed-loop control of balance due to ageing [160]. COP CFREQ could reflect the time required for the body to return to its initial position [43]. Our results may imply that ageing could cause latency and, thus, increase the response time. Reduced COP FREQD may also suggest a rigidity and stiffness of the body in senior adults compared to young adults during quiet standing [242].

We observed reduced inter-segment coordination in senior adults, which may lead to a greater body sway in this population. Trunk-leg MSC at lower sway frequencies ($f \leq 1$ Hz) was significantly reduced in senior adults. This reflects a reduced degree of in-phase action between trunk and leg at lower sway oscillations resulting in an impaired ankle strategy. As we expected, pelvis-leg and trunk-leg MSC reduced as sway frequency increased from 1.0 to 5.0 Hz in both populations. This shows the transition from the ankle strategy to the ankle-hip strategy at higher frequencies [116], [136]. Nevertheless, senior adults showed significantly larger MSC at higher frequencies compared to young adults, which may indicate less ability to adapt their inter-segment coordination from the ankle strategy to the ankle-hip strategy at higher sway oscillations ($f > 1$ Hz).

In summary, IMU-based balance biomarkers, in contrast to observational clinical tests, could potentially objectively diagnose different aspects of impaired balance with high sensitivity. Such quantitative measures could be essential for implementing targeted interventions, which may lead to achieving a higher rehabilitation efficacy.

6.4.2 Senior adults at admission versus discharge: effect of rehabilitation

Although all COP measures tended to improve post-rehabilitation, we observed no statistical significance ($P > 0.05$). Among the COM acceleration measures, only RDIST, MDIST, and MVELO in ML direction significantly improved. These results imply that rehabilitative interventions resulted in a reduced sway acceleration and sway jerkiness in the ML direction. However, the body sway displacement and velocity were not significantly reduced post-rehabilitation as indicated by COP measures. Reduced jerkiness in the ML direction may indicate a more effective active correction made by the central nervous system against body sway. The literature showed that balance biomarkers in the ML direction, including ML-RDIST, ML-MDIST, and ML-MVELO, are the best distinguisher between future fallers and non-fallers in senior adults [160]. Therefore, our results objectively may show a potentially reduced risk of future falls among our participants post-rehabilitation. Previous studies have suggested that IMUs provide impairment-level measures that characterize the functional performance of balance with increased sensitivity to not only movement disorders but also rehabilitation and mild changes in postural stability [24], [27]. In agreement with these studies, the results of the present study highlighted the capability of IMUs in identifying subtle changes to balance due to rehabilitative interventions in senior adults. Such objective outcome evaluation allows the physical therapist to identify the improved and yet impaired aspects of balance post-rehabilitation in senior adults. Although a reduced jerkiness in the ML direction implies reduced future fall risk, high sway displacement and velocity in senior adults still reflect high intrinsic risk factors in this population. This conclusion could only be achieved by objective outcome evaluation using IMUs, rather than only the BBS assessment. This implies the importance of quantitative evaluation of rehabilitation efficacy using IMUs, as an add-on to the BBS assessment procedure without the need to complete separate tests.

High body sway post-rehabilitation could be attributed to reduced cutaneous sensation, decreased proprioception, impaired joint receptors, and visual impairment due to ageing, which would affect the contribution of sensory inputs to postural control [160]. Consequently, compensatory reactions for reducing body sway would be delayed due to the reduced ability to sense the COP displacement under the feet [160] and a faulty internal map of stability limits [126]. Furthermore, previous studies have shown that muscle strength declines due to atrophy associated with ageing (e.g., dorsiflexion weakness due to reduced ankle muscle strength) [160]. The presence

of muscle weakness may also contribute to high body sway after therapy. Nevertheless, the reduced distance and velocity measures of COM acceleration in the ML direction may imply better sway control post-rehabilitation. Inter-segment coordination did not significantly improve post-rehabilitation. This suggests that therapy may not eliminate the difficulty in adapting from ankle strategy to ankle-hip strategy in senior adults. Therefore, a lack of reciprocal action between the body segments may be a factor contributing to high body sway displacement post-rehabilitation. This fact highlights the need for a more targeted intervention aimed at improving the underlying causes of impaired balance, such as inter-segment coordination.

Note, although most COP-based and COM acceleration-based measures did not significantly improve after rehabilitation, such minor improvement in many biomarkers could lead to an overall improvement in balance performance post-rehabilitation. Such objective outcome evaluation and interpretations allow therapists to understand the extent of improvement in different aspects of balance post-rehabilitation. Hence, they will be able to determine the efficacy of retrospective treatments and implement prospective interventions, targeting less-improved aspects of balance.

6.4.3 IMU-based balance biomarkers versus BBS

The BBS total scores pre- and post-rehabilitation were [34, 40, 43.5] and [41.5, 45.5, 50], respectively, as [25%, 50%, 75%] percentiles. O'Sullivan et al. [144] reported BBS total scores of 44.2 ± 6.2 and 49.8 ± 6.2 for elderly fallers and non-fallers, respectively. Ghahramani et al. [171] reported BBS total scores of 52.2 ± 2.2, 51.1 ± 2.1, and 49.9 ± 4.0 for non-fallers, once-faller, and multiple-fallers, respectively. This suggests that the BBS scores reported in this study were within the range of the scores reported in the literature for similar populations of elderly fallers. The BBS total score showed a significant balance improvement post-rehabilitation in the senior adults. Among the balance biomarkers, only MSC ($f > 1$ Hz) had significant Spearman's correlation with BBS total score for both the admission ($\rho = -0.55$, $P < 0.05$) and discharge ($\rho = -0.37$, $P < 0.05$) test sessions. This result may show that a higher BBS total score at discharge could be attributed to better inter-segment coordination. We previously have shown the high reliability of MSC in identifying balance impairments in different test conditions in patients with impaired balance [78]. We did not observe any significant Spearman's correlation between other balance biomarkers and BBS total score nor between each balance biomarker and each BBS task score at both admission and discharge test sessions (see *Supplementary Material*). This observation implies a lack of

association between BBS and IMU-based balance biomarkers. Such lack of association between BBS and balance biomarkers, along with previous studies supporting the capability of IMU-based balance biomarkers in identifying subtle changes in the balance due to rehabilitation stability [24], [27] suggest that IMU-based balance biomarkers may be able to quantify balance characteristics that BBS alone cannot simply identify and characterize. For instance, comparing BBS total scores at admission and discharge test sessions indicates a significantly reduced fall risk. By contrast, balance biomarkers obtained using IMUs during the BBS test suggested that only sway jerkiness in ML direction improved after therapy while body sway and inter-segment coordination were not significantly improved. Such an advantage highlights the capability of the IMU-based balance biomarkers, in addition to the BBS, to identify different aspects of balance characteristics and underlying risk factors post-therapy that are not easily observable via BBS. Such an additional advantage may lead to increased efficacy of rehabilitation outcome evaluation. On the other hand, postural control is a complex task that is regulated via the integration of sensory information and the interaction of the body with a dynamic environment [29]. Therefore, it is likely that many non-significant improvements in COP-based and COM acceleration-based balance biomarkers would have led to an overall improvement in balance performance as captured by BBS scores. Therefore, the use of IMUs integrated into BBS is recommended since they may characterize different aspects of balance that may be ignored when each method is employed separately.

Nevertheless, although the BBS is a useful and practical clinical test for balance evaluation, it may not be able to provide all the detailed information needed to identify all the aspects of impaired balance and all the underlying causes of impaired balance pre-rehabilitation. Therefore, the little information provided by the BBS scores may limit therapists' ability to introduce targeted interventions focusing on underlying causes of impairment. In addition, the BBS does not provide objective outcome evaluation regarding the efficacy of the rehabilitation and its effect on different aspects of balance. Particularly, the BBS could only show the overall changes in balance post-rehabilitation and not the improved and yet impaired aspect of balance. Therefore, BBS may not be able to characterize risk factors associated with remaining impaired aspects of balance after rehabilitation. By contrast, the efficacy of the rehabilitation, as well as post-therapy fall risk factors and their underlying causes, could be identified by the instrumented balance evaluation.

Furthermore, the BBS tends to be, in part, subjective in nature due to the involvement of human opinion in score assignment, whereas IMUs enable objective balance evaluation with a

high sensitivity to subtle changes. The subjectivity of the BBS could also contribute to a lack of association between the BBS total scores and balance biomarkers. One possible explanation could be the effect of inter-rater variability on the BBS scores since multiple physical therapists were involved in this study which further shows the necessity of using an objective instrumented approach.

In addition, the use of IMUs may allow for a faster balance assessment in large cohorts in clinical settings as they used data from only two minutes of quiet standing rather than several tasks performed to obtain the BBS score. This is particularly important due to the worldwide increase in the ageing population and insufficient healthcare resources to identify high-risk fallers in a timely manner for implementing more effective early interventions. Early diagnosis of balance impairments, introducing targeted interventions, and objective outcome evaluation of balance performance after rehabilitation for senior adults can significantly reduce future fall incidences and prolonged complications of fall-related injuries and their impact on the healthcare systems.

In summary, an instrumented BBS test may provide physical therapists with a more sensitive objective balance assessment tool. Therefore, a preventative intervention can be precisely focused on the underlying causes of impaired balance, and therapists can follow the patient's progress over time, evaluate the efficacy of the retrospective interventions on different aspects of balance, and introduce prospective interventions to reduce post-rehabilitation fall incidences [37].

6.4.4 Clinical relevance and translation of IMU-based balance biomarkers

Identifying IMU-based balance biomarkers of standing balance does not necessarily mean that they can be addressed clinically. Extensive research is required to determine the clinical relevance of a variety of IMU-based balance biomarkers in individuals with different underlying impairments. However, in the present study, we only focused on balance biomarkers with proven clinical relevance in the literature. Previous studies [37], [49], [253] have provided the clinical relevance of conventional balance biomarkers used in the present study to evaluate the balance of individuals with different conditions. Nevertheless, introducing new biomarkers requires extensive clinical research to determine their clinical value.

In addition, Horak et al. [37] discussed the potential impact of conventional IMU-based balance biomarkers for clinical balance assessment and the development of guided rehabilitative interventions for improving balance in the elderly as well as individuals with Parkinson's disease.

They have suggested [37], [49] that such balance measures can provide clinically-relevant characterizations on how and why balance is impaired with increased sensitivity to mild impairments and change with rehabilitation compared to clinical functional tests. They also suggested that instrumenting clinical functional tests with IMUs adds a multitude of balance characteristics to what functional tests alone can provide [37], [49]. For example, BBS measures whether an individual can accomplish a task; however, the addition of IMUs provides an objective measure of the level of impairment [37].

It is critical for therapists to fully understand the advantages and limitations of emerging balance assessment technologies when translating them into clinical practice. Therefore, translating balance assessment technologies into clinical settings requires the involvement of physical therapists in the process of developing methodologies to promote technologies that are valid, sensitive, and responsive enough for clinical practice. The literature suggests that therapists are interested in balance biomarkers that have been validated against gold-standard references and are associated with clinically-relevant outcomes such as fall risk and severity of impairment [37]. The therapists require assessment technologies that are easy to use while providing quick and meaningful reports for both referring physicians and their patients. Such technologies must demonstrate sensitivity to the quality of balance such that patients with a high level of balance performance can enhance their function or prevent a decline in function. In addition, they must reflect information regarding the severity of impairment that can guide interventions while being responsive to the changes [37]. As assessment technologies become more accessible, companies developing such technologies must engage and communicate with physical therapists to better understand the clinical needs and direct their resources toward addressing the abovementioned concerns regarding sensitivity, validity, and responsiveness.

6.4.5 Limitations

The data used in this study were collected from a relatively small population of senior adults and a small population of young adults. Utilizing IMUs for balance evaluation in a large cohort can shed light on the feasibility of the instrumented BBS in clinical practice on a large scale. In-patient senior adults received personalized rehabilitation programs. The type and length of the program were tailored for each patient based on the impact of patient-specific medical conditions on initial balance performance and on progress over the course of the program. Information on the type of rehabilitation interventions that each patient received was not available to the authors due

to the patients' privacy policy. Future studies should determine the sensitivity of instrumented tests for identifying changes in balance biomarkers due to unique rehabilitation programs among in-patient senior adults in clinical settings. The methodologies of such studies would require the stratification of patients into groups with similar stability performance and similar impairments. Finally, we did not record prospective falls in this study. Recording fall incidences after discharge would enable identifying the best predictors of future falls among balance biomarkers and BBS scores.

6.5 Conclusion

In the present study, we provided a balance evaluation of senior adults pre- and post-rehabilitation in a clinical setting using both the BBS and balance biomarkers obtained using IMUs during quiet standing. COP time-domain and frequency-domain measures, COM acceleration time-domain measures, and inter-segment coordination measures were able to identify age-related changes in the balance of senior adults compared to young adults. Particularly, the instrumenting BBS test with IMUs allowed for objective outcome evaluation of rehabilitative interventions with high sensitivity to subtle changes in balance without a significant increase in assessment time. Objective balance assessment showed that rehabilitation improved efforts for active postural correction in the elderly while it could not improve sway displacement/velocity. Therefore, balance biomarkers may enable characterizing underlying causes of impaired balance and may allow identifying the improved and yet impaired aspects of balance post-rehabilitation. Hence, they may be appropriate to characterize risk factors post-rehabilitation for elderly fallers; however, BBS scores may only show changes in overall balance. Therefore, we recommend the use of IMUs along with the BBS test in clinical environments. Note that information on the type of rehabilitation interventions that each patient received was not available to the authors. Therefore, it was not possible to investigate the capability of IMU-based balance biomarkers for evaluating the efficacy of a specific intervention. Nevertheless, instrumented balance assessment may provide the physical therapists with a more sensitive objective assessment tool and may facilitate objective outcome evaluation of rehabilitative interventions. Furthermore, IMUs may contribute to a timelier balance evaluation of elderly cohorts. Future studies should investigate the capability of instrumented balance assessment tools for an early diagnosis of those susceptible to falls and for the implementation of more effective rehabilitative interventions.

6.5.1 What is next?

We developed and validated an algorithm for reliable assessment of static standing balance, based on wearable technology measurements, with the capability of being integrated into clinical tests for individuals with neuromuscular impairments such as ambulatory individuals with iSCI with mild balance deficits as well as the elderly with moderate-to-severe balance impairments (Chapters 3 to 6). In the next chapter, we investigated the limit of dynamic balance to assess the risk of loss of balance during dynamic conditions. Note, since there is a need for a standard biomechanical criterion that particularly quantifies the limits of dynamic balance during sitting due to complexities associated with human trunk structure and its control, the next chapters (Chapters 7 to 9) focused on providing insights into the control strategy employed by the neuromusculoskeletal system for dynamic balance of sitting.

Chapter 7

This chapter shows how the feasible stability region can be obtained for seated stability and how an algorithm can be used to obtain the margin of stability during perturbed sitting using wearable technology. This chapter has been adopted and/or edited from:

A. Noamani, K. Agarwal, A. H. Vette, and H. Rouhani, "Predicted Threshold for Seated Stability: Estimation of Margin of Stability Using Wearable Inertial Sensors," IEEE J. Biomed. Heal. Informatics, vol. 25, no. 9, pp. 3361–3372, 2021, doi: 10.1109/JBHI.2021.3073352.

7 Feasible Seated Stability Region

7.1 Introduction

Each year, about 22,000 new cases of spinal cord injury are reported in the USA and Canada, and the total number of individuals with spinal cord injury living in these countries is estimated to be around 380,000 [73], [74]. Due to the impaired neuromuscular function of the trunk and pelvic musculature, individuals with spinal cord injury are frequently unable to adequately control their sitting balance.

More than 60% of individuals with spinal cord injury use wheelchairs or scooters for daily mobility [22]. Many of them experience higher postural sway during sitting compared to able-bodied individuals because of impaired trunk stability [24]. Thus, these individuals are at high risk of falling when exposed to sitting perturbations, such as hitting a bump during daily wheeling, making tips and falls the leading cause of injury in this population [27]. Consequently, they view sitting stability during daily activities as one of their most essential needs, even outweighing their desire to walk again [34]. In this light, an assistive device that can evaluate and improve their sitting stability during daily life would dramatically improve their quality of life while moving in a wheelchair.

Recent studies have shown that the development of neuroprostheses using functional electrical stimulation (FES) could be beneficial for restoring trunk stability during seated posture by activating the paralyzed trunk musculature. It has been suggested that closed-loop control of stimulation using kinematic feedback of the trunk can reduce muscle fatigue, ensure smoother

muscle contractions, and result in improved joint trajectory tracking [181]. Hence, motion states (i.e., position and velocity) of the trunk center of mass (COM) can be of significant importance in utilizing closed-loop FES control for stabilizing the trunk. However, to the best of the author's knowledge, there is no standard biomechanical criterion that particularly quantifies the relationship between the motion states of the trunk COM and sitting balance and is validated against a gold-standard reference.

Previous studies have used biomechanical models of the human body to characterize stability using the motion states of the body's COM with respect to its base of support (BOS) [52]–[58]. To quantify the relationship between the COM states and stability during gait and standing, two concepts have been introduced: the extrapolated COM [182] and feasible stability region (FSR) [57], [183]. In static conditions, the projection of the COM position should remain within the BOS boundaries to achieve stability. However, in dynamic conditions, the COM velocity must also be considered [52]. When the COM position is within the BOS, a COM velocity directed outward may lead to an unstable condition. Similarly, when the COM position is not within the BOS, a COM velocity toward the BOS may lead to a stable condition [52]. This concept is quantified by the extrapolated COM. The concept of the extrapolated COM suggests that the position of the COM plus its velocity, multiplied by a factor, should remain within the BOS for dynamic stability. This factor is identified based on a simple one-segment inverted pendulum biomechanical model and is equal to the inverse of the natural frequency of the pendulum. At the same time, the FSR is defined as the range of feasible COM velocities for an initial COM position that would bring the COM to the edge of the BOS with a velocity of zero. Hence, the FSR is a subspace of the COM motion states with boundaries that determine the limits of dynamic stability. Therefore, the dynamic stability is achieved as long as the COM motion states remain within the FSR. If the COM states during a gait cycle or standing fall within the boundaries of FSR, the occurrence of loss of balance is unlikely. However, COM states falling outside of the FSR boundaries indicate a high possibility of loss of balance. Hence, measuring the motion states of the body's COM during real-world perturbed conditions and comparing them with the previously obtained FSR boundaries in the state-space plane can characterize the risk of loss of balance.

The FSR allows using complex biomechanical models of the body for quantification of dynamic stability during various task-specific motions and postures. The FSR boundaries in the COM state space can be obtained as nonlinear curves and as a function of the complex body motion

and posture, and external perturbations [58], unlike the extrapolated COM, which obtains the stability limit using a linear combination of the COM motion states. FSR has been identified using biomechanical models along with dynamics optimizations and then validated against experimental data for standing [54], [189] and walking [56], [57], [187], as well as during gait following a slip [188] and BOS perturbations [58]. However, to the best of our knowledge, FSR has not been identified and validated against experimental data for quantifying the relationship between the trunk COM states and seated stability following BOS perturbations.

Assessment of stability using both extrapolated COM and FSR requires measuring the COM motion states. In-lab equipment such as motion capture cameras has been used in the past to validate the use of the extrapolated COM and FSR for quantifying standing [54], [189] and walking stability [58]. However, the use of such approaches during activities of daily living requires a portable device for measuring the COM motion states. Wearable technologies such as inertial measurement units (IMUs) could be useful for this purpose. Unlike motion capture cameras, wearable technologies can be used during activities of daily living and in spaces other than an equipped lab space. Wearable IMU can be a low-cost, user-friendly tool for out-of-lab assessment of seated stability. Nevertheless, their accuracy for obtaining COM motion states must first be validated against motion capture cameras as a gold-standard reference.

To address the abovementioned gaps and to quantify the relationship between the dynamic posture of the trunk and fall risk during sitting, this study aims to: (a) obtain the limit of stability against forward loss of balance based on the concept of FSR following BOS perturbations using mathematical simulations; (b) experimentally validate the obtained FSR using a motion capture system; (c) compare the predicted FSR and extrapolated COM for quantifying seated stability using experimental data; and (d) investigate the accuracy of using wearable IMUs for assessing the dynamic sitting posture and fall risk against the motion capture system as the gold-standard reference using experimental data.

In the following section, first, we explain how the FSR can be obtained for seated stability using mathematical simulation. Second, we describe our experimental study with fifteen individuals during perturbed sitting to obtain the trunk COM motion states using motion capture cameras. Third, we explore the validity of the FSR using the experimental data and compared the margin of stability obtained via FSR with the extrapolated COM. Finally, we identify the accuracy

of the IMUs against the motion capture for estimating trunk COM motion states and the margin of stability.

7.2 Methods

7.2.1 Simulation Study: FSR Modelling

We used a mathematical simulation approach including forward dynamics and dynamic optimization to determine the threshold of the trunk COM position and velocity relative to the BOS against forward loss of balance. To this end, we used a six-segment model of the human body in the sagittal plane during sitting in this study for simulating seated stability when a BOS perturbation is applied. The implemented model consisted of the head and neck, thorax and upper limbs (crossed over the chest), lumbar segment, pelvic segment, thighs, and lower legs (Figure 7-1). Segments were connected to each other by revolute joints. Body segment parameters, including mass, moments of inertia, COM, and joint center of rotation positions, were derived according to the cadaveric data provided by Vette et al. (upper body) [254] and Winter (lower limbs) [223]. The inputs to the model were the initial angle and angular velocity $(\theta, \dot{\theta})$ of each joint as well as the muscle excitation history, $u(t)$, as explained in previous studies [58], [187], [188]. Similar to previous studies, joint moments were estimated based on anatomical maximum flexion and extension limits and an activation level as follows:

$$\tau_i = \begin{cases} a_i(t) {T_i}^E & a_i(t) \geq 0 \\ a_i(t) {T_i}^F & a_i(t) < 0 \end{cases} \quad (1)$$

where τ_i is the joint moment, a_i is the activation level, and ${T_i}^E$ and ${T_i}^F$ are the physiological moment range of joint i for extension and flexion, respectively [233], [255], [256]. The activation level, used in Eq. 1, was computed via a first-order differential equation as follows:

$$\dot{a}(t) = \frac{u(t) - a(t)}{\tau_{act}}, -1 \leq u(t), a(t) \leq 1 \quad (2)$$

where $u(t)$ is the muscle excitation that was controlled by a series of control nodes (11 nodes per joint), and τ_{act} is the activation time constant [58], [188]. The initial activation levels required for solving Equation (2) and initial joint moments were obtained using an initial configuration of the model, selected to show different initial trunk COM positions. The initial trunk COM positions in the anteroposterior direction were chosen to be $[-1.5, -1.25, -1, -0.75, -0.70, -0.5,$

$-0.25,\ 0] \times \text{BOS length}$ with respect to the COM position in the stable, maximum forward bending condition. The choice of these initial COM positions was based on previous studies that obtained the FSR for walking [58], [187], [188]. The BOS length was chosen to be 75% of the thigh length (from the hip to the knee), similar to previous studies [242], [257]–[259]. The configurations of the segments with respect to each other were adopted, for which we observed the abovementioned initial trunk COM positions in experimental kinematic data (averaged across participants).

For each initial trunk COM position, we used a genetic optimization algorithm (Figure 7-2) to obtain the maximum feasible initial trunk COM velocities that would bring the trunk COM position to the anterior edge of the BOS. This maximum velocity corresponding to each initial trunk COM position indicates the threshold against forward loss of balance. Any initial velocity leading to an unstable condition would cause divergence of the optimization process.

Optimization variables were initial joint angular velocity and muscle excitation history for each joint. Note that having one time series for $u(t)$ per joint as an optimization variable significantly increases the computational cost. Therefore, a set of independent linearly interpolated variables known as control nodes were used in the literature [58], [188] to define $u(t)$. In the present study, 11 control nodes per joint were defined as the optimization variables. Subsequently, a corresponding time series for $u(t)$ was constructed by interpolating the control nodes over the simulation time. Therefore, we used 12 optimization variables for each joint including initial angular velocity and 11 control nodes. Following previous studies [58], [188], a cost function was defined to characterize trunk stability during BOS perturbations while guaranteeing a smooth and natural motion of each trunk segment.

$$
\begin{aligned}
Cost\ Function = \ & \frac{w_1}{\dot{x}_{COM}^{initial}} + w_2\left|\dot{x}_{COM}^{final}\right| + \\
& w_3\left|\ddot{x}_{COM}^{final}\right| + \ w_4 \int_{t_i}^{t_f} e\big(F_y(t)\big)dt + w_5 \int_{t_i}^{t_f} e(\Theta(t))dt + \\
& w_6 \int_{t_i}^{t_f} e\left(\dot{\Theta}(t)\right) dt + w_7 \sum_{i=1}^{4} \int_{t_i}^{t_f} \tau(t)^2 dt + w_8 \sum_{i=1}^{6} \int_{t_i}^{t_f} SD(\Theta_i)\, dt + \\
& w_9\left|x_{COM}^{final} - x_{BOS\ edge}\right| + \\
& w_{10}\left|y_{Head\ COM}^{final} - y_{Pelvis\ COM}^{final}\right| + \\
& w_{11}\left|y_{Thorax\ COM}^{final} - y_{Pelvis\ COM}^{final}\right|
\end{aligned}
\tag{3}
$$

$$w_{12}\left|y^{final}_{Lumbar\ COM} - y^{final}_{Pelvis\ COM}\right| +$$

$$w_{13}\left|y^{final}_{Pelvis\ COM} - y^{final}_{Thigh\ COM}\right|$$

where t_i and t_f are the initial and final time instances of the simulation; x, $\dot{x}$, and $\ddot{x}$ are the linear position, velocity, and acceleration, respectively, in the anteroposterior direction; y is the vertical position; τ is the joint moment; SD is the standard-deviation; F_y is the vertical ground reaction force; and w_i is the weight for the i^{th} term. Note that we used linear kinematics of the COM rather than angular kinematics to obtain the FSR. This is consistent with previous studies that identified the FSR during standing [54], [189] and walking [56], [57], [187].

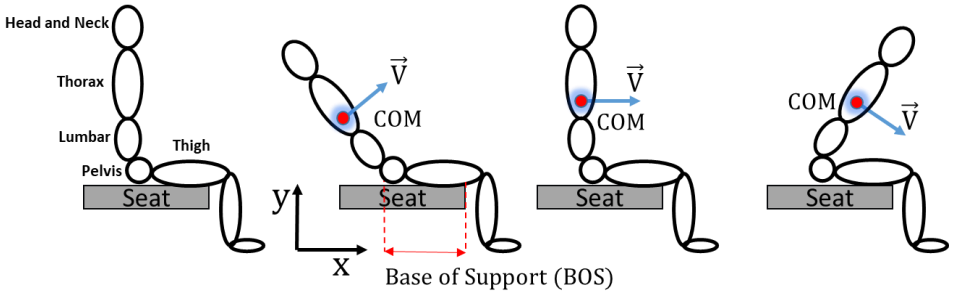

Figure 7-1. The biomechanical model, used for dynamic optimization and simulation, consisted of the head and neck, thorax and upper limbs, lumbar segment, pelvis segment, thighs, and lower legs and feet as one segment. The base of support (BOS) was determined to be located at 75% of the thigh length. The position and velocity of the trunk center of mass (COM) were then used to obtain the feasible stability region (FSR) during perturbed sitting for different initial positions of the trunk COM with respect to the front edge of the BOS.

The rationale for using terms 1 to 9 was explained in detail by Yang et al. [188] and Bahari et al. [58]. We added terms 10 to 13 to terms 1 to 9 to ensure faster convergence and to avoid non-physiological motion of segments with respect to each other. The first term ensures that the maximum initial velocity, which brings the trunk COM position to the front end of the BOS, is achieved. The second and third terms are to bring the trunk COM to a stationary condition at the front end of the BOS. The fourth term ensures that the resultant vertical ground reaction force under the thighs remains positive. The fifth and sixth terms ensure that θ and $\dot{\theta}$ at each joint remain within the physiological limits. The seventh term is to minimize the integral of the square of the joint moments leading to faster convergence. The eighth term ensures smooth changes of the joint angles and minimizes their rapid changes. The ninth term requires the final trunk COM position to stay inside the BOS limit at the end of the simulation.

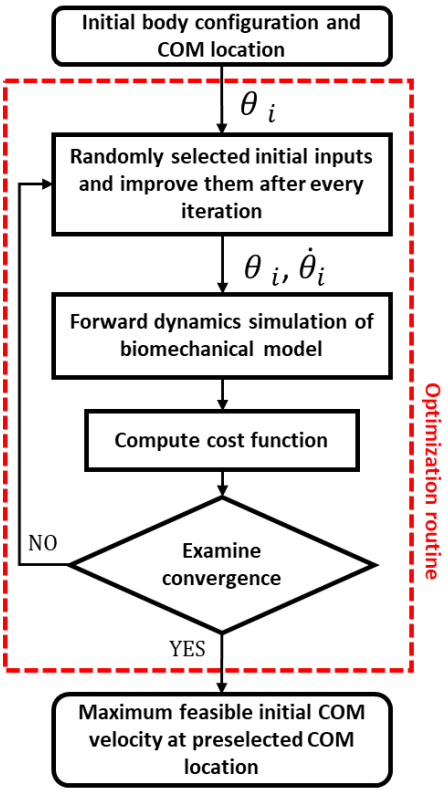

Figure 7-2. Flowchart of dynamic optimization and simulation.

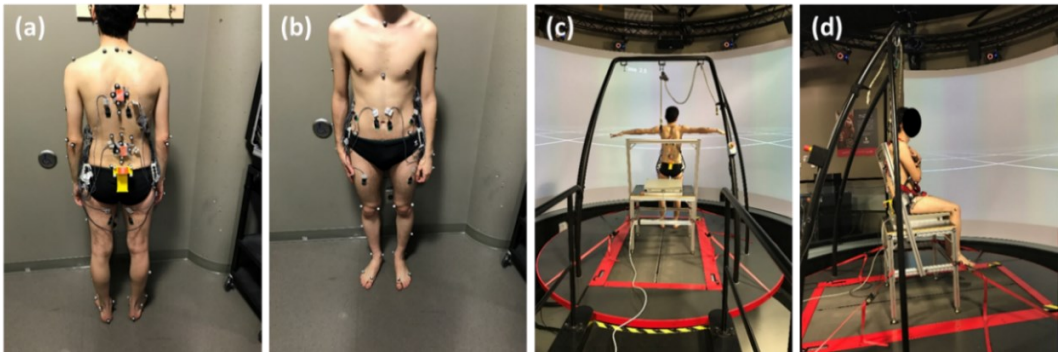

Figure 7-3. (a, b) Anatomical markers and inertial measurement units (IMUs) were placed on the body; (c) A T-pose anatomical calibration was performed at the beginning of the data collection; and (d) Perturbed sitting trials were performed while the participant sat on a customized seat fixed on the Stewart platform of a Computer Assisted Rehabilitation Environment (CAREN). Note that the recordings of electromyography electrodes shown in this figure were not used for the present study.

Terms ten to thirteen ensure the trunk segments have physiologically meaningful motions during the seated condition and facilitate faster convergence of the simulation. Our previous experimental studies [233], [260] indicate that the vertical COM positions of the trunk segments (head, thorax, and lumbar) remain above the pelvis while the COM of the pelvis remains above

the thighs. Thus, terms ten to thirteen ensure that such conditions are maintained over the course of the simulation. Functions $e(x(t))$ and $\lfloor x \rfloor$ were defined by Yang et al. [188] as follows:

$$e\big(x(t)\big) = \sum_{i=1}^{q} \emptyset(x_i(t)) \tag{4}$$

$$\emptyset(x_i(t)) = \begin{cases} x_i^{LB} - x_i, & x_i < x_i^{LB} \\ 0, & x_i^{LB} \le x_i \le x_i^{UB} \\ x_i - x_i^{UB}, & x_i \ge x_i^{UB} \end{cases} \tag{5}$$

$$\lfloor x \rfloor = \begin{cases} -x, & x \le 0 \\ 0, & x > 0 \end{cases} \tag{6}$$

where x_i^{LB} and x_i^{UB} are the lower and upper bounds of the variable x_i, respectively, used to account for the physically feasible ranges of angle and angular velocity for each joint. The cost function defined in Equation (3) is particularly important in modelling perturbed sitting where relative intersegmental motion is large compared to unperturbed sitting. The weights (w_i) were determined using an initial multi-objective optimization where each term in Equation (3) was used as a separate cost function. The weights were then calculated to ensure all terms fall within the same range without outweighing one another in the main optimization. The role of the weights was to scale each term, in the cost function, so all terms would fall within the same range and would equally contribute to the cost value. Therefore, the optimization algorithm could simultaneously minimize all terms in the cost function [58]. In all simulations, the BOS perturbation was modelled as a ramp signal, and the thigh segment was assumed to be fixed on the BOS. Simulations were performed with MATLAB R2018b (MathWorks, Natick, MA, USA).

7.2.2 Experimental Study

7.2.2.1 Participants

Fifteen abled-bodied male individuals (mass: 75.9±11.2 kg, height: 178±7 cm, age: 24±4 years) with no history of neuromuscular or musculoskeletal impairments or any disorders that may have affected their seated stability participated in this study. Participants were informed about the experimental protocol and provided written consent prior to participation. The Research Ethics Board of the University of Alberta approved the study protocol (Study ID: Pro00063998).

7.2.2.2 Experimental Protocol

Each participant was asked to sit, with their arms crossed over the chest, on a customized seat without foot support equipped with a force plate (AMTI, Watertown, MA, USA) on top

(Figure 7-3). The seat was fixed on the Stewart platform of a Computer Assisted Rehabilitation Environment (CAREN; Motekforce Link, Amsterdam, The Netherlands). The platform was connected to six hydraulic actuators that allowed three-dimensional translation and three-dimensional rotation of the platform. A 180-degree curved virtual-reality projection screen was in front of the participants. White two-dimensional grid lines on a black background were projected onto the virtual-reality screen by four F-10 AS3D projectors (Barco, Fredrikstad, Norway) to provide a similar sensory condition for all participants prior to the perturbation. Sudden BOS perturbations in the form of a ramp-shaped horizontal anteroposterior displacement of the platform were applied to the seat. Perturbations were applied with three different amplitudes increasing from low to high (Figure 7-4).

Table 7-1. Markers were placed on the anatomical landmarks of the head, spine, trunk, arms, pelvis, and lower limb, including thighs, legs, and feet.

Segment	Retro-reflective markers on anatomical landmarks
Head	Condyloid process and mastoid process (left and right)
Spine	C7, T12, and L5 vertebrae, and 5 cm bilaterally to each vertebra
Trunk	T9 vertebra, Suprasternal and xiphoid
Arms	Acromion, lateral epicondylitis, and olecranon (left and right)
Hands	Distal ulna bone, little finger metacarpal head, middle finger distal phalanges
Pelvis	Anterior and posterior superior iliac spine (left and right)
Legs	Greater trochanter, medial and lateral epicondylitis, medial and lateral malleolus
Feet	Calcaneus, 1st and 5th metatarsal heads

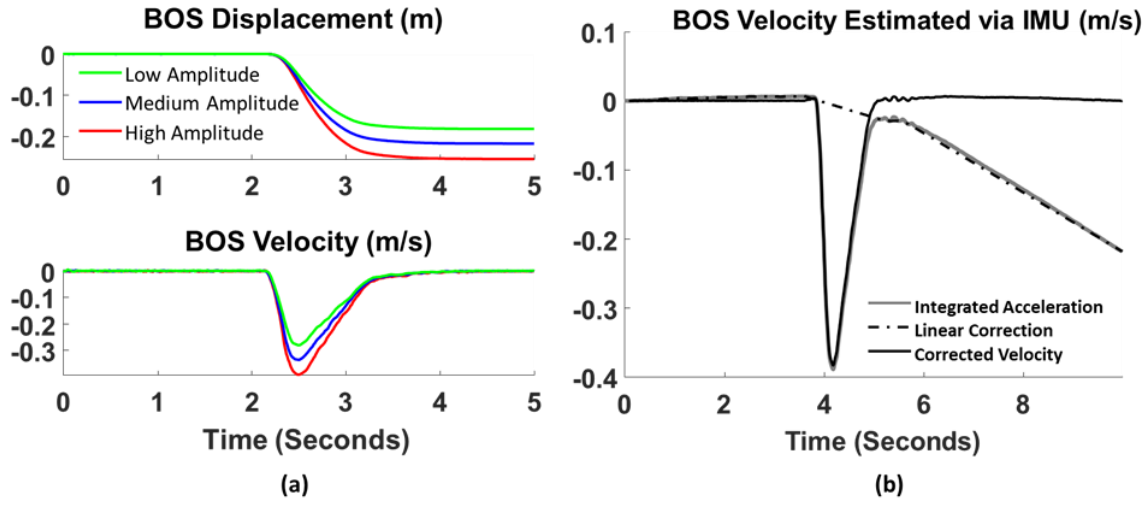

Figure 7-4. **(a)** Base of support (BOS) perturbation characteristics. **(b)** Calculation of the BOS velocity based on the anteroposterior acceleration as measured by an inertial measurement unit (IMU) placed on the seat.

The amplitudes of the perturbations were designed to duplicate a near-fall experience while ensuring the safety of the participants. The amplitudes were determined by trial and error in our preliminary experiments and based on the experience of the CAREN operator. The participants were instructed to fixate on the screen, keep their legs hanging vertically downward, and maintain their sitting balance without using their lower limbs. Three trials were performed for each perturbation amplitude. Rest breaks were provided between the trials as needed.

7.2.2.3 Data Acquisition

Retro-reflective markers were placed on the anatomical landmarks of the head, spine, trunk, arms, hands, pelvis, legs, and feet (Table 7-1 and Figure 7-3). A twelve-camera motion capture system (Vicon Motion Systems Ltd., Oxford, UK) recorded the trajectory of the markers at a sampling frequency of 100 Hz. In addition, four markers were placed on the seat to record BOS motion.

Three inertial measurement units (IMUs) (MTws, XSENS Technologies, NL) measured the kinematics of the thorax, lumbar segment, and pelvic segment at a sampling rate of 100 Hz. One IMU was also attached to the seat. Each IMU was composed of a tri-axial gyroscope (range: ±2000 deg/s), a tri-axial accelerometer (range: ±16g), and a tri-axial magnetometer (range: ±1.9 Gauss) and mounted on a rigid plate equipped with four retro-reflective markers (Figure 7-3). The raw IMU and marker data were low-pass filtered via a zero-lag 4^{th}-order Butterworth filter with a cut-off frequency of 30 Hz and 10 Hz, respectively. The cut-off frequency was selected based on the frequency content of the time series obtained via the Fast Fourier Transform. The synchronization between the motion capture system and the IMUs was conducted by sending an analog trigger from the IMUs to the motion capture system at the beginning and end of each trial. A T-pose anatomical calibration was performed by each participant (Figure 7-3c). Anatomical markers of the thorax, lumbar segment, and pelvic segment were removed prior to perturbation trials and were subsequently reconstructed using anatomical calibration data.

7.2.3 Data Analysis

The FSR, obtained via simulations, was validated against the motion states of the trunk COM, computed using experimental data. Individual-specific body segment parameters were obtained via scaling of the data from the simulation using each participant's body weight and height, similar to our previous studies [233], [260]. The kinematics of each segment during

perturbation trials were computed using the trajectories of the markers and forming anatomical frames (*see Additional Information*), similar to the procedure described in our previous studies [233], [260]. The position and velocity of the trunk COM in the anteroposterior direction were then estimated as follows:

$$P_{COM}(t) = \frac{\sum_{i=1}^{n} Mass_i \,.\, P_{COM_i}(t)}{\sum_{i=1}^{n} Mass_i} \tag{7}$$

$$V_{COM}(t) = \frac{dP_{COM}(t)}{dt} = \frac{P_{COM}(t+1) - P_{COM}(t-1)}{2\,\Delta t} \tag{8}$$

where $P_{COM}(t)$ and $V_{COM}(t)$ are the position and velocity of the trunk COM at time t, respectively; $Mass_i$ and $P_{COM_i}(t)$ are the mass and COM position of segment i, respectively, and n is the number of segments, including head and neck, thorax, arms, lumbar segment, and pelvic segment. To quantify the risk of loss of balance, the margin of stability (a_{margin}) was then calculated as the shortest distance from the trunk COM states to the boundary of the obtained FSR in the state-space plane (velocity-position). Note that the trunk COM states were normalized using the trunk height and BOS length prior to the calculation of a_{margin} as follows:

$$V_{COM}^{Normal} = \frac{V_{COM}}{\sqrt{g \times Trunk\ Height}} \tag{9}$$

$$P_{COM}^{Normal} = \frac{P_{COM} - P_{BOS\ front\ end}}{Length\ of\ BOS} \tag{10}$$

where V_{COM}^{Normal} and P_{COM}^{Normal} are the normalized velocity and position of the trunk COM, respectively; trunk height was measured as the distance between the C7 and L5 markers, and BOS length was measured as 75% of the thigh length (from the hip to the knee). In addition, the extrapolated COM in the anteroposterior direction was computed as follows [182]:

$$XCOM(t) = P_{COM}(t) + \frac{V_{COM}(t)}{\omega_0}, \quad \omega_0 = \sqrt{\frac{g}{l_{COM}}} \tag{11}$$

where $XCOM$ is the extrapolated COM; g is the gravitational acceleration; and l_{COM} is the equivalent length between the hip joint and the trunk COM position for each participant. The margin of stability (b_{margin}) was calculated as the shortest distance between the XCOM and the front edge of the BOS.

To investigate the accuracy of wearable IMUs in measuring the motion states of the trunk COM, we used IMUs attached to the thorax segment, lumbar segment, and pelvic segment. The IMUs were calibrated by aligning the accelerometer's vertical axis with gravity during quiet sitting at the beginning of each trial [93], [227]. We used the sensor's built-in Kalman filter to obtain the orientation of each segment (expressed as quaternions). The angle and angular velocity of each segment were calculated using its orientation and used along with the estimated body-segment parameters to estimate the motion states of the trunk COM. Equations for calculating angle and angular velocity using quaternions are provided by [261] (see *Additional Information*). Furthermore, the velocity of the BOS was estimated using the accelerometer's reading. The acceleration signal was integrated using a trapezoidal numerical integration and then corrected for the drift using linear interpolation (Figure 7-4b), similar to previous studies [235], [236], [262], [263]. We used linear interpolation because of the short correction period (just over 1 second in Figure 7-4b). Finally, the margin of stability (a_{margin}^{IMU}) with respect to the FSR boundary was then estimated using only IMUs recordings.

7.2.4 Statistical Analysis

We used Spearman's correlation between a_{margin} and b_{margin} to compare the margin of stability obtained using FSR and the extrapolated COM. Furthermore, to compare the margin of stability estimated by the IMUs with that estimated by the motion capture system, we performed statistical analyses between a_{margin} and a_{margin}^{IMU}. The Kolmogorov-Smirnov test rejected the null hypothesis that the data followed a normal distribution. Therefore, we used a non-parametric statistical test (Wilcoxon signed-rank test) at a 0.05 significance level for the comparison. We also calculated the correlation coefficient and root-mean-square (RMS) difference between the time series obtained via the motion capture system and IMUs for the motion states of the trunk. We used the statistical F-test between the margins of stability associated with different perturbation amplitudes to compare the variance of the margin of stability within our sample population between the two perturbation conditions. All analyses were performed with MATLAB R2018b (MathWorks, Natick, MA, USA).

7.3 Results

Figure 7-5 shows the boundary of FSR, known as the limit of stability, obtained from the simulations. All experimentally obtained trunk COM states for all perturbation trials fell within the FSR (Figure 7-5). Trunk COM states for the perturbations with higher amplitudes were more scattered and closer to the limit of stability. The variances of the margin of stability among participants for low, medium, and high perturbation amplitudes were [0.009, 0.010, 0.012], respectively. The statistical F-test between the margins of stability associated with different perturbation amplitudes revealed a significantly larger variance among participants for the high amplitude compared to the low amplitude ($p = 0.039$). No significant differences were observed between the low and medium amplitudes, and the medium and high amplitudes. However, the variance of the margin of stability among participants tended to increase when increasing the perturbation amplitude.

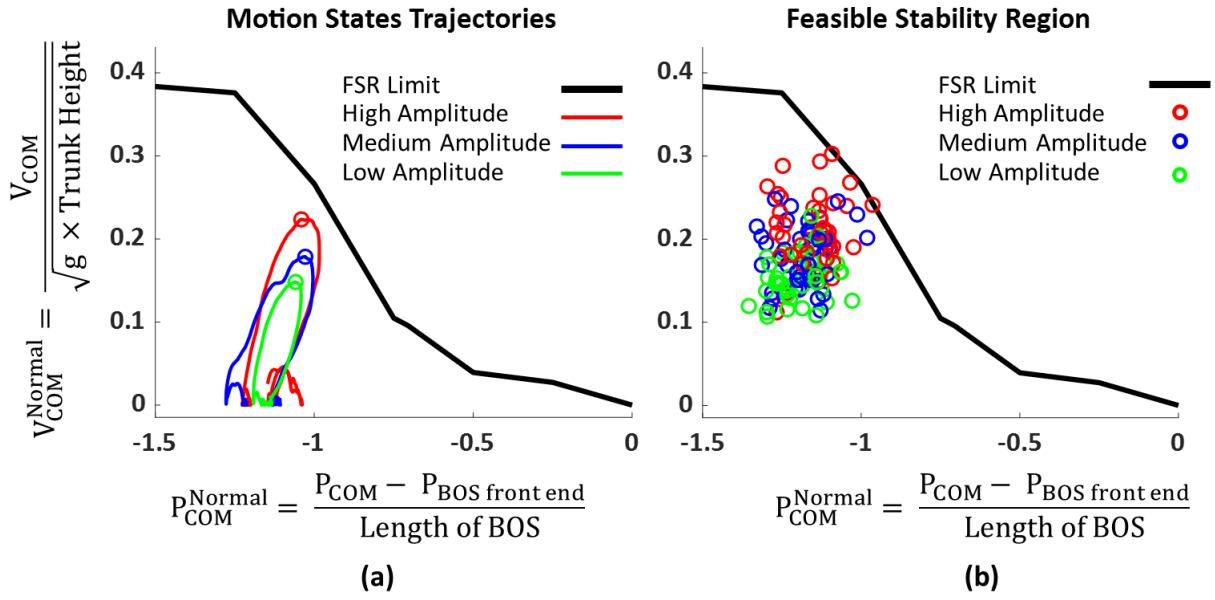

Figure 7-5. **(a)** Feasible stability region (FSR) estimated via dynamic optimization (solid black line) and three representative trajectories of motion states of the trunk COM during perturbation trials for different perturbation amplitudes measured for one participant (left); and **(b)** the motion states of the trunk center of mass (COM) at the minimum margin of stability (the most unstable moment) during experimental trials with sudden horizontal perturbations with different amplitudes for all participants (right).

Spearman's correlation between a_{margin} and b_{margin} showed a medium correlation coefficient (ρ = 0.430, p < 0.001). The statistical comparison between the FSR margin of stability obtained via the motion capture system and the IMUs showed no significant difference (p = 0.753) (Figure 7-6). The correlation coefficient between the motion capture system and IMUs for estimating the trunk COM position and velocity were [0.916, 0.956, 0.975] and [0.862, 0.893, 0.935], respectively, as the [25%, 50%, 75%] percentiles across participants (Figure 7-6). Moreover, the RMS difference between the motion capture system and IMUs for estimating the trunk COM position and velocity were [0.004, 0.006, 0.009] and [0.015, 0.018, 0.021], respectively, as the [25%, 50%, 75%] percentiles across participants (Figure 7-6). Figure 7-7 shows a sample time series of the trunk COM states and platform velocity as estimated via the IMUs compared to the motion capture system, with a high correlation and small magnitude of the error.

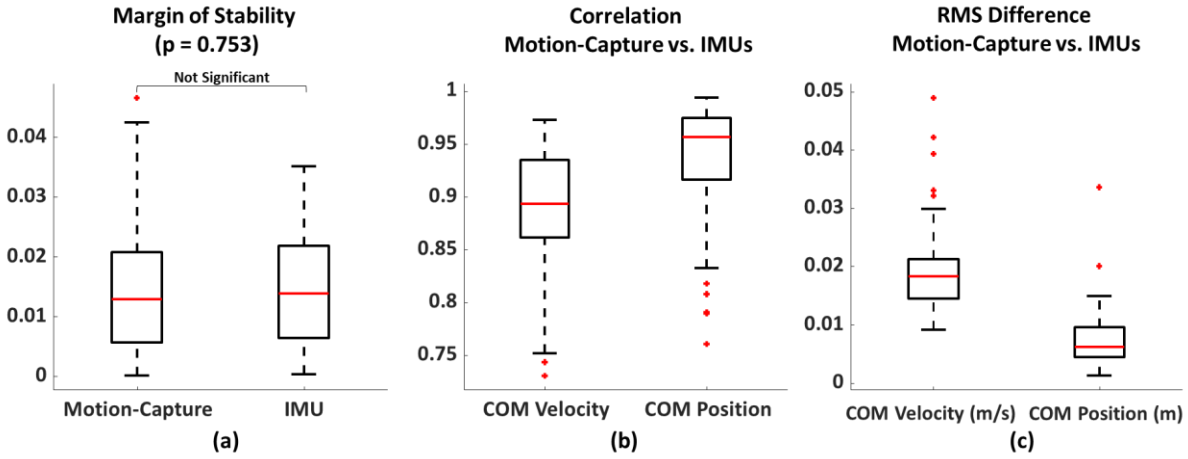

Figure 7-6. **(a)** The margin of stability was obtained experimentally using the motion capture system and the inertial measurement units (IMUs). No significant difference was observed between the two measures; (**b**) and **(c)** The correlation coefficient and root-mean-square (RMS) difference, respectively, between the normalized trunk COM position and velocity obtained by the motion capture system and those obtained by the IMUs.

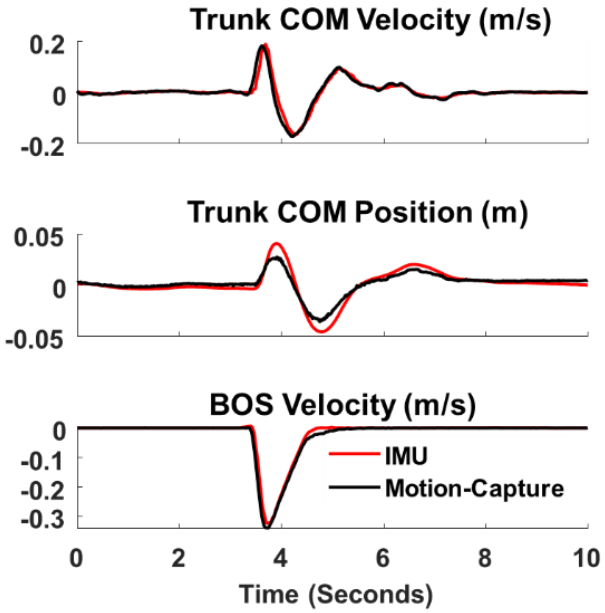

Figure 7-7. Trunk center of mass (COM) velocity and position, as well as the base of support (BOS) velocity, were estimated via the motion capture system (black line) and via inertial measurement units (IMUs) (red line) for one trial and one participant.

7.4 Discussion

This study presented a predicted threshold against forward loss of balance during sitting using dynamic optimization and simulation to quantify the relationship between the trunk COM states and seated stability. We obtained FSR for the sitting condition using a six-segment biomechanical model (Objective (a)). We used experimental data from fifteen able-bodied individuals who maintained their seated stability following BOS perturbations to validate the obtained FSR (Objective (b)). We measured the trunk COM states using a motion capture system and computed the margin of stability with respect to the boundary of FSR as an indication of loss of balance (Objective (c)). We also validated the use of wearable IMUs against the motion capture system for estimation of the margin of stability (Objective (d)). Such wearable technology may be of significant importance, in the future, for (a) alarming wheelchair users regarding a potential fall risk during wheeling as a function of wheeling speed and body posture; (b) training users to improve dynamic sitting balance in rehabilitation programs; and (c) the development of a neuroprosthesis for improving seated stability using a closed-loop FES system. Each of these applications requires extensive investigation. Nevertheless, the present study took a step forward

toward the quantification of seated stability under dynamic conditions, which could pave the way for future research studies.

7.4.1 Experimental Validation of FSR

FSR against forward loss of balance obtained for the sitting condition (Figure 7-5) shows a more nonlinear limit of stability in the state-space plane compared to that obtained for walking [58], [188] and standing [54], [189]. This could be due to larger intersegmental motions between trunk segments during perturbed sitting compared to walking and standing. Previous studies [54], [58], [188] neglected the intersegmental motion between the trunk segments during gait and standing, which cannot be neglected during perturbed sitting [260]. As indicated by Figure 7-5a, all the experimentally measured trunk COM motion states were located within the FSR for all perturbation trials, which suggests the maintained balance of the participants.

The represented motion states in the state-space plane were chosen to be those that had the trunk COM velocity reach its maximum following the BOS perturbation (Figure 7-5a and Figure 7-5b). Since the BOS perturbation was applied as a ramp-shaped displacement in a short period of time, the trunk COM velocity increased and then decreased, similar to the BOS velocity. Therefore, the selected point in the state-space plane represented the instance of the most unstable condition with a minimum margin of stability (Figure 7-5b). In reality, BOS disturbances oftentimes have the shape of a horizontal impulse displacement; however, in the laboratory condition, the BOS disturbance was realized in the form of a ramp-shaped displacement to prevent potential harm to the study participants.

By increasing the BOS perturbation amplitude, the trunk COM motion states became more scattered. Our statistical analysis revealed that the high perturbation amplitude led to a large variance in the margin of stability compared to the low perturbation amplitude. This could be due to the increased variability of the trunk intersegmental motions and neuromuscular control strategy as the BOS perturbation amplitude increased. In addition, trunk stiffness acts as a passive mechanism in stabilizing the trunk in response to the perturbation by producing a resistive torque. The literature indicates that trunk stiffness is much lower for small perturbations [212] and linearly increases proportionally to the load [264]. By increasing the perturbation amplitude, the effect of the variability in trunk stiffness among participants may have become more apparent, which would further explain why the motion states of the trunk became more scattered.

In agreement with previous studies [58], [188], we also observed that the trunk COM states were closer to the limit of stability for larger amplitudes of perturbation, which indicates a more challenged sitting posture and smaller margin of stability (Figure 7-5a and Figure 7-5b). The trajectory of the trunk COM motion states (Figure 7-5b) showed that the margin of stability tended to decrease when increasing the perturbation amplitude; however, no statistical significance was observed between the margins of stability for different perturbation amplitudes. Larger differences between the perturbation amplitudes (which might not be safe) would be needed to observe a clearer difference among the margins of stability within a small-size population.

7.4.2 FSR vs. Extrapolated Center of Mass

To quantify the risk of loss of balance, we estimated the margin of stability (a_{margin}) as the shortest distance from the trunk COM states to the boundary of the FSR in the state-space plane using experimental data. We also calculated the margin of stability (b_{margin}) using the concept of XCOM introduced by Hof et al. for standing [52] and walking [182], i.e., as the shortest distance between the XCOM and the front edge of the BOS. Spearman's correlation between the two measures was moderate. This is due to the fact that the XCOM (Equation (10)) assumes a linear limit of stability in the state-space plane between the velocity and position of the COM. However, the FSR obtained in this study using a multi-segment biomechanical model (Figure 7-5) showed a nonlinear limit of stability, which could explain the moderate correlation between the two measures. Moreover, the nonlinear FSR presented by the current study provides a more conservative limit of stability compared to the XCOM-based limit, particularly in larger initial COM velocities. Quantifying the risk of loss of balance based on a more conservative nonlinear limit of stability obtained specifically for the sitting condition could provide better insights into the seated stability of an individual. Nevertheless, larger perturbations, which would bring the COM position close to the front end of the BOS, are needed to investigate the highly nonlinear portion of the FSR limit of stability. This is particularly important since the relation between seated stability and the dynamics of the trunk COM is different compared to the relations obtained for standing and walking at different COM motion states.

7.4.3 Margin of Stability: IMUs vs. Motion Capture

We also used IMUs placed over the thorax, lumbar segment, and pelvic segment to estimate the states of the trunk COM. We also used an accelerometer placed on the seat to estimate the

velocity of BOS. The accuracy of a segment's orientation estimate using an IMU may deteriorate over time due to the drift associated with the gyroscope output. Complex sensor fusion algorithms, such as extended Kalman filters or complementary filters, can reduce the error in orientation estimation and are integrated into some commercially available IMUs. Here, we used the built-in Kalman filter of the sensors to obtain the segment's orientation. Furthermore, numerical trapezoidal integration of the BOS accelerometer's recording showed a systematic drift (Figure 7-4b). To overcome this problem, a correction time series was generated and subtracted from the integrated accelerometer's recording to estimate the BOS velocity. High correlations were observed between the position and velocity time series obtained with the motion capture system and the IMUs, with a small RMS difference (Figure 7-6 and Figure 7-7). The comparison between the margins of stability estimated using the IMUs and the motion capture system revealed no significant difference. These findings imply that a wearable device composed of IMUs along with the estimated FSR could be used to estimate the margin of stability. Such assessment methodology, in the future, may contribute to assessing the risk of loss of balance outside a laboratory volume and during seated daily activities and wheeling in a wheelchair; however, it requires further investigations under real-world conditions.

Moreover, recent studies have shown that the development of an FES-based neuroprosthesis within a closed-loop control strategy using the inclination angle of the trunk as a feedback signal could be beneficial for restoring trunk stability during seated posture [27], [72], [176]–[178]. These studies used accelerometers to estimate the trunk inclination angle for a closed-loop FES control strategy [27], [72], [176], [177], [265]. However, the use of an accelerometer for estimating trunk kinematics in dynamic conditions (e.g., BOS perturbations) is prone to errors and may yield inconsistent results since it is not possible to isolate gravity from the acceleration associated with the dynamic motion. Therefore, such methods for monitoring trunk stability may not be error-free when a significant BOS perturbation is imposed, whereas the method presented in this study is preferable since it would be less prone to artifacts due to more dynamic movements resulting from energetic external perturbations. The present study validated an algorithm for monitoring trunk stability using wearable technology and based on the concept of the margin of stability during dynamic conditions. Using the methodology presented in this study may facilitate the development of a closed-loop FES system for improving trunk stability by providing real-time feedback on trunk stability based on both trunk COM position and velocity. Nevertheless, further

investigations are required to assess the validity of this approach for FES systems and populations with impaired trunk stability.

7.4.4 Limitations

We only recruited able-bodied male participants for the present study. Notably, a majority of terms in the optimization cost function corresponded to the geometrical and physiological constraints of seated posture and are in common for all populations. Yet, the range of joint angles and moments might vary among populations and, thus, a more diverse population is needed for further generalization of the obtained FSR. Particularly, the physiological ranges of flexion and extension moments used in our simulation were based on data from able-bodied individuals [260]. These ranges could be affected by neuromuscular impairments and, thus, the model parameters may vary, which is a limitation. Therefore, a safety factor could be used for estimating the margin of stability when the physiological strength of the trunk musculature cannot be measured for each individual.

We estimated body-segment parameters for each individual by scaling cadaveric data using an individual's body weight and height, which may induce uncertainty in the calculations [233]. However, normalization of the trunk COM states prior to calculating the margin of stability could reduce the effect of this uncertainty. Moreover, our simulation predicted FSR based on a 'biomechanical' model of loss of balance. The limit of stability may change under different physiological and cognitive conditions [58].

In addition, we assumed a three-segment trunk model (consisting of the head-neck, thorax, and lumbar) and pelvic segments, and we neglected the intervertebral motions within each segment as well as the effect of potential upper limb motion. Future studies may perform a sensitivity analysis to investigate the effect of segmentation on the predicted FSR. The FSR must be obtained for different trunk models from single- to multi-segment models to determine the differences in the predicted limit of dynamic stability.

Previous studies used high perturbation amplitudes, causing loss of balance during standing or walking conditions, to investigate if an actual loss of balance could be identified based on their calculated FSR [58], [187], [188]. Loss of balance during standing or walking does not always result in falling, but requires action for recovery, such as taking a step forward or backward. Therefore, they identified those recovery actions and compared them with the FSR to see if the

body's COM motion states would fall outside the FSR boundaries. However, during perturbed sitting, loss of balance may lead to whiplash-related brain or spinal cord injuries due to a lack of recovery action since participants were instructed to cross their arms over their chest during the perturbation trials and, therefore, they could not use their arms for recovery. Therefore, the amplitudes of the perturbations for the present study were designed to only simulate near-fall conditions while ensuring the participants' safety. Since all experimental COM motion states during perturbed sitting fell within the FSR, this could indicate the validity of our approach. Nevertheless, not having an actual loss of balance in our experimental data is a limitation of our study.

Finally, we only considered the motions and FSR in the sagittal plane. Finding the limit of stability in the frontal plane could be a future research direction. Nevertheless, the present study took a step forward toward the quantification of seated stability, which could pave the way for further investigations.

7.5 Conclusion

This study presented the FSR against forward loss of balance during sitting based on the velocity and position of the trunk COM, validated the FSR against experimental data for perturbed sitting as measured by the motion capture system, and developed and validated an algorithm for estimating the margin of stability using wearable technology composed of IMUs for quantification of seated stability and risk of loss of balance. Our results indicate a more nonlinear limit of stability compared to those obtained for walking and standing. The margin of stability estimated via IMUs showed small differences compared to that estimated via the motion capture system. Such wearable technology may be applicable (a) as an alarming device for wheelchair users during wheeling and activities of daily living regarding the risk of falling; (b) for targeted rehabilitation and intervention to improve seated stability; and (c) as feedback in the development of neuroprostheses using a closed-loop FES system. Future studies should conduct extensive experimental studies to investigate the applicability of the proposed methodology to the abovementioned domains.

7.5.1 What is next?

We developed and validated an algorithm for assessing the dynamic stability and risk of loss of balance during sitting using wearable technology. Although this algorithm is helpful for

assessing the dynamic stability during sitting, it does not provide any information about the underlying neuromuscular stabilization mechanisms involved in maintaining dynamic balance. In the next chapter, a methodology to characterize the underlying neuromuscular mechanisms that regulate dynamic stability was investigated.

7.6 Additional Information

7.6.1 Quaternion Conversions to Euler Angle and Rotation Matrix

The Euler angles (α, β, γ) representing roll, pitch, and yaw angles can be calculated from the quaternion $(q_0 + iq_1 + jq_2 + kq_3)$ at each instant of time as follows:

$$\begin{bmatrix}\alpha\\ \beta\\ \gamma\end{bmatrix} = \begin{bmatrix}atan2(2(q_0q_1 + q_2q_3, 1 - 2(q_1^2 + q_2^2))\\ asin(2(q_0q_2 - q_3q_1))\\ atan2(2(q_0q_3 + q_1q_2, 1 - 2(q_2^2 + q_3^2))\end{bmatrix}$$

In addition, the rotation matrix from the segment-fixed frame (local) to the global frame $({}^G_L R)$ corresponding to the quaternion $(q_0 + iq_1 + jq_2 + kq_3)$ can be obtained as follows:

$${}^G_L R = \begin{bmatrix} q_0^2 + q_1^2 - q_2^2 - q_3^2 & 2(q_1q_2 - q_0q_3) & 2(q_0q_2 + q_1q_3) \\ 2(q_1q_2 + q_0q_3) & q_0^2 - q_1^2 + q_2^2 - q_3^2 & 2(q_2q_3 - q_0q_1) \\ 2(q_1q_3 - q_0q_2) & 2(q_0q_1 + q_2q_3) & q_0^2 - q_1^2 - q_2^2 + q_3^2 \end{bmatrix}$$

The angular velocity can also be obtained using the rotation matrix as follows:

$$W_{t-1} = F_s.\ ({}^G_L R^T_{t-1} \times {}^G_L R_t - I_{3\times3})$$

$$\vec{\omega}_{t-1} = \begin{bmatrix} W_{t-1}(3,2) \\ W_{t-1}(1,3) \\ W_{t-1}(2,1) \end{bmatrix}$$

In Eq. 3, W_{t-1} is a 3×3 spin matrix at time instant $t-1$, ${}^G_L R_{t-1}$ and ${}^G_L R_t$ are the rotation matrices at time instances $t-1$ and t, respectively, F_s is the sampling frequency, and $I_{3\times3}$ is a 3×3 identity matrix. In Eq. 4, $\vec{\omega}_{t-1}$ is the angular velocity at time instant $t-1$ and W_{t-1} is the spin matrix obtained using Eq. 3.

7.6.2 Cost function weights

Table 7-2. Weights of the cost function for each initial position of the COM with respect to the front end of the BOS.

	(COM initial position with respect to the front end of BOS) / BOS length													
	W_1	W_2	W_3	W_4	W_5	W_6	W_7	W_8	W_9	W_{10}	W_{11}	W_{12}	W_{13}	W_{14}
-1.5	1	400	10	12	150	2	0.004	0.1	1400	100	100	100	100	1000
-1.25	1	400	10	12	150	2	0.004	0.1	1400	100	100	100	100	1000
-1	1	400	10	12	150	2	0.004	0.1	700	100	100	100	100	1000
-0.75	1	400	10	12	150	2	0.004	0.1	700	100	100	100	100	1000
-0.7	1	400	10	12	150	2	0.004	0.1	700	100	100	100	100	1000
-0.5	1	200	10	6	150	2	0.004	0.1	350	100	100	100	100	1000
-0.25	1	200	10	6	150	2	0.004	0.1	350	100	100	100	100	1000
0	0.01	200	10	6	600	8	0.004	0.1	350	1000	1000	100	100	1000

7.6.3 Definition of the anatomical frames based on anatomical landmarks

Table 7-3. Definition of the anatomical frames based on the location of the anatomical landmarks of each segment, including head, thorax, lumbar, pelvis, and arms.

Anatomical Frame for the head segment	
z-axis	Pointed to the right as a vector from the mid-point of the left Condyloid and mastoid processes to the mid-point of the right Condyloid and mastoid processes.
y-axis	Pointing vertically perpendicular to the plane defined by the z-axis and an auxiliary vector from mid-mastoid processes to mid-Condyloid processes.
x-axis	Pointing anteriorly to form an orthogonal right-handed coordinate system

Anatomical Frame for the thorax segment	
y-axis	A vector pointing vertically from T12 to C7.
x-axis	A vector pointing anteriorly perpendicular to the plane defined by the y-axis and an auxiliary vector from left to right formed by bilateral C7 markers.
z-axis	Pointing to the right to form an orthogonal right-handed coordinate system.

Anatomical Frame for the lumbar segment	
y-axis	A vector pointing vertically from L5 to T12.
x-axis	A vector pointing anteriorly perpendicular to the plane defined by the y-axis and an auxiliary vector from left to right formed by bilateral T12 markers.
z-axis	Pointing to the right to form an orthogonal right-handed coordinate system.

Anatomical Frame for the pelvis segment	
z-axis	A vector pointing to the right from left ASIS to right ASIS.
y-axis	A vector pointing vertically perpendicular to the plane defined by left and right ASIS markers and mid-point of left and right PSIS markers.
x-axis	Pointing anteriorly to form an orthogonal right-handed coordinate system.

Anatomical Frame for the arms	
x-axis (lower arm)	Pointed distally from the mid-point of the lateral epicondylitis and olecranon to the marker placed on the wrist (ulnar styloid process).
x-axis (upper arm)	Pointed proximally from the mid-point of the lateral epicondylitis and olecranon to the marker placed on the shoulder (acromion).
y-axis	The cross-product of the z-axis and x-axis, pointing anteriorly
z-axis	Cross product of the x-axis of the lower and upper arm segments at each side of the body

Chapter 8

This chapter shows an approach to characterize the roles of active and passive mechanisms of seated stability using a nonlinear neuromechanical model. This chapter has been adopted and/or edited from:

A. Noamani, A. H. Vette, and H. Rouhani, "Nonlinear Response of Human Trunk Musculature Explains Neuromuscular Stabilization Mechanisms in Sitting Posture," 2022, J. of Neural Eng. 19(2), 026045.

8 Neuromuscular Control of Seated Stability

8.1 Introduction

Several components of the sensorimotor system interact to maintain an upright seated posture by stabilizing the inherently unstable trunk. Characterizing the roles of underlying neuromuscular mechanisms involved in stabilizing the human trunk has been a long-term challenge in human motor control research [23]. Indeed, the complex interrelation between neuromuscular mechanisms hinders our mechanistic understanding of the roles carried out by these mechanisms toward maintaining seated stability [44]. Many individuals with neuromusculoskeletal conditions, including two-thirds (range: 59.2% to 86.5% depending on the number of years post-injury) of individuals with spinal cord injury (SCI), are wheelchair users [22], and often show degraded trunk control, which requires assistance in seated stability during activities of daily living [23]. Affected individuals are commonly unable to maintain an upright seated posture due to neuromuscular impairment of the trunk [24]. As a result, external perturbations during sitting can cause injurious falls: 69% (95% confidence interval 60–76%) of wheelchair users experience at least one fall each year [12], [28], and falls are the leading cause of injury in this population [27], often requiring hospitalization [29]. The literature has shown that a mechanistic understanding of neuromuscular control in healthy individuals contributes to diagnosing and improving impaired balance as well as developing assistive technologies for restoring trunk stability during impaired sitting [59]. In this light, an approach to quantifying neuromuscular stabilization mechanisms could enable objective assessments and targeted rehabilitative interventions for impaired balance [60], [67] and allow for the design of bio-inspired

assistive technologies [25], [60], [72]. The development of therapies and interventions to improve seated stability in affected individuals could significantly improve their functional ability in activities of daily living and thus increase their quality of life [34].

The seated human body is generally modelled as an inverted pendulum, with its stability achieved via two control mechanisms [46]: (a) passive control without time delay [60], which results from the mechanical stiffness and damping of the muscles and connective tissue generating resistive joint moments to stabilize the trunk [46]; and (b) active control with a time delay that complements the passive control by generating additional phasic joint moments to stabilize the trunk, especially in response to external perturbations [25], [60]. Active joint moments are generated by the sensorimotor system, which activates relevant muscles based on sensory information and anticipated, predictable perturbations [44], [46], [61].

The passive and active control mechanisms of sitting and standing stability have been identified using closed-loop system identification techniques applied to body motion and muscle activation data recorded when the body was perturbed via external stimuli (e.g., external forces, moving support surface, or moving visual surround) [46], [65]. Previous work has identified the dynamics of standing stability [45], [197], including passive as well as active control [44], sensory dynamics [61], [198], [199], muscular dynamics, and sensorimotor time-delay [44], [46], and of seated stability both with [67] and without modeling the muscular dynamics [60], [199]. Nevertheless, all previous work assumed time-invariant linear behaviour for the neuromuscular control that maintains sitting or standing stability and neglected time-variant or nonlinear dynamics. Additionally, previous studies used offline optimization techniques that require time-consuming post-processing of acquired data. This limits the applicability of such models for fast identification of impaired balance or when designing assistive technologies that are robust against time-varying nonlinear neuromuscular dynamics of the body (e.g., due to disturbances and muscle fatigue) and physiological uncertainties in real-world conditions [68]–[71]. In this light, there is a paramount need for a nonlinear neuromechanical model of seated stability that explains the roles of passive and active stabilization mechanisms while accounting for time-varying properties of the neuromuscular system.

Recent work has proposed the use of Extended Kalman filters (EKF) [69], [214] and adaptive fuzzy modelling [71], [215] for online identification of nonlinear time-varying neuromechanical models associated with the human shoulder and knee. Such models can be used

to define robust muscle stimulation patterns and enable online adaptation of the stimulation by estimating relevant neuromuscular information [69]. However, despite their potential, these approaches have not been exploited for identifying nonlinear trunk dynamics and characterizing mechanisms of seated stability.

Therefore, the overall goal of this study was to characterize the roles of passive and active stabilization mechanisms involved in human sitting stability by experimentally identifying nonlinear trunk dynamics in healthy individuals. Specifically, we used an Adaptive Unscented Kalman Filter (AUKF) to identify the parameters of a nonlinear model while accounting for the time-varying process and measurement noise. We assumed that exploiting the adaptive property of the AUKF enabled dynamic adaptation of its properties under uncertain conditions without requiring offline optimization.

8.2 Methods

8.2.1 Participants

Ten able-bodied, young, and male individuals participated in this study (age: 24 ± 4 years; mass: 76 ± 13 kg; height: 178 ± 78 cm; Body Mass Index (BMI): 24 ± 3; mean ± standard deviation). All participants reported no history of neuromusculoskeletal impairments or any disorders that may have affected their seated stability. They gave written informed consent to the experimental procedures, which were approved by the local research ethics board.

8.2.2 Data acquisition

A 16-channel Bagnoli electromyograms (EMG) system including bipolar surface EMG electrodes (DELSYS, Natick, MA, USA) was used. Each EMG sensor had two electrodes with an inter-electrode gap of 10 mm and contact dimensions of 10.0 × 1.0 mm. The EMG system had a peak-to-peak baseline noise of 5 to 10 μV. The common-mode rejection ratio and the input impedance of the electrodes were -92 dB, and 10^{15} Ω, respectively. The analog-to-digital converter generated 16-bit offset binary conversions from analog sources. Surface EMGs were recorded from twelve trunk and upper leg muscles known to contribute to trunk stability and its control during sitting [266]. Bipolar surface EMG electrodes (Bagnoli, DELSYS, Natick, MA, USA) were placed bilaterally over the muscle belly of the rectus abdominis, external oblique, rectus femoris, erector spinae (T9 level), erector spinae (L3 level), and biceps femoris (Figure 8-1) [67]. A self-

adhesive reference electrode was placed over the right iliac crest. EMG data were amplified (gain was muscle- and participant-dependent varying from 10^2 to 10^4), sampled and digitized at 2 kHz. Note that we used surface EMG electrodes in the present study. The literature suggested caution when interpreting data recorded via surface EMG electrodes compared to indwelling EMG electrodes [267]. Nevertheless, many studies have used surface EMG to study trunk muscles' activation [25], [266], [268] and identify neuromuscular parameters [44], [59], [62].

The motion of the body and base-of-support was recorded during the sitting task at 100 Hz using a twelve-camera motion capture system (Vicon Motion Systems Ltd., Oxford, UK). Retroreflective markers were placed bilaterally on the anatomical landmarks [259] of the head, thoracic and lumbar segments of the trunk, arms, hands, pelvis, legs, and feet (Table 8-1 and Figure 8-1). Four markers were placed on the four corners of the seat to record the motion of the base of support.

8.2.3 Experimental protocol

The participants were asked to lie in the supine position with their eyes closed for 60 seconds to establish baseline muscle activity and then performed a series of exercises [67] to determine the maximum voluntary contraction (MVC) for each muscle. Each MVC exercise lasted 30 seconds [269] and was performed three times consecutively [25]. A resting break of 30 seconds was given between exercises to minimize fatigue [269]. Note that there was no observed decrease in muscle activity across the repetitions of each MVC exercise. Next, a T-pose anatomical calibration trial was performed (Figure 8-1) since the anatomical markers of the thoracic and lumbar segments of the trunk and pelvis were removed prior to the main trials. These anatomical markers were reconstructed for the main trials using data from the anatomical calibration.

Participants were subsequently asked to sit, with their arms crossed over the chest and their legs hanging vertically downward, on a customized seat without foot support (Figure 8-1). The seat was fixed on the perturbation platform of a Computer-Assisted Rehabilitation Environment (CAREN; Motek Medical, Amsterdam, The Netherlands). Two-dimensional, white grid lines on a black background were projected on a 180-degree curved virtual-reality projection screen to provide a consistent visual field (Figure 8-1C and Figure 8-1D). Participants were instructed to fix their vision on the screen and maintain their sitting stability without using their lower limbs, while base-of-support perturbations were applied via anteroposterior translation of the platform (Figure

8-1). First, a sudden low-amplitude ramp-shaped perturbation was applied (Figure 8-1E). Next, three 240-second trials with white noise perturbation profiles were performed. Each profile had a mean power spectral density of 4 cm^2/Hz and was filtered via dual-pass first-order high-pass and eight-order low-pass Butterworth filters with cut-off frequencies of 0.1 Hz and 5 Hz, respectively [44]. The first (last) 10 seconds of each profile consisted of a 5-second hold followed (preceded) by increasing (decreasing) ramp motions to avoid abrupt initiation (termination). We used only the middle 220 seconds of each trial to eliminate the initiation and termination effects for analyses. Rest breaks were provided between trials on participant request.

Table 8-1. Retroreflective markers were placed over the anatomical landmarks.

Segment	**Retroreflective markers on anatomical landmarks**
Head	Condyloid process and mastoid process (left and right)
Spine (thorax)	C7, 5 cm bilaterally to C7, and T12 vertebra
Spine (lumbar)	T12, 5 cm bilaterally to T12, and L5
Trunk	T9 vertebra, Suprasternal and xiphoid
Arms	Acromion, lateral epicondylitis, and olecranon (left and right)
Hands	Distal ulna bone, little finger metacarpal head, middle finger distal phalanges
Pelvis	Anterior and posterior superior iliac spine (left and right)
Legs	Greater trochanter, medial and lateral epicondylitis, medial and lateral malleolus
Feet	Calcaneus, 1st and 5th metatarsal heads

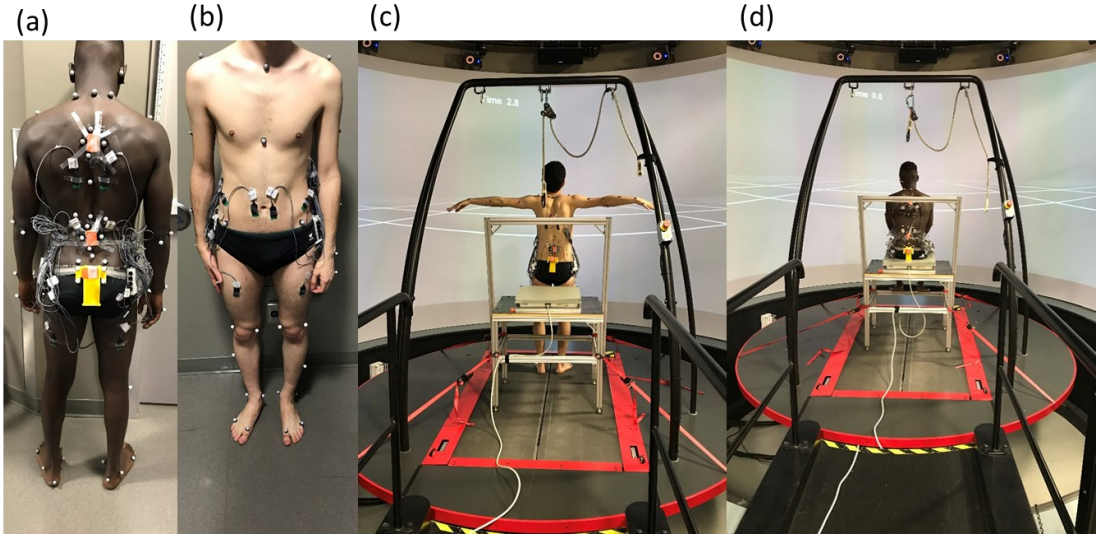

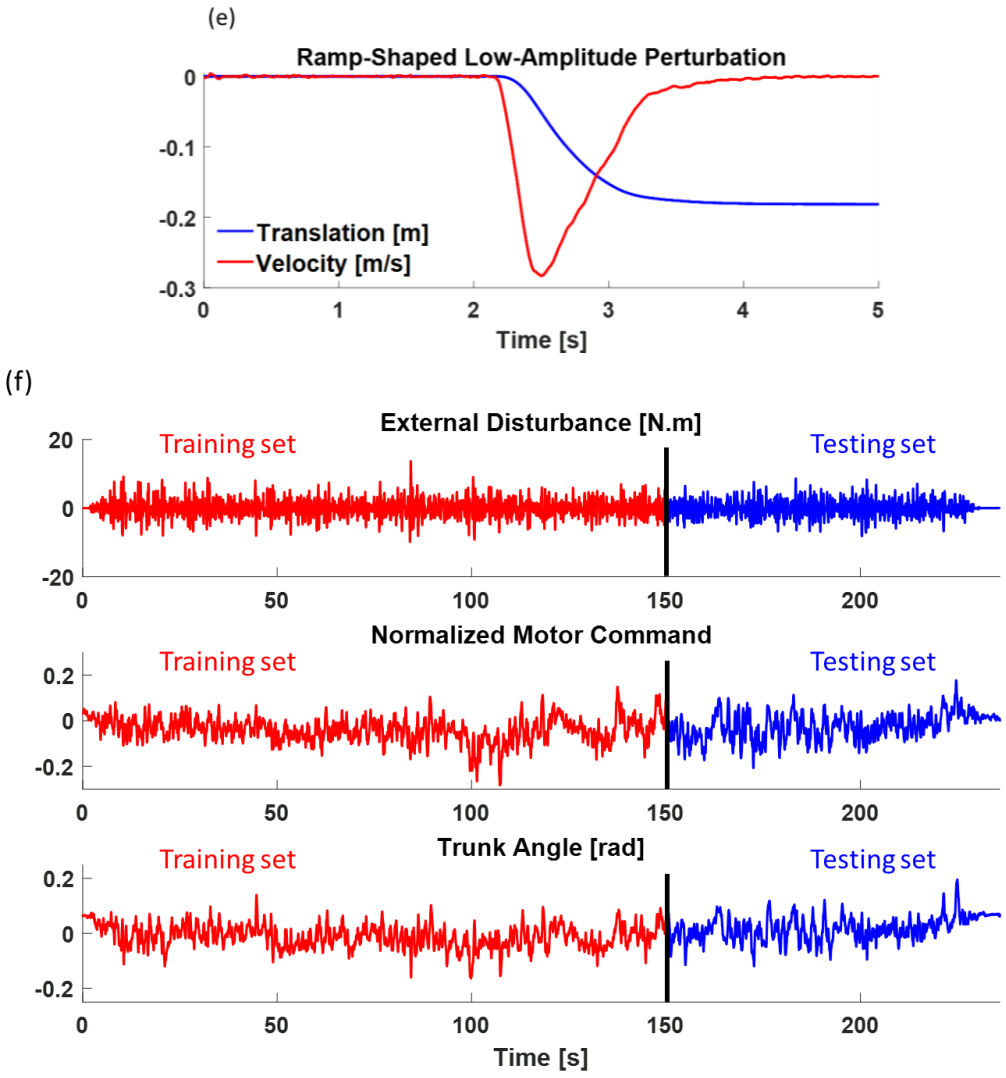

Figure 8-1. Experimental setup at a Computer Assisted Rehabilitation Environment (CAREN): **(a, b)** Retroreflective markers were placed bilaterally on the anatomical landmarks of the head, spine, trunk, arms, hands, pelvis, legs, and feet. Twelve bipolar surface electromyography (EMG) electrodes were placed bilaterally over the muscle belly of rectus abdominis, external oblique, rectus femoris, erector spinae (T9 level), erector spinae (L3 level), and biceps femoris; **(c)** A T-pose anatomical calibration. Note that the recordings of inertial measurement units shown in this figure were not used for the present study; **(d)** Participants sat on a seat fixed on the CAREN platform while base-of-support perturbations were applied to the seat; **(e)** Sudden base of support perturbation characteristics applied to the seat in the form of a ramp-shaped displacement; **(f)** The external disturbance was calculated as the moment applied to the trunk due to the acceleration of the base-of-support measured via the trajectories of retroreflective markers placed on the CAREN platform. The normalized motor command was obtained as the summation of the back muscles' normalized EMG (extensors) subtracted by the summation of the front muscles' normalized EMG (flexors). Trunk sway angle was calculated as the angle between the vertical axis of the lab frame and the line connecting the instantaneous positions of the trunk's center-of-mass and the L5 marker.

8.2.4 Data pre-processing

The EMG time series were divided by gain, demeaned, rectified, and filtered using a moving-average filter with a window size of 100 milliseconds [270]. The EMG time series for the perturbation trials were then normalized using the baseline, and maximum MVC values among the three recorded MVCs:

$$EMG_i^{normal}(t) = \frac{EMG_i(t) - Baseline_i}{MVC_i - Baseline_i} \quad (1)$$

where $EMG_i^{normal}(t)$ and $EMG_i(t)$ are the normalized and measured activity level of muscle i at time t, respectively; $Baseline_i$ is the mean activity level of muscle i during the baseline tests; and MVC_i is the maximum activity level of muscle i during the MVC exercises.

The marker trajectories were low-pass filtered using a dual-pass fourth-order Butterworth filter with a cut-off frequency of 10 Hz. Body segment parameters, including mass, moments of inertia, center-of-mass (COM), and joint center of rotation positions, were derived from cadaveric data of the upper body [254] and lower limbs [223]. Participant-specific body segment parameters were estimated by scaling the cadaveric data using each participant's height and mass [233], [260]. The trunk sway angle modelled the motion of the COM of the upper body during sitting as an inverted pendulum rotating about the L5-S1 joint. Segment kinematics were calculated using the marker trajectories as described in [76], [80]. Subsequently, the position of the trunk COM position at time t ($P_{COM}(t)$) was calculated based on the COM position and mass of the head and neck, thorax, arms, lumbar, and pelvic segments as follows:

$$P_{COM}(t) = \frac{\sum_{i=1}^{N} Mass_i \,.\, P_{COM_i}(t)}{\sum_{i=1}^{N} Mass_i} \quad (2)$$

where $Mass_i$ and $P_{COM_i}(t)$ are the mass and COM position of segment i, respectively, and N is the number of segments, including head and neck, thorax, arms, lumbar, and pelvis. The trunk sway angle ($\theta(t)$) was then calculated as the angle between the vertical axis of the lab frame and the line connecting P_{COM} and the L5 marker (i.e., the inverted pendulum length).

8.2.5 Nonlinear neuromechanical representation

The nonlinear neuromechanical model of trunk stability used in this study is shown in Figure 8-2. The plant, as an inverted pendulum, presents a joint moment due to the gravitational force acting on the trunk's COM. The inherent uncertainties of the system include unmodelled

internal dynamics (e.g., spinal reflexes), system parameter variations (e.g., muscle fatigue), and external disturbances [68]. Hence, the total joint moment acting on the L5-S1 joint is as follows:

$$M_{total} = M_g + M_e + M_v + M_a + M_{unc} + M_{dist} \quad (3)$$

where M_g is the gravitational joint moment; M_e is the passive elastic joint moment; M_v is the passive viscous joint moment; M_a is the active joint moment; M_{unc} represents the joint moment produced by the uncertainty dynamics associated with unmodelled internal dynamics and system parameter variations; and M_{dist} represents joint moments due to external disturbances (Figure 8-2). The passive joint moment (M_p) is the summation of M_e and M_v. M_g, M_e, and M_v are obtained as follows:

$$M_g = -mglsin(x_1 - \theta_0) \quad (4)$$

$$M_e = -K_1 \exp(-K_2 x_1)(x_1 - K_3) \quad (5)$$

$$M_v = -B_1 \, \text{sign}(x_2) \, |x_2|^{B_2} \quad (6)$$

In Equation 4, m is the total mass of the upper body; g is the gravitational acceleration; l is the length of the inverted pendulum; x_1 is the trunk sway angle; and θ_0 is the deviation of the trunk angle from the vertical axis during upright sitting. In Equation 5, $K_1, K_2,$ and K_3 represent the stiffness coefficient, exponential elasticity, and resting elastic angle of the trunk, respectively [69], [271]. In Equation 6, B_1 and B_2 are positive constants representing the damping coefficient and exponential term, respectively; and x_2 is the angular velocity of the inverted pendulum [68].

M_a is modelled based on three components: a muscle recruitment curve followed by critically-damped second-order activation dynamics multiplied by a nonlinear static contraction function, which are described in the following (Figure 8-2) [69]. The recruitment curve is the motor command (u) from the CNS for activating each muscle as a piece-wise saturation function with the lower and upper bounds represented by the baseline and MVC, respectively:

$$u = \begin{cases} 0, & EMG < Baseline \\ EMG^{normal} & Baseline \leq EMG \leq MVC \\ 0, & EMG > MVC \end{cases} \quad (7)$$

where u is the motor command; $Baseline$ is the mean activity level of muscle during the baseline tests; MVC is the maximum muscle activity measured during the MVC tests; and EMG^{normal} is the normalized EMG as calculated in Equation (1). The total motor command (u_{total}) is obtained

as the summation of the back muscles' motor commands (extensors) subtracted by the summation of the front muscles' motor commands (flexors):

$$u_{total} = \sum_{i=1}^{6} [u_i]_{Extensors} - \sum_{j=1}^{6} [u_j]_{flexors} \quad (8)$$

where i and j are summation indices for extensor and flexor muscles, respectively. u_{total} is converted to a normalized activation with a time delay using a second-order transfer function. This transfer function represents the dynamic behaviour of the muscle activation due to calcium release dynamics, muscle fibre conduction velocities, and the time delay associated with chemical reactions [69], [211]:

$$\dot{x}_3 = x_4, \qquad \dot{x}_4 = -2\omega_0\beta x_4 - {\omega_0}^2 x_3 + {\omega_0}^2 u_{total}(t - T_d) \quad (9)$$

where x_3 is the normalized activation; ω_0 is the natural frequency; β is a damping coefficient equal to unity; and T_d is the input time delay. M_a is obtained as the normalized activation multiplied by a nonlinear contraction function ($\mathcal{F}_m$) under non-isometric muscle contraction conditions (Figure 8-2) [69]:

$$M_a = \mathcal{F}_m(x_1, x_2)x_3 \quad (10)$$

where $\mathcal{F}_m$ is the maximal active moment in the case of full muscle activation based on the trunk angular position(x_1) and velocity (x_2) represented by a normalized radial-basis function (RBF) neural network [69]. We used nine RBFs to describe $\mathcal{F}_m$. The center of the associated Gaussian functions was selected using grid-partitioning over the range of x_1 and x_2 during non-isometric muscle contraction with equal variances and high overlapping [69]. Therefore, $\mathcal{F}_m$ acts as a state-varying gain for the muscle activation dynamics.

The joint moment due to external disturbances (M_{dist}) was calculated based on the motion of the base of support as follows:

$$M_{dist} = -m.\, a_{BOS}.\, l.\, cos(x_1) \quad (11)$$

where m is the total mass of the upper body; l is the length of the inverted pendulum; x_1 is the trunk sway angle, and a_{BOS} is the acceleration of the base of support.

M_{unc} is modelled via a second-order recursive Autoregressive with Extra Input (ARX) in parallel:

$$M_{unc} = J * Unc(t) \tag{12}$$

$$Unc(t) = -\sum_{i=1}^{2} a_i Unc(t-i) + \sum_{i=0}^{2} [\, b_{1,i} x_1(t-i) + b_{2,i} x_2(t-i) + b_{3,i} u_{total}(t-T_d-i) \,] \tag{13}$$

where J is the moment of inertia of the inverted pendulum; and Unc is the uncertainty as a function of x_1, x_2, and u_{total}. The model coefficients are $a_i, b_{1,i}, b_{2,i}, b_{3,i}$ (i: summation index) adjusted by a recursive least squares (RLS) algorithm to account for time-varying uncertainties when an identified model is used in real-time. The cost function was defined to minimize the difference between the actual ($\ddot{\theta}_{t,\ actual}$) and estimated ($\ddot{\theta}_{t,\ model}$) angular acceleration as follows [68]:

$$Cost = \frac{1}{2}\sum_{t=1}^{T} {e_t}^2 = \frac{1}{2}\sum_{t=1}^{T} (\ddot{\theta}_{t,\ actual} - \ddot{\theta}_{t,\ model})^2 \tag{14}$$

where T is the duration of a trial; e_t is the error between the actual ($\ddot{\theta}_{t,\ actual}$) and estimated ($\ddot{\theta}_{t,\ model}$) angular acceleration at time sample t.

8.2.6 State-space representation

The nonlinear dynamics of the trunk depicted in Figure 8-2 can be represented in state-space form with four state variables and one input as follows:

$$\dot{x} = \begin{bmatrix} \dot{x}_1 \\ \dot{x}_2 \\ \dot{x}_3 \\ \dot{x}_4 \end{bmatrix} = f(x,\ u_{total}) \tag{15}$$

$$f(x,\ u_{total}) = \begin{bmatrix} x_2 \\ \frac{1}{J}[M_g(x_1) + M_e(x_1) + M_v(x_2) + M_a(x_1, x_2, x_3) + M_{unc}(x_1, x_2) + M_{dist}] \\ x_4 \\ -2\omega_0\beta x_4 - {\omega_0}^2 x_3 + {\omega_0}^2 u_{total}(t - T_d) \end{bmatrix} \tag{16}$$

$$y = Cx = [1\ 0\ 0\ 0] \begin{bmatrix} x_1 \\ x_2 \\ x_3 \\ x_4 \end{bmatrix} \tag{17}$$

where $\dot{x}$ is the time derivative of the state-vector x and y is the system measurement.

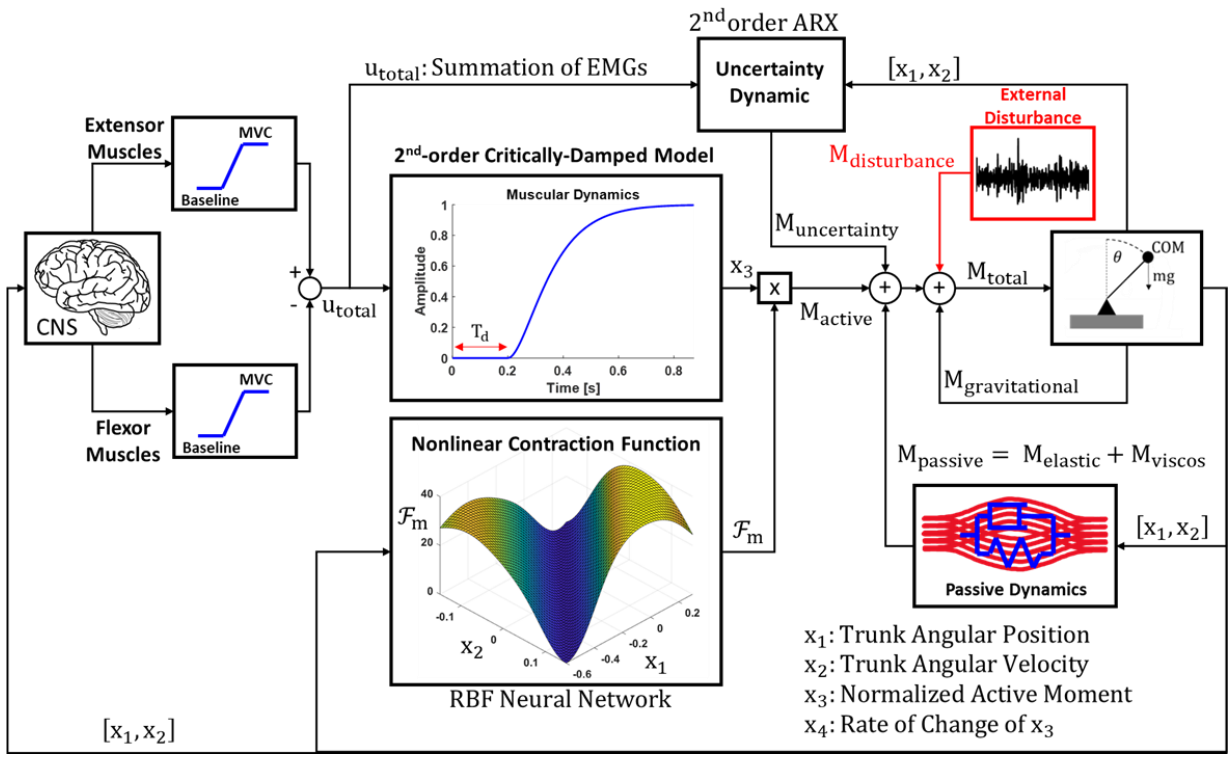

Figure 8-2. The nonlinear neuromechanical model of the trunk consists of passive control, active control, and the plant modelled as an inverted pendulum. This model also accounts for the system's inherent uncertainties, including unmodelled internal dynamics (e.g., spinal reflexes) and system parameter variations (e.g., muscle fatigue) as well as external disturbances [68]. The total joint moment acting on the L5-S1 joint (M_{total}) is obtained as the summation of the gravitational joint moment (M_g), passive elastic joint moment (M_e), passive viscous joint moment (M_v), active joint moment (M_a), joint moment produced by the uncertainty dynamics (M_{unc}), and joint moments due to external disturbances (M_{dist}). m is the total mass of the upper body, g is the gravitational acceleration, l is the length of the inverted pendulum (i.e., the distance between the trunk's center-of-mass and the L5 marker), x_1 and x_2 are the sway angle and angular velocity of the inverted pendulum. M_e shows the nonlinear elasticity of the trunk [69], [271]. M_v shows the nonlinear damping function [68]. M_a consists of a muscle recruitment curve followed by a critically damped 2nd-order activation dynamics multiplied by a nonlinear static contraction function [69]. The recruitment curve shows the activated motor command (u) from the CNS for activating each muscle as a piece-wise saturation function with the lower and upper bounds represented by the baseline and MVC, respectively. The total motor command (u_{total}) is the summation of the back muscles' motor commands (extensors) subtracted by the summation of the front muscles' motor commands (flexors). The total motor command is converted to a normalized activation with a time delay (T_d) using a 2nd-order transfer function. This transfer function represents the dynamic behavior of the muscle activation due to calcium release dynamics, muscle fiber conduction velocities, and time delay associated with the chemical reactions [69], [211]. $\mathcal{F}_m$ is the nonlinear contraction function defined as the maximal active moment in case of full muscle activation and is a function of the angle (x_1) and angular velocity (x_2) of the trunk [69]. M_{unc} is modelled via a 2nd-order recursive ARX in parallel. The inputs of the uncertainty dynamics are the angular position and velocity as well as the motor command. The model coefficients are adjusted by a recursive least squares algorithm for accounting for time-varying uncertainties when an identified model is being used in real-time [68].

8.2.7 Identification of passive control

In accordance with the literature [212], we assumed that low-amplitude perturbations mostly elicit passive mechanisms rather than active postural control mechanisms. Therefore, we

used the experimental data for the sudden low-amplitude, ramp-shaped perturbation and a nonlinear least-squares algorithm to find the participant-specific passive stiffness (K_1, K_2, K_3) and damping (B_1, B_2) parameters of the neuromechanical model. The initial value of these parameters were obtained from the literature [212], [271].

8.2.8 Identification of active control

The active control parameters ($\emptyset$) were taken to be the natural frequency (ω_0) of the activation dynamics and the weights (ψ) of the RBF neural network describing $\mathcal{F}_m$. We assumed that the active control parameters were slowly varying in comparison to the process dynamics [69]. We used a dual-estimation scheme by forming an augmented state vector (z) as follows:

$$\dot{z} = \begin{bmatrix} \dot{x} \\ \dot{\emptyset} \end{bmatrix} = \begin{bmatrix} f(x, u_{total}, \emptyset) \\ 0 \end{bmatrix} = g(z, u_{total}), \qquad z = \begin{bmatrix} x \\ \emptyset \end{bmatrix}, \qquad \emptyset = \begin{bmatrix} \omega_0 \\ \psi \end{bmatrix} \tag{18}$$

We used a UKF according to [272] (Table 8-2, *Algorithm 1*) to estimate the augmented state vector using the augmented state-space model together with the experimental data for the three 240-second perturbation trials. We assumed that the available observation of the system was the discrete-time trunk sway angle, and the input and measurement signals were constant between two consecutive discrete samples. Hence, the discrete-time model for state-estimation is as follows:

$$z_k = g\left(z_{k-1}, u_{total,k-1}\right) + w_k \tag{19}$$

$$y_k = h(z_k) + v_k$$

where $g\left(z_{k-1}, u_{total,k-1}\right)$ is the state transition function; w_k and v_k are uncorrelated sampled white noise signals describing the process and measurement noises with covariance matrices Q_k and R_k, respectively; and h is the measurement function. The initial augmented state vector was $[y(0), 0, 0, 0, \hat{\omega}_0(0), \hat{\psi}_0(0)]'$, where $y(0)$ is the initial measured trunk angular position; $\hat{\omega}_0(0)$ is equal to 8.33 rad/s, as reported in the literature [178]; and $\hat{\psi}(0)$ was randomly generated in the range [-0.01, 0.01] [69]. We employed two approaches to optimize the parameters associated with the UKF for maximizing the accuracy of the estimation: (a) offline optimization, using a genetic algorithm [273], on the first 240-second perturbation trial for each participant; and (b) online optimization, using an AUKF [274], [275], on the second and third 240-second perturbation trials for each participant.

8.2.9 UKF with offline optimization of filter parameters

We used a custom genetic algorithm implemented in MATLAB R2020a (MathWorks, Natick, MA, USA) to optimize the UKF parameters. The optimization variable vector (Θ) was defined as the scaling parameters associated with the unscented transform (α, β, κ), the process noise covariance matrix (Q) elements, and the measurement noise covariance (R). Process noises were assumed to be uncorrelated and, thus, Q was a diagonal matrix. The cost function was defined to maximize the log-likelihood of the measurement, according to [273], as follows:

$$\log p(Y|\Theta) = \frac{\sum_{t=1}^{T} \log\left(\mathcal{N}\left(y(t)\middle|\hat{y}(t),\, S(t)\right)\right)}{T}; \tag{20}$$

$$\mathcal{N}(x|\mu,\, \sigma) = \frac{1}{\sqrt{2\pi\sigma^2}} \exp\left(-\frac{(x-\mu)^2}{2\sigma^2}\right); \tag{21}$$

where $y(t)$ is the measurement at time t; $\hat{y}(t)$ and $S(t)$ are, respectively, the mean and covariance of the measurement estimate resulting from the UKF with filter parameters Θ; and $\mathcal{N}(x|\mu,\, \sigma)$ is the likelihood of x, given a normal distribution with a mean of μ and standard deviation of σ.

Table 8-2.The standard Unscented Kalman filter (UKF) (Algorithm 1) and the Adaptive UKF (AUKF) (Algorithm 2) algorithms where $g(*)$ and $h(*)$ denote state transition function and measurement function, respectively; x and y represent state and measurement vectors, respectively; X and Y represent sigma points associated with the state and measurement vectors, respectively, resulting from the unscented transform; P represents error covariance matrix; Q and R represents process and measurement noise covariance matrices; α, β, κ represents filter scaling parameters; L represents the number of states; $W_i^{(c)}$ and $W_i^{(m)}$ are the weights associated with the covariance and mean of the sigma points, respectively, and $\hat{K}_k$ represents the Kalman gain. In AUKF, $\chi^2_{\sigma,s}$ represent a chi-square distribution with s degree of freedom to detect a fault with a reliability level of $1-\sigma$; φ_k is a statistical function to detect the fault; γ is a weighting factor showing the adaptation strength, and δ describes the distance between the mean of the state $\hat{x}$ and the sigma points. Note, k shows the time step and $k|k$ and $k|k-1$ represent the a posteriori and a priori estimates, respectively.

Algorithm 1. The standard Unscented Kalman filter (UKF) [272]	
Inputs	$g(*), h(*), \hat{x}_0, \hat{P}_0^{xx}, Q, R, \alpha, \beta, \kappa, L$
1:	**Initialize Unscented Transform weights:**
2:	$\lambda = \alpha^2(L+\kappa) - L$
3:	$W_0^{(m)} = \lambda/(L+\lambda)$; $W_0^{(c)} = \lambda/(L+\lambda) + (1-\alpha^2+\beta)$;
4:	$W_i^{(m)} = W_i^{(c)} = \lambda/2(L+\lambda)$; $i = 1 \rightarrow 2L$
5:	**for** time-step k = 1 → K do
6:	Calculate sigma points:
7:	$X_{k-1\|k-1} = [\hat{x}_{k-1\|k-1}, \hat{x}_{k-1\|k-1} \pm \sqrt{(L+\lambda)\hat{P}^{xx}_{k-1\|k-1}}]$;
8:	Time update:

9: $X_{k|k-1} = \mathcal{g}(X_{k-1|k-1})$;
10: $\hat{x}_{k|k-1} = \sum_{i=0}^{2L} W_i^{(m)} X_{k|k-1}^i$;
11: $\hat{P}_{k|k-1}^{xx} = \sum_{i=0}^{2L} W_i^{(c)} \left[X_{k|k-1}^i - \hat{x}_{k|k-1}\right]\left[X_{k|k-1}^i - \hat{x}_{k|k-1}\right]^T + Q$;
12 $Y_{k|k-1} = \mathcal{h}(X_{k|k-1})$;
13: $\hat{y}_{k|k-1} = \sum_{i=0}^{2L} W_i^{(m)} Y_{i,k|k-1}$;
14: Measurement update:
15: $\hat{P}_{k|k-1}^{yy} = \sum_{j=0}^{2L} W_i^{(C)} \left[Y_{k|k-1}^i - \hat{y}_{k|k-1}\right]\left[Y_{k|k-1}^i - \hat{y}_{k|k-1}\right]^T + R$;
16: $\bar{P}_{k|k-1}^{xy} = \sum_{i=0}^{2L} W_i^{(c)} \left[X_{k|k-1}^i - \hat{x}_{k|k-1}\right][Y_{k|k-1}^i - \hat{y}_{k|k-1}]^T$;
17: $\hat{K}_k = \bar{P}_{k|k-1}^{xy}(\hat{P}_{k|k-1}^{yy})^{-1}$;
18: $\hat{x}_{k|k} = \hat{x}_{k|k-1} + \hat{K}_k\left(y_k - \hat{y}_{k|k-1}\right)$,
19: $\hat{P}_{k|k}^{xx} = \hat{P}_{k|k-1}^{xx} - \hat{K}_k \hat{P}_{k|k-1}^{yy}(\hat{K}_k)^T$;
20: Save $\hat{x}_{k|k}$ and $\hat{P}_{k|k}^{xx}$
21: **end for**

Algorithm 2. The Adaptive Unscented Kalman filter (AUKF) [274], [276]

Inputs $\mathcal{g}(*), \mathcal{h}(*), \hat{x}_0, \hat{P}_0^{xx}, Q_0, R_1, \alpha_1, \beta, \kappa, \chi_{\sigma,s}^2$
1: Initialize standard UKF $\rightarrow W_i^{(m)}, W_i^{(c)}, X_{k-1|k-1}$
2: **for** time-step k = 1 → K do
3: Perform standard UKF: $\hat{x}_{k|k}, K_k, P_{k|k-1}^{yy}, P_{k|k}^{xx}$
4: Perform the fault-detection mechanism: $\varphi_k = \mu_k^T[P_{k|k-1}^{yy} + R_k]^{-1}\mu_k$
5: **if** $\varphi_k > \chi_{\sigma,s}^2$ then
6: Update Q_{k-1} and R_k;
7: Innovation: $\mu_k = y_k - h(\bar{x}_{k|k-1})$, Residual: $\varepsilon_k = y_k - h(\hat{x}_{k|k})$;
8: $\hat{S}_{k|k}^{yy} = \sum_{j=0}^{2L} W_i^{(c)} [\mathcal{h}\left(X_{k|k}^i\right) - \bar{y}_{k|k}][h\left(X_{k|k}^i\right) - \bar{y}_{k|k}]^T$;
9: $\gamma = \max\{\gamma_0, (\varphi_k - a \times \chi_{\sigma,s}^2)/\varphi_k\}$
10: $Q_{k-1} = (1-\gamma)Q_{k-1} + \gamma(K_k \mu_k \mu_k^T K_k^T), R_k = (1-\gamma)R_k + \gamma\left(\varepsilon_k \varepsilon_k^T + \hat{S}_{k|k}^{yy}\right)$;
11: Correct the state estimate:
12 $\hat{y}_{k|k} = \sum_{i=0}^{2L} W_i^{(m)} h\left(X_{k|k}^i\right)$;
13: $\bar{P}_{k|k}^{xx} = \sum_{i=0}^{2L} W_i^{(c)} \left[X_{k|k}^i - \hat{x}_{k|k}\right]\left[X_{k|k}^i - \hat{x}_{k|k}\right]^T + Q_{k-1}$;
14: $\bar{P}_{k|k}^{xy} = \sum_{i=0}^{2L} W_i^{(c)} \left[X_{k|k}^i - \hat{x}_{k|k}\right][h\left(X_{k|k}^i\right) - \hat{y}_{k|k}]^T$;
15: $\hat{P}_{k|k}^{yy} = \hat{S}_{k|k}^{yy} + R_k$, $\hat{K}_k = \bar{P}_{k|k}^{xy}(\hat{P}_{k|k}^{yy})^{-1}$;
16: $\hat{x}_{k|k} = \hat{x}_{k|k} + \hat{K}_k\left(y_k - \hat{y}_{k|k}\right)$, $\hat{P}_{k|k}^{xx} = \bar{P}_{k|k}^{xx} - \hat{K}_k \hat{P}_{k|k}^{yy}(\hat{K}_k)^T$;
17: **end if**
18: $Q_k \leftarrow Q_{k-1}$ and $R_{k+1} \leftarrow R_k$
19: Save $\hat{x}_{k|k}$ and $\hat{P}_{k|k}^{xx}$
20: $\delta_k = [\sqrt{(L+\kappa)P_k}]_i$, $\delta_k^{max} = \max\{\delta_k(i,i)\}$;
21: $\alpha_{k+1} = \sqrt{trace(P_k)}/\delta_k^{max}$;
22: **end for**

8.2.10 AUKF for online optimization of filter parameters

The UKF performance can deteriorate or even diverge over time due to errors between the actual and modelled noise distributions [274]. Moreover, previous studies have suggested that when the UKF is applied to highly nonlinear models with a constant scaling parameter (α), it can lack robustness [276], [277]. To address these issues, we used the robust adaptive UKF (AUKF) proposed by Zheng et al. [274] to account for uncertain process and measurement noise distributions. The robust AUKF [274] runs a standard UKF at each time step, but employs an online fault-detection mechanism to determine if the process and measurement noise covariance matrices should be updated. Additionally, we used the self-adaptive UKF proposed by Yongfang et al. [276], [277] to account for the time-varying scaling parameter of the filter. Such an approach provided a robust estimate of the augmented state vector despite uncertain conditions, which can facilitate potential online system identification with minimized computation time in future studies. Mathematical details of the robust AUKF and self-tuning scaling parameter are provided in Table 8-2, *Algorithm 2*.

8.2.11 Analysis of model performance

To analyze the performance of the identified neuromechanical model for each participant and trial, we divided each 240-second trial into two sets: (a) a training set, as the first 150 seconds of the trial, used to identify the active control parameters ($\emptyset$); and (b) a testing set, as the last 90 seconds of the trial, used to cross-validate the performance of the identified model. We used the mean squared error (MSE) and correlation coefficient between the actual measurements of the trunk sway angle and the output of the identified model on the testing set to quantify model performance.

8.3 Results

The stiffness parameters (K_1, K_2, K_3) shown schematically in Figure 8-2 were identified to be 139.05 ± 22.97 [N.m/rad], 0.52 ± 1.08 [1/rad], and 0.00 ± 0.00 [rad] (mean ± standard deviation across participants), respectively. The damping parameters (B_1, B_2) in Figure 8-2 were identified to be 12.78 ± 5.78 [N.m.s/rad] and 1.19 ± 0.29 [1/rad], respectively. Figure 8-3 shows a representative time series obtained for the gravitational (M_g) and passive moments (M_p) during a low-amplitude ramp-shaped perturbation.

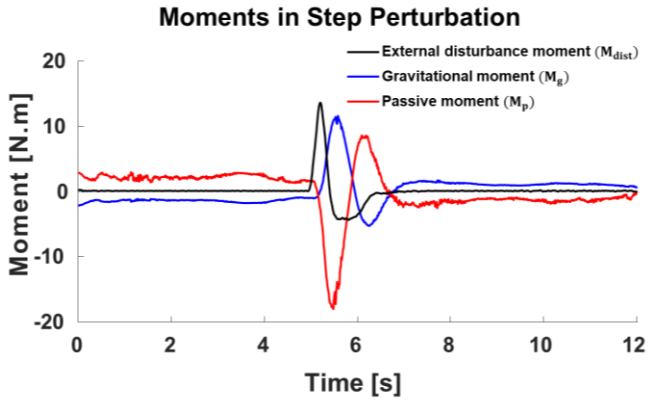

Figure 8-3. A representative time series of the joint moments involved in the low-amplitude step perturbation trial are presented.

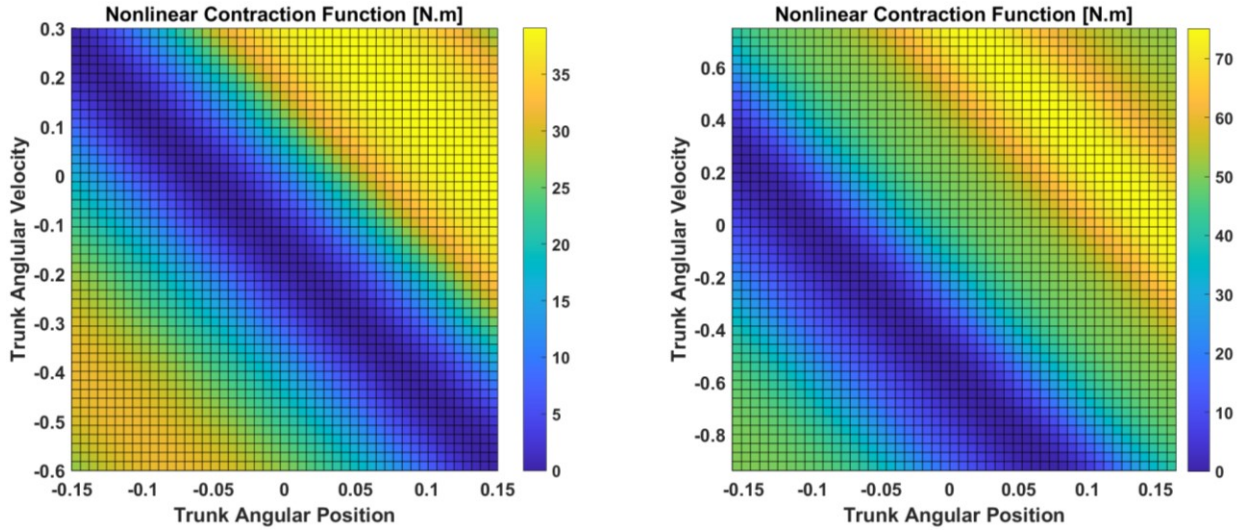

Figure 8-4. Nonlinear contraction function presented as a surface based on the angular position and velocity of the trunk for two representative participants. The nonlinear contraction function shows the maximal active moment in the case of full muscle activation.

The identified natural frequency associated with the muscle activation dynamics (ω_0 in Figure 8-2) was consistent across the three 240-second perturbation trials, with values of 11.35 ± 2.61 [1/s], 12.22 ± 2.98 [1/s], and 12.15 ± 2.82 [1/s] for the first, second, and third trials, respectively, despite UKF being used for identification on the first trial and AUKF being used on the second and third trials. The time delay between the measured feedback and motor command (T_d), which was estimated using correlation analysis, was also consistent across the perturbation trials, with values of 227.50 ± 34.12 [ms], 227.50 ± 27.12 [ms], and 226.25 ± 26.69 [ms]. The nonlinear contraction function ($\mathcal{F}_m$) showed the non-isometric behaviour of the maximal active

moment (Figure 8-4). $\mathcal{F}_m$ decreased (shown in blue in Figure 8-4) when the trunk was in the neutral state (i.e., upright) or when the angular position and velocity exhibited anti-phase behaviour to move the trunk toward the neutral state. By contrast, $\mathcal{F}_m$ increased (shown in yellow in Figure 8-4) when the angular position and velocity increased in the same direction (in-phase behaviour). Figure 8-5A illustrates how the active and passive control mechanisms coordinated to stabilize the trunk against external disturbances and gravitational moments during a 30-second segment of a representative perturbation trial. The total moment (M_{total}) estimated by the identified model could predict the measured inertial moment (top panel of Figure 8-5A). The passive joint moment ($M_p = M_e + M_v$) stabilized the trunk against the gravitational moment without time delay (middle panel of Figure 8-5A), whereas the active joint moment (M_a) played a significant role in stabilizing the trunk against external disturbances (M_{dist}) with time delay (bottom panel of Figure 8-5A). Figure 8-5B demonstrates that including the uncertainty dynamics in the model provided a better estimation of the measured stabilizing joint moment by accounting for unmodelled dynamics and system parameter variations over time.

The goodness of fit of the identified models, as quantified by MSE, was 0.0008 ± 0.0004 [rad^2], 0.0007 ± 0.0003 [rad^2], and 0.0007 ± 0.0006 [rad^2] for the first, second, and third perturbation trials, obtained by UKF, AUKF, and AUKF, respectively. The corresponding correlation coefficients were 84.77 ± 4.91 [%], 86.82 ± 4.70 [%], and 86.72 ± 6.70 [%], respectively. Figure 8-6 shows the ability of the AUKF to estimate the parameters of the nonlinear model over the 150-second segment for characterizing the stabilization mechanisms as well as the trunk sway angle time series obtained by the identified model.

(a)

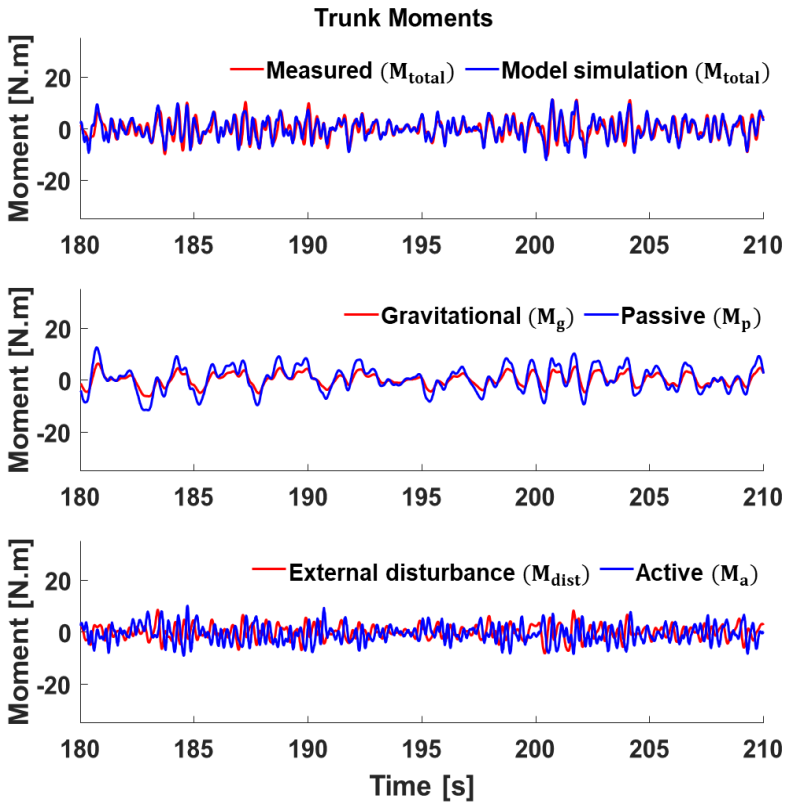
Trunk Moments
Measured (M_{total})
Model simulation (M_{total})
Gravitational (M_g)
Passive (M_p)
External disturbance (M_{dist})
Active (M_a)
Moment [N.m]
20
0
-20
180
185
190
195
200
205
210
Time [s]

(b)

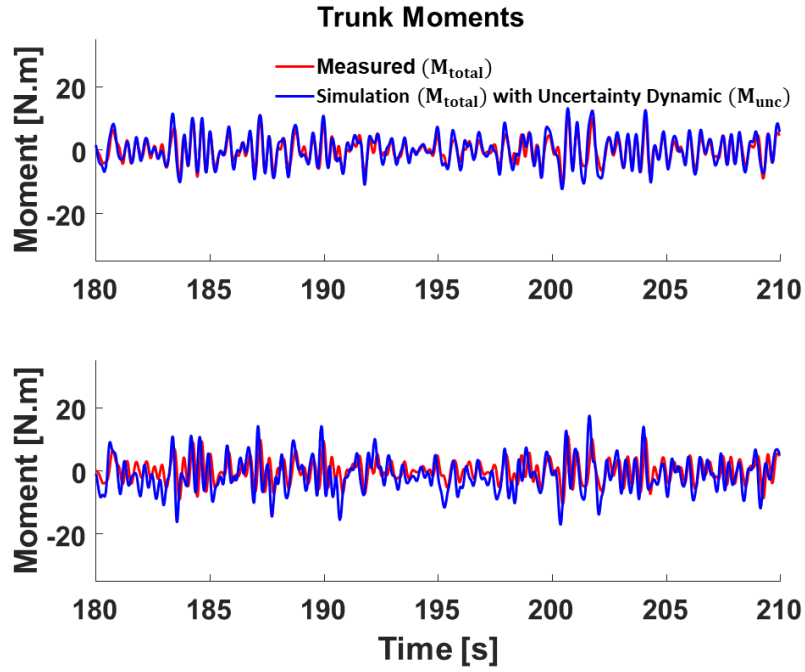
Trunk Moments
Measured (M_{total})
Simulation (M_{total}) with Uncertainty Dynamic (M_{unc})
Moment [N.m]
20
0
-20
180
185
190
195
200
205
210
Time [s]

Figure 8-5. (a) The measured and modelled trunk moments (M_{total}) for a representative perturbation trial (top), decomposed into the gravitational (M_g) and passive moments ($M_p = M_e + M_v$): M_p resists against M_g without a time delay (middle), and external (M_{dist}) and active moments (M_a): M_a resists against M_{dist} with a time delay (bottom). (b) The modelled trunk moment was compared to the measured trunk moment when the model included the uncertainty dynamics to account for unmodelled dynamics and system parameter variations (top). The modelled trunk compared to the measured trunk moment when the model did not include uncertainty dynamics (bottom).

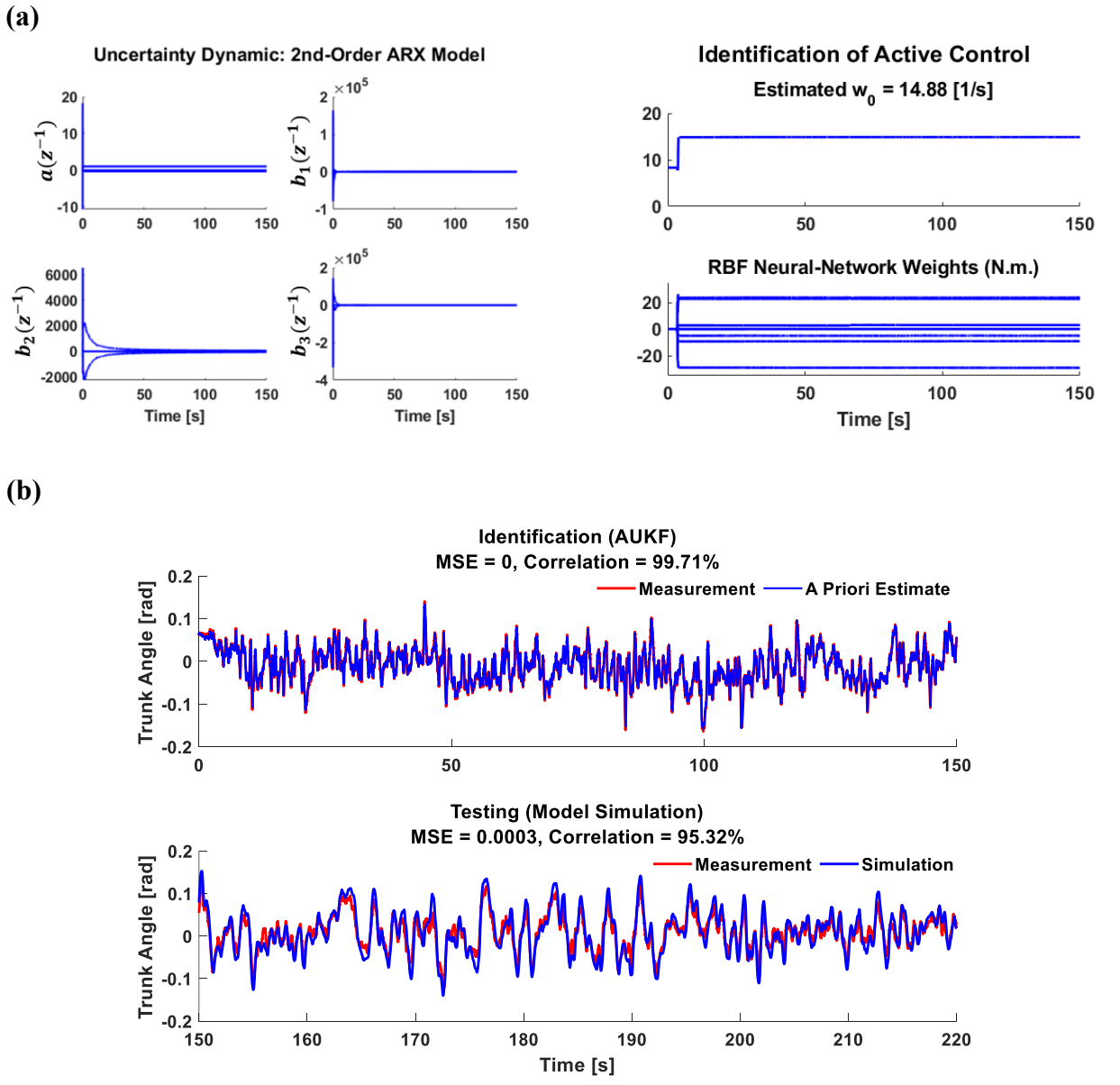

Figure 8-6. (a) Identification of the parameters associated with the uncertainty dynamics (left) and the active control (right) over the first 150 seconds of each trial presented for one trial. (b) The trunk sway angle obtained by the nonlinear neuromechanical model identified in Figure 8-2 compared to the actual measurement (MSE: mean squared error). The adaptive Unscented Kalman filter (AUKF) was applied to the first 150 seconds of the trial to identify the parameters associated with the active control (top). The performance of the identified model was then examined using the rest of the trial (bottom). Note, the first (last) 10 seconds of each 240-second perturbation trial consisted of a 5-second hold followed by increasing (decreasing) ramp motions to avoid abrupt initiation (termination) and therefore, we only used the middle 220 seconds for analyses.

Table 8-3. Summary of the identified passive and active controls' parameters expressed as mean ± standard deviation. The sudden perturbation trial was used to identify passive control parameters using a nonlinear least-squares algorithm. The first 240-second perturbation trial was used to identify active control parameters using a UKF tuned with offline optimization. The second and third 240-second perturbation trials were used to identify active control parameters using an AUKF.

	Sudden Perturbation Trial	**240-Second Perturbation Trial 1**	**240-Second Perturbation Trial 2**	**240-Second Perturbation Trial 3**
$\mathbf{K_1}$ $[\mathbf{N.m/rad}]$	139.05 ± 22.97	-	-	-
$\mathbf{K_2}$ $[\mathbf{1/rad}]$	0.52 ± 1.08	-	-	
$\mathbf{K_3}$ $[\mathbf{rad}]$	0.0001 ± 0.0001	-	-	-
$\mathbf{B_1}$ $[\mathbf{N.m.s/rad}]$	12.78 ± 5.78	-	-	-
$\mathbf{B_2}$ $[\mathbf{1/rad}]$	1.19 ± 0.29	-	-	-
$\boldsymbol{\omega_0}$ $[\mathbf{1/s}]$	-	11.35 ± 2.61	12.22 ± 2.98	12.15 ± 2.82
$\mathbf{T_d}$ $[\mathbf{ms}]$	-	227.50 ± 34.12	227.50 ± 27.12	226.25 ± 26.69

8.4 Discussion

This study aimed to characterize the roles of the passive and active control mechanisms involved in trunk stabilization during sitting by experimentally identifying a neuromechanical model of nonlinear trunk dynamics in healthy individuals using UKF and AUKF. We used an AUKF to identify the parameters of the neuromechanical model to account for the time-varying process and measurement noise.

8.4.1 Developed neuromechanical model and its validity

Identifying the passive control mechanism is challenging since it requires differentiating the M_p from M_a during perturbed sitting. Previous studies [26], [212] have suggested that the contribution of M_a to trunk stabilization is negligible compared to that of M_p during low-amplitude seated perturbations. Accordingly, we used a low-amplitude, ramp-shaped base-of-support perturbation to quantify the behavior of the passive mechanism. Notably, low-level tonic muscle activation may present as co-contractions when a low-amplitude perturbation is applied. Nevertheless, such tonic muscle activation contributes to the passive mechanism by increasing the stiffness and damping properties of the trunk without time delay [25], [26].

Previous studies [271] have suggested that a nonlinear component, expressed as an exponential term, improves the estimation of the stiffness characteristic, and that the resting elastic angle (K_3) could differ from the natural upright angle [271]. Accordingly, we used a nonlinear stiffness model that accounts for the nonlinear elasticity behavior and resting elastic angle of the trunk. Our obtained stiffness and damping coefficients were comparable to the findings of previous

studies that reported the trunk stiffness (K_1), damping (B_1), and nonlinear elasticity (K_2) from 100 to 200 [N.m/rad] [212], 10 to 15 [N.m.s/rad] [212] , and -0.486 to 2.024 [1/rad] [271], respectively. We also found that the identified K_3 was negligible compared to the natural upright trunk angle during sitting.

We followed previous studies [66], [194] that demonstrated the capability of filtered white noise as an external disturbance for characterizing the active mechanism of stability during standing. The recruitment curve was used to introduce the physiological nonlinearity due to the constraints imposed by the minimum and maximum possible muscle excitation levels for each muscle. Opposing signs were used when calculating the total motor commands for posterior and anterior trunk muscles to account for the fact that they generate joint moments in opposing directions [44]. While we used a delayed, critically-damped second-order model to quantify the muscle activation dynamics similar to [62], [278], we used a nonlinear contraction function ($\mathcal{F}_m$), instead of a constant gain, to account for the non-isometric muscle activation condition. Hence, we quantified the muscle activation dynamics by the following parameters: ω_0, T_d, and $\mathcal{F}_m$ (see Figure 8-2). Since the total motor command was an input to the muscle activation dynamics, the identified ω_0 is an average representation of twitch contraction frequency across all relevant muscles. Previous studies [44], [62], [69] reported the twitch contraction frequency from 4 to 25 [rad/s] for different muscles, which agrees with our results (Figure 8-4). The identified T_d captures the latency between the sensory feedback and the M_a. The identified T_d in Figure 8-2 is within the range of values reported by Audu and Triolo [60] (200 [ms]) as well as Goodworth and Peterka [199] (280 [ms], termed the long-latency). We used a normalized RBF neural network to represent $\mathcal{F}_m$ for explaining the state-varying gain due to non-isometric muscle contraction. Previous studies [44], [62] used a constant gain for the activation dynamics under isometric conditions for quiet standing. However, this assumption may not be valid during seated tasks such as reaching and bending, which involve a change of length of the trunk muscles. The identified $\mathcal{F}_m$ in Figure 8-4 indicates the necessity of accounting for non-isometric conditions by exhibiting highly nonlinear state-varying behavior with respect to the trunk angular position and velocity.

The performance of the identified neuromechanical model was examined for each participant and trial using MSE and correlation coefficient. Audu and Triolo [60], [62] reported an average root-mean-square error of 0.011 [rad] between their model simulation and measurement; However, they did not describe how the results of their model simulation varied with respect to

measurement. The goodness of fit of our identified neuromechanical model, quantified by MSE, was 0.0007 ± 0.0004 [rad^2] across participants. This value is within the range of accuracy of the motion measurement device, implying that the identified neuromechanical model is highly accurate in comparison to previous studies [60], [62].

8.4.2 Roles of passive and active mechanisms in trunk stabilization

When an external perturbation is applied, the deviation of the trunk from its neutral position generates M_g that is compensated for by a delay-free and resistive M_p due to the intrinsic stiffness and damping properties of the trunk (Figure 8-5A). Previous studies [62] have suggested that M_p contributes up to 91% of the trunk stabilizing moment. Our results confirm that a large majority of the stabilizing joint moment is provided by M_p (Figure 8-5A). However, M_p cannot stabilize the trunk against both gravitational and acceleration effects [60], [62], and an additional phasic response from the active mechanism is needed in response to external disturbances (Figure 8-5A). While M_p acts instantly to stabilize the trunk against undesired trunk motion, the central nervous system (CNS) receives and processes sensory information to generate a delayed phasic joint moment (M_a) by activating relevant trunk muscles in a synergistic manner. We observed that the dynamic behavior of M_a is correlated with that of the external disturbance (Figure 8-5A), indicating that M_a is required to complement M_p, at least in the presence of external disturbances.

We observed that $\mathcal{F}_m$ increased when the angular position and velocity increased in the same direction whereas, when the trunk was in, or moving toward, its neutral position, $\mathcal{F}_m$ decreased (Figure 8-4). The non-isometric behaviour of $\mathcal{F}_m$ showed an increased contribution of M_a to trunk stabilization during extreme motion states where M_p is not likely to stabilize the trunk alone. Note that, unlike M_p, M_a is a time-varying process affected by internal disturbances, muscle fatigue, and strength condition [68], [69]. Although adding the uncertainty dynamics did not change the overall behaviour of the model, it did improve the association between the measured and modelled moments, as shown in Figure 8-5B. This highlights the importance of accounting for the unmodelled internal dynamics in the overall neuromechanical model.

8.4.3 Importance of developing a nonlinear model of neuromuscular mechanisms of seated stability control

Most previous studies assumed time-invariance and linearity of the neuromechanical model for identifying the passive and active mechanisms of seated stability control [44]–[46], [60],

[61], [65], [67], [197]–[199]. This assumption is valid only for small perturbation conditions around an upright posture. Therefore, it limits the understanding of the inherently nonlinear system. Additionally, the offline optimization techniques for model identification reported in the literature do not allow for online correction of the time-varying properties of the identified model (e.g., due to muscle fatigue) after the optimization has been performed. As a result, the applicability of such models is limited when designing control strategies for assistive technologies such as closed-loop FES systems or exoskeletons for long-term operation [70], [71].

The time-varying nonlinear neuromuscular dynamics and high inter-subject variation of the muscle response [68], [70], [71], [215], [279] are reported to be major challenges toward developing a neuroprosthesis utilizing closed-loop control (e.g., FES). Our developed neuromechanical model of seated stability may address these challenges by accounting for the nonlinear behaviour of the active and passive control mechanisms as well as uncertainties due to unmodelled dynamics. Such a bio-inspired neuromechanical model may provide a physiologically meaningful plant model when developing a closed-loop control system. In particular, AUKF, utilized for identifying the properties of the nonlinear neuromechanical model, enables real-time correction of the model parameters (e.g., using forgetting factors), which may allow for tracking system variations due to external disturbances, muscle fatigue, and physiological uncertainties. However, future studies are needed to investigate the applicability of the proposed identification scheme to identify changes in active and passive control mechanisms, and system variations, under uncertain conditions such as fatigue-induced conditions or in individuals with neuromuscular impairments who may exhibit different stabilization mechanisms due to the motor and/or sensory deficits. Furthermore, the identification method used by previous studies [44]–[46], [60], [61], [65], [67], [197]–[199] does not address the adverse effect of the time-varying process and measurement noise on the identification of the neuromechanical model. This adverse effect could impact the performance of assistive technologies in long-term operation, as characteristics of process and measurement noise change appreciably. The noise covariance adaptation mechanism used by AUKF accounts for uncertain process and measurement noise distributions, which could minimize the adverse effect of time-varying noise on the identification of the neuromechanical model. The adaptative property of AUKF could therefore increase the performance of the identified neuromechanical model and may be useful, in the future, for developing more robust assistive technologies under real-world conditions. Moreover, the lower computational cost of

such an identification scheme allows for participant-specific identification of the neuromechanical model, which can facilitate the tailored design of assistive technologies. Nevertheless, future studies may employ the proposed methodology, including the neuromechanical model and the identification scheme to investigate the value of this approach for designing robust assistive technologies aimed at improving stability.

8.4.4 Limitations of the experimental procedure

Since all study participants were able-bodied, young, and male, future studies should investigate the applicability of our findings to other populations requiring assistive technologies. Future studies may investigate between-gender differences in neuromechanical model parameters as well as differences between healthy participants and individuals with impaired seated stability (e.g., due to ageing or any neuromuscular impairments). Future studies may also perform time series analyses based on fractal dimension and Lyapunov exponent to investigate the predictability and convergence of EMG time series for identifying between-gender and age-related differences. We estimated participant-specific body-segment parameters by scaling cadaveric data by participant anthropometric data, which may have introduced uncertainty into the model parameters [233]. We assumed a single-segment inverted pendulum of the trunk, which did not account for intervertebral and upper limb motion. Future studies should investigate the effect of trunk segmentation on the neuromechanical model of seated stability. Using multi-segment models for identifying the neuromechanical model requires uncorrelated external perturbation profiles simultaneously applied to each segment level. Further investigations and sensitivity analysis are needed to determine the effect of segmentation on the passive and active parameters describing the neuromechanical model. In the present study, we used AUKF to identify the parameters of the neuromechanical model in young, healthy individuals during a short amount of time while assuming the active control parameters were slowly varying in comparison to the process dynamics. Future studies may investigate the utilization of AUKF with a forgetting factor to track variations of active control parameters due to muscle fatigues over longer durations. Finally, we only investigated motion in the sagittal plane; however, the trunk muscles selected for this study also contribute to the trunk's motion in the frontal and transverse planes. Therefore, future work should extend our model to seated stability in the frontal and transverse planes. Nevertheless, the present study took a step toward the quantification of seated stability, which could provide the foundation for further related work.

8.5 Conclusions

This study experimentally identified a nonlinear, time-varying neuromechanical model of seated stability that captures both passive and active control mechanisms under non-isometric conditions in healthy individuals. The developed model predicted the role of the active and passive mechanisms involved in trunk stability of able-bodied young adults during perturbed sitting with high accuracy. This model may enable a comprehensive mechanistic understanding of the various components of the neuromuscular control system involved in the seated stability of able-bodied young adults.

8.5.1 What is next?

We validated a methodology for a mechanistic understating of the passive and active stabilization mechanisms involved in dynamic stability. However, the role of the neural control in regulating dynamic stability and how it appears to operate still require investigation. In the next chapter, the high-level task goals of the neural control that regulates dynamic stability were investigated.

Chapter 9

This chapter shows an approach to characterize neural control and its task goals to regulate seated stability using a nonlinear neuromechanical model and nonlinear control theory. This chapter has been adopted and/or edited from:

A. Noamani, A. H. Vette, and H. Rouhani, "Nonlinear Neural Feedback Explains Task Goals of Central Nervous System for Trunk Stability in Sitting Posture," ready for submission.

9 CNS Task Goals of Seated Stability

9.1 Introduction

Maintaining stability of the inherently unstable human trunk during sitting requires the complex interaction of several components of the sensorimotor system [44], [59]. Individuals with moderate-to-severe sensorimotor impairments, e.g., up to two-thirds of individuals with spinal cord injury, suffer from reduced trunk stability and the inability to sit unassisted [22]–[24]. Consequently, they are at risk of injurious falls when exposed to external sitting disturbances, with nearly 70% of wheelchair users experiencing at least one fall each year [28]. Such falls are the leading cause of injury in this population [27] and often require hospital care [29]. In this light, previous work has demonstrated that an understanding of healthy neuromuscular control can be utilized to identify and restore impaired balance in individuals with neuromuscular impairments [23], [59], [66]. Hence, the characterization of neuromuscular control can contribute to objective balance evaluation and the development of targeted rehabilitative interventions for improving impaired balance [60], [67]. Furthermore, assistive technologies based on neuromodulation, such as functional electrical stimulation (FES), have shown potential for restoring seated stability by stimulating impaired trunk muscles via both open- [175] and closed-loop [27], [176]–[180] control strategies. However, designing bio-inspired controllers for FES systems is challenging [25], [60], [72], since such complex technologies must provide physiological actions similar to those of motor commands (e.g., muscle activation) produced by the healthy neural control system [25]. Therefore, characterizing the neural control of non-impaired seated stability is a prerequisite for bio-inspired closed-loop neuromodulation technology [60].

To characterize neural control, it is essential to determine the task goals representing high-level functional goals of the CNS that regulate seated stability. However, characterizing the task goals for given motor behaviour, such as seated stability, and how the CNS accomplishes these goals via neural control, has been a long-standing question in human motor control research [23]. The literature has proposed different task goals for maintaining an upright standing posture based on the reduction of the body center of mass (COM) sway and pace of sway [44]. Nevertheless, determining the task goals for seated stability, their relative importance in the neural control strategy, and how the neural control regulates this motor task is still an open question. Answering this question requires characterizing the complex interrelation between the underlying neuromuscular stabilization mechanisms and a mechanistic understanding of the closed-loop control system for seated stability.

To characterize the closed-loop postural control system and the interrelation between neuromuscular mechanisms, previous studies have proposed neuromechanical models of human stability. The closed-loop postural control system during sitting can be explained using an inverted pendulum with passive and active stabilization control mechanisms [25], [44], [46], [60], [61]. Identifying the dynamics associated with the process of converting sensory information into motor commands through active feedback control by the CNS characterizes the neural control and its task goals.

Previous studies have identified the neural control as well as the passive and active control of standing and seated stability using linear closed-loop system identification techniques applied to body kinematics and muscle activation data recorded when the body was perturbed via external stimuli (e.g., moving support surface, external forces, or perturbed visual surround) [46], [65]. This work proposed that the neural control generates motor commands based on task goals of minimizing the angular position and velocity [44], [59], [62], [94] as well as acceleration [44], [59] with respect to the static upright posture. Many studies have provided non-parametric estimates of the neural dynamics in both standing and sitting postures using linear closed-loop system identification [44], [59], [60], [197]. Other studies have provided parametric estimates of the neural dynamics by using linear controllers such as proportional-integral-derivative (PID) control [60], [61], [198], [199], proportional-derivative (PD) control [62], [65], and PD control with acceleration feedback [59], [207] to model the neural control functioning for controlling postural stability.

Another approach has been proposed to use linear optimal control theory to characterize the task goals for motor behaviour [44]. This theory characterizes task goals as the minimization of cost functions to obtain optimal performance of the neural control system [280], [281]. In contrast to classic models (e.g., PD or PID) for neural control, the optimal feedback control theory relies on a performance criterion allowing the motor task and neuromechanical model of the body to dictate a control scheme that best describes the actual physiological process and, thus, results in a control law that leads to the best performance [281]. Oftentimes, this approach assumes that the neural feedback is minimizing a cost function that penalizes large motor commands (e.g., muscle activations) and state variables (e.g., body angular kinematics) toward minimizing energy expenditure and guaranteeing stability, respectively. Parameterizing the cost function enables prioritizing the task goals of the neural control for motor behaviour [44]. For a given neuromechanical model of the body, there is optimal neural feedback that minimizes this cost function. Hence, identifying the neural feedback control strategy for a given motor task (e.g., seated stability) would allow us to interpret the cost function and, therefore, explain the relative importance of the task goals [44].

Despite its potential, optimal control theory has not been utilized to characterize neural control and its task goals for regulating seated stability. Characterizing the neural control using PD or PID control schemes along with linear time-invariant neuromechanical models ignores the time-varying nonlinear behaviour of the underlying neuromechanical dynamics associated with physiological uncertainties in real-world conditions [68]–[71]. In addition, the use of control structures such as PID does not reflect optimal neural control strategies and psychological task goals for regulating seated stability. Therefore, utilizing a nonlinear neuromechanical model along with the nonlinear control theory for identifying the neural control would lead to a better mechanistic understanding of the task goals for a given motor behaviour (e.g., seated stability). Such an identification approach may help researchers to overcome a fundamental challenge in human motor control, may facilitate the mathematical identification of neuromechanical mechanisms, and may contribute to objective balance evaluation, development of targeted rehabilitative interventions, and bio-inspired design of assistive technologies, all aimed to improve impaired balance.

This study aimed to address the abovementioned issues by identifying the task goals of the intact neural control associated with seated stability. First, we used a nonlinear neuromechanical

model of the seated human along with a full-state feedback linearization approach and optimal control theory for identifying the neural control. Second, we identified the parameters associated with a cost function that penalizes the motor commands and state variables to achieve seated stability via nonlinear neural feedback. Third, we characterized the task goals for seated stability by interpreting the identified cost function.

9.2 Methods

9.2.1 Participants

Ten healthy, young male individuals volunteered to participate in this study (age: 24 ± 4 years; weight: 76 ± 13 kg; height: 178 ± 8 cm; mean ± standard deviation). All volunteers reported no history of neuromusculoskeletal disorders or any impairments that may have affected their seated stability. Participants gave written informed consent to the experimental procedures, which were approved by the research ethics board of the University of Alberta (Study ID: Pro00063998).

9.2.2 Data acquisition

We placed retro-reflective markers, bilaterally, on the anatomical landmarks [259] of the head, thoracic and lumbar segments of the trunk, arms, hands, pelvis, legs, and feet (Figure 9-1). We also placed four markers on the four corners of the seat. We recorded the trajectory of the body and base-of-support during the experiments using a twelve-camera motion capture system (Vicon Motion Systems Ltd., Oxford, UK) at a sampling rate of 100 Hz.

We placed bipolar electromyography (EMG) electrodes (Bagnoli, DELSYS, Natick, MA, USA) bilaterally over the muscle belly of the erector spinae (T9 level and L3 level), biceps femoris, rectus abdominis, external oblique, and rectus femoris (Figure 9-1) [67]. The selected muscles are known for their major contribution to seated stability [266]. We used a self-adhesive reference electrode placed over the right iliac crest. We amplified EMG data with a muscle- and participant-dependent gain varying from 10^2 to 10^4, sampled and digitized at 2 kHz.

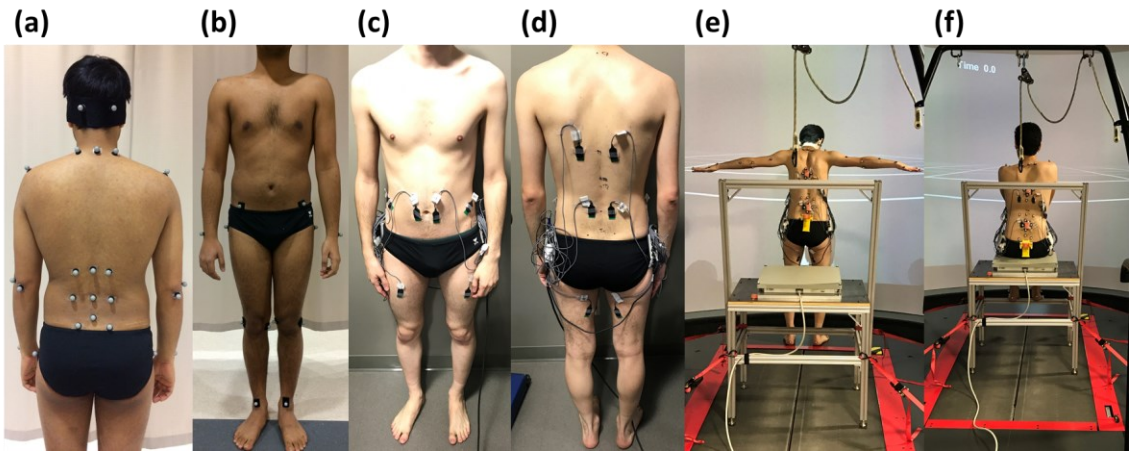

Figure 9-1 The experimental study was conducted at a Computer Assisted Rehabilitation Environment (CAREN): (a, b) Placement of the retroreflective markers; (c, d) Placement of electromyography (EMG) electrodes; (e) A T-pose anatomical calibration was carried out; (f) Participants were asked to sit on a customized seat fastened to the CAREN platform, while base-of-support perturbations in the form of anteroposterior translation of the platform were applied to the seat.

9.2.3 Experimental procedure

We recorded the baseline muscle activity while the participants lay down in the supine position with their eyes closed for 60 seconds. We also recorded the maximum voluntary contraction (MVC) for each muscle while participants performed a series of exercises [67]. Each MVC was performed three times consecutively, with each time lasting 30 seconds. Participants were given a 30-second resting break between MVC exercises to minimize the effect of fatigue. A T-pose anatomical calibration trial was conducted (Figure 9-1). The anatomical markers of the thoracic, lumbar, and pelvic segments were removed prior to the main trials. The anatomical calibration data were then later used to reconstruct the anatomical markers for the main trials.

We fastened a customized seat on a six-degree-of-freedom Stewart platform of a Computer-Assisted Rehabilitation Environment (CAREN; Motek Medical, Amsterdam, The Netherlands) before the session started. A consistent visual surround was provided for all participants by projecting two-dimensional, white grid lines on a black background on a 180-degree curved virtual-reality projection screen (Figure 9-1). Participants sat on a customized seat with their arms crossed over the chest and their legs hanging vertically downward without foot support (Figure 9-1). We asked the participants to keep their vision on the virtual-reality screen and maintain their seated stability while external disturbances were applied in the form of anteroposterior translation of the platform. First, we used a low-amplitude ramp-shaped perturbation suddenly applied to the seat. Subsequently, we used three 240-second white noise

profiles as the perturbation. We designed the white noise profiles with a mean power spectral density of 4 cm^2/Hz, filtered via zero-lag first-order high-pass and eight-order low-pass Butterworth filters with cut-off frequencies of 0.1 Hz and 5 Hz, respectively. Each profile was initiated with a 5-second hold followed by a 5-second increasing ramp and terminated with a 5-second decreasing ramp followed by a 5-second hold to eliminate any abrupt initiation and termination effects. Therefore, the middle 220 seconds of each trial were used for analyses. Between-trial rest breaks were given upon request by the participant.

9.2.4 Data pre-processing

We filtered the motion trajectories via a zero-lag fourth-order low-pass Butterworth filter with a cut-off frequency of 10 Hz. We estimated participant-specific body segment parameters, including mass, moments of inertia, COM, and joint center of rotation positions, by scaling cadaveric data of the upper body [254] and lower limbs [223] using each participant's weight and height [233], [260]. We obtained segmental kinematics based on the marker trajectories as explained in our previous studies [76], [80]. We calculated the instantaneous position of the upper body COM using the weighted summation of the instantaneous COM position of the head and neck, thoracic, lumbar, arms, and pelvic segments. We used an inverted pendulum model to obtain the trunk sway angle as the motion of the upper body COM rotating about the L5-S1 joint.

We divided the EMG time series by gain, and we then demeaned, rectified, and filtered the scaled time series using a moving-average filter with a window size of 100 milliseconds [270]. We down-sampled the EMG time series to 100 Hz and normalized them for the perturbation trials using a Min-Max Scaling approach based on the baseline and maximum MVC (highest values among the three recorded MVCs) of each muscle as the minimum and maximum values, respectively.

9.2.5 Nonlinear neuromechanical model

This section is explained in detail in our previous study [81] and is briefly described here. The nonlinear neuromechanical dynamics of the seated stability were modelled, as illustrated in Figure 9-2. A state-space representation of this model has four state variables, one input and one output. The first two state variables represent the angular position and velocity of the trunk modelled as an inverted pendulum controlled by gravitational, active, and passive joint moments. The other state variables represent critically-damped second-order transfer function associated

with the muscle activation dynamics due to calcium release dynamics, muscle fibre conduction velocities, and the time delay associated with chemical reactions [69], [211]. The state-space representation is as follows:

$$\dot{x} = \begin{bmatrix} \dot{x}_1 \\ \dot{x}_2 \\ \dot{x}_3 \\ \dot{x}_4 \end{bmatrix} = F(x, u, \emptyset) = f(x) + g(x, u) \tag{1}$$

$$f(x) = \begin{bmatrix} x_2 \\ \frac{1}{J}[M_g(x_1) + M_e(x_1) + M_v(x_2) + M_a(x_1, x_2, x_3) + M_{dist}] \\ x_4 \\ -2\omega_0\beta x_4 - {\omega_0}^2 x_3 \end{bmatrix} \tag{2}$$

$$g(x, u) = \begin{bmatrix} 0 \\ 0 \\ 0 \\ {\omega_0}^2 \end{bmatrix} u(t - T_d) \tag{3}$$

$$y = h(x) = x_1 \tag{4}$$

In Equations 1-4, f and g are the system functions; h is the measurement function; $\dot{x}$ is the time derivative of the state-vector x; u is the total motor command; y is the system measurement; x_1 is the trunk sway angle; x_2 is the angular velocity; x_3 is the normalized activation; x_4 is the rate of change of activation; M_g is the gravitational joint moment; M_e is the passive elastic joint moment; M_v is the passive viscous joint moment; M_a is the active joint moment; M_{dist} is the joint moment due to external disturbances; J is the moment of inertia; ω_0 is the natural frequency; β is a damping coefficient equal to unity; and T_d is the input time delay.

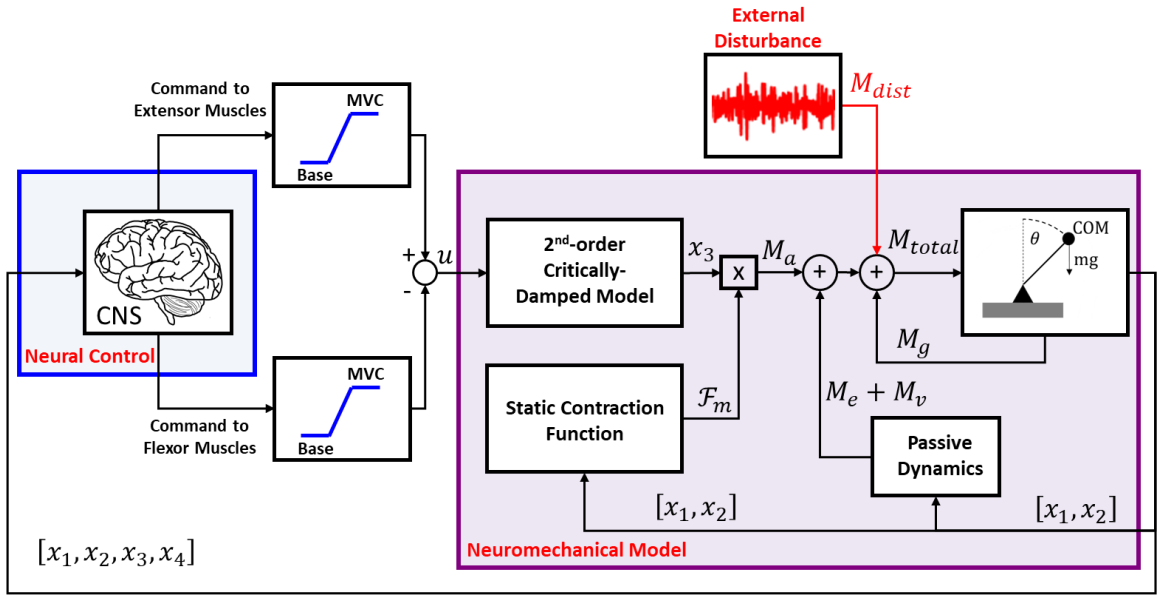

Figure 9-2. The nonlinear neuromechanical model of seated stability was validated in our previous study [81]. A state-space representation of this model has four state variables, and one input and one output. The first two state variables represent the angular position (x_1) and velocity (x_2) of the trunk center of mass (COM) controlled by gravitational ($M_g = -mgl\ sin(x_1 - \theta_0)$), active ($M_a = \mathcal{F}_m(x_1, x_2)x_3$), and passive joint moments ($M_p = M_e + M_v$) composed of elastic ($M_e = -K_1 e^{(-K_2 x_1)(x_1 - K_3)}$) and viscous ($M_v = B_1\ \text{sign}(x_2)\ |x_2|^{B_2}$) components where m is the total mass of the upper body; g is the gravitational acceleration; l is the length of the inverted pendulum, θ_0 is the trunk angle deviation from the vertical axis during upright posture; K_1, K_2, and K_3 are the stiffness coefficient, exponential elasticity, and resting elastic angle of the trunk, respectively [69], [271]; B_1 and B_2 are the damping coefficient and exponential term, respectively [68]; and $\mathcal{F}_m$ is an arbitrary function (e.g., a polynomial or a neural network) modelling the maximal active moment in the case of full muscle activation based on the trunk angular position (x_1) and velocity (x_2). The other state variables (x_3 and x_4) represent a critically damped second-order transfer function associated with the dynamic behaviour of the muscle activation due to calcium release dynamics and muscle fibre conduction velocities, with the parameters ω_0 as the natural frequency and β as a damping coefficient equal to unity as well as the time delay (T_d) associated with chemical reactions. The total motor command (u) was calculated as the summation of the back muscles' motor commands (extensors) subtracted by the summation of the front muscles' motor commands (flexors): Each muscle activation was normalized via Min-Max scaling using its Maximum Voluntary Contraction (MVC) and baseline. External disturbances were modelled as a joint moment M_{dist}.

9.2.6 Identification of passive-active controls

This section is explained in detail in our previous study and is briefly described here [81]. We used the nonlinear neuromechanical model to characterize the passive and active stabilization mechanisms (Figure 9-2). We used the data of the sudden perturbation trial to estimate the parameters of the passive stiffness (K_1, K_2, K_3) and damping (B_1, B_2) by using a Nonlinear Least Squares algorithm by assuming that low-amplitude perturbations mostly elicit passive mechanisms rather than active postural control mechanisms [212]. Subsequently, we used an Unscented Kalman Filter (UKF) [272] on three 240-second perturbation trials to estimate the parameters of the active control in addition to the state variables for each participant using a dual-estimation scheme by forming an augmented state vector:

$$\dot{X} = \begin{bmatrix} \dot{x} \\ \dot{\emptyset} \end{bmatrix} = \begin{bmatrix} F(x, u, \emptyset) \\ 0 \end{bmatrix} = \not{f}(X, u), \qquad X = \begin{bmatrix} x \\ \emptyset \end{bmatrix}, \qquad \emptyset = \begin{bmatrix} \omega_0 \\ \psi \end{bmatrix} \tag{5}$$

Where X is the augmented state vector; $\not{f}$ is the state-space representation of the augmented state-space model, and $\emptyset$ is the active control parameters, including the natural frequency (ω_0) of the activation dynamics and the coefficients (ψ) of the arbitrary function $\mathcal{F}_m$. It was assumed that $\emptyset$ was slowly varying compared to the process dynamics [69]. We have previously shown that such an identification approach, along with the nonlinear neuromechanical model, allows us to quantitatively characterize the active and passive postural control mechanisms with high accuracy [81].

9.2.7 Nonlinear neural feedback: full-state feedback linearization

The use of UKF in the previous study allowed us to observe the state vector (x) of the nonlinear system based on the measurement of the trunk sway angle (y) and the total motor command (u) [81]. In the present study, to characterize the task goals of the neural control, we assumed that

(1) the neural control system acts as an optimal linear quadratic regulator (LQR) that receives full-state linearized feedback from the neuromechanical model, and
(2) the neural feedback minimizes a quadratic cost function that penalizes the motor commands and poor stability performance expressed as the state variables in the linearized space.

Hence, identifying the neural control is to determine:

(1) a diffeomorphism that transforms the state variables of the nonlinear neuromechanical model into a linear space where LQR can be applied.
(2) the weights of the quadratic cost function associated with the LQR control; and
(3) the gains of the LQR that minimizes the quadratic cost function.

This allows us to interpret the cost function and the optimal neural control and, therefore, explain the task goals used by the neural control for seated stability [44]. The process of identifying the neural control is depicted in Figure 9-3, and the details are provided in the following sections. First, we prove that there exists a transformation that transforms the nonlinear neuromechanical model into a linear space where linear optimal control theory can be applied.

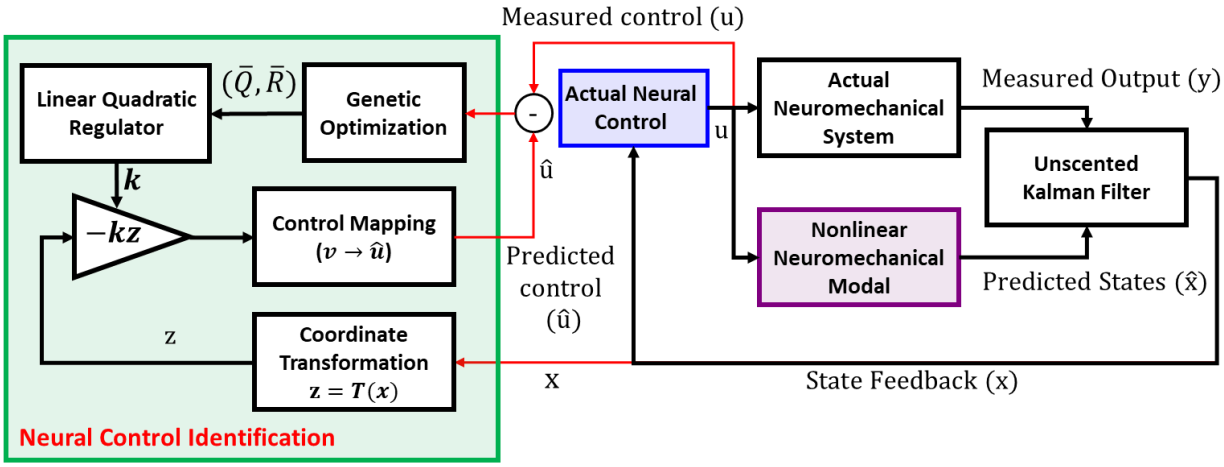

Figure 9-3. We used an unscented Kalman filter (UKF) along with the identified neuromechanical model (shown in purple in both Figure 9-2 and Figure 9-3) to obtain full-state neural feedback. We used a full-state feedback linearization approach to linearize the nonlinear neural feedback and then employed optimal control theory to identify the actual neural control (shown in blue in both Figure 9-2 and Figure 9-3) and its task goals associated with seated stability. We assumed that the neural control acts as a linear quadratic regulator (LQR), and the neural feedback minimizes a quadratic cost function that penalizes the motor commands and state variables in the linearized space. We used a genetic algorithm to obtain $\bar{Q}$ and $\bar{R}$ that minimized the difference between the predicted motor command ($\hat{u}$) and the actual motor command (u) measured by EMG.

9.2.7.1 Proof of existence of a transformation

We obtained a diffeomorphism $z = T(x)$ that transformed our nonlinear system $\dot{x} = f(x) + g(x)u$ into the linear space with $(A,\ B)$ controllable and $W(x)$ nonsingular on a domain $D \subset \Re^n$, for all $x \in D$:

$$\dot{z} = Az + Bv \tag{6}$$

$$u = \varphi(x) + W^{-1}(x)v \tag{7}$$

$$A = \begin{bmatrix} 0_{n-1\times 1} & I_{n-1\times n-1} \\ 0 & 0_{1\times n-1} \end{bmatrix};\ B = \begin{bmatrix} 0_{n-1\times 1} \\ 1 \end{bmatrix} \tag{8}$$

where z and v are the transformed state vector and control command in linearized space, respectively; $\varphi(x)$ and $W(x)$ are the control mapping functions; A and B are linear system matrices in a canonical form, and n is the number of state variables ($n = 4$ in our study).

Accordingly, our nonlinear system $\dot{x} = f(x) + g(x)u$ is feedback linearizable if and only if there is a domain $D_0 \subset D$ such that: (1) set of vector fields $\{g,\ ad_f g,\ \ldots, ad_f^{n-1} g\}$ are linearly independent for all $x \in D_0$; and (2) the set $\{g,\ ad_f g,\ \ldots, ad_f^{n-2} g\}$ is involutive in D_0. Note, $ad_f^i g$

represents the i-order Lie bracket of f and g [282]. We investigated these two conditions for our nonlinear neuromechanical model as follows:

Condition (1): it shows the controllability of the nonlinear system and is satisfied if $G(x) = \left[g,\ ad_f g,\ \ldots, ad_f^{n-1} g\right]$ has rank $n = 4$ for all $x \in D_0$. Based on our neuromechanical model, we can show:

$$G(x) = \begin{bmatrix} 0 & 0 & 0 & -\frac{1}{J}\mathcal{F}_m {\omega_0}^2 \\ 0 & 0 & \frac{1}{J}\mathcal{F}_m {\omega_0}^2 & \frac{1}{J^2}\mathcal{F}_m {\omega_0}^2 \left(\frac{\partial M_v}{\partial x_2} + \frac{\partial \mathcal{F}_m}{\partial x_2} x_3 + 2J\omega_0\right) \\ 0 & -{\omega_0}^2 & -2{\omega_0}^3 & -3{\omega_0}^4 \\ {\omega_0}^2 & 2{\omega_0}^3 & 3{\omega_0}^4 & 4{\omega_0}^5 \end{bmatrix} \tag{9}$$

Since $rank\{G(x)\} = 4$, Condition (1) is satisfied.

Condition (2): The distribution $span\{g(x),\ ad_f g(x),\ \ldots, ad_f^{n-2} g(x)\}$ is involutive $\{\forall x \in D\ and\ \forall i, j \in [0, n-2]\}$ if and only if:

$$rank\{g,\ ad_f g,\ \ldots, ad_f^{n-2} g\} = rank\{[g,\ ad_f g,\ \ldots, ad_f^{n-2} g,\ [ad_f^i g, ad_f^j g]]\} \tag{10}$$

Using our nonlinear neuromechanical model, we can obtain:

$$rank\{g,\ ad_f g,\ \ldots, ad_f^{n-2} g\} = rank\left\{\begin{bmatrix} 0 & 0 & 0 \\ 0 & 0 & \frac{1}{J}\mathcal{F}_m {\omega_0}^2 \\ 0 & -{\omega_0}^2 & -2{\omega_0}^3 \\ {\omega_0}^2 & 2{\omega_0}^3 & 3{\omega_0}^4 \end{bmatrix}\right\} = 3 \tag{11}$$

$$rank\{[g,\ ad_f g, ad_f^2 g, [ad_f^i g, ad_f^j g]]\} = rank\left\{\begin{bmatrix} 0 & 0 & 0 & 0 \\ 0 & 0 & \frac{1}{J}\mathcal{F}_m {\omega_0}^2 & 0 \\ 0 & -{\omega_0}^2 & -2{\omega_0}^3 & 0 \\ {\omega_0}^2 & 2{\omega_0}^3 & 3{\omega_0}^4 & 0 \end{bmatrix}\right\} = 3 \tag{12}$$

Based on Equations 15-17, Condition (2) is also satisfied. Therefore, the existence of full-state feedback linearization is proved.

9.2.7.2 Linearized full-state feedback

We obtained the linearized full-state feedback as the input of the neural control by solving a set of partial differential equations for the diffeomorphism $z = T(x)$. Combining Equations 1-3 and Equations 6-8 gives:

$$\dot{z} = \frac{\partial T(x)}{\partial x}\dot{x} = \frac{\partial T(x)}{\partial x}(f(x) + g(x)u) \tag{13}$$

$$\dot{z} = Az + Bv = Az + BW(x)(u - \varphi(x)) \tag{14}$$

Since Equation 13 and Equation 14 are equal, we can obtain:

$$\frac{\partial T(x)}{\partial x} f(x) = AT(x) - BW(x)\varphi(x) \tag{15}$$

$$\frac{\partial T(x)}{\partial x} g(x) = BW(x) \tag{16}$$

$T(x)$ is not uniquely defined by this system of differential equations and any linear transformation M that leads to $\tilde{T}(x) = M.T(x)$ will also satisfy this set of equations; however, with $\tilde{A} = MAM^{-1}$ and $\tilde{B} = MB$. One possible solution to this set of equations can be obtained as follows [282]:

$$z_1 = T_1(x) = h(x) = x_1 \tag{17}$$

$$z_2 = T_2(x) = L_f h(x) = x_2 \tag{18}$$

$$z_3 = T_3(x) = L_f^2 h(x) = \dot{x}_2 = \frac{1}{J}(M_g + M_e + M_v + \mathcal{F}_m . x_3) \tag{19}$$

$$z_4 = T_4(x) = L_f^3 h(x) = \frac{1}{J}\left(\frac{\partial M_g}{\partial x_1} + \frac{\partial M_e}{\partial x_1} + \frac{\partial \mathcal{F}_m}{\partial x_1} x_3\right) x_2 + \frac{1}{J}\left(\frac{\partial M_v}{\partial x_2} + \frac{\partial \mathcal{F}_m}{\partial x_2} x_3\right) T_3 + \frac{1}{J} F_m x_4 \tag{20}$$

$$W(x) = \frac{1}{J}\mathcal{F}_m {\omega_0}^2 \tag{21}$$

$$\varphi(x) = \frac{-1}{W(x)}\left(\frac{\partial T_4(x)}{\partial x_1} f_1 + \frac{\partial T_4(x)}{\partial x_2} f_2 + \frac{\partial T_4(x)}{\partial x_3} f_3 + \frac{\partial T_4(x)}{\partial x_3} f_4\right) \tag{22}$$

where $L_f^i h(x)$ is the i-order Lie derivative of h with respect to f. Interestingly, the linear state-space z represents the angular kinematics of the trunk with z_1, z_2, z_3, and z_4 having the dimension of angular position [rad], velocity [rad/s], acceleration [rad/s^2], and jerk [rad/s^3], respectively. Therefore, the input of the neural control would be the angular kinematics of the trunk.

9.2.7.3 Neural control identification

The process of identifying the neural control is depicted in Figure 9-3. The UKF provided the state vector x based on the measured trunk angle y using the processed motion capture data and the measured total motor command using the EMG data for each participant and each trial. We used the transformation matrix $T(x)$ (Equations 17-20) to obtain the state vector z in the linear space expressing the trunk's angular kinematics and fed it into the neural control defined as an LQR with a quadratic cost function. The neural control then output linearized control command v which was then converted into the motor command $\hat{u}$ in the nonlinear space using control mapping functions, $W(x)$ and $\varphi(x)$, based on Equations 7, 21, and 22.

The quadratic cost function penalized the motor commands (muscle activations), and linearized state variables as follows:

$$Cost = \int_{t=0}^{\infty} (z^T Q z + v^T R v)\, dt \tag{23}$$

Q is a diagonal four-by-four and R one-by-one positive definite matrices. To quantify the task goals associated with seated stability, we used a genetic algorithm to obtain Q and R that minimized the difference between predicted motor command ($\hat{u}$) via the neural control model and the actual motor command (u) measured by EMG. The obtained Q and R were then used to calculate LQR gains according to Equations 24 and 25 below. The algebraic Riccati equation (Equation 24) is solved to obtain S based on Q and R. The LQR gain vector (k) is obtained based on Equation 25 (see Figure 9-3). Note that Equation 24 has multiple answers; however, the answer that makes the closed-loop system stable via k is selected. Also, inferring the obtained cost function via comparing the values of elements in Q and R allows us to characterize the task goals associated with seated stability.

$$A^T S + SA - SBR^{-1}B^T S + Q = 0 \tag{24}$$

$$k = R^{-1}B^T S \tag{25}$$

9.2.8 Analysis of neural control model performance

We divided each 240-second trial into two sets to assess the performance of the identified neural control for each participant and trial: (1) an identification set, as the first 150 seconds of each trial, used to identify the neural control (Q, R); and (2) a test set, as the last 90 seconds of the

trial, used to cross-validate the performance of the identified model. We used the Friedman test with a significance level of 0.05 to statistically compare the weights of the LQR quadratic cost function (Q, R) as well as the LQR gains among all participants and trials. We used the Friedman test for statistical comparison since the normal distribution condition was not met for our data. We used the mean squared error (MSE) and correlation coefficient between the actual measurements (u) and the output of the identified model $(\hat{u})$ on the test set to quantify the performance. Finally, we investigated the robustness of the estimated neural control by deviating the neuromechanical parameters by ten percent to see the effect of erroneous neuromechanical model parameters. We used the Friedman test with a significance level of 0.05 to find any significant differences between the predictions before and after deviating the parameters in terms of accuracy and correlation.

9.3 Results

9.3.1 Identification of the neural control

We identified the passive and active control components of a nonlinear neuromechanical model of seated stability (Figure 9-2) based on our previous study [81]. We used data collected during the sudden perturbation trial to identify the passive control parameters using a Nonlinear Least Squares algorithm [81]. We used the data of the 240-second trials to identify the active control parameters using an Unscented Kalman Filter (UKF) according to our previous study [81]. The use of UKF, along with the identified neuromechanical model in our previous study [81] enabled us to obtain full-state feedback as the input to the neural control.

In the present study, we used a full-state feedback linearization approach to globally linearize the nonlinear neural feedback and then employed optimal control theory to identify the neural control and the task goals associated with seated stability, as follows:

Feedback linearization: We mathematically proved that the neuromechanical model, used to quantify passive and active controls of seated stability, is full-state feedback linearizable. Then, we obtained a diffeomorphism that transformed the state variables of the nonlinear neuromechanical model into a linear space where linear optimal control theory could be applied. This mapping was bioinspired since the linearized full-state neural feedback variables were the angular position, velocity, acceleration, and jerk of the trunk COM during sitting representing sensory information received by the neural control (see *Methods* for details).

Characterization of the neural control: We used a full-state feedback linearization approach to globally linearize the feedback from the nonlinear neuromechanical model and then employed optimal control theory to identify the neural control and the task goals associated with seated stability (Figure 9-2 and Figure 9-3). We assumed that the neural control receives full-state linearized feedback from the neuromechanical model and penalizes the muscle activations and poor stability performance [44], [281]. To implement this assumption, we modelled the neural control as an optimal linear quadratic regulator (LQR), with a quadratic cost function that penalizes the motor commands and state variables in the linearized space using weight matrices R and Q, respectively (Figure 9-3) (see *Methods* for details). We used a genetic algorithm to obtain the weights of the LQR quadratic cost function that minimized the difference between the predicted motor command via the neural control model ($\hat{u}$) and the actual motor command (u) measured by EMG sensors.

9.3.2 Characterized task goals of the neural control

Figure 9-4a shows the normalized weights of the quadratic cost function associated with the LQR control for all participants and trials. The obtained cost function weights, Q and R, were normalized by the maximum absolute value of the associated state variables and motor command, respectively, for comparison. Q_1, Q_2, Q_3, and Q_4 penalized poor angular position, velocity, acceleration, and jerk, respectively, while R penalized the motor command representing muscle activations. Friedman test showed that R was significantly larger than Q_2 and Q_4 ($P < 0.0001$). Among the state variables, we observed that Q_1 and Q_3 were significantly larger than Q_2 and Q_4 ($P < 0.05$).

The LQR gains k_1, k_2, k_3, and k_4 were normalized by the maximum absolute value of the linearized feedback: angular position, velocity, acceleration, and jerk, respectively. We observed that acceleration feedback had a significantly higher gain compared to other kinematics information (Figure 9-4b).

(a)

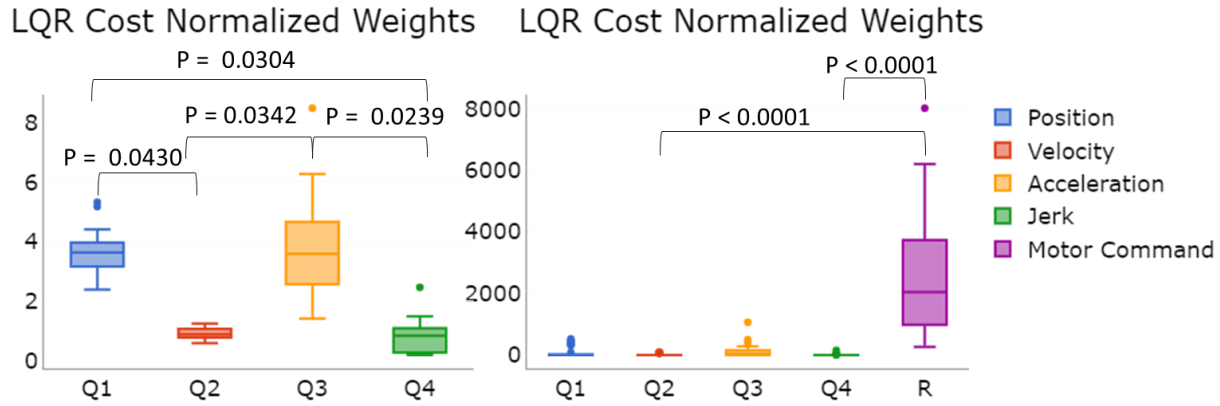

(b)

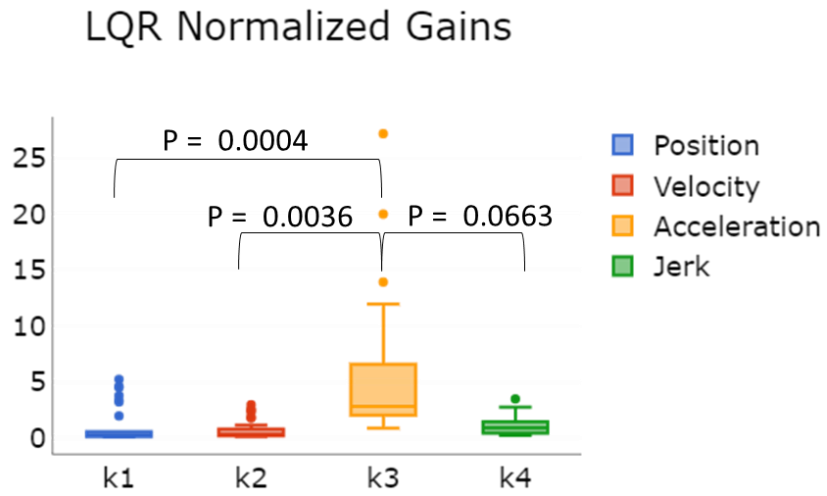

Figure 9-4. **(a)** Optimized weights of the quadratic cost function. The obtained weights in Figure 9-3, Q and R, were normalized by the maximum absolute value of the associated state variables and motor command, respectively, for comparison among weights. Q_1, Q_2, Q_3, and Q_4 penalized poor angular position, velocity, acceleration, and jerk, respectively, while R penalized the motor command representing muscle activations; **(b)** The linear quadratic regulator (LQR) gains k_1, k_2, k_3, and k_4 were normalized by the maximum absolute value of the linearized feedback: angular position, velocity, acceleration, and jerk, respectively. Statistical Friedman test was performed to identify significant differences at a significance level of 0.05.

We observed that the mean squared error (MSE) between the predicted motor command ($\hat{u}$) and measured motor command (u) was less than 0.6% of the Min-Max scaled value among all trials and participants for both identification and test sets (Figure 9-5). The correlation coefficient between $\hat{u}$ and u was higher than 90% as the median among all trials and participants for both identification and test sets. The most and least accurate estimations of the motor command had a correlation coefficient of 99.3% and 82.02%, respectively (Figure 9-6a). In addition, Figure 9-6b

shows an example of the performance of the identified neural control and neuromechanical model compared to the measured inertial trunk moment for one participant and trial.

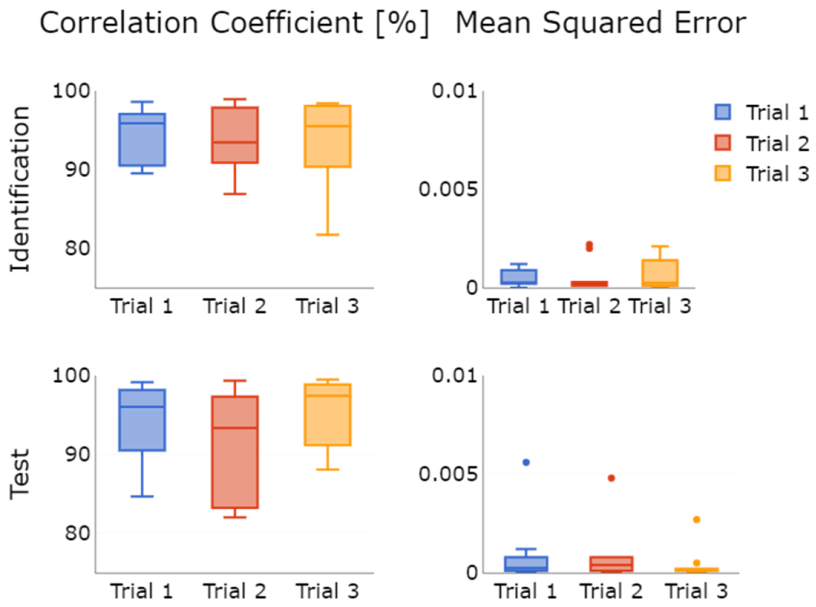

Figure 9-5. The correlation coefficient and mean squared error between the predicted motor command ($\hat{u}$) and actual motor command (u) evaluated on the identification and test datasets to quantify the accuracy of the modelled neural control in Figure 9-3.

(a)

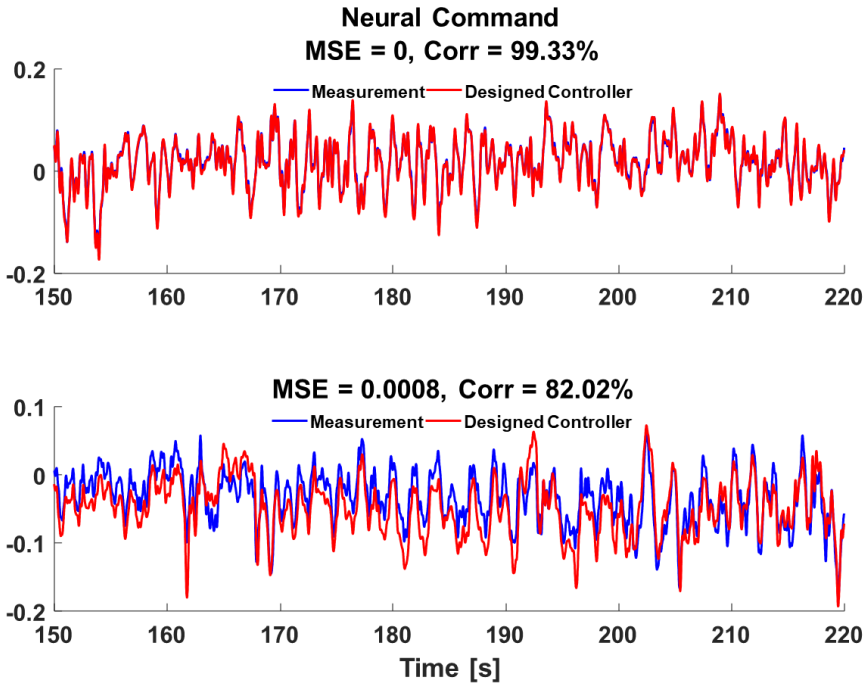

(b)

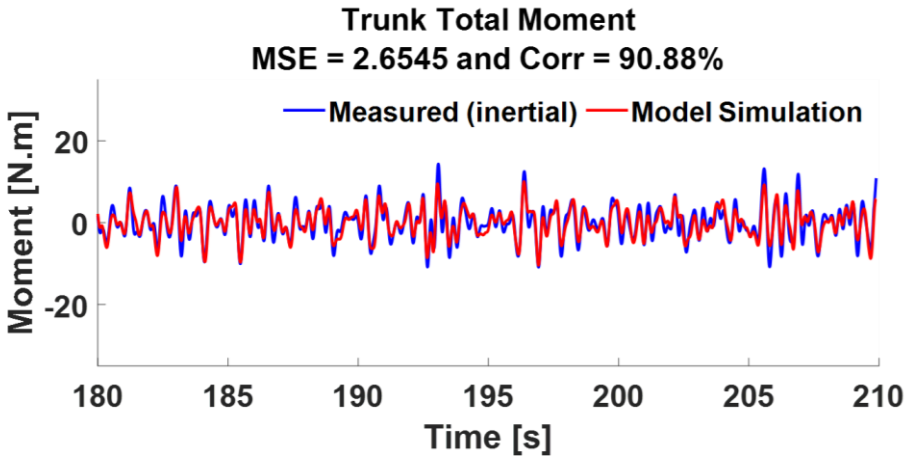

Figure 9-6. **(a)** The most and least accurate estimations of the motor command had a correlation coefficient of 99.3% and 82.02%, respectively; **(b)** an example of the performance of the identified neural control and neuromechanical model when used in a simulation compared to the measured inertial trunk moment for one participant and trial.

We investigated the effect of erroneous neuromechanical parameters on the performance of the identified neural control. To this end, we deviated the neuromechanical parameters by 10%. We observed no significant effect on the performance of the identified neural control in terms of the correlation coefficient and MSE (Figure 9-7).

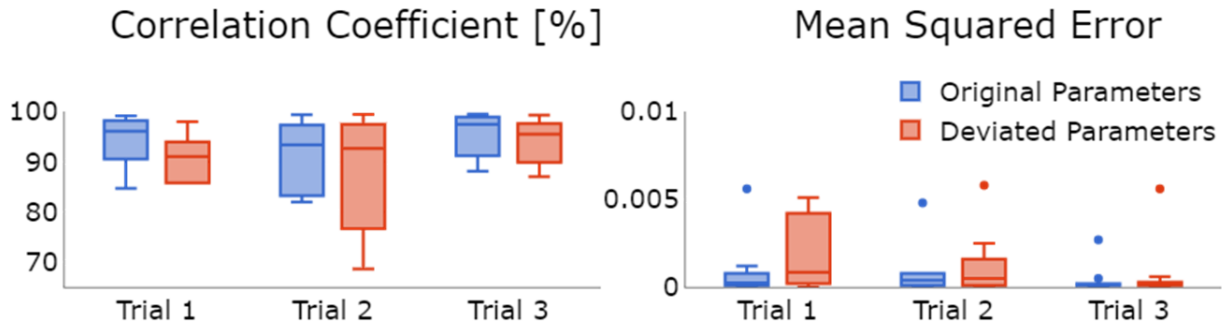

Figure 9-7. The performance of the identified neural control in terms of correlation coefficient and mean squared error (MSE) for three 240-second perturbation trials when the neuromechanical parameters were deviated by 10% to introduce error into the feedback linearization and control mapping.

9.4 Discussion

This study aimed to characterize the task goals of the neural control system for seated stability by experimentally applying a nonlinear neural feedback model in able-bodied individuals. We obtained full-state feedback from a nonlinear neuromechanical model of seated stability via a

UKF and then used a full-state feedback linearization along with optimal control theory to quantify the neural control and its task goals.

9.4.1 Task goals of neural control for seated stability

To infer the task goals, we assumed the neural control system acted as an optimal controller that receives full-state linearized feedback from the nonlinear neuromechanical model of seated stability. Full-state feedback linearization transformed the nonlinear state vector into linear space where the state vector included trunk COM angular position, velocity, acceleration, and jerk. Therefore, the quadratic cost function of the LQR penalized the motor commands (e.g., muscle activations) and COM angular kinematics representing sensory information. Inferring the optimized weights of the cost function allowed us to determine the task goals for seated stability via the optimal control theory [44]. The obtained weights showed that the neural control had significantly higher penalties for the motor command, and the COM angular position and acceleration compared to the COM angular velocity and jerk (Figure 9-4a). This suggests that the identified neural feedback stabilizes the trunk while achieving near-minimum muscle activations as a task goal.

Kiemel et al. [44] showed that the neural control adopted minimization of muscle activation for stabilizing upright stance, and the neural feedback did not substantially increase muscle activation to reduce deviations of the COM position. A significantly high penalty for the motor command may suggest that there is no functional benefit to further minimizing COM angular sway that would demand higher muscle activation when sitting is stable. In addition to what Kiemel et al. [44] observed for standing stability, the high penalty associated with COM angular position in our study may reflect that the neural control attempted to sufficiently minimize the deviation of the COM angular position from upright sitting posture while maintaining minimum muscle activation. Todorov [281] explained that such behaviour is due to the 'minimal intervention principle,' meaning that there is no need to correct deviations away from the average behaviour unless such deviations hinder the task performance. This is because correction is expensive due to the energy costs, i.e., muscle activation. Satisfying task goals of simultaneously minimizing both muscle activation and COM angular position seems to be conflicting in terms of energy expenditure since minimizing COM position demands high muscle activation. However, the neural feedback law that maintains the deviations of COM sufficiently smaller than the size of the base of support can achieve seated stability while keeping muscle activation to a minimum [44]. Such

a stabilization strategy, while ensuring stable posture, avoids overcorrection of COM position and high muscle activation that could lead to a rapid onset of muscle fatigue.

We also found that, in addition to the COM angular position, the neural control penalized the COM angular acceleration significantly more than COM angular velocity and jerk. This suggests that acceleration information plays a more important role than velocity information which may be different from previous studies that modelled the neural control via PD control with no acceleration feedback [62], [65]. The literature has highlighted that acceleration feedback provides reliable information on the trunk's inertia during the stabilization task [283]. Furthermore, angular acceleration information provides sensory input about the sum of joint moments applied to the trunk. The literature has shown that COM acceleration during standing is highly correlated with the distance between the COP and the vertical projection of the COM position [164]. This distance reflects the relationship between the controlling and controlled variables of postural control [164]. As a result, COM acceleration contains information on the neural control system's performance in correcting sitting or standing posture. Therefore, such information can be relevant and employed by the neural control to generate motor commands resulting in proper stabilizing active joint moments in response to external disturbances. Moreover, we observed significantly higher LQR gain associated with acceleration input compared to position and velocity (Figure 9-4b). This may reflect a larger contribution of the trunk COM angular acceleration to optimal motor command and, thus, active joint moments, further highlighting the importance of acceleration feedback. One additional reason that COM angular acceleration had more contribution to the motor command compared to COM angular position might be due to minimizing the muscle activation without overcorrecting COM position that would demand higher muscle activation levels.

Overall, inferring the cost function of the optimal neural feedback revealed that the task goals of the neural control for seated stability could be to achieve near-minimum muscle activation while keeping the deviations of the COM angular position and acceleration sufficiently small. To achieve seated stability, the neural control system may predominantly use COM angular acceleration information to generate motor commands resulting in activating relevant muscles and generating active joint moments against external disturbances while avoiding overcorrecting COM angular position and rapid onset of muscle fatigue.

9.4.2 Nonlinear neural feedback model and its validity

The inherently nonlinear dynamics of neuromuscular mechanisms involved in seated stability and their complex interrelations hinder our mechanistic understanding of how the CNS stabilizes the human trunk during sitting. Previous studies have assumed linear neuromechanical models of stability to quantify neural control by using linear controllers such as PID control [60], [61], [198], [199], PD control [62], [65], PD control with acceleration feedback [59], [207], and LQR optimal control [44]. For the approximation of the human body dynamics during sitting as a linear model, the COM motion must be small, which is not necessarily true under challenging conditions or in the presence of significant perturbations [44]. Therefore, neglecting the nonlinear behaviour of the underlying neuromechanical system could lead to an erroneous estimation of the neural control, which, consequently, affects our understanding of the task goals used by the neural control system to regulate stability. To address this challenge, we proposed a two-step approach. First, we used our previously validated nonlinear neuromechanical model of seated stability [81]. Second, in the present study, we identified the nonlinear neural feedback control strategy in the CNS for seated stability by employing a full-state feedback linearization technique along with a linear optimal control model, i.e., LQR.

In contrast to the literature, our identified neural feedback is not limited to a small range of motions and is applicable to a wide range of COM motion states. This is due to the global transformation from the nonlinear state-space into a linear state-space where linear optimal control theory is globally valid. By modelling the nonlinearity, we showed that the identified neural feedback could not be approximated using a PD control and linear neuromechanical models, previously reported in the literature [62], [65]. We showed that the neural feedback depends not only on the COM angular position and velocity but also on the COM angular acceleration and jerk, while the COM position and acceleration information contributed significantly more to the motor command compared to its velocity and jerk. As such, using PD control with a linear neuromechanical model limits our ability to explain the task goals used by the neural control for seated stability. In contrast, the use of optimal control with quadratic cost function may allow us to infer the task goals associated with seated stability.

An optimal control scheme relies on a performance criterion (e.g., cost function) explaining what the goal is and subsequently finds the control law that leads to the best performance [280], [281]. Therefore, instead of assuming what control schemes the neural control might utilize (e.g.,

PD or PID), optimal feedback control allows the task and the neuromechanical model to dictate the control scheme that best describes the process of regulating seated stability [281]. This gives the optimal control a generality in practice [281]. Moreover, since the sensorimotor system consists of components with actions aimed to continuously enhance behavioural performance (e.g., natural optimality), the optimal control can precisely describe the optimal nature of the sensorimotor function compared to PD or PID control schemes [280], [281]. This gives the optimal control a theoretical advantage over classic alternatives (e.g., PD or PID) for describing the behaviour of the neural control [281].

It should be noted that by using LQR control, we assumed the external perturbations used in the study do not alter the neural feedback law. This assumption was based on previous studies that suggested mechanical perturbations do not significantly change neural feedback law, in contrast to sensory perturbations, which may cause alteration in sensory reweighting and, consequently, may change the neural feedback law [44], [45].

9.4.3 Accuracy of the identified parameters of the neural feedback model

We examined the performance of the identified neural control for each participant and trial using MSE and correlation coefficient. The MSE between the predicted motor command and measured motor command (i.e., EMG recording) was less than 0.6% among all trials and participants, while the correlation coefficient between them was higher than 90% as the median among all trials and participants for both identification and test sets (Figure 9-5). The MSE values were within the range of accuracy of the measurement devices, suggesting that the identified neural feedback model was highly accurate. This accuracy can be seen in Figure 9-6 for the most and least accurate estimations of the motor command as the output of the neural control system among all trials.

We also examined the robustness of the identified neural control by introducing errors into the parameters of the identified neuromechanical model. We deviated neuromechanical parameters by 10%. The introduced error affects the feedback linearization and control mapping processes. We observed that the addition of these errors in neuromechanical parameters did not significantly change the performance of the identified neural control (Figure 9-7). This shows that the identified neural controls were robust against potential variation in the neuromechanical properties (e.g., due to muscle fatigue). Note that we utilized UKF and a dual-estimation scheme for identifying the

properties of the nonlinear neuromechanical model as well as the state vector (Figure 9-2 and Equation 1) [81]. This may allow for online correction of the neuromechanical parameters (e.g., using forgetting factors), which may enable tracking system variations due to muscle fatigue and physiological uncertainties [81]. However, future research studies should be conducted to investigate the applicability of the proposed identification scheme to identify changes in neural control under uncertain conditions, such as a fatigue-induced condition or in individuals with neuromuscular impairments who may exhibit different control mechanisms due to the motor and/or sensory deficits.

9.4.4 Limitations

First, we only recruited healthy, young, and male participants highlighting the need for further investigation on other populations with different sex, age group, and/or neuromuscular impairments. Second, we scaled cadaveric anthropometric data by participant's height and weight to obtain individual-specific body-segment parameters, which may have introduced errors into the neuromechanical parameters [233]. Third, we used a one-segment model of the trunk, assuming intervertebral motions are negligible. Future studies should investigate the effect of multi-segment trunk models on seated stability [233], [260]. Utilizing multi-segment models requires uncorrelated external perturbation profiles simultaneously applied to each segment level. Fourth, in future studies, the external perturbation should also be applied in mediolateral directions to investigate seated stability in the frontal plane. Fifth, we used a quadratic cost function for the LQR, assumed as the neural control scheme. The type of the cost function could also be an optimization variable, among others. Nevertheless, the present study took a step toward understanding the neural control system's task goals associated with seated stability, which could provide the foundation for future work.

It is worth mentioning that the similarity between the behaviour of the neuromechanical and neural control models and the behaviour of the actual system does not necessarily imply that these models can predict every aspect of the actual physiological mechanisms and their performance. However, such modelling approaches may lead to a better understanding of how the CNS and the musculoskeletal system interact to produce movement or maintain postural stability. Audu and Triolo [60] suggested that modelling the behaviour of the neuromusculoskeletal system contributes to expanding our knowledge about how the balance mechanisms operate. Such knowledge may be helpful for identifying differences between able-bodied individuals and those

with neuromuscular impairment (e.g., iSCI) and, consequently, would be invaluable toward the development of control systems for restoring seated stability and guiding the rehabilitative efforts toward a better outcome [60].

Todorov [281] explained that many motor function theories were described based on "optimal performance" by applying sophisticated optimal control theory to achieve behavioural predictions. Although the assumption of optimality is not without its limitations, such methodology has enabled explaining many empirical phenomena compared to other modelling methods [281]. Moreover, the sensorimotor system is comprised of natural processes with continuous actions aimed at improving behavioural performance (e.g., natural optimality). Therefore, the optimal control potentially has a theoretical advantage compared to other modelling approaches to describe the optimal nature of the sensorimotor function. Hence, Todorov [281] stated that "optimality provides a natural starting point for computational investigations of sensorimotor function."

9.5 Conclusion

In this study, we experimentally identified a nonlinear model for neural feedback control of seated stability. By using a nonlinear neuromechanical model along with feedback linearization and optimal control theory, we inferred the task goals used by the neural control system to regulate seated stability. We showed that the neural feedback may use angular position, velocity, acceleration, and jerk in a linearized space. We observed that the neural control may try to achieve near-minimum muscle activation while keeping the deviations of the trunk COM angular position and acceleration sufficiently small. To achieve seated stability, the neural control may use COM angular acceleration information to activate relevant muscles to generate required active joint moments against external disturbances. Our proposed approach to identifying the neural feedback control facilitates a better mechanistic understanding of the neuromuscular mechanisms involved in seated stability while enabling inferring the task goals used by the neural control system to achieve the targeted motor behaviour.

9.6 What is next?

The algorithms proposed in Chapters 7 to 9 for assessing dynamic stability and characterizing neuromuscular mechanisms were validated for able-bodied individuals. Future

studies may investigate the feasibility and validity of using the developed algorithms for assessing the dynamic stability in individuals with impaired balance. Future studies may investigate the feasibility of using the algorithm developed in Chapter 7 to assess the risk of loss of balance in individuals with degraded trunk control in real-world conditions. This algorithm may also be useful for evaluating the effect of rehabilitation on the dynamic seated balance by measuring the margin of stability pre- and post-rehabilitation in individuals with impaired seated balance with the aim of improving the margin of stability post-rehabilitation. Future studies may also investigate the use of methodologies introduced in Chapter 8 and Chapter 9 to characterize the changes in neuromuscular stabilization mechanisms due to neuromuscular impairments with the aim of understanding the underlying mechanisms associated with balance difficulties pre-therapy. Such methodologies may also be helpful in investigating the effect of therapy on neuromuscular mechanisms as an objective method of assessment. Future studies may also investigate the feasibility of utilizing the algorithms proposed in Chapters 7 to 9 to design assistive technologies focused on improving the dynamic seated stability in individuals with impaired trunk control during activities of daily living. Nevertheless, extensive research studies must be conducted to investigate the applicability of the proposed method to developing effective assistive technologies.

Chapter 10

This chapter provides a summary of the outcomes and future directions for this research.

10 Conclusions & Future Perspectives

10.1 Main Outcomes and Original Contributions

We developed and validated an algorithm that allows for obtaining clinically meaningful balance biomarkers using wearable technology. This technology allows for (a) the characterization of complex balance mechanisms without a dedicated laboratory; (b) an increase in the sensitivity of characterizing impaired balance in individuals with mild balance deficits (e.g., individuals with iSCI AIS level D); (c) the capability of integration into conventional clinical tests; and (d) the objective outcome evaluation of rehabilitative interventions in clinical environments for elderly patients with moderate-to-severe balance difficulty.

We identified the limits of dynamic seated stability based on the concept of the FSR and developed an algorithm for assessing dynamic seated stability using wearable technology out of equipped laboratories. We provided a detailed characterization of the underlying neuromuscular stabilization mechanisms involved in human sitting to address a long-lasting issue in motor control. We proposed a method that allows for a mechanistic understanding of the task goals used by the CNS to achieve seated stability. The original contributions of each of Chapters 3 to 9 are described below.

10.1.1 Wearable Technology for Balance Assessment (Chapter 3)

A review of the literature showed a lack of a validation study comparing the accuracy of the wearable technology against gold-standard in-lab equipment for assessing the dynamics of standing balance. We validated an algorithm to obtain the kinematics and kinetics of standing balance using wearable technology. The primary outcome of this research was a wearable technology consisting of three accelerometers mounted on the leg, sacrum, and sternum along with an algorithm that exhibited sufficient accuracy for estimating segments' orientation, joint moments, 3D GRF, and COP position and could be recommended for standing balance assessment.

10.1.2 Characterization of Standing Balance after iSCI (Chapter 4)

A review of the literature revealed that the use of body-worn IMUs to obtain clinically meaningful measures of standing balance in individuals with iSCI has not been fully investigated. We used our validated algorithm to perform a comprehensive balance evaluation using wearable technology for a group of ambulatory individuals with iSCI (AIS level D) during standing on HS and FS with EO and EC conditions. Our method allowed us to characterize standing balance in individuals with iSCI AIS level D compared to able-bodied individuals. Our proposed methodology could potentially identify reduced stability performance, increased control demand, and less effective active correction in the iSCI group in all test conditions. The iSCI group exhibited higher and lower reliance on visual and somatosensory information, respectively, for maintaining balance caused by the impaired somatosensory feedback. Our proposed technology and methodology exhibited sufficient resolution with the discriminatory ability for objective balance evaluation based on unperturbed static standing in a group of ambulatory individuals with iSCI (AIS level D).

10.1.3 Postural Control Strategy after iSCI (Chapter 5)

A review of the literature showed that identifying alteration of postural control strategies post-iSCI under different sensory conditions has not been investigated. We used our validated algorithm to assess the postural control strategy using wearable technology based on the coherence between the trunk and leg accelerations for a group of ambulatory individuals with iSCI (AIS level D) during standing on HS and FS with EO and EC conditions. The iSCI group exhibited a similar balance strategy at lower frequencies compared to able-bodied populations. However, they showed difficulty in adapting inter-segment coordination from ankle strategy to hip strategy as the sway frequency increases. The alteration of somatosensory input had an adverse effect on trunk-leg movement coordination in both groups. Our proposed technology and methodology showed sufficient sensitivity, discriminatory ability and excellent test-retest reliability to identify changes in postural control strategy in ambulatory individuals with iSCI (AIS level D).

10.1.4 Instrumented Clinical Balance Evaluation (Chapter 6)

A review of the literature showed that balance assessment using wearable IMUs has not been employed in a clinical setting to obtain an objective outcome evaluation of rehabilitative interventions. We investigated, in a clinical setting, the use of our validated wearable technology

integrated into the BBS test for objective outcome evaluation of balance rehabilitation in elderly fallers compared to conventional BBS scores. Our proposed methodology enabled objective outcome evaluation of rehabilitative interventions with high sensitivity to detect subtle changes in balance without a significant increase in assessment time. Our proposed methodology enabled characterizing underlying causes of impaired balance pre-rehabilitation and allowed identifying the improved and yet impaired aspects of balance post-rehabilitation.

10.1.5 Feasible Seated Stability Region (Chapter 7)

We found the FSR against loss of balance during sitting and validated the FSR against experimental data for perturbed sitting. We developed and validated a wearable device composed of IMUs for estimating the margin of stability for quantification of seated stability and risk of loss of balance. The primary outcome of this research was a wearable device that can assess the risk of loss of balance based on the margin of stability calculated from the real-time trunk kinematics and the pre-obtained FSR.

10.1.6 Neuromuscular Control of Seated Stability (Chapter 8)

A survey of the literature revealed that determining the roles of underlying neuromuscular mechanisms involved in stabilizing the human trunk during sitting is a fundamental challenge in human motor control. We characterized the underlying passive and active stabilization mechanisms involved in human sitting by identifying a nonlinear physiologically meaningful neuromechanical model of seated stability. Our proposed model predicted the trunk sway behaviour during perturbed sitting with high accuracy and correlation, allowing a better mechanistic understanding of the roles of passive and active stabilization mechanisms involved in sitting. The primary outcome of our research was a nonlinear characterization of the neuromuscular control that accounts for physiological uncertainties. Such an identification approach may allow for real-time tracking and correction of parameters' variations due to external disturbances and muscle fatigue.

10.1.7 CNS Task Goals of Seated Stability (Chapter 9)

We identified the task goals of the CNS for regulating dynamic seated stability using a nonlinear neuromechanical model along with feedback linearization and optimal control. We observed the neural dynamics may use trunk angular kinematics as the input to achieve near-minimum muscle activation while keeping the deviations of the trunk angular position and

acceleration sufficiently small. To achieve these high-level task goals, the neural control may significantly use trunk angular acceleration information to generate motor commands leading to proper active joint moments against external disturbances.

10.2 Future Perspectives

10.2.1 Static Balance

10.2.1.1 Personalized Therapy

Future studies should determine the sensitivity of instrumented tests with IMUs for detecting changes in balance biomarkers due to specific rehabilitation programs among patients with impaired balance in clinical settings. Future studies should also evaluate the effectiveness of such targeted interventions to reduce future fall incidences and their adverse consequences among individuals with impaired balance. First, future studies may use IMU-based objective measures to diagnose balance disorders that BBS may miss and determine the underlying causes by comparing balance biomarkers of the patients with those of able-bodied individuals as the baseline. Second, a personalized therapy could be implemented to target the underlying causes determined by the balance biomarkers. Third, an IMU-based objective balance assessment methodology has the potential to be used by researchers to track subtle changes in a patient's balance and follow the patient's progress over the course of the rehabilitation. Fourth, the balance biomarkers obtained pre- and post-rehabilitation may be used objectively evaluate the effectiveness of the introduced interventions.

10.2.1.2 Remote Health Monitoring

Future studies should investigate the use of IMUs for remote balance evaluation at patients' homes. This enables remote health monitoring without requiring the physical presence of healthcare professionals, wherever professional resources are limited or during healthcare crises, such as the COVID-19 pandemic when access to healthcare is a challenge for high-risk individuals with other underlying medical conditions.

10.2.2 Dynamic Balance

10.2.2.1 Fall Risk Assessment

Future studies should pursue the application of our proposed algorithm to fall prevention for wheelchair users in several ways. Our algorithm may be used for alarming wheelchair users on

fall risk during daily wheeling quantified by the margin of stability. This technology may also be used for training individuals with impaired trunk stability to improve dynamic sitting balance in rehabilitation programs with the aim of increasing the margin of stability under challenging sitting conditions.

10.2.2.2 Neuromuscular Characterization

The identification approach, along with the nonlinear neuromechanical model of seated stability used in this thesis research, allows for frequent tracking and correction of model parameters' variations due to external disturbances and muscle fatigue. Future studies should investigate the application of the proposed approach to identify changes in active control in a fatigue-induced condition or any condition that may affect the neuromuscular mechanism. Future research should also investigate the capability of our proposed system identification scheme in detecting changes in neuromuscular mechanisms in impaired individuals. Particularly, future studies should investigate how a neurological condition affects the active and passive control mechanisms. They should also investigate how neuromuscular impairment could affect the task goals of the CNS for regulating seated stability. Future research may focus on using our system identification scheme for the objective evaluation of sitting balance and introducing targeted rehabilitative interventions.

10.2.2.3 Closed-loop FES Control

The margin of stability, obtained via the identified FSR and validated algorithm using wearable technology in this study, can be used as feedback to a neuroprosthesis for activating relevant muscles in case of increased risk of loss of balance using a closed-loop FES system. Future work can also benefit from the proposed system identification scheme to design bio-inspired assistive technologies for improving trunk instability. The neural dynamics identified in the present study may also be used to develop bio-inspired controllers for closed-loop FES systems. The gains of the LQR feedback linearization controller may be dynamically adapted based on online tracking and correction of the parameters associated with the neuromechanical model of seated stability.

10.2.2.4 Technical Considerations

The present study characterized active and passive control mechanisms of seated stability and determined the task goals of the neural control for regulating seated stability in the sagittal plane. Future studies may look into how the neuromechanical model of seated stability and the

task goals of the neural control would differ in the frontal plane. Furthermore, we assumed a single-segment model of the trunk, which did not account for intervertebral and upper limb motion. Future studies should investigate the effect of trunk segmentation on the neuromechanical model and neural control task goals of seated stability.

References

[1] E. R. Burns, J. A. Stevens, and R. Lee, "The direct costs of fatal and non-fatal falls among older adults — United States," *J. Safety Res.*, vol. 58, pp. 99–103, 2016, doi: 10.1016/j.jsr.2016.05.001.

[2] "Web-based injury statistics query and reporting system (WISQARS). National Center for Injury Prevention and Control, Centers for Disease Control and Prevention." [Online]. Available: https://www.cdc.gov/injury/wisqars/index.html.

[3] R. L. Ganz, DA, Bao Y, Shekelle PG, "Will My Patient Fall ?," *Am. Med. Assoc.*, vol. 297, no. 1, pp. 77–86, 2007, doi: 10.1001/jama.297.1.77.

[4] R. P. Hubble, G. A. Naughton, P. A. Silburn, and M. H. Cole, "Wearable sensor use for assessing standing balance and walking stability in people with Parkinson's disease: A systematic review," *PLoS One*, vol. 10, no. 4, pp. 1–22, 2015, doi: 10.1371/journal.pone.0123705.

[5] M. M. Noohu, A. B. Dey, and M. E. Hussain, "Relevance of balance measurement tools and balance training for fall prevention in older adults," *J. Clin. Gerontol. Geriatr.*, vol. 5, no. 2, pp. 31–35, 2014, doi: 10.1016/j.jcgg.2013.05.002.

[6] W. Zijlstra and K. Aminian, "Mobility assessment in older people: New possibilities and challenges," *Eur. J. Ageing*, vol. 4, no. 1, pp. 3–12, 2007, doi: 10.1007/s10433-007-0041-9.

[7] J. A. Stevens, K. A. Mack, L. J. Paulozzi, and M. F. Ballesteros, "Self-Reported Falls and Fall-Related Injuries Among Persons Aged ≥ 65 Years-United States, 2006," *J. Safety Res.*, vol. 39, no. 3, pp. 345–349, 2008, doi: 10.1016/j.jsr.2008.05.002.

[8] L. Yu, Y. Zhao, H. Wang, T. L. Sun, T. E. Murphy, and K. L. Tsui, “Assessing elderly’s functional balance and mobility via analyzing data from waist-mounted tri-axial wearable accelerometers in timed up and go tests,” *BMC Med. Inform. Decis. Mak.*, vol. 21, no. 1, pp. 1–14, 2021, doi: 10.1186/s12911-021-01463-4.

[9] A. F. Ambrose, G. Paul, and J. M. Hausdorff, “Risk factors for falls among older adults: A review of the literature,” *Maturitas*, vol. 75, no. 1, pp. 51–61, 2013, doi: 10.1016/j.maturitas.2013.02.009.

[10] T. Arora *et al.*, “Current state of balance assessment during transferring , sitting , standing and walking activities for the spinal cord injured population : A systematic review,” *J. Spinal Cord Med.*, vol. 0, no. 0, pp. 1–14, 2018, doi: 10.1080/10790268.2018.1481692.

[11] S. S. Brotherton, J. S. Krause, and P. J. Nietert, “Falls in individuals with incomplete spinal cord injury,” *Spinal Cord*, vol. 45, pp. 37–40, 2007, doi: 10.1038/sj.sc.3101909.

[12] A. Khan *et al.*, “Falls after spinal cord injury: a systematic review and meta-analysis of incidence proportion and contributing factors,” *Spinal Cord*, vol. 57, no. 7, pp. 526–539, 2019, doi: 10.1038/s41393-019-0274-4.

[13] S. Amatachaya, J. Wannapakhe, P. Arrayawichanon, W. Siritarathiwat, and P. Wattanapun, “Functional abilities , incidences of complications and falls of patients with spinal cord injury 6 months after discharge,” *Spinal Cord*, pp. 520–524, 2011, doi: 10.1038/sc.2010.163.

[14] S. S. Brotherton *et al.*, “A Pilot Study of Factors Associated With Falls in Individuals With Incomplete Spinal Cord Injury,” *J. Spinal Cord Med. ISSN*, vol. 30, no. 3, pp. 243–250, 2007, doi: 10.1080/10790268.2007.11753932.

[15] G. Shah *et al.*, “Measuring balance confidence after spinal cord injury: the reliability and

validity of the Activities- specific Balance Confidence Scale," *J. Spinal Cord Med.*, vol. 40, no. 6, pp. 768–776, 2017, doi: 10.1080/10790268.2017.1369212.

[16] J. Lemay and S. Nadeau, "Standing balance assessment in ASIA D paraplegic and tetraplegic participants : concurrent validity of the Berg Balance Scale," *Spinal Cord*, vol. 48, pp. 245–250, 2010, doi: 10.1038/sc.2009.119.

[17] J. Lemay, D. Gagnon, C. Duclos, M. Grangeon, C. Gauthier, and S. Nadeau, "Influence of visual inputs on quasi-static standing postural steadiness in individuals with spinal cord injury," *Gait Posture*, vol. 38, pp. 357–360, 2013, doi: 10.1016/j.gaitpost.2012.11.029.

[18] J. Lemay, D. H. Gagnon, S. Nadeau, M. Grangeon, C. Gauthier, and C. Duclos, "Center-of-pressure total trajectory length is a complementary measure to maximum excursion to better differentiate multidirectional standing limits of stability between individuals with incomplete spinal cord injury and able-bodied individuals," *Lemay al. J. NeuroEngineering Rehabil.*, vol. 11, no. 8, pp. 1–11, 2014.

[19] G. Scivoletto *et al.*, "Clinical factors that affect walking level and performance in chronic spinal cord lesion patients," *Spine (Phila. Pa. 1976).*, vol. 33, no. 3, pp. 259–264, 2008, doi: 10.1097/BRS.0b013e3181626ab0.

[20] D. G. Sayenko, M. I. Alekhina, K. Masani, A. H. Vette, H. Obata, and K. Nakazawa, "Positive effect of balance training with visual feedback on standing balance abilities in people with incomplete spinal cord injury," *Spinal Cord*, vol. 48, pp. 886–893, 2010, doi: 10.1038/sc.2010.41.

[21] K. E. Musselman, J. Lemay, K. Walden, A. Harris, D. H. Gagnon, and M. C. Verrier, "The standing and walking assessment tool for individuals with spinal cord injury : A qualitative study of validity and clinical use," *J. Spinal Cord Med.*, vol. 42, pp. 108–118, 2019, doi:

10.1080/10790268.2019.1616148.

[22] "Complete Public Version of the 2019 Annual Statistical Report for the Spinal Cord Injury Model System," 2019.

[23] A. D. Goodworth, Y. H. Wu, D. Felmlee, E. Dunklebarger, and S. Saavedra, "A trunk support system to identify posture control mechanisms in populations lacking independent sitting," *IEEE Trans. Neural Syst. Rehabil. Eng.*, vol. 25, no. 1, pp. 19–27, 2017, doi: 10.1109/TNSRE.2016.2541021.

[24] M. Milosevic *et al.*, "Trunk control impairment is responsible for postural instability during quiet sitting in individuals with cervical spinal cord injury," *Clin. Biomech.*, vol. 30, no. 5, pp. 507–512, 2015, doi: 10.1016/j.clinbiomech.2015.03.002.

[25] K. Masani *et al.*, "Postural reactions of the trunk muscles to multi-directional perturbations in sitting," *Clin. Biomech.*, vol. 24, no. 2, pp. 176–182, 2009, doi: 10.1016/j.clinbiomech.2008.12.001.

[26] A. H. Vette, N. Wu, K. Masani, and M. R. Popovic, "Low-intensity functional electrical stimulation can increase multidirectional trunk stiffness in able-bodied individuals during sitting," *Med. Eng. Phys.*, vol. 37, no. 8, pp. 777–782, 2015, doi: 10.1016/j.medengphy.2015.05.008.

[27] K. L. Armstrong, L. M. Lombardo, K. M. Foglyano, M. L. Audu, and R. J. Triolo, "Automatic application of neural stimulation during wheelchair propulsion after SCI enhances recovery of upright sitting from destabilizing events," *J. Neuroeng. Rehabil.*, vol. 15, no. 1, pp. 1–13, 2018, doi: 10.1186/s12984-018-0362-2.

[28] H. Singh *et al.*, "Perspectives of wheelchair users with spinal cord injury on fall circumstances and fall prevention: A mixed methods approach using photovoice," *PLoS*

One, vol. 15, no. 8 august, pp. 1–22, 2020, doi: 10.1371/journal.pone.0238116.

[29] H. Xiang, A. M. Chany, and G. A. Smith, "Wheelchair related injuries treated in US emergency departments," *Inj. Prev.*, vol. 12, no. 1, pp. 8–11, 2006, doi: 10.1136/ip.2005.010033.

[30] C. L. Chen, K. T. Yeung, L. I. Bih, C. H. Wang, M. I. Chen, and J. C. Chien, "The relationship between sitting stability and functional performance in patients with paraplegia," *Arch. Phys. Med. Rehabil.*, vol. 84, no. 9, pp. 1276–1281, 2003, doi: 10.1016/S0003-9993(03)00200-4.

[31] N. Hart *et al.*, "Respiratory effects of combined truncal and abdominal support in patients with spinal cord injury," *Arch. Phys. Med. Rehabil.*, vol. 86, no. 7, pp. 1447–1451, 2005, doi: 10.1016/j.apmr.2004.12.025.

[32] R. Chen, B. Kayser, S. Yan, and P. T. Macklem, "Twitch transdiaphragmatic pressure depends critically on thoracoabdominal configuration," *J. Appl. Physiol.*, vol. 88, no. 1, pp. 54–60, 2000, doi: 10.1152/jappl.2000.88.1.54.

[33] I. Bolin, P. Bodin, and M. Kreuter, "Sitting position - Posture and performance in C5-C6 tetraplegia," *Spinal Cord*, vol. 38, no. 7, pp. 425–434, 2000, doi: 10.1038/sj.sc.3101031.

[34] K. D. Anderson, "Targeting recovery: Priorities of the spinal cord-injured population," *J. Neurotrauma*, vol. 21, no. 10, pp. 1371–1383, 2004, doi: 10.1089/neu.2004.21.1371.

[35] K. Chan *et al.*, "Quantifying balance control after spinal cord injury : Reliability and validity of the mini-BESTest Quantifying balance control after spinal cord injury : Reliability and validity of the mini-BESTest," *J. Spinal Cord Med.*, vol. 42, no. 1, pp. 141–148, 2019, doi: 10.1080/10790268.2019.1647930.

[36] J. Lemay and S. Nadeau, "Potential of The Smart Balance Master System to Assess

Standing Balance in People with Incomplete Spinal Cord Injury," *J. Rehabil. Med.*, vol. 45, pp. 55–60, 2013, doi: 10.2340/16501977-1067.

[37] F. Horak, L. King, and M. Mancini, "Role of Body-Worn Movement Monitor Technology for Balance and Gait Rehabilitation," *Phys. Ther.*, vol. 95, no. 3, pp. 461–470, 2015.

[38] J. J. Collins and C. J. De Luca, "The effects of visual input on open-loop and closed-loop postural control mechanisms," *Exp. Brain Res.*, vol. 103, no. 1, pp. 151–163, 1995, doi: 10.1007/BF00241972.

[39] J. J. Collins, C. J. De Luca, A. Burrows, and L. A. Lipsitz, "Age-related changes in open-loop and closed-loop postural control mechanisms," *Exp. Brain Res.*, vol. 104, no. 3, pp. 480–492, 1995, doi: 10.1007/BF00231982.

[40] Collins, J. J. and C. J. De Luca, "Open-loop and closed-loop control of posture: A random-walk analysis of center-of-pressure trajectories," *Exp. Brain Res.*, vol. 95, pp. 309–318, 1993, doi: 10.1109/HICSS.2001.927267.

[41] T. E. T. E. Prieto, J. B. J. B. Myklebust, R. G. R. G. Hoffmann, E. G. E. G. Lovett, and B. M. B. M. Myklebust, "Measures of postural steadiness: Differences between healthy young and elderly adults," *IEEE Trans. Biomed. Eng.*, vol. 43, no. 9, pp. 956–966, 1996, doi: 10.1109/10.532130.

[42] C. Maurer and R. J. Peterka, "A new interpretation of spontaneous sway measures based on a simple model of human postural control," *J. Neurophysiol.*, vol. 93, no. 1, pp. 189–200, 2005, doi: 10.1152/jn.00221.2004.

[43] A. H. Vette, K. Masani, V. Sin, and M. R. Popovic, "Posturographic measures in healthy young adults during quiet sitting in comparison with quiet standing," *Med. Eng. Phys.*, vol. 32, no. 1, pp. 32–38, 2010, doi: 10.1016/j.medengphy.2009.10.005.

[44] T. Kiemel, Y. Zhang, and J. J. Jeka, “Identification of neural feedback for upright stance in humans: Stabilization rather than sway minimization,” *J. Neurosci.*, vol. 31, no. 42, pp. 15144–15153, 2011, doi: 10.1523/JNEUROSCI.1013-11.2011.

[45] T. Kiemel, A. J. Elahi, and J. J. Jeka, “Identification of the plant for upright stance in humans: Multiple movement patterns from a single neural strategy,” *J. Neurophysiol.*, vol. 100, no. 6, pp. 3394–3406, 2008, doi: 10.1152/jn.01272.2007.

[46] H. Van Der Kooij, E. Van Asseldonk, and F. C. T. Van Der Helm, “Comparison of different methods to identify and quantify balance control,” *J. Neurosci. Methods*, vol. 145, no. 1–2, pp. 175–203, 2005, doi: 10.1016/j.jneumeth.2005.01.003.

[47] A. Merlo *et al.*, “Postural stability and history of falls in cognitively able older adults: The Canton Ticino study,” *Gait Posture*, vol. 36, no. 4, pp. 662–666, 2012, doi: 10.1016/j.gaitpost.2012.06.016.

[48] L. Rocchi, L. Chiari, A. Cappello, and F. B. Horak, “Identification of distinct characteristics of postural sway in Parkinson’s disease: A feature selection procedure based on principal component analysis,” *Neurosci. Lett.*, vol. 394, no. 2, pp. 140–145, 2006, doi: 10.1016/j.neulet.2005.10.020.

[49] F. B. Horak and M. Mancini, “Objective biomarkers of balance and gait for Parkinson’s disease using body-worn sensors,” *Mov. Disord.*, vol. 28, no. 11, pp. 1544–1551, 2013, doi: 10.1002/mds.25684.

[50] A. R. Marinho-buzelli, H. Rouhani, B. Catharine, J. Angelo, B. Milos, and M. C. Verrier, “Effects of water immersion on quasi-static standing exploring center of pressure sway and trunk acceleration : a case series after incomplete spinal cord injury,” *Spinal Cord Ser. Cases*, 2019, doi: 10.1038/s41394-019-0147-2.

[51] S. Tyson, “How to measure balance in clinical practice . A systematic review of the psychometrics and clinical utility of measures of balance activity for neurological conditions,” *Clin. Rehabil.*, vol. 23, pp. 824–840, 2009.

[52] A. L. Hof, M. G. J. Gazendam, and W. E. Sinke, “The condition for dynamic stability,” *J. Biomech.*, vol. 38, no. 1, pp. 1–8, 2005, doi: 10.1016/j.jbiomech.2004.03.025.

[53] K. Iqbal and Y. C. Pai, “Predicted region of stability for balance recovery: Motion at the knee joint can improve termination of forward movement,” *J. Biomech.*, vol. 33, no. 12, pp. 1619–1627, 2000, doi: 10.1016/S0021-9290(00)00129-9.

[54] Y.-C. Pai and J. Patton, “Center of Mass Velocity-Position Predictions for Balance Control,” *J. Biomech.*, vol. 30, no. 4, pp. 347–354, 1997.

[55] Y. C. Pai and K. Iqbal, “Simulated movement termination for balance recovery: Can movement strategies be sought to maintain stability in the presence of slipping or forced sliding?,” *J. Biomech.*, vol. 32, no. 8, pp. 779–786, 1999, doi: 10.1016/S0021-9290(99)00074-3.

[56] F. Yang, F. C. Anderson, and Y. C. Pai, “Predicted threshold against backward balance loss in gait,” *J. Biomech.*, vol. 41, no. 9, pp. 1823–1831, 2008, doi: 10.1016/j.jbiomech.2008.04.005.

[57] F. Yang, D. Espy, and Y. C. Pai, “Feasible stability region in the frontal plane during human gait,” *Ann. Biomed. Eng.*, vol. 37, no. 12, pp. 2606–2614, 2009, doi: 10.1007/s10439-009-9798-7.

[58] H. Bahari, A. H. Vette, J. S. Hebert, and H. Rouhani, “Predicted threshold against forward and backward loss of balance for perturbed walking,” *J. Biomech.*, vol. 95, p. 109315, 2019, doi: 10.1016/j.jbiomech.2019.109315.

[59] J. H. Pasma, J. Van Kordelaar, D. De Kam, V. Weerdesteyn, A. C. Schouten, and H. Van Der Kooij, "Assessment of the underlying systems involved in standing balance: The additional value of electromyography in system identification and parameter estimation," *J. Neuroeng. Rehabil.*, vol. 14, no. 1, pp. 1–17, 2017, doi: 10.1186/s12984-017-0299-x.

[60] M. L. Audu and R. J. Triolo, "Intrinsic and extrinsic contributions to seated balance in the sagittal and coronal planes: Implications for trunk control after spinal cord injury," *J. Appl. Biomech.*, vol. 31, no. 4, pp. 221–228, 2015, doi: 10.1123/jab.2013-0307.

[61] R. J. Peterka, "Sensorimotor integration in human postural control," *J. Neurophysiol.*, vol. 88, no. 3, pp. 1097–1118, 2002, doi: 10.1152/jn.2002.88.3.1097.

[62] A. H. Vette, K. Masani, K. Nakazawa, and M. R. Popovic, "Neural-mechanical feedback control scheme generates physiological ankle torque fluctuation during quiet stance," *IEEE Trans. Neural Syst. Rehabil. Eng.*, vol. 18, no. 1, pp. 86–95, 2010, doi: 10.1109/TNSRE.2009.2037891.

[63] K. Masani, M. R. Popovic, K. Nakazawa, M. Kouzaki, and D. Nozaki, "Importance of Body Sway Velocity Information in Controlling Ankle Extensor Activities during Quiet Stance," *J. Neurophysiol.*, vol. 90, no. 6, pp. 3774–3782, 2003, doi: 10.1152/jn.00730.2002.

[64] J. H. Pasma *et al.*, "Reliability of system identification techniques to assess standing balance in healthy elderly," *PLoS One*, vol. 11, no. 3, 2016, doi: 10.1371/journal.pone.0151012.

[65] A. D. Goodworth and R. J. Peterka, "Identifying mechanisms of stance control: A single stimulus multiple output model-fit approach," *J. Neurosci. Methods*, vol. 296, pp. 44–56, 2018, doi: 10.1016/j.jneumeth.2017.12.015.

[66] T. A. Boonstra, A. C. Schouten, and H. Van Der Kooij, "Identification of the contribution of the ankle and hip joints to multi-segmental balance control," *J. Neuroeng. Rehabil.*, vol.

10, no. 1, 2013, doi: 10.1186/1743-0003-10-23.

[67] K. Agarwal, “Quantification of Mechanisms of Human Seated Balance using System,” University of Alberta, 2018.

[68] A. Ajoudani and A. Erfanian, “A neuro-sliding-mode control with adaptive modeling of uncertainty for control of movement in paralyzed limbs using functional electrical stimulation,” *IEEE Trans. Biomed. Eng.*, vol. 56, no. 7, pp. 1771–1780, 2009, doi: 10.1109/TBME.2009.2017030.

[69] T. Schauer *et al.*, “Online identification and nonlinear control of the electrically stimulated quadriceps muscle,” *Control Eng. Pract.*, vol. 13, no. 9, pp. 1207–1219, 2005, doi: 10.1016/j.conengprac.2004.10.006.

[70] A. Farhoud and A. Erfanian, “Fully automatic control of paraplegic FES pedaling using higher-order sliding mode and fuzzy logic control,” *IEEE Trans. Neural Syst. Rehabil. Eng.*, vol. 22, no. 3, pp. 533–542, 2014, doi: 10.1109/TNSRE.2013.2296334.

[71] V. Nekoukar and A. Erfanian, “A decentralized modular control framework for robust control of FES-activated walker-assisted paraplegic walking using terminal sliding mode and fuzzy logic control,” *IEEE Trans. Biomed. Eng.*, vol. 59, no. 10, pp. 2818–2827, 2012, doi: 10.1109/TBME.2012.2208963.

[72] M. Vanoncini, W. Holderbaum, and B. J. Andrews, “Development of closed loop FES controllers for trunk stabilization in paraplegia,” *13th Int. FES Soc. Conf.*, vol. 11, no. 4, pp. 365–367, 2008.

[73] “Spinal Cord Injury in Canada, Praxis Institute.” [Online]. Available: https://sci-bc.ca/info-centre/spinal-cord-injury/. [Accessed: 29-Jul-2020].

[74] “Spinal Cord Injury (SCI) Facts and Figures at a Glance. The National Spinal Cord Injury

Statistical Center. The University of Alabama at Birmingham Department of Physical Medicine and Rehabilitation," *National Spinal Cord Injury Statistical Center*, 2020. [Online]. Available: https://www.nscisc.uab.edu/Public/Facts and Figures 2020.pdf. [Accessed: 28-Jul-2020].

[75] M. T. Do, V. C. Chang, N. Kuran, and W. Thompson, "Fall-related injuries among Canadian seniors, 2005–2013: An analysis of the Canadian community health survey," *Heal. Promot. Chronic Dis. Prev. Canada*, vol. 35, no. 7, pp. 99–108, 2015, doi: 10.24095/hpcdp.35.7.01.

[76] A. Noamani, M. Nazarahari, J. Lewicke, A. H. Vette, and H. Rouhani, "Validity of using wearable inertial sensors for assessing the dynamics of standing balance," *Med. Eng. Phys.*, vol. 77, pp. 53–59, 2020, doi: 10.1016/j.medengphy.2019.10.018.

[77] A. Noamani, J. F. Lemay, K. E. Musselman, and H. Rouhani, "Characterization of standing balance after incomplete spinal cord injury: Alteration in integration of sensory information in ambulatory individuals," *Gait Posture*, vol. 83, no. October 2020, pp. 152–159, 2021, doi: 10.1016/j.gaitpost.2020.10.027.

[78] A. Noamani, J.-F. Lemay, K. E. Musselman, and H. Rouhani, "Postural control strategy after incomplete spinal cord injury: effect of sensory inputs on trunk–leg movement coordination," *J. Neuroeng. Rehabil.*, vol. 17, no. 1, 2020, doi: 10.1186/s12984-020-00775-2.

[79] A. Noamani, A. H. Vette, and H. Rouhani, "Instrumented Functional Test for Objective Outcome Evaluation of Balance Rehabilitation in Elderly Fallers : A Clinical Study," *Gerontology*, 2022, doi: 10.1159/000521001.

[80] A. Noamani, K. Agarwal, A. H. Vette, and H. Rouhani, "Predicted Threshold for Seated Stability : Estimation of Margin of Stability Using Wearable Inertial Sensors," *IEEE J.*

Biomed. Heal. Informatics, vol. 25, no. 9, pp. 3361–3372, 2021, doi: 10.1109/JBHI.2021.3073352.

[81] A. Noamani, A. H. Vette, and H. Rouhani, "Nonlinear response of human trunk musculature explains neuromuscular stabilization mechanisms in sitting posture," *J. Neural Eng.*, vol. 19, p. 026045, 2022, doi: https://doi.org/10.1088/1741-2552/ac63ed.

[82] Y. Aramaki, D. Nozaki, K. Masani, T. Sato, K. Nakazawa, and H. Yano, "Reciprocal angular acceleration of the ankle and hip joints during quiet standing in humans," *Exp. Brain Res.*, vol. 136, no. 4, pp. 463–473, 2001, doi: 10.1007/s002210000603.

[83] K. Masani, A. H. Vette, and M. R. Popovic, "Controlling balance during quiet standing: Proportional and derivative controller generates preceding motor command to body sway position observed in experiments," *Gait Posture*, vol. 23, no. 2, pp. 164–172, 2006, doi: 10.1016/j.gaitpost.2005.01.006.

[84] W.-L. Hsu, J. P. Scholz, G. Schoner, J. J. Jeka, and T. Kiemel, "Control and Estimation of Posture During Quiet Stance Depends on Multijoint Coordination," *J. Neurophysiol.*, vol. 97, no. 4, pp. 3024–3035, 2007, doi: 10.1152/jn.01142.2006.

[85] M. Mancini *et al.*, "ISway: A sensitive, valid and reliable measure of postural control," *J. Neuroeng. Rehabil.*, vol. 9, no. 1, pp. 1–8, 2012, doi: 10.1186/1743-0003-9-59.

[86] K. Masani, A. H. Vette, M. O. Abe, K. Nakazawa, and M. R. Popovic, "Smaller sway size during quiet standing is associated with longer preceding time of motor command to body sway," *Gait Posture*, vol. 33, no. 1, pp. 14–17, 2011, doi: 10.1016/j.gaitpost.2010.08.012.

[87] T. Kato, S. ichiro Yamamoto, T. Miyoshi, K. Nakazawa, K. Masani, and D. Nozaki, "Anti-phase action between the angular accelerations of trunk and leg is reduced in the elderly," *Gait Posture*, vol. 40, no. 1, pp. 107–112, 2014, doi: 10.1016/j.gaitpost.2014.03.006.

[88] D. A. Winter, “Human blance and posture control during standing and walking,” *Gait Posture*, vol. 3, no. 4, pp. 193–214, 1995, doi: 10.1016/0966-6362(96)82849-9.

[89] S. B. Richmond, B. W. Fling, H. Lee, and D. S. Peterson, “The assessment of center of mass and center of pressure during quiet stance: Current applications and future directions,” *J. Biomech.*, vol. 123, p. 110485, 2021, doi: 10.1016/j.jbiomech.2021.110485.

[90] M. R. Popovic, I. P. I. Pappas, K. Nakazawa, T. Keller, M. Morari, and V. Dietz, “Stability criterion for controlling standing in able-bodied subjects,” *J. Biomech.*, vol. 33, no. 11, pp. 1359–1368, 2000, doi: 10.1016/S0021-9290(00)00123-8.

[91] J. Howcroft, J. Kofman, and E. D. Lemaire, “Review of fall risk assessment in geriatric populations using inertial sensors,” *J. Neuroeng. Rehabil.*, vol. 10, no. 1, pp. 1–12, 2013, doi: 10.1186/1743-0003-10-91.

[92] M. Nazarahari and H. Rouhani, “Detection of daily postures and walking modalities using a single chest-mounted tri-axial accelerometer,” *Med. Eng. Phys.*, vol. 57, pp. 75–81, 2018, doi: 10.1016/j.medengphy.2018.04.008.

[93] A. Noamani, M. Nazarahari, J. Lewicke, A. H. Vette, and H. Rouhani, “Validity of using wearable inertial sensors for assessing the dynamics of standing balance,” *Med. Eng. Phys.*, vol. 77, pp. 53–59, 2020, doi: 10.1016/j.medengphy.2019.10.018.

[94] J. Jeka, T. Kiemel, R. Creath, F. Horak, and R. Peterka, “Controlling human upright posture: Velocity information is more accurate than position or acceleration,” *J. Neurophysiol.*, vol. 92, no. 4, pp. 2368–2379, 2004, doi: 10.1152/jn.00983.2003.

[95] O. Caron, B. Faure, and Y. Brenière, “Estimating the centre of gravity of the body on the basis of the centre of pressure in standing posture,” *J. Biomech.*, vol. 30, no. 11–12, pp. 1169–1171, 1997, doi: 10.1016/S0021-9290(97)00094-8.

[96] H. Amoud, M. Abadi, D. J. Hewson, V. Michel-Pellegrino, M. Doussot, and J. Duchêne, "Fractal time series analysis of postural stability in elderly and control subjects," *J. Neuroeng. Rehabil.*, vol. 4, pp. 1–12, 2007, doi: 10.1186/1743-0003-4-12.

[97] L. Montesinos, R. Castaldo, and L. Pecchia, "On the use of approximate entropy and sample entropy with centre of pressure time-series," *J. Neuroeng. Rehabil.*, vol. 15, no. 1, pp. 1–15, 2018, doi: 10.1186/s12984-018-0465-9.

[98] C. Hansen, Q. Wei, J. S. Shieh, P. Fourcade, B. Isableu, and L. Majed, "Sample entropy, univariate, and multivariate multi-scale entropy in comparison with classical postural sway parameters in young healthy adults," *Front. Hum. Neurosci.*, vol. 11, no. April, 2017, doi: 10.3389/fnhum.2017.00206.

[99] A. M. Sabatini, "Analysis of postural sway using entropy measures of signal complexity," *Med. Biol. Eng. Comput.*, vol. 38, no. 6, pp. 617–624, 2000, doi: 10.1007/BF02344866.

[100] U. R. Acharya, S. C. Goh, K. Iijima, M. Sekine, and T. Tamura, "Analysis of body responses to an accelerating platform by the largest-Lyapunov-exponent method," *Proc. Inst. Mech. Eng. Part H J. Eng. Med.*, vol. 223, no. 1, pp. 111–120, 2009, doi: 10.1243/09544119JEIM454.

[101] M. Grangeon, D. Gagnon, C. Duclos, C. Gauthier, C. Larivière, and P. Gourdou, "Characterizing Postural Stability in a Quasi-Static Sitting Position among Individuals with Sensorimotor Impairments Following Spinal Cord Injury," *J. Bioeng. Biomed. Sci.*, vol. 03, no. 01, pp. 1–10, 2013, doi: 10.4172/2155-9538.1000124.

[102] N. Genthon, N. Vuillerme, J. P. Monnet, C. Petit, and P. Rougier, "Biomechanical assessment of the sitting posture maintenance in patients with stroke," *Clin. Biomech.*, vol. 22, no. 9, pp. 1024–1029, 2007, doi: 10.1016/j.clinbiomech.2007.07.011.

[103] A. Hufschmidt, J. Dichgans, K. H. Mauritz, and M. Hufschmidt, “Some Methods and Parameters of Body Sway Quantification and Their Neurological Applications*. Arch. Psychiat. Nervenkr. 228, 135-150 (1980),” *Arch Psychiatr Nervenkr*, vol. 150, no. 228, pp. 135–150, 1980.

[104] A. C. H. Geurts, B. Nienhuis, and T. W. Mulder, “Intrasubject variability of selected force-platform parameters in the quantification of postural control,” *Arch. Phys. Med. Rehabil.*, vol. 74, no. 11, pp. 1144–1150, 1993.

[105] J. E. Fitzgerald, A. Murray, C. Elliott, and J. P. Birchall, “Comparison of body sway analysis techniques: Assessment with subjects standing on a stable surface,” *Acta Otolaryngol.*, vol. 114, no. 2, pp. 115–119, 1994, doi: 10.3109/00016489409126028.

[106] C. Elliott, J. E. FitzGerald, and A. Murray, “Postural stability of normal subjects measured by sway magnetometry: Pathlength and area for the age range 15 to 64 years,” *Physiol. Meas.*, vol. 19, no. 1, pp. 103–109, 1998, doi: 10.1088/0967-3334/19/1/009.

[107] V. Cornilleau-Pérès, N. Shabana, J. Droulez, J. C. H. Goh, G. S. M. Lee, and P. T. K. Chew, “Measurement of the visual contribution to postural steadiness from the COP movement: Methodology and reliability,” *Gait Posture*, vol. 22, no. 2, pp. 96–106, 2005, doi: 10.1016/j.gaitpost.2004.07.009.

[108] S. Norrlin, A. Karlsson, G. Ahlsten, H. Lanshammar, H. Cson Silander, and M. Dahl, “Force measurements of postural sway and rapid arm lift in seated children with and without MMC,” *Clin. Biomech.*, vol. 17, no. 3, pp. 197–202, 2002, doi: 10.1016/S0268-0033(02)00006-2.

[109] S. Demura, T. Kitabayashi, and N. Masahiro, “Power spectrum characteristics of sway position and velocity of the center of pressure during static upright posture for healthy

people," *Percept. Mot. Ski.*, vol. 106, pp. 307–316, 2008.

[110] L. Rocchi, L. Chiari, and A. Cappello, "Feature selection of stabilometric parameters based on principal component analysis," *Med. Biol. Eng. Comput.*, vol. 42, no. 1, pp. 71–79, 2004, doi: 10.1007/BF02351013.

[111] D. A. Winter, A. E. Patla, F. Prince, M. Ishac, and K. Gielo-perczak, "Stiffness control of balance in quiet standing," *J. Neurophysiol.*, vol. 80, no. 3, pp. 1211–1221, 1998, doi: 10.1152/jn.1998.80.3.1211.

[112] W. H. Gage, D. A. Winter, J. S. Frank, and A. L. Adkin, "Kinematic and kinetic validity of the inverted pendulum model in quiet standing," *Gait Posture*, vol. 19, no. 2, pp. 124–132, 2004, doi: 10.1016/S0966-6362(03)00037-7.

[113] K. L. Fok, J. Lee, A. H. Vette, and K. Masani, "Kinematic error magnitude in the single-mass inverted pendulum model of human standing posture," *Gait Posture*, vol. 63, no. April, pp. 23–26, 2018, doi: 10.1016/j.gaitpost.2018.04.021.

[114] R. Fitzpatrick, D. K. Rogers, and D. I. McCloskey, "Stable human standing with lower-limb muscle afferents providing the only sensory input.," *J. Physiol.*, vol. 480, no. 2, pp. 395–403, 1994, doi: 10.1113/jphysiol.1994.sp020369.

[115] A. Alexandrov, A. Frolov, F. Horak, P. Carlson-Kuhta, and S. Park, "Feedback equilibrium control during human standing," *Biol. Cybern.*, vol. 93, no. 5, pp. 309–322, 2005, doi: 10.1007/s00422-005-0004-1.

[116] R. Creath, T. Kiemel, F. Horak, R. Peterka, and J. Jeka, "A unified view of quiet and perturbed stance: Simultaneous co-existing excitable modes," *Neurosci. Lett.*, vol. 377, no. 2, pp. 75–80, 2005, doi: 10.1016/j.neulet.2004.11.071.

[117] Y. Zhang, T. Kiemel, and J. Jeka, "The influence of sensory information on two-component

coordination during quiet stance," *Gait Posture*, vol. 26, no. 2, pp. 263–271, 2007, doi: 10.1016/j.gaitpost.2006.09.007.

[118] S. Sasagawa, J. Ushiyama, M. Kouzaki, and H. Kanehisa, "Effect of the hip motion on the body kinematics in the sagittal plane during human quiet standing," *Neurosci. Lett.*, vol. 450, no. 1, pp. 27–31, 2009, doi: 10.1016/j.neulet.2008.11.027.

[119] D. C. Hay and M. P. Wachowiak, "Analysis of free moment and center of pressure frequency components during quiet standing using magnitude squared coherence," *Hum. Mov. Sci.*, vol. 54, no. March, pp. 101–109, 2017, doi: 10.1016/j.humov.2017.04.002.

[120] M. Saffer, T. Kiemel, and J. Jeka, "Coherence analysis of muscle activity during quiet stance," *Exp. Brain Res.*, vol. 185, no. 2, pp. 215–226, 2008, doi: 10.1007/s00221-007-1145-3.

[121] L. E. Dibble and M. Lange, "Predicting Falls In Individuals with Parkinson Disease: A Reconsideration of Clinical Balance Measures," *J. Neurol. Phys. Ther.*, vol. 30, no. 2, pp. 60–67, 2006.

[122] A. K. Adlerton, U. Moritz, and R. Moe-Nilssen, "Forceplate and accelerometer measures for evaluating the effect of muscle fatigue on postural control during one-legged stance.," *Physiother. Res. Int.*, vol. 8, no. 4, pp. 187–199, 2003, doi: 10.1002/pri.289.

[123] S. L. Whitney *et al.*, "A comparison of accelerometry and center of pressure measures during computerized dynamic posturography: A measure of balance," *Gait Posture*, vol. 33, no. 4, pp. 594–599, 2011, doi: 10.1016/j.gaitpost.2011.01.015.

[124] R. E. Mayagoitia, J. C. Lötters, P. H. Veltink, and H. Hermens, "Standing balance evaluation using a triaxial accelerometer," *Gait Posture*, vol. 16, no. 1, pp. 55–59, 2002, doi: 10.1016/S0966-6362(01)00199-0.

[125] B. Najafi, D. Horn, S. Marclay, R. T. Crews, S. Wu, and J. S. Wrobel, "Assessing postural control and postural control strategy in diabetes patients using innovative and wearable technology," *J. Diabetes Sci. Technol.*, vol. 4, no. 4, pp. 780–791, 2010, doi: 10.1177/193229681000400403.

[126] M. Mancini, F. B. Horak, C. Zampieri, P. Carlson-Kuhta, J. G. Nutt, and L. Chiari, "Trunk accelerometry reveals postural instability in untreated Parkinson's disease," *Park. Relat. Disord.*, vol. 17, no. 7, pp. 557–562, 2011, doi: 10.1016/j.parkreldis.2011.05.010.

[127] J. L. Alberts *et al.*, "Using Accelerometer and Gyroscopic Measures to Quantify Postural Stability," *J. Athl. Train.*, vol. 50, no. 6, pp. 578–588, 2015, doi: 10.4085/1062-6050-50.2.01.

[128] N. R. Heebner, J. S. Akins, S. M. Lephart, and T. C. Sell, "Reliability and validity of an accelerometry based measure of static and dynamic postural stability in healthy and active individuals," *Gait Posture*, vol. 41, no. 2, pp. 535–539, 2015, doi: 10.1016/j.gaitpost.2014.12.009.

[129] E. E. Hansson and Å. Tornberg, "Coherence and reliability of a wearable inertial measurement unit for measuring postural sway," *BMC Res. Notes*, vol. 12, no. 1, pp. 1–5, 2019, doi: 10.1186/s13104-019-4238-8.

[130] M. Ghislieri, L. Gastaldi, S. Pastorelli, S. Tadano, and V. Agostini, "Wearable inertial sensors to assess standing balance: a systematic review," *Sensors (Switzerland)*, vol. 19, no. 19, pp. 1–25, 2019, doi: 10.3390/s19194075.

[131] G. Bonora *et al.*, "Investigation of anticipatory postural adjustments during One-Leg Stance using inertial sensors: Evidence from subjects with Parkinsonism," *Front. Neurol.*, vol. 8, no. JUL, 2017, doi: 10.3389/fneur.2017.00361.

[132] C. Baston, M. Mancini, L. Rocchi, and F. Horak, “Effects of Levodopa on Postural Strategies in Parkinson’s disease,” *Gait Posture*, vol. 46, pp. 26–29, 2016, doi: 10.1016/j.gaitpost.2016.02.009.

[133] N. Hasegawa *et al.*, “Functional limits of stability and standing balance in people with Parkinson’s disease with and without freezing of gait using wearable sensors,” *Gait Posture*, vol. 87, no. April, pp. 123–129, 2021, doi: 10.1016/j.gaitpost.2021.04.023.

[134] A. C. Albán-Cadena, F. Villalba-Meneses, K. O. Pila-Varela, A. Moreno-Calvo, C. P. Villalba-Meneses, and D. A. Almeida-Galárraga, “Wearable sensors in the diagnosis and study of Parkinson’s disease symptoms: a systematic review,” *J. Med. Eng. Technol.*, vol. 45, no. 7, pp. 532–545, 2021, doi: 10.1080/03091902.2021.1922528.

[135] J. M. Huisinga, R. J. St George, R. Spain, S. Overs, and F. B. Horak, “Postural response latencies are related to balance control during standing and walking in patients with multiple sclerosis,” *Arch. Phys. Med. Rehabil.*, vol. 95, no. 7, pp. 1390–1397, 2014, doi: 10.1016/j.apmr.2014.01.004.

[136] J. Huisinga, M. Mancini, C. Veys, R. Spain, and F. Horak, “Coherence analysis of trunk and leg acceleration reveals altered postural sway strategy during standing in persons with multiple sclerosis,” *Hum. Mov. Sci.*, vol. 58, no. October 2017, pp. 330–336, 2018, doi: 10.1016/j.humov.2017.12.009.

[137] N. Baker, C. Gough, and S. J. Gordon, “Inertial sensor reliability and validity for static and dynamic balance in healthy adults: A systematic review,” *Sensors*, vol. 21, no. 15, 2021, doi: 10.3390/s21155167.

[138] A. Dalton, H. Khalil, M. Busse, A. Rosser, R. van Deursen, and G. ÓLaighin, “Analysis of gait and balance through a single triaxial accelerometer in presymptomatic and symptomatic

Huntington's disease," *Gait Posture*, vol. 37, no. 1, pp. 49–54, 2013, doi: 10.1016/j.gaitpost.2012.05.028.

[139] M. K. O'brien *et al.*, "Augmenting clinical outcome measures of gait and balance with a single inertial sensor in age-ranged healthy adults," *Sensors (Switzerland)*, vol. 19, no. 20, pp. 1–28, 2019, doi: 10.3390/s19204537.

[140] M. Mancini, L. Chiari, L. Holmstrom, A. Salarian, and F. B. Horak, "Validity and reliability of an IMU-based method to detect APAs prior to gait initiation," *Gait Posture*, vol. 43, pp. 125–131, 2016, doi: 10.1016/j.gaitpost.2015.08.015.

[141] M. Patel, A. Pavic, and V. A. Goodwin, "Wearable inertial sensors to measure gait and posture characteristic differences in older adult fallers and non-fallers: A scoping review," *Gait Posture*, vol. 76, no. February 2019, pp. 110–121, 2020, doi: 10.1016/j.gaitpost.2019.10.039.

[142] J. M. Leach, M. Mancini, R. J. Peterka, T. L. Hayes, and F. B. Horak, "Validating and calibrating the Nintendo Wii balance board to derive reliable center of pressure measures," *Sensors (Switzerland)*, vol. 14, no. 10, pp. 18244–18267, 2014, doi: 10.3390/s141018244.

[143] H. Barbeau, M. Ladouceur, and K. E. Norman, "Walking After Spinal Cord Injury: and Functional Recovery," *Arch Phys Med Rehabil*, vol. 80, pp. 225–235, 1999.

[144] G. Scivoletto and V. Di Donna, "Prediction of walking recovery after spinal cord injury," *Brain Res. Bull.*, vol. 78, no. 1, pp. 43–51, 2009, doi: 10.1016/j.brainresbull.2008.06.002.

[145] G. E. Lee, H. Bae, T. S. Yoon, J. S. Kim, T. I. Yi, and J. S. Park, "Factors that Influence Quiet Standing Balance of Patients with Incomplete Cervical Spinal Cord Injuries," *Ann. Rehabil. Med.*, vol. 36, pp. 530–537, 2012.

[146] F. Tamburella, G. Scivoletto, M. Iosa, and M. Molinari, "Reliability , validity , and

effectiveness of center of pressure parameters in assessing stabilometric platform in subjects with incomplete spinal cord injury : a serial cross-sectional study," *J. Neuroeng. Rehabil.*, vol. 11, no. 86, pp. 1–13, 2014.

[147] S. Datta, D. J. Lorenz, and S. J. Harkema, "Dynamic longitudinal evaluation of the utility of the berg balance scale in individuals with motor incomplete spinal cord injury," *Arch. Phys. Med. Rehabil.*, vol. 93, no. 9, pp. 1565–1573, 2012, doi: 10.1016/j.apmr.2012.01.026.

[148] S. Sprigle, C. Maurer, and M. Holowka, "Development of valid and reliable measures of postural stability," *J. Spinal Cord Med.*, vol. 30, no. 1, pp. 40–49, 2007, doi: 10.1080/10790268.2007.11753913.

[149] S. M. Lynch, P. Leahy, and S. P. Barker, "Reliability of measurements obtained with a modified functional reach test in subjects with spinal cord injury," *Phys. Ther.*, vol. 78, no. 2, pp. 128–133, 1998, doi: 10.1093/ptj/78.2.128.

[150] M. Wirz, R. Müller, and C. Bastiaenen, "Falls in Persons With Spinal Cord Injury: Validity and Reliability of the Berg Balance Scale," *Neurorehabil. Neural Repair*, vol. 24, no. 1, pp. 70–77, 2010, doi: 10.1177/1545968309341059.

[151] S. Datta, D. J. Lorenz, S. Morrison, E. Ardolino, and S. J. Harkema, "A Multivariate Examination of Temporal Changes in Berg Balance Scale Items for Patients With ASIA Impairment Scale C and D Spinal Cord Injuries," *Arch. Phys. Med. Rehabil.*, vol. 90, no. 7, pp. 1208–1217, 2009, doi: 10.1016/j.apmr.2008.09.577.

[152] K. Srisim, J. Saengsuwan, and S. Amatachaya, "Functional assessments for predicting a risk of multiple falls in independent ambulatory patients with spinal cord injury," *J. Spinal Cord Med.*, vol. 38, no. 4, pp. 439–445, 2015, doi: 10.1179/2045772313Y.0000000186.

[153] K. E. Musselman *et al.*, "Evaluating Intrinsic Fall Risk Factors After Incomplete Spinal

Cord Injury: Distinguishing Fallers From Nonfallers," *Arch. Rehabil. Res. Clin. Transl.*, vol. 3, no. 1, p. 100096, 2021, doi: 10.1016/j.arrct.2020.100096.

[154] T. Shany, S. J. Redmond, M. R. Narayanan, and N. H. Lovell, "Sensors-based wearable systems for monitoring of human movement and falls," *IEEE Sens. J.*, vol. 12, no. 3, pp. 658–670, 2012, doi: 10.1109/JSEN.2011.2146246.

[155] J. Hamm, A. G. Money, A. Atwal, and I. Paraskevopoulos, "Fall prevention intervention technologies: A conceptual framework and survey of the state of the art," *J. Biomed. Inform.*, vol. 59, pp. 319–345, 2016, doi: 10.1016/j.jbi.2015.12.013.

[156] C. Wang, M. Patriquin, A. Vaziri, and B. Najafi, "Mobility Performance in Community-Dwelling Older Adults: Potential Digital Biomarkers of Concern about Falling," *Gerontology*, vol. 77030, 2021, doi: 10.1159/000512977.

[157] M. O'sullivan, C. Blake, C. Cunningham, G. Boyle, and C. Finucane, "Correlation of accelerometry with clinical balance tests in older fallers and non-fallers," *Age Ageing*, vol. 38, no. 3, pp. 308–313, 2009, doi: 10.1093/ageing/afp009.

[158] D. Roman-Liu, "Age-related changes in the range and velocity of postural sway," *Arch. Gerontol. Geriatr.*, vol. 77, no. September 2017, pp. 68–80, 2018, doi: 10.1016/j.archger.2018.04.007.

[159] J. Howcroft, E. D. Lemaire, J. Kofman, and W. E. McIlroy, "Elderly fall risk prediction using static posturography," *PLoS One*, vol. 12, no. 2, pp. 1–13, 2017, doi: 10.1371/journal.pone.0172398.

[160] L. Pizzigalli, M. Micheletti Cremasco, A. Mulasso, and A. Rainoldi, "The contribution of postural balance analysis in older adult fallers: A narrative review," *J. Bodyw. Mov. Ther.*, vol. 20, no. 2, pp. 409–417, 2016, doi: 10.1016/j.jbmt.2015.12.008.

[161] V. P. Panzer, S. Bandinelli, and M. Hallett, “Biomechanical assessment of quiet standing and changes associated with aging,” *Arch. Phys. Med. Rehabil.*, vol. 76, no. 2, pp. 151–157, 1995, doi: 10.1016/S0003-9993(95)80024-7.

[162] S. M. S. F. Freitas, S. A. Wieczorek, P. H. Marchetti, and M. Duarte, “Age-related changes in human postural control of prolonged standing,” *Gait Posture*, vol. 22, no. 4, pp. 322–330, 2005, doi: 10.1016/j.gaitpost.2004.11.001.

[163] J. A. Raymakers, M. M. Samson, and H. J. J. Verhaar, “The assessment of body sway and the choice of the stability parameter(s),” *Gait Posture*, vol. 21, no. 1, pp. 48–58, 2005, doi: 10.1016/j.gaitpost.2003.11.006.

[164] K. Masani, A. H. Vette, M. Kouzaki, H. Kanehisa, T. Fukunaga, and M. R. Popovic, “Larger center of pressure minus center of gravity in the elderly induces larger body acceleration during quiet standing,” *Neurosci. Lett.*, vol. 422, no. 3, pp. 202–206, 2007, doi: 10.1016/j.neulet.2007.06.019.

[165] D. Lin, H. Seol, M. A. Nussbaum, and M. L. Madigan, “Reliability of COP-based postural sway measures and age-related differences,” *Gait Posture*, vol. 28, no. 2, pp. 337–342, 2008, doi: 10.1016/j.gaitpost.2008.01.005.

[166] M. G. Tucker, J. J. Kavanagh, R. S. Barrett, and S. Morrison, “Age-related differences in postural reaction time and coordination during voluntary sway movements,” *Hum. Mov. Sci.*, vol. 27, no. 5, pp. 728–737, 2008, doi: 10.1016/j.humov.2008.03.002.

[167] N. B. Singh, W. R. Taylor, M. L. Madigan, and M. A. Nussbaum, “The spectral content of postural sway during quiet stance: Influences of age, vision and somatosensory inputs,” *J. Electromyogr. Kinesiol.*, vol. 22, no. 1, pp. 131–136, 2012, doi: 10.1016/j.jelekin.2011.10.007.

[168] C. Fujimoto, N. Egami, S. Demura, T. Yamasoba, and S. Iwasaki, “The effect of aging on the center-of-pressure power spectrum in foam posturography,” *Neurosci. Lett.*, vol. 585, pp. 92–97, 2015, doi: 10.1016/j.neulet.2014.11.033.

[169] T. Kato, S. ichiro Yamamoto, T. Miyoshi, K. Nakazawa, K. Masani, and D. Nozaki, “Anti-phase action between the angular accelerations of trunk and leg is reduced in the elderly,” *Gait Posture*, vol. 40, no. 1, pp. 107–112, 2014, doi: 10.1016/j.gaitpost.2014.03.006.

[170] Z. Li, Y. Y. Liang, L. Wang, J. Sheng, and S. J. Ma, “Reliability and validity of center of pressure measures for balance assessment in older adults,” *J. Phys. Ther. Sci.*, vol. 28, no. 4, pp. 1364–1367, 2016, doi: 10.1589/jpts.28.1364.

[171] M. Ghahramani, D. Stirling, F. Naghdy, G. Naghdy, and J. Potter, “Body postural sway analysis in older people with different fall histories,” *Med. Biol. Eng. Comput.*, vol. 57, no. 2, pp. 533–542, 2019, doi: 10.1007/s11517-018-1901-5.

[172] J. Johansson, A. Nordström, Y. Gustafson, G. Westling, and P. Nordström, “Increased postural sway during quiet stance as a risk factor for prospective falls in community-dwelling elderly individuals,” *Age Ageing*, vol. 46, no. 6, pp. 964–970, 2017, doi: 10.1093/ageing/afx083.

[173] L. Montesinos, R. Castaldo, and L. Pecchia, “Wearable inertial sensors for fall risk assessment and prediction in older adults: A systematic review and meta-analysis,” *IEEE Trans. Neural Syst. Rehabil. Eng.*, vol. 26, no. 3, pp. 573–582, 2018, doi: 10.1109/TNSRE.2017.2771383.

[174] R. Sun and J. J. Sosnoff, “Novel sensing technology in fall risk assessment in older adults: A systematic review,” *BMC Geriatr.*, vol. 18, no. 1, 2018, doi: 10.1186/s12877-018-0706-6.

[175] K. Patel, M. Milosevic, K. Nakazawa, M. R. Popovic, and K. Masani, "Wheelchair neuroprosthesis for improving dynamic trunk stability," *IEEE Trans. Neural Syst. Rehabil. Eng.*, vol. 25, no. 12, pp. 2472–2479, 2017, doi: 10.1109/TNSRE.2017.2727072.

[176] M. L. Audu, L. M. Lombardo, J. R. Schnellenberger, K. M. Foglyano, M. E. Miller, and R. J. Triolo, "A neuroprosthesis for control of seated balance after spinal cord injury," *J. Neuroeng. Rehabil.*, vol. 12, no. 1, pp. 1–12, 2015, doi: 10.1186/1743-0003-12-8.

[177] J. O. Murphy, M. L. Audu, L. M. Lombardo, K. M. Foglyano, and R. J. Triolo, "Feasibility of closed-loop controller for righting seated posture after spinal cord injury," *J. Rehabil. Res. Dev.*, vol. 51, no. 5, pp. 747–760, 2014, doi: 10.1682/JRRD.2013.09.0200.

[178] M. Milosevic, K. Masani, N. Wu, K. M. V. McConville, and M. R. Popovic, "Trunk muscle co-activation using functional electrical stimulation modifies center of pressure fluctuations during quiet sitting by increasing trunk stiffness," *J. Neuroeng. Rehabil.*, vol. 12, no. 1, pp. 1–9, 2015, doi: 10.1186/s12984-015-0091-8.

[179] A. Bheemreddy *et al.*, "A closed-loop self-righting controller for seated balance in the coronal and diagonal planes following spinal cord injury," *Med. Eng. Phys.*, vol. 86, pp. 47–56, 2020, doi: 10.1016/j.medengphy.2020.10.010.

[180] A. R. W. Friederich, M. L. Audu, and R. J. Triolo, "Characterization of the Force Production Capabilities of Paralyzed Trunk Muscles Activated with Functional Neuromuscular Stimulation in Individuals with Spinal Cord Injury," *IEEE Trans. Biomed. Eng.*, vol. 68, no. 8, pp. 2389–2399, 2021, doi: 10.1109/TBME.2020.3039404.

[181] R. Davoodi, B. J. Andrews, G. D. Wheeler, and R. Lederer, "Development of an indoor rowing machine with manual FES controller for total body exercise in paraplegia," *IEEE Trans. Neural Syst. Rehabil. Eng.*, vol. 10, no. 3, pp. 197–203, 2002, doi:

10.1109/TNSRE.2002.802880.

[182] A. L. Hof, "The 'extrapolated center of mass' concept suggests a simple control of balance in walking," *Hum. Mov. Sci.*, vol. 27, no. 1, pp. 112–125, 2008, doi: 10.1016/j.humov.2007.08.003.

[183] Y. C. Pai, B. E. Maki, K. Iqbal, W. E. McIlroy, and S. D. Perry, "Thresholds for step initiation induced by support-surface translation: A dynamic center-of-mass model provides much better prediction than a static model," *J. Biomech.*, vol. 33, no. 3, pp. 387–392, 2000, doi: 10.1016/S0021-9290(99)00199-2.

[184] Y. C. Pai, M. W. Rogers, J. Patton, T. D. Cain, and T. A. Hanke, "Static versus dynamic predictions of protective stepping following waist-pull perturbations in young and older adults," *J. Biomech.*, vol. 31, no. 12, pp. 1111–1118, 1998, doi: 10.1016/S0021-9290(98)00124-9.

[185] J. L. Patton, Y. C. Pai, and W. A. Lee, "Evaluation of a model that determines the stability limits of dynamic balance," *Gait Posture*, vol. 9, no. 1, pp. 38–49, 1999, doi: 10.1016/S0966-6362(98)00037-X.

[186] J. L. Patton, W. A. Lee, and Y. C. Pai, "Relative stability improves with experience in a dynamic standing task," *Exp. Brain Res.*, vol. 135, no. 1, pp. 117–126, 2000, doi: 10.1007/s002210000500.

[187] F. Yang, F. C. Anderson, and Y. C. Pai, "Predicted threshold against backward balance loss in gait," *J. Biomech.*, vol. 40, no. 4, pp. 804–811, 2007, doi: 10.1016/j.jbiomech.2006.03.015.

[188] F. Yang, F. C. Anderson, and Y. C. Pai, "Predicted threshold against backward balance loss following a slip in gait," *J. Biomech.*, vol. 41, no. 9, pp. 1823–1831, 2008, doi:

10.1016/j.jbiomech.2008.04.005.

[189] Y. C. Pai, “Movement termination and stability in standing,” *Exerc. Sport Sci. Rev.*, vol. 31, no. 1, pp. 19–25, 2003, doi: 10.1097/00003677-200301000-00005.

[190] P. J. Lee, E. L. Rogers, and K. P. Granata, “Active trunk stiffness increases with co-contraction,” *J. Electromyogr. Kinesiol.*, vol. 16, no. 1, pp. 51–57, 2006, doi: 10.1016/j.jelekin.2005.06.006.

[191] M. Freddolini, S. Strike, and R. Y. W. Lee, “The role of trunk muscles in sitting balance control in people with low back pain,” *J. Electromyogr. Kinesiol.*, vol. 24, no. 6, pp. 947–953, 2014, doi: 10.1016/j.jelekin.2014.09.009.

[192] F. B. Horak, “Postural orientation and equilibrium: What do we need to know about neural control of balance to prevent falls?,” *Age Ageing*, vol. 35, no. SUPPL.2, pp. 7–11, 2006, doi: 10.1093/ageing/afl077.

[193] R. A. Preuss, S. G. Grenier, and S. M. McGill, “Postural control of the lumbar spine in unstable sitting,” *Arch. Phys. Med. Rehabil.*, vol. 86, no. 12, pp. 2309–2315, 2005, doi: 10.1016/j.apmr.2005.07.302.

[194] D. Engelhart, T. A. Boonstra, R. G. K. M. Aarts, A. C. Schouten, and H. Van Der Kooij, “Comparison of closed-loop system identification techniques to quantify multi-joint human balance control,” *Annu. Rev. Control*, vol. 41, pp. 58–70, 2016, doi: 10.1016/j.arcontrol.2016.04.010.

[195] D. Engelhart, A. C. Schouten, R. G. K. M. Aarts, and H. Van Der Kooij, “Assessment of Multi-Joint Coordination and Adaptation in Standing Balance: A Novel Device and System Identification Technique,” *IEEE Trans. Neural Syst. Rehabil. Eng.*, vol. 23, no. 6, pp. 973–982, 2015, doi: 10.1109/TNSRE.2014.2372172.

[196] D. Engelhart *et al.*, "Impaired Standing Balance in Elderly: A New Engineering Method Helps to Unravel Causes and Effects," *J. Am. Med. Dir. Assoc.*, vol. 15, no. 3, pp. 227.e1-227.e6, 2014, doi: 10.1016/j.jamda.2013.09.009.

[197] J. H. Pasma *et al.*, "Assessing Standing Balance using MIMO Closed Loop System Identification Techniques," *IFAC-PapersOnLine*, vol. 48, no. 28, pp. 1381–1385, 2015, doi: 10.1016/j.ifacol.2015.12.325.

[198] R. J. Peterka, P. J. Loughlin, R. J. Peterka, and P. J. Loughlin, "Dynamic Regulation of Sensorimotor Integration in Human Postural Control," *J. Neurophysiol.*, vol. 91, pp. 410–423, 2004, doi: 10.1152/jn.00516.2003.

[199] A. D. Goodworth and R. J. Peterka, "Contribution of Sensorimotor Integration to Spinal Stabilization in Humans," *J. Neurophysiol.*, vol. 102, no. 1, pp. 496–512, 2009, doi: 10.1152/jn.00118.2009.

[200] H. Van Der Kooij and R. J. Peterka, "Non-linear stimulus-response behavior of the human stance control system is predicted by optimization of a system with sensory and motor noise," *J. Comput. Neurosci.*, vol. 30, no. 3, pp. 759–778, 2011, doi: 10.1007/s10827-010-0291-y.

[201] E. E. Hansson, A. Beckman, and A. Håkansson, "Effect of vision, proprioception, and the position of the vestibular organ on postural sway," *Acta Otolaryngol.*, vol. 130, no. 12, pp. 1358–1363, 2010, doi: 10.3109/00016489.2010.498024.

[202] R. C. Fitzpatrick and B. L. Day, "Probing the human vestibular system with galvanic stimulation," *J. Appl. Physiol.*, vol. 96, no. 6, pp. 2301–2316, 2004, doi: 10.1152/japplphysiol.00008.2004.

[203] J. F. Iles, R. Baderin, R. Tanner, and A. Simon, "Human standing and walking: Comparison

of the effects of stimulation of the vestibular system," *Exp. Brain Res.*, vol. 178, no. 2, pp. 151–166, 2007, doi: 10.1007/s00221-006-0721-2.

[204] P. van Drunen, Y. Koumans, F. C. T. van der Helm, J. H. van Dieën, and R. Happee, "Modulation of intrinsic and reflexive contributions to low-back stabilization due to vision, task instruction, and perturbation bandwidth," *Exp. Brain Res.*, vol. 233, no. 3, pp. 735–749, 2015, doi: 10.1007/s00221-014-4151-2.

[205] A. Kavounoudias, J. C. Gilhodes, R. Roll, and J. P. Roll, "From balance regulation to body orientation: Two goals for muscle proprioceptive information processing?," *Exp. Brain Res.*, vol. 124, no. 1, pp. 80–88, 1999, doi: 10.1007/s002210050602.

[206] L. M. Nashner and P. Wolfson, "Influence of head position and proprioceptive cues on short latency postural reflexes evoked by galvanic stimulation of the human labyrinth," *Brain Res.*, vol. 67, no. 2, pp. 255–268, 1974, doi: 10.1016/0006-8993(74)90276-5.

[207] T. D. J. Welch and L. H. Ting, "A feedback model reproduces muscle activity during human postural responses to support-surface translations," *J. Neurophysiol.*, vol. 99, no. 2, pp. 1032–1038, 2008, doi: 10.1152/jn.01110.2007.

[208] H. Rouhani, M. Same, K. Masani, Y. Q. Li, and M. R. Popovic, "PID controller design for FES applied to ankle muscles in neuroprosthesis for standing balance," *Front. Neurosci.*, vol. 11, no. JUN, pp. 1–14, 2017, doi: 10.3389/fnins.2017.00347.

[209] H. Rouhani, M. R. Popovic, M. Same, Y. Q. Li, and K. Masani, "Identification of ankle plantar-flexors dynamics in response to electrical stimulation," *Med. Eng. Phys.*, vol. 38, no. 11, pp. 1166–1171, 2016, doi: 10.1016/j.medengphy.2016.07.011.

[210] T. S. Buchanan, D. G. Lloyd, K. Manal, and T. F. Besier, "Neuromusculoskeletal Modeling: Estimation of Muscle Forces and Joint Moments and Movements From Measurements of

Neural Command," *J. Appl. Biomech.*, vol. 20, no. 4, pp. 367–395, 2004, doi: 10.3998/ark.5550190.0011.815.

[211] R. Riener, A. Member, T. Fuhr, and S. Member, "Patient-Driven Control of FES-Supported Standing Up : A Simulation Study," *IEEE Trans. Rehabil. Eng.*, vol. 6, no. 2, pp. 113–124, 1998, doi: 10.1109/86.681177.

[212] A. H. Vette, K. Masani, N. Wu, and M. R. Popovic, "Multidirectional quantification of trunk stiffness and damping during unloaded natural sitting," *Med. Eng. Phys.*, vol. 36, no. 1, pp. 102–109, 2014, doi: 10.1016/j.medengphy.2013.10.005.

[213] J. H. Pasma, D. Engelhart, A. C. Schouten, H. van der Kooij, A. B. Maier, and C. G. M. Meskers, "Impaired standing balance: The clinical need for closing the loop," *Neuroscience*, vol. 267, pp. 157–165, 2014, doi: 10.1016/j.neuroscience.2014.02.030.

[214] P. Spagnol, C. Klauer, F. Previdi, J. Raisch, and T. Schauer, "Modeling and Online-Identification of Electrically Stimulated Antagonistic Muscles for Horizontal Shoulder Abduction and Adduction," in *European Control Conference (ECC)*, 2013, pp. 3979–3984, doi: doi: 10.23919/ECC.2013.6669599.

[215] V. Nekoukar and A. Erfanian, "An Adaptive Fuzzy Sliding-Mode Controller Design for Walking Control with Functional Electrical Stimulation : A Computer Simulation Study," *Int. J. Control. Autom. Syst.*, vol. 9, no. 6, pp. 1124–1135, 2011, doi: 10.1007/s12555-011-0614-4.

[216] ko Berg, S. Wood-Dauphinee, and J. Williams, "The Balance Scale: reliability assessment with elderly residents and patients with an acute stroke.," *Can. J. Public Heal.*, vol. 27, no. 1, pp. 27–36, 1995.

[217] C. P. Carty, N. J. Cronin, G. A. Lichtwark, P. M. Mills, and R. S. Barrett, "Lower limb

muscle moments and power during recovery from forward loss of balance in male and female single and multiple steppers," *Clin. Biomech.*, vol. 27, no. 10, pp. 1031–1037, 2012, doi: 10.1016/j.clinbiomech.2012.07.009.

[218] M. K. Y. Mak, O. Levin, J. Mizrahi, and C. W. Y. Hui-Chan, "Joint torques during sit-to-stand in healthy subjects and people with Parkinson's disease," *Clin. Biomech.*, vol. 18, no. 3, pp. 197–206, 2003, doi: 10.1016/S0268-0033(02)00191-2.

[219] S. R. Goldberg, S. Õunpuu, A. S. Arnold, J. R. Gage, and S. L. Delp, "Kinematic and kinetic factors that correlate with improved knee flexion following treatment for stiff-knee gait," *J. Biomech.*, vol. 39, no. 4, pp. 689–698, 2006, doi: 10.1016/j.jbiomech.2005.01.015.

[220] H. Rouhani, J. Favre, X. Crevoisier, and K. Aminian, "A wearable system for multi-segment foot kinetics measurement," *J. Biomech.*, vol. 47, no. 7, pp. 1704–1711, 2014, doi: 10.1016/j.jbiomech.2014.02.027.

[221] H. Rouhani, J. Favre, X. Crevoisier, and K. Aminian, "Ambulatory measurement of ankle kinetics for clinical applications," *J. Biomech.*, vol. 44, no. 15, pp. 2712–2718, 2011, doi: 10.1016/j.jbiomech.2011.07.021.

[222] K. Lebel, P. Boissy, M. Hamel, and C. Duval, "Inertial measures of motion for clinical biomechanics: Comparative assessment of accuracy under controlled conditions - Changes in accuracy over time," *PLoS One*, vol. 10, no. 3, pp. 1–12, 2015, doi: 10.1371/journal.pone.0118361.

[223] D. A. Winter, *Biomechanics and Motor Control of Human Movement*, Fourth Edi. Hoboken, NJ, USA: John Wiley & Sons, Inc., 2009.

[224] A. Cappozzo, F. Catani, U. Della Croce, and A. Leardini, "Position and orietnation in space of bones during movement," *Clin. Biomech.*, vol. 10, no. 4, pp. 171–178, 1995.

[225] Rolf Moe-Nilssen and Jorunn L. Helbostad, “Trunk accelerometry as a measure of balance control during quiet standing,” *Gait Posture*, vol. 16, no. 1, pp. 60–68, 2002.

[226] M. Nazarahari and H. Rouhani, “Semi-automatic Sensor-to-Body Calibration of Inertial Sensors on Lower Limb Using Gait Recording,” *IEEE Sens. J.*, vol. (In Press), 2019, doi: 10.1109/JSEN.2019.2939981.

[227] M. Nazarahari, A. Noamani, N. Ahmadian, and H. Rouhani, “Sensor-to-Body Calibration Procedure for Clinical Motion Analysis of Lower Limb Using Magnetic and Inertial Measurement Units,” *J. Biomech.*, vol. 85, pp. 224–229, 2019.

[228] A. Karatsidis, G. Bellusci, H. Schepers, M. de Zee, M. Andersen, and P. Veltink, “Estimation of Ground Reaction Forces and Moments During Gait Using Only Inertial Motion Capture,” *Sensors*, vol. 17, no. 1, p. 75, 2016, doi: 10.3390/s17010075.

[229] G. S. Faber, C. C. Chang, I. Kingma, J. T. Dennerlein, and J. H. Van Dieën, “Estimating 3D L5 / S1 moments and ground reaction forces during trunk bending using a full-body ambulatory inertial motion capture system,” *J. Biomech.*, vol. 49, no. 6, pp. 904–912, 2016, doi: 10.1016/j.jbiomech.2015.11.042.

[230] J. Kodama and T. Watanabe, “Examination of inertial sensor-based estimation methods of lower limb joint moments and ground reaction force: Results for squat and sit-to-stand movements in the sagittal plane,” *Sensors (Switzerland)*, vol. 16, no. 8, 2016, doi: 10.3390/s16081209.

[231] A. S. Koopman, I. Kingma, G. S. Faber, J. Bornmann, and J. H. van Dieën, “Estimating the L5S1 flexion/extension moment in symmetrical lifting using a simplified ambulatory measurement system,” *J. Biomech.*, vol. 70, pp. 242–248, 2018, doi: 10.1016/j.jbiomech.2017.10.001.

[232] A. Noamani, A. H. Vette, R. Preuss, M. R. Popovic, and H. Rouhani, “Quantification of multi-segment trunk kinetics during multi-directional trunk bending,” *Gait Posture*, vol. 64, no. June, pp. 205–212, 2018, doi: 10.1016/j.gaitpost.2018.06.027.

[233] A. Noamani, A. H. A. H. Vette, R. Preuss, M. R. M. R. Popovic, and H. Rouhani, “Optimal Estimation of Anthropometric Parameters for Quantifying Multi-Segment Trunk Kinetics,” *J. Biomech. Eng.*, vol. 140, no. 10, pp. 101003-1–10, 2018, doi: 10.1115/1.4040247.

[234] M. Windolf, N. Gotzen, and M. Morlock, “Systematic accuracy and precision analysis of video motion capturing systems — exemplified on the Vicon-460 system,” *J. Biomech.*, vol. 41, pp. 2776–2780, 2008, doi: 10.1016/j.jbiomech.2008.06.024.

[235] B. Mariani, C. Hoskovec, S. Rochat, C. Bula, J. Penders, and K. Aminian, “3D gait assessment in young and elderly subjects using foot-worn inertial sensors,” *J. Biomech.*, vol. 43, no. 15, pp. 2999–3006, 2010, doi: 10.1016/j.jbiomech.2010.07.003.

[236] H. Rouhani, J. Favre, X. Crevoisier, and K. Aminian, “Measurement of Multi-segment Foot Joint Angles During Gait Using a Wearable System,” *J. Biomech. Eng.*, vol. 134, no. June 2012, pp. 061006 1–8, 2012, doi: 10.1115/1.4006674.

[237] C. Mazzà, M. Donati, J. McCamley, P. Picerno, and A. Cappozzo, “An optimized Kalman filter for the estimate of trunk orientation from inertial sensors data during treadmill walking,” *Gait Posture*, vol. 35, no. 1, pp. 138–142, 2012, doi: 10.1016/j.gaitpost.2011.08.024.

[238] S. Mahallati, H. Rouhani, R. Preuss, K. Masani, and M. R. Popovic, “Multisegment Kinematics of the Spinal Column: Soft Tissue Artifacts Assessment,” *J. Biomech. Eng.*, vol. 138, no. 7, p. 071003, 2016, doi: 10.1115/1.4033545.

[239] W. L. Hsu, L. S. Chou, and M. Woollacott, “Age-related changes in joint coordination

during balance recovery," *Age (Omaha).*, vol. 35, no. 4, pp. 1299–1309, 2013, doi: 10.1007/s11357-012-9422-x.

[240] T. Arora, K. E. Musselman, J. Lanovaz, and A. Oates, "Effect of haptic input on standing balance among individuals with incomplete spinal cord injury," *Neurosci. Lett.*, vol. 642, pp. 91–96, 2017, doi: 10.1016/j.neulet.2017.02.001.

[241] T. E. Prieto, J. B. Myklebust, R. G. Hoffmann, E. G. Lovett, and B. M. Myklebust, "Measures of postural steadiness: differences between healthy young and elderly adults," *IEEE Trans. Biomed. Eng.*, vol. 43, no. 9, pp. 956–966, 1996, doi: 10.1109/10.532130.

[242] M. Grangeon, C. Gauthier, C. Duclos, F. Lemay, and D. Gagnon, "Unsupported Eyes Closed Sitting and Quiet Standing Share Postural Control Strategies in Healthy Individuals," *Motor Control*, vol. 19, pp. 10–24, 2015.

[243] A. Karlsson, S. Norrlin, H. C. Silander, M. Dahl, and H. Lanshammar, "Amplitude and frequency analysis of force plate data in sitting children with and without MMC," *Clin. Biomech.*, vol. 15, no. 7, pp. 541–545, 2000, doi: 10.1016/S0268-0033(00)00010-3.

[244] A. R. Marinho-buzelli, H. Rouhani, K. Masani, M. C. Verrier, and M. R. Popovic, "The influence of the aquatic environment on the control of postural sway," *Gait Posture*, vol. 51, pp. 70–76, 2017, doi: 10.1016/j.gaitpost.2016.09.009.

[245] A. Noamani, J. Lemay, K. E. Musselman, and H. Rouhani, "Characterization of Standing Balance after Incomplete Spinal Cord Injury: Alteration in Integration of Sensory Information," *Gait Posture*, vol. submitted, 2020.

[246] F. B. Horak and L. M. Nashner, "Central programming of postural movements: Adaptation to altered support-surface configurations," *J. Neurophysiol.*, vol. 55, no. 6, pp. 1369–1381, 1986, doi: 10.1152/jn.1986.55.6.1369.

[247] F. B. Horak, L. M. Nashner, and H. C. Diener, “Postural strategies associated with somatosensory and vestibular loss,” *Exp. Brain Res.*, vol. 82, no. 1, pp. 167–177, 1990, doi: 10.1007/BF00230848.

[248] J. Huisinga, M. Mancini, C. Veys, R. Spain, and F. Horak, “Coherence analysis of trunk and leg acceleration reveals altered postural sway strategy during standing in persons with multiple sclerosis,” *Hum. Mov. Sci.*, vol. 58, no. October 2017, pp. 330–336, 2018, doi: 10.1016/j.humov.2017.12.009.

[249] A. C. Scheffer, M. J. Schuurmans, N. Van dijk, T. Van der hooft, and S. E. De rooij, “Fear of falling: Measurement strategy, prevalence, risk factors and consequences among older persons,” *Age Ageing*, vol. 37, no. 1, pp. 19–24, 2008, doi: 10.1093/ageing/afm169.

[250] G. A. R. Zijlstra, J. C. M. van Haastregt, J. T. M. van Eijk, E. van Rossum, P. A. Stalenhoef, and G. I. J. M. Kempen, “Prevalence and correlates of fear of falling, and associated avoidance of activity in the general population of community-living older people,” *Age Ageing*, vol. 36, no. 3, pp. 304–309, 2007, doi: 10.1093/ageing/afm021.

[251] L. Dierking, K. Markides, S. Al Snih, and M. Kristen Peek, “Fear of Falling in Older Mexican Americans: A Longitudinal Study of Incidence and Predictive Factors,” *J. Am. Geriatr. Soc.*, vol. 64, no. 12, pp. 2560–2565, 2016, doi: 10.1111/jgs.14496.

[252] M. Nazarahari and H. Rouhani, “Semi-automatic Sensor-to-Body Calibration of Inertial Sensors on Lower Limb Using Gait Recording,” *IEEE Sens. J.*, vol. 19, no. 24, pp. 1–1, 2019, doi: 10.1109/jsen.2019.2939981.

[253] F. B. Horak, C. L. Shupert, and A. Mirka, “Components of postural dyscontrol in the elderly: A review,” *Neurobiol. Aging*, vol. 10, no. 6, pp. 727–738, 1989, doi: 10.1016/0197-4580(89)90010-9.

[254] A. H. Vette, T. Yoshida, T. A. Thrasher, K. Masani, and M. R. Popovic, "A complete, non-lumped, and verifiable set of upper body segment parameters for three-dimensional dynamic modeling," *Med. Eng. Phys.*, vol. 33, no. 1, pp. 70–79, 2011, doi: 10.1016/j.medengphy.2010.09.008.

[255] F. Ghezelbash, Z. El Ouaaid, A. Shirazi-Adl, A. Plamondon, and N. Arjmand, "Trunk musculoskeletal response in maximum voluntary exertions: A combined measurement-modeling investigation," *J. Biomech.*, vol. 70, pp. 124–133, 2018, doi: 10.1016/j.jbiomech.2017.11.007.

[256] F. C. Anderson and M. G. Pandy, "Dynamic optimization of human walking," *J. Biomech. Eng.*, vol. 123, no. 5, pp. 381–390, 2001, doi: 10.1115/1.1392310.

[257] M. Milosevic, D. H. Gagnon, P. Gourdou, and K. Nakazawa, "Postural regulatory strategies during quiet sitting are affected in individuals with thoracic spinal cord injury," *Gait Posture*, vol. 58, no. August, pp. 446–452, 2017, doi: 10.1016/j.gaitpost.2017.08.032.

[258] R. A. Preuss and M. R. Popovic, "Quantitative analysis of the limits of stability in sitting," *J. Appl. Biomech.*, vol. 26, no. 3, pp. 265–272, 2010, doi: 10.1007/BF02099629.

[259] R. A. Preuss and M. R. Popovic, "Three-dimensional spine kinematics during multidirectional, target-directed trunk movement in sitting," *J. Electromyogr. Kinesiol.*, vol. 20, no. 5, pp. 823–832, 2010, doi: 10.1016/j.jelekin.2009.07.005.

[260] A. Noamani, A. H. Vette, R. Preuss, M. R. Popovic, and H. Rouhani, "Quantification of multi-segment trunk kinetics during multi-directional trunk bending," *Gait Posture*, vol. 64, pp. 205–212, 2018, doi: 10.1016/j.gaitpost.2018.06.027.

[261] C. J. Craig, *Introduction to robotics: mechanics and control*, 3rd Editio. New Jersey: Pearson, 2005.

[262] N. Ahmadian, M. Nazarahari, J. L. Whittaker, and H. Rouhani, “Quantification of triple single-leg hop test temporospatial parameters: A validated method using body-worn sensors for functional evaluation after knee injury,” *Sensors (Switzerland)*, vol. 20, no. 12, pp. 1–15, 2020, doi: 10.3390/s20123464.

[263] A. M. Sabatini, “Inertial Sensing To Gait Analysis,” *Med. Biol. Eng.*, vol. 43, no. 2002, pp. 94–101, 2005.

[264] K. M. Moorhouse and K. P. Granata, “Trunk stiffness and dynamics during active extension exertions,” *J. Biomech.*, vol. 38, no. 10, pp. 2000–2007, 2005, doi: 10.1016/j.jbiomech.2004.09.014.

[265] M. Vanoncini, W. Holderbaum, and B. J. Andrews, “Electrical Stimulation for trunk control in paraplegia: A feasibility study,” *Control Eng. Pract.*, vol. 20, no. 12, pp. 1247–1258, 2012, doi: 10.1016/j.conengprac.2012.06.007.

[266] B. W. R. Roberts, F. Gholibeigian, J. Lewicke, and A. H. Vette, “Spatial and temporal relation of kinematics and muscle activity during unstable sitting,” *J. Electromyogr. Kinesiol.*, vol. 52, no. November 2019, p. 102418, 2020, doi: 10.1016/j.jelekin.2020.102418.

[267] T. R. Allen, R. L. Brookham, A. C. Cudlip, and C. R. Dickerson, “Comparing surface and indwelling electromyographic signals of the supraspinatus and infraspinatus muscles during submaximal axial humeral rotation,” *J. Electromyogr. Kinesiol.*, vol. 23, no. 6, pp. 1343–1349, 2013, doi: 10.1016/j.jelekin.2013.08.002.

[268] J. Bobet, K. Masani, M. R. Popovic, and A. H. Vette, “Kinematics-based prediction of trunk muscle activity in response to multi-directional perturbations during sitting,” *Med. Eng. Phys.*, vol. 58, pp. 56–63, 2018, doi: 10.1016/j.medengphy.2018.05.004.

[269] S. H. M. Brown, M. L. Haumann, and J. R. Potvin, “The responses of leg and trunk muscles to sudden unloading of the hands: Implications for balance and spine stability,” *Clin. Biomech.*, vol. 18, no. 9, pp. 812–820, 2003, doi: 10.1016/S0268-0033(03)00167-0.

[270] P. Konrad, *Noraxon: The ABC of EMG A Practical Introduction to Kinesiological Electromyography*, no. April. Noraxon INC. USA, 2005.

[271] M. Ferrarin and A. Pedotti, “The Relationship Between Electrical Stimulus and Joint Torque : A Dynamic Model,” *IEEE Trans. Rehabil. Eng.*, vol. 8, no. 3, pp. 342–352, 2000.

[272] E. A. Wan and R. Van Der Merwe, “The unscented Kalman filter for nonlinear estimation,” *IEEE 2000 Adapt. Syst. Signal Process. Commun. Control Symp. AS-SPCC 2000*, pp. 153–158, 2000, doi: 10.1109/ASSPCC.2000.882463.

[273] L. A. Scardua and J. J. da Cruz, “Complete offline tuning of the unscented Kalman filter,” *Automatica*, vol. 80, pp. 54–61, 2017, doi: 10.1016/j.automatica.2017.01.008.

[274] B. Zheng, P. Fu, B. Li, and X. Yuan, “A robust adaptive unscented kalman filter for nonlinear estimation with uncertain noise covariance,” *Sensors (Switzerland)*, vol. 18, no. 3, p. 808, 2018, doi: 10.3390/s18030808.

[275] S. Yong, H. Chongzhao, and L. Yongqi, “Adaptive UKF for target tracking with unknown process noise statistics,” *2009 12th Int. Conf. Inf. Fusion, FUSION 2009*, no. 1, pp. 1815–1820, 2009.

[276] N. Yongfang and T. Zhang, “Scaling parameters selection principle for the scaled unscented Kalman filter,” *J. Syst. Eng. Electron.*, vol. 29, no. 3, pp. 601–610, 2018, doi: 10.21629/JSEE.2018.03.17.

[277] N. Yongfang and T. Zhang, “A self-Adaptive scaling parameter selection algorithm for the Unscented Kalman Filter,” *Proc. - 2015 Chinese Autom. Congr. CAC 2015*, pp. 86–90,

2016, doi: 10.1109/CAC.2015.7382475.

[278] T. Kiemel, K. S. Oie, and J. J. Jeka, “Multisensory fusion and the stochastic structure of postural sway,” *Biol. Cybern.*, vol. 87, no. 4, pp. 262–277, 2002, doi: 10.1007/s00422-002-0333-2.

[279] V. Nekoukar and A. Erfanian, “Adaptive fuzzy terminal sliding mode control for a class of MIMO uncertain nonlinear systems,” *Fuzzy Sets Syst.*, vol. 179, no. 1, pp. 34–49, 2011, doi: 10.1016/j.fss.2011.05.009.

[280] E. Todorov and M. I. Jordan, “Optimal feedback control as a theory of motor coordination,” *Nat. Neurosci.*, vol. 5, no. 11, pp. 1226–1235, 2002, doi: 10.1038/nn963.

[281] E. Todorov, “Optimality principles in sensorimotor control,” *Nat. Neurosci.*, vol. 7, no. 9, pp. 907–915, 2004, doi: 10.1038/nn1309.

[282] H. K. Khalil, *Nonlinear systems.*, 3rd ed. Prentice Hall, 2002.

[283] T. D. J. Welch and L. H. Ting, “A feedback model explains the differential scaling of human postural responses to perturbation acceleration and velocity,” *J. Neurophysiol.*, vol. 101, no. 6, pp. 3294–3309, 2009, doi: 10.1152/jn.90775.2008.

[284] R. Betz *et al.*, “The 2019 revision of the International Standards for Neurological Classification of Spinal Cord Injury (ISNCSCI)—What’s new?,” *Spinal Cord*, vol. 57, no. 10, pp. 815–817, 2019, doi: 10.1038/s41393-019-0350-9.

[285] S. C. Kirshblum *et al.*, “International standards for neurological classification of spinal cord injury (Revised 2011),” *J. Spinal Cord Med.*, vol. 34, no. 6, pp. 535–546, 2011, doi: 10.1179/204577211X13207446293695.

[286] D. Jackson *et al.*, “American Spinal Cord Injury Association (ASIA) Impairment Scale.” [Online]. Available: https://www.physio-

pedia.com/American_Spinal_Cord_Injury_Association_(ASIA)_Impairment_Scale#cite_note-:0-1. [Accessed: 07-Nov-2022].

Supplementary Material

Supplementary Material of Chapter 4

American Spinal Injury Association Impairment Scale

The International Standards for Neurological Classification of Spinal Cord Injury (ISNCSCI) was introduced by the American Spinal Injury Association (ASIA) as a standard tool to categorize spinal cord injuries based on sensory and motor assessments [284]. It consists of a motor and sensory examination to determine the sensory level and motor level for the right and left sides of the body, the Neurological Level of Injury (NLI) and whether the injury is complete or incomplete [285]. ASIA impairment scale (AIS) is used to describe the functional impairment of an individual as a consequence of SCI. The AIS is a measure of how much sensation an individual feels after light touch and a pin prick at several locations on both sides of the person's body. The AIS has five levels, ranging from complete loss of neural function (Grade A) to completely normal (Grade E).

Supp Table 1 AIS grading system [286]

Grade A	Complete. No sensory or motor function is preserved in the sacral segments S4-5.
Grade B	Sensory Incomplete. Sensory but not Motor Function is preserved below the neurological level and includes the Sacral Segments S4-S5, AND no motor Function is preserved more than three levels below the Motor Level on either side of the body
Grade C	Motor Function is preserved below the Neurological Level, AND more than half of key muscle functions below the Neurological Level of Injury have a muscle grade less than 3 (Grades 0-2)
Grade D	Motor function is preserved below the neurological level, AND at least half (half or more) of key muscle functions below the NLI have a muscle grade ≥ 3
Grade E	If sensation and motor function as tested with the ISNCSCI are graded as normal in all segments AND the patient had prior deficits, then the AIS Grade is E.

Sensory Score

The key sensory points are located with respect to bony anatomical landmarks as shown in the dermatomes C2 to S5 in Supp Figure 1. These points are bilaterally examined using light touch and pin-prick. In clinical settings, a cotton tip is used for the light touch, and a neuro-tip or safety pin is used for the pin-prick. The reference for comparing the sensory key points is commonly the sensation on the patient's cheek [285]. Scoring is based on a three-point scale as follows [285], [286]:

- 0: Absent
- 1: Altered - Impaired or partial appreciation, including Hyperesthesia (increased sensitivity of any of the senses, such as sight, sound, touch, and smell)
- 2: Normal or intact - similar as on the cheek
- NT: Not stable

The sensory level is defined as the most caudal, intact dermatome for both light touch and pin-prick sensations [285], [286]. The sensory level is determined by conducting the abovementioned sensory examination of the key sensory points (28 dermatomes) on each side of the body which may differ for the right and left sides. The sensory level is the dermatome level that is intact and located immediately rostral to the first impaired dermatome or the first dermatome with an absent light touch or pin-prick sensation [285], [286]. The sensory level should be determined for each side. Four sensory levels may be determined for each dermatome, including (1, 2) right pin-prick and light, and (3, 4) left pin-prick and light touch. The overall single sensory level is the most rostral intact sensory point [285], [286]. The overall sensory level is determined as the most rostral intact sensory point. Finally, the sensory scores of each dermatome for both light touch and pin-prick are added up across the dermatomes and body side to have two summary scores for pin-prick and light touch. The maximum score for each pin-prick and light touch is 56 [285], [286].

Motor Examination

The motor function is examined bilaterally for ten paired myotomes (a group of muscles innervated by a single spinal nerve root) for C5-T1 and L2-S (Supp Table 2). Scoring is based on a six-point scale as follows [285], [286]:

- 0: Total paralysis

- 1: Palpable or visible contraction
- 2: Active movement, full range of motion with gravity eliminated
- 3: Active movement, full range of motion against gravity
- 4: Active movement, full range of movement against gravity and moderate resistance in a muscle-specific position
- 5: Normal active movement, full range of motion against gravity and full resistance in a muscle-specific position expected from an unimpaired person
- 5*: Normal active movement, full range of motion against gravity and sufficient resistance to be considered normal if identified inhibiting factors (i.e., pain, disuse) were not present
- NT: Not testable, i.e., due to immobilization, severe pain such that the patient cannot be graded, amputation of the limb, or contracture of >50% of the range of motion

For conducting the test, the patient must be in a supine-lying position throughout the test, except during the examination of the rectal, which must be in a side-lying position.

Supp Table 2. Key motor function [285], [286]

Level	Key Muscle Function	Description of Muscle Function Testing Position for Grade 4 or 5
C5	Elbow Flexion Biceps Brachii Biceps Brachialis	Elbow Flexed at 90, Forearm Supinated
C6	Wrist Extension Extensor Carpi Radialis Longus Extensor Carpi Radialis Brevis	Full Wrist Extension
C7	Elbow Extension Triceps Brachii	Shoulder Neutral Rotation, Adducted at 90 Flexion with Elbow at 45 Flexion
C8	Flexion of Middle Finger Flexor Digitorum Profundus	Full Flexed Distal Phalanx with Proximal Finger Joint Stabilised in Extension
T1	Abduction of Little Finger Abductor Digiti Minimi	Full Abduction Fingers
L2	Hip Flexion Iliopsoas	Hip Flexed at 90
L3	Knee Extension Quadriceps	Knee Flexed at 15
L4	Ankle Dorsiflexion Tibialis Anterior	Full Dorsiflexion
L5	Long Toe Extensors Extensor Hallucis Longus	Full Extension 1st Toe
S1	Ankle Plantarflexion Gastrocnemius Soleus	Hip Neutral with Full Knee Extension and Full Ankle Plantarflexion

The motor level is the lowest key muscle function that shows a grade of at least 3 on supine testing, and the key muscle functions at the level above should grade as intact. The motor level is determined by examining the key muscle functions for each of the myotomes on the right and left sides of the body. The motor scores for each myotome are then obtained by adding up the score across myotomes and sides of the body to determine a single motor score for each of the upper limbs and lower limbs. There are five key muscle functions for each upper extremity which would give a maximum score of 25 for each upper extremity and a total score of 50 for the upper limbs. There are five key muscle functions for each lower extremity which would give a maximum score of 25 for each lower extremity and a total score of 50 for the lower limbs [285], [286].

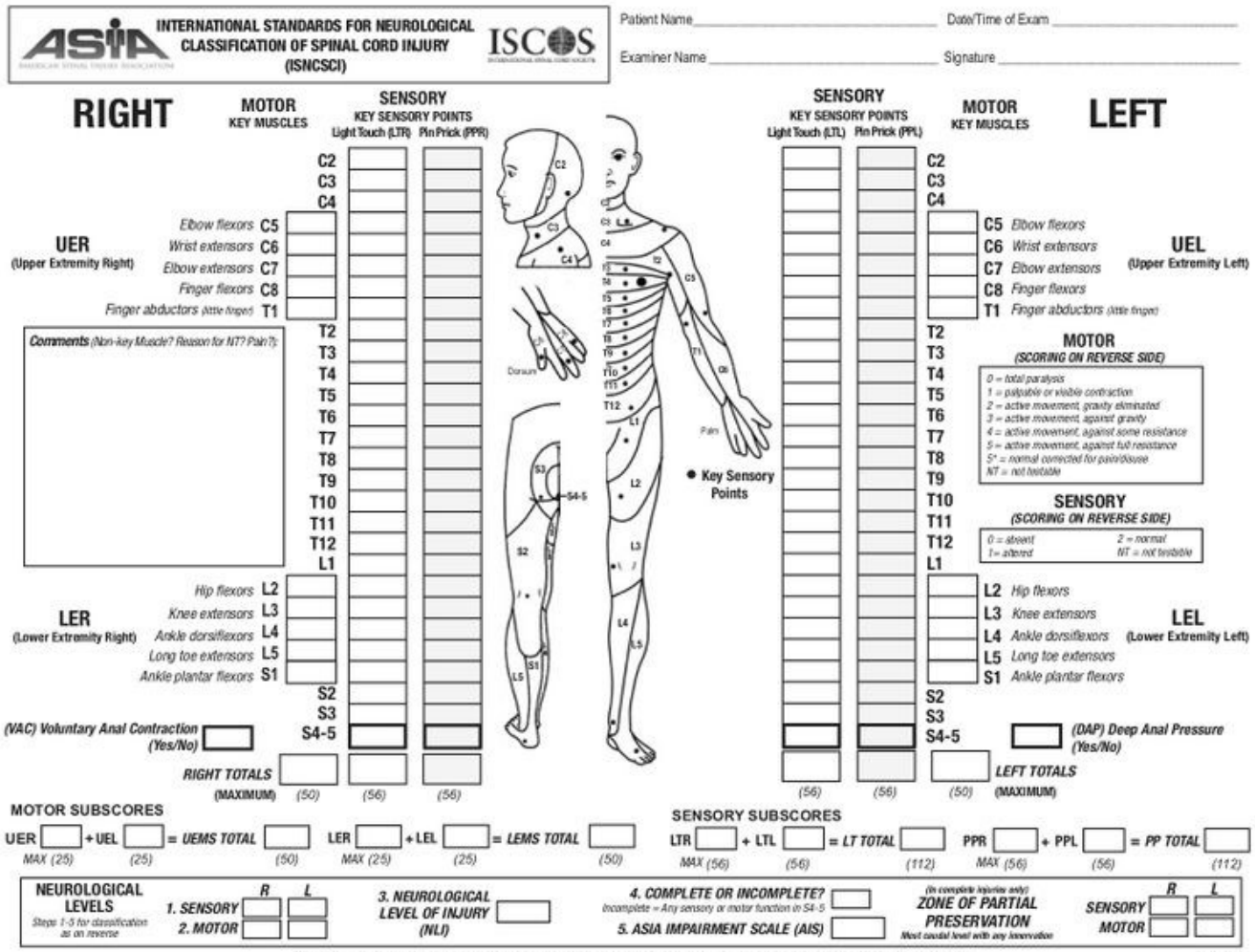
INTERNATIONAL STANDARDS FOR NEUROLOGICAL CLASSIFICATION OF SPINAL CORD INJURY (ISNCSCI)
ISCOS
Patient Name
Date/Time of Exam
Examiner Name
Signature
RIGHT
MOTOR
KEY MUSCLES
SENSORY
KEY SENSORY POINTS
Light Touch (LTR)
Pin Prick (PPR)
UER
(Upper Extremity Right)
Elbow flexors C5
Wrist extensors C6
Elbow extensors C7
Finger flexors C8
Finger abductors (little finger) T1
Comments (Non-key Muscle? Reason for NT? Pain?):
LER
(Lower Extremity Right)
Hip flexors L2
Knee extensors L3
Ankle dorsiflexors L4
Long toe extensors L5
Ankle plantar flexors S1
(VAC) Voluntary Anal Contraction (Yes/No)
RIGHT TOTALS
(MAXIMUM)
(50)
(56)
(56)
C2
C3
C4
T2
T3
T4
T5
T6
T7
T8
T9
T10
T11
T12
L1
S2
S3
S4-5
Dorsum
Palm
Key Sensory Points
SENSORY
KEY SENSORY POINTS
Light Touch (LTL)
Pin Prick (PPL)
MOTOR
KEY MUSCLES
LEFT
C5 Elbow flexors
C6 Wrist extensors
C7 Elbow extensors
C8 Finger flexors
T1 Finger abductors (little finger)
UEL
(Upper Extremity Left)
MOTOR
(SCORING ON REVERSE SIDE)
0 = total paralysis
1 = palpable or visible contraction
2 = active movement, gravity eliminated
3 = active movement, against gravity
4 = active movement, against some resistance
5 = active movement, against full resistance
5* = normal corrected for pain/disuse
NT = not testable
SENSORY
(SCORING ON REVERSE SIDE)
0 = absent
1= altered
2 = normal
NT = not testable
L2 Hip flexors
L3 Knee extensors
L4 Ankle dorsiflexors
L5 Long toe extensors
S1 Ankle plantar flexors
LEL
(Lower Extremity Left)
(DAP) Deep Anal Pressure (Yes/No)
LEFT TOTALS
(MAXIMUM)
(56)
(56)
(50)
MOTOR SUBSCORES
UER + UEL = UEMS TOTAL
MAX (25)
(25)
(50)
LER + LEL = LEMS TOTAL
MAX (25)
(25)
(50)
SENSORY SUBSCORES
LTR + LTL = LT TOTAL
MAX (56)
(56)
(112)
PPR + PPL = PP TOTAL
MAX (56)
(56)
(112)
NEUROLOGICAL LEVELS
Steps 1-5 for classification as on reverse
R
L
1. SENSORY
2. MOTOR
3. NEUROLOGICAL LEVEL OF INJURY (NLI)
4. COMPLETE OR INCOMPLETE?
Incomplete = Any sensory or motor function in S4-5
5. ASIA IMPAIRMENT SCALE (AIS)
(In complete injuries only)
ZONE OF PARTIAL PRESERVATION
Most caudal level with any innervation
SENSORY
MOTOR
This form may be copied freely but should not be altered without permission from the American Spinal Injury Association.
REV 11/15

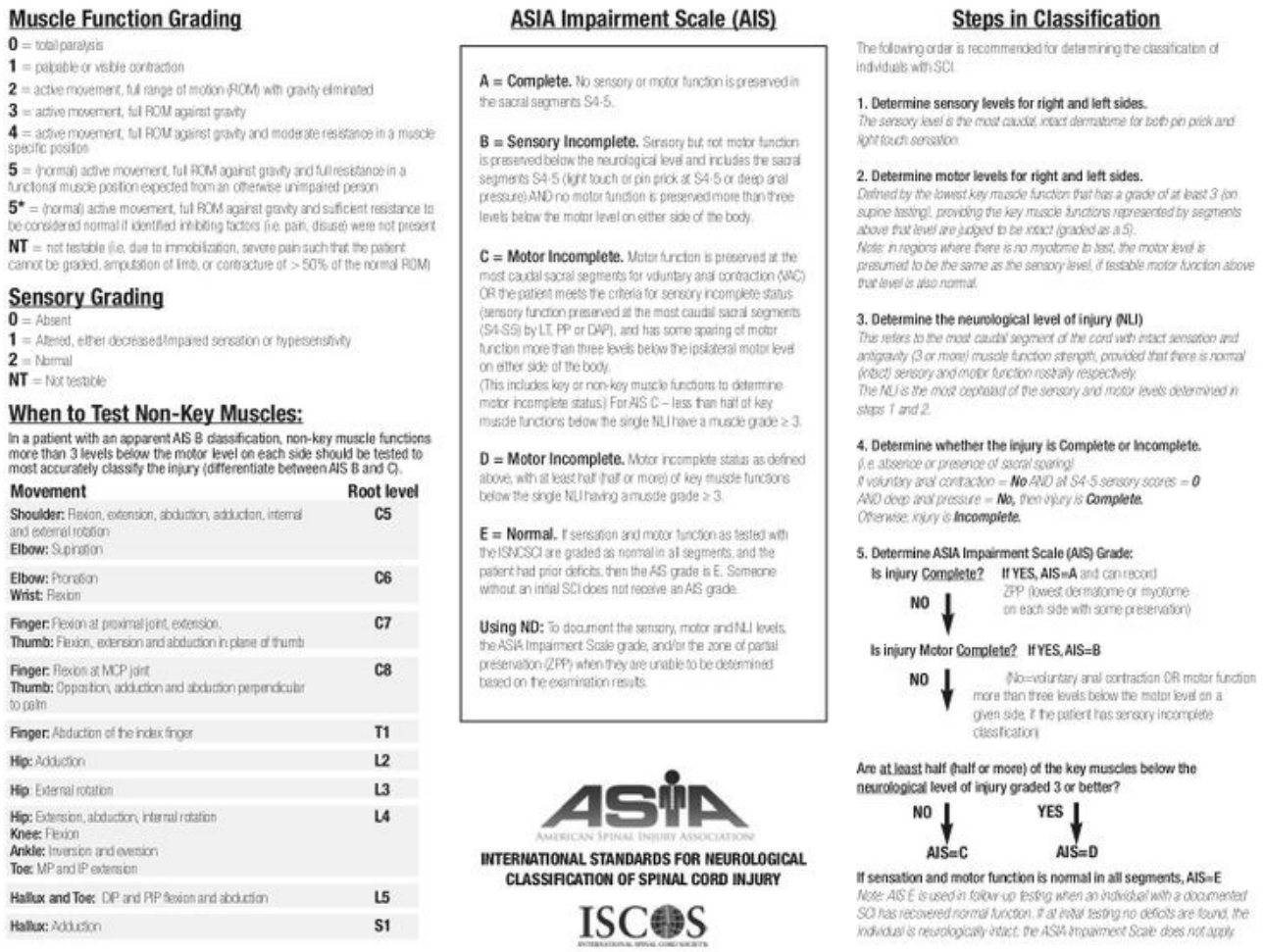

Muscle Function Grading

0 = total paralysis

1 = palpable or visible contraction

2 = active movement, full range of motion (ROM) with gravity eliminated

3 = active movement, full ROM against gravity

4 = active movement, full ROM against gravity and moderate resistance in a muscle specific position

5 = (normal) active movement, full ROM against gravity and full resistance in a functional muscle position expected from an otherwise unimpaired person

5* = (normal) active movement, full ROM against gravity and sufficient resistance to be considered normal if identified inhibiting factors (i.e. pain, disuse) were not present

NT = not testable (i.e. due to immobilization, severe pain such that the patient cannot be graded, amputation of limb, or contracture of >50% of the normal ROM)

Sensory Grading

0 = Absent

1 = Altered, either decreased/impaired sensation or hypersensitivity

2 = Normal

NT = Not testable

When to Test Non-Key Muscles:

In a patient with an apparent AIS B classification, non-key muscle functions more than 3 levels below the motor level on each side should be tested to most accurately classify the injury (differentiate between AIS B and C).

Movement	Root level
Shoulder: Flexion, extension, abduction, adduction, internal and external rotation **Elbow:** Supination	C5
Elbow: Pronation **Wrist:** Flexion	C6
Finger: Flexion at proximal joint, extension. **Thumb:** Flexion, extension and abduction in plane of thumb	C7
Finger: Flexion at MCP joint **Thumb:** Opposition, adduction and abduction perpendicular to palm	C8
Finger: Abduction of the index finger	T1
Hip: Adduction	L2
Hip: External rotation	L3
Hip: Extension, abduction, internal rotation **Knee:** Flexion **Ankle:** Inversion and eversion **Toe:** MP and IP extension	L4
Hallux and Toe: DIP and PIP flexion and abduction	L5
Hallux: Adduction	S1

ASIA Impairment Scale (AIS)

A = Complete. No sensory or motor function is preserved in the sacral segments S4-5.

B = Sensory Incomplete. Sensory but not motor function is preserved below the neurological level and includes the sacral segments S4-5 (light touch or pin prick at S4-5 or deep anal pressure) AND no motor function is preserved more than three levels below the motor level on either side of the body.

C = Motor Incomplete. Motor function is preserved at the most caudal sacral segments for voluntary anal contraction (VAC) OR the patient meets the criteria for sensory incomplete status (sensory function preserved at the most caudal sacral segments (S4-S5) by LT, PP or DAP), and has some sparing of motor function more than three levels below the ipsilateral motor level on either side of the body.
(This includes key or non-key muscle functions to determine motor incomplete status.) For AIS C – less than half of key muscle functions below the single NLI have a muscle grade ≥ 3.

D = Motor Incomplete. Motor incomplete status as defined above, with at least half (half or more) of key muscle functions below the single NLI having a muscle grade ≥ 3.

E = Normal. If sensation and motor function as tested with the ISNCSCI are graded as normal in all segments, and the patient had prior deficits, then the AIS grade is E. Someone without an initial SCI does not receive an AIS grade.

Using ND: To document the sensory, motor and NLI levels, the ASIA Impairment Scale grade, and/or the zone of partial preservation (ZPP) when they are unable to be determined based on the examination results.

ASIA
AMERICAN SPINAL INJURY ASSOCIATION

INTERNATIONAL STANDARDS FOR NEUROLOGICAL CLASSIFICATION OF SPINAL CORD INJURY

ISCOS
INTERNATIONAL SPINAL CORD SOCIETY

Steps in Classification

The following order is recommended for determining the classification of individuals with SCI.

1. Determine sensory levels for right and left sides.
The sensory level is the most caudal, intact dermatome for both pin prick and light touch sensation.

2. Determine motor levels for right and left sides.
Defined by the lowest key muscle function that has a grade of at least 3 (on supine testing), providing the key muscle functions represented by segments above that level are judged to be intact (graded as a 5).
Note: in regions where there is no myotome to test, the motor level is presumed to be the same as the sensory level, if testable motor function above that level is also normal.

3. Determine the neurological level of injury (NLI)
This refers to the most caudal segment of the cord with intact sensation and antigravity (3 or more) muscle function strength, provided that there is normal (intact) sensory and motor function rostrally respectively.
The NLI is the most cephalad of the sensory and motor levels determined in steps 1 and 2.

4. Determine whether the injury is Complete or Incomplete.
(i.e. absence or presence of sacral sparing)
*If voluntary anal contraction = **No** AND all S4-5 sensory scores = **0***
*AND deep anal pressure = **No,** then injury is **Complete.***
*Otherwise, injury is **Incomplete.***

5. Determine ASIA Impairment Scale (AIS) Grade:

Is injury Complete? If YES, AIS=A and can record ZPP (lowest dermatome or myotome on each side with some preservation)

NO ↓

Is injury Motor Complete? If YES, AIS=B

NO ↓ (No=voluntary anal contraction OR motor function more than three levels below the motor level on a given side, if the patient has sensory incomplete classification)

Are at least half (half or more) of the key muscles below the neurological level of injury graded 3 or better?

NO ↓ AIS=C

YES ↓ AIS=D

If sensation and motor function is normal in all segments, AIS=E
Note: AIS E is used in follow up testing when an individual with a documented SCI has recovered normal function. If at initial testing no deficits are found, the individual is neurologically intact; the ASIA Impairment Scale does not apply.

Supp Figure 1. Standard Neurological Classification of Spinal Cord Injury

Supplementary Material of Chapter 6

Supp Table 3. Berg Balance Scale (BBS) scores for each task and participant at admission and discharge test sessions.

	Task 1		Task 2		Task 3		Task 4	
ID	**Admission**	**Discharge**	**Admission**	**Discharge**	**Admission**	**Discharge**	**Admission**	**Discharge**
1	3	4	4	4	4	4	3	4
2	3	4	4	4	4	4	3	4
3	4	4	4	4	4	4	4	4
4	4	4	4	4	4	4	4	4
5	4	4	4	4	4	4	4	4
6	2	3	1	4	4	4	0	3
7	3	3	4	4	4	4	3	4
8	3	3	4	4	4	4	3	4
9	3	3	4	4	4	4	4	4
10	3	4	4	4	4	4	3	4
11	4	4	3	4	4	4	3	4
12	1	3	3	4	4	4	1	4
13	3	3	4	4	4	4	4	3
14	4	4	4	4	4	4	4	4
15	4	4	4	4	4	4	4	4
16	3	3	4	4	4	4	3	3
17	4	4	4	4	4	4	4	4
18	0	4	3	4	4	4	3	4
19	4	4	4	4	4	4	4	4
20	4	4	4	4	4	4	4	4
21	1	3	3	4	4	4	2	3
22	1	3	4	4	4	4	3	4
23	4	4	4	4	4	4	4	4
24	3	4	4	4	4	4	3	4
25	4	4	4	4	4	4	4	4
26	4	4	4	4	4	4	4	4
27	3	3	4	4	4	4	3	4
28	1	4	3	3	4	4	3	4
29	3	4	4	4	4	4	3	4
30	3	4	4	4	4	4	4	4
31	4	4	4	4	4	4	4	4
32	4	4	4	4	4	4	4	4
33	3	4	3	4	4	4	2	4
34	3	4	4	4	4	4	3	4
35	3	3	4	4	4	4	4	4
36	3	3	4	4	4	4	1	2

	Task 5		Task 6		Task 7		Task 8	
ID	**Admission**	**Discharge**	**Admission**	**Discharge**	**Admission**	**Discharge**	**Admission**	**Discharge**
1	3	3	4	4	4	4	3	3
2	3	3	4	4	3	4	3	3
3	4	4	4	4	4	4	3	3
4	4	4	4	4	3	4	2	2
5	4	4	4	4	4	4	3	3
6	1	2	3	4	1	4	0	0
7	4	4	4	4	4	4	3	3
8	3	3	3	4	3	4	3	3
9	4	4	4	4	4	4	3	3
10	2	3	4	4	3	3	3	3
11	4	4	3	4	2	3	3	3
12	1	3	3	4	2	3	1	3
13	4	3	3	4	1	1	2	3
14	4	4	4	4	4	4	3	3
15	4	4	4	4	4	4	3	3
16	3	3	3	4	1	1	2	3
17	4	4	4	4	4	2	2	4
18	3	4	3	4	3	3	2	4
19	4	4	4	4	3	4	3	3
20	4	4	4	4	4	4	4	4
21	2	3	3	4	0	0	1	2
22	3	3	3	4	1	4	0	0
23	4	4	4	4	3	4	3	4
24	3	4	3	4	3	4	3	3
25	4	4	4	4	2	4	3	3
26	4	4	4	4	3	4	3	3
27	3	3	3	4	4	4	3	4
28	1	4	3	3	1	3	1	3
29	4	4	3	4	2	3	3	3
30	4	4	4	4	0	1	3	1
31	4	4	4	4	3	3	4	3
32	4	4	4	4	4	4	4	4
33	3	4	3	4	0	0	1	3
34	3	4	4	4	1	3	2	2
35	3	3	4	4	3	4	3	4
36	3	2	2	3	1	1	2	3

	Task 9		Task 10		Task 11		Task 12	
ID	**Admission**	**Discharge**	**Admission**	**Discharge**	**Admission**	**Discharge**	**Admission**	**Discharge**
1	4	4	2	2	0	2	0	3
2	3	4	2	2	1	2	0	0
3	4	4	2	2	2	3	2	4
4	1	3	2	2	2	2	1	2
5	3	4	2	3	2	2	2	4
6	3	0	2	2	0	1	0	0
7	4	4	2	3	2	2	3	3
8	3	3	2	3	1	1	1	1
9	3	4	2	2	2	2	4	3
10	3	3	4	4	1	1	1	1
11	3	3	2	3	2	2	1	1
12	0	4	1	4	0	2	0	2
13	3	4	2	4	2	3	0	3
14	4	4	4	4	4	4	4	4
15	3	4	2	3	2	4	4	4
16	3	4	2	4	0	2	0	0
17	4	4	4	4	4	4	4	4
18	0	4	3	4	2	2	4	4
19	4	4	4	4	1	2	2	2
20	4	4	4	4	4	4	4	4
21	0	3	1	2	0	1	0	0
22	3	4	3	3	2	2	0	1
23	3	4	4	4	1	4	1	4
24	3	4	4	4	3	4	0	4
25	4	4	2	3	2	2	4	4
26	4	4	2	4	2	2	1	3
27	4	4	3	4	2	2	0	3
28	0	3	1	2	0	2	0	2
29	3	4	3	4	2	3	3	4
30	4	4	4	4	0	2	3	3
31	3	4	2	3	1	2	2	4
32	4	4	2	4	4	4	0	4
33	3	4	1	2	1	3	2	4
34	4	4	3	3	3	3	0	2
35	3	4	4	3	1	4	1	4
36	3	4	4	2	0	1	0	0

ID	Task 13		Task 14		Total Score		Improvement
	Admission	Discharge	Admission	Discharge	Admission	Discharge	
1	2	2	1	1	37	44	7
2	2	2	1	1	36	41	5
3	2	3	1	1	44	48	4
4	3	3	1	2	39	44	5
5	0	4	0	2	40	50	10
6	0	1	0	1	17	29	12
7	3	3	1	1	44	46	2
8	3	3	1	1	37	41	4
9	3	3	1	1	45	45	0
10	3	3	0	0	38	41	3
11	1	2	1	1	36	42	6
12	2	3	0	1	19	44	25
13	2	2	0	1	34	42	8
14	2	2	2	2	51	51	0
15	2	3	2	2	46	51	5
16	2	3	0	1	30	39	9
17	3	3	1	1	50	50	0
18	2	2	2	2	34	49	15
19	3	3	1	1	45	47	2
20	4	4	2	2	54	54	0
21	0	1	0	0	17	30	13
22	2	2	1	1	30	39	9
23	3	3	1	2	43	53	10
24	2	3	2	3	40	53	13
25	3	3	1	1	45	48	3
26	3	3	0	1	42	48	6
27	4	4	1	1	41	48	7
28	2	3	0	1	20	41	21
29	2	3	1	2	40	50	10
30	3	2	0	1	40	42	2
31	3	3	1	1	43	47	4
32	0	2	0	1	42	51	9
33	2	3	0	1	28	44	16
34	2	3	1	1	37	45	8
35	3	2	1	4	41	51	10
36	2	2	0	1	29	32	3

Supp Table 4. Spearman's correlation between each Berg Balance Scale (BBS) task score and center-of-pressure (COP) balance biomarkers presented as [ρ, P] at both admission and discharge test sessions. Highlighted cells are significant values (P < 0.05).

		Task 1		Task 2		Task 3	
COP-based Biomarkers		**Admission**	**Discharge**	**Admission**	**Discharge**	**Admission**	**Discharge**
RD	**RDIST**	[0.11, 0.5403]	[0.07, 0.6691]	[-0.05, 0.7673]	[-0.06, 0.7415]	[NaN, NaN]	[NaN, NaN]
	MDIST	[0.03, 0.8604]	[0.1, 0.5535]	[-0.12, 0.4983]	[-0.06, 0.7415]	[NaN, NaN]	[NaN, NaN]
	TOTEX	[-0.02, 0.9145]	[0.13, 0.4482]	[0.17, 0.3283]	[-0.22, 0.198]	[NaN, NaN]	[NaN, NaN]
	MVELO	[-0.05, 0.7862]	[0.14, 0.4094]	[0.1, 0.5635]	[-0.22, 0.198]	[NaN, NaN]	[NaN, NaN]
	95% Conf. Ellipse	[0.2, 0.2452]	[0.05, 0.7927]	[0.09, 0.6161]	[0.01, 0.9624]	[NaN, NaN]	[NaN, NaN]
	Sway Area	[0.02, 0.8947]	[0.09, 0.5986]	[0.03, 0.8735]	[-0.14, 0.4212]	[NaN, NaN]	[NaN, NaN]
	MFREQ	[-0.17, 0.3259]	[0.07, 0.6932]	[0.18, 0.2843]	[-0.24, 0.166]	[NaN, NaN]	[NaN, NaN]
	MEDFREQ	[0.14, 0.404]	[0.02, 0.9215]	[0.23, 0.1787]	[0.04, 0.8138]	[NaN, NaN]	[NaN, NaN]
	CFREQ	[-0.05, 0.7627]	[0.07, 0.6691]	[0.24, 0.1544]	[-0.19, 0.2745]	[NaN, NaN]	[NaN, NaN]
	FREQD	[0.11, 0.521]	[-0.05, 0.7675]	[-0.16, 0.3439]	[0.11, 0.5393]	[NaN, NaN]	[NaN, NaN]
AP	**RDIST**	[0.18, 0.304]	[0.13, 0.4482]	[0.01, 0.9758]	[-0.09, 0.6037]	[NaN, NaN]	[NaN, NaN]
	MDIST	[0.05, 0.7553]	[0.09, 0.6217]	[-0.09, 0.6054]	[-0.09, 0.6037]	[NaN, NaN]	[NaN, NaN]
	TOTEX	[0.01, 0.9762]	[0.15, 0.3907]	[0.25, 0.1389]	[-0.22, 0.198]	[NaN, NaN]	[NaN, NaN]
	MVELO	[-0.06, 0.7394]	[0.15, 0.3725]	[0.1, 0.5635]	[-0.22, 0.198]	[NaN, NaN]	[NaN, NaN]
	MFREQ	[-0.14, 0.4208]	[0.06, 0.7425]	[0.14, 0.4149]	[-0.22, 0.198]	[NaN, NaN]	[NaN, NaN]
	MEDFREQ	[-0.2, 0.2531]	[0.08, 0.6452]	[0.02, 0.8914]	[-0.01, 0.9624]	[NaN, NaN]	[NaN, NaN]
	CFREQ	[-0.15, 0.3751]	[0.01, 0.9476]	[0.16, 0.34]	[-0.12, 0.4783]	[NaN, NaN]	[NaN, NaN]
	FREQD	[0.25, 0.1483]	[-0.19, 0.2743]	[0.01, 0.9396]	[0.14, 0.4212]	[NaN, NaN]	[NaN, NaN]
ML	**RDIST**	[0.02, 0.919]	[0.09, 0.5986]	[-0.13, 0.4509]	[-0.02, 0.8876]	[NaN, NaN]	[NaN, NaN]
	MDIST	[-0.05, 0.759]	[0.11, 0.5315]	[-0.2, 0.254]	[-0.02, 0.8876]	[NaN, NaN]	[NaN, NaN]
	TOTEX	[-0.01, 0.9665]	[0.15, 0.3725]	[0.05, 0.7848]	[-0.24, 0.166]	[NaN, NaN]	[NaN, NaN]
	MVELO	[0, 0.9981]	[0.14, 0.4285]	[0.03, 0.8735]	[-0.22, 0.198]	[NaN, NaN]	[NaN, NaN]
	MFREQ	[-0.09, 0.6043]	[-0.05, 0.7927]	[0.17, 0.317]	[-0.24, 0.166]	[NaN, NaN]	[NaN, NaN]
	MEDFREQ	[-0.18, 0.2979]	[-0.01, 0.9476]	[0.05, 0.7906]	[-0.19, 0.2745]	[NaN, NaN]	[NaN, NaN]
	CFREQ	[-0.23, 0.177]	[-0.21, 0.2192]	[0.12, 0.4935]	[-0.19, 0.2745]	[NaN, NaN]	[NaN, NaN]
	FREQD	[0.12, 0.5037]	[-0.14, 0.4285]	[-0.13, 0.4418]	[0.17, 0.3191]	[NaN, NaN]	[NaN, NaN]

		Task 4		Task 5		Task 6	
COP-based Biomarkers		**Admission**	**Discharge**	**Admission**	**Discharge**	**Admission**	**Discharge**
RD	**RDIST**	[-0.05, 0.7798]	[-0.07, 0.6909]	[0.14, 0.4038]	[0.02, 0.9163]	[-0.08, 0.6465]	[-0.01, 0.9461]
	MDIST	[-0.11, 0.5228]	[-0.05, 0.7562]	[0.05, 0.7676]	[0.04, 0.8217]	[-0.13, 0.4635]	[-0.01, 0.9461]
	TOTEX	[0.06, 0.7197]	[0.01, 0.9505]	[0.16, 0.3392]	[0.04, 0.8148]	[0.11, 0.51]	[0, 1]
	MVELO	[0.04, 0.8297]	[0.03, 0.8718]	[0.14, 0.4283]	[0.04, 0.8059]	[0.07, 0.6779]	[0.02, 0.8925]
	95% Conf. Ellipse	[0.2, 0.249]	[-0.16, 0.3424]	**[0.34, 0.0415]**	[0.01, 0.9493]	[0.11, 0.5327]	[0.07, 0.6848]
	Sway Area	[0.01, 0.9636]	[-0.09, 0.5928]	[0.14, 0.4014]	[-0.01, 0.931]	[0.02, 0.9243]	[0, 1]
	MFREQ	[0.07, 0.6684]	[0.05, 0.7704]	[0.06, 0.7338]	[0.05, 0.7685]	[0.18, 0.3062]	[0.01, 0.9461]
	MEDFREQ	[0.15, 0.3984]	[0.08, 0.6411]	[0.28, 0.0936]	[-0.01, 0.9472]	[0.08, 0.6465]	[0.21, 0.2187]
	CFREQ	[0.15, 0.3861]	[0.13, 0.4623]	[0.15, 0.3944]	[-0.07, 0.6692]	[0.25, 0.1426]	[0.06, 0.7353]
	FREQD	[-0.13, 0.4497]	[0.1, 0.5545]	[-0.19, 0.2749]	[-0.08, 0.6296]	[-0.1, 0.5587]	[0, 1]
AP	**RDIST**	[-0.02, 0.8956]	[0.05, 0.7609]	[0.21, 0.2283]	[0.1, 0.5794]	[-0.03, 0.8798]	[-0.02, 0.8925]
	MDIST	[-0.13, 0.4374]	[0.02, 0.8963]	[0.07, 0.6821]	[0.04, 0.8093]	[-0.09, 0.6064]	[-0.02, 0.8925]
	TOTEX	[0.14, 0.4181]	[0.05, 0.7895]	[0.23, 0.1822]	[0.06, 0.7369]	[0.17, 0.3254]	[-0.02, 0.8925]
	MVELO	[0.02, 0.9098]	[0.06, 0.7421]	[0.13, 0.4637]	[0.05, 0.7509]	[0.1, 0.5794]	[0.01, 0.9461]
	MFREQ	[0.12, 0.4866]	[-0.09, 0.6015]	[0.09, 0.5877]	[0.04, 0.8272]	[0.2, 0.2332]	[-0.04, 0.8393]
	MEDFREQ	[0.06, 0.732]	[-0.19, 0.2705]	[0.11, 0.5285]	[-0.03, 0.8472]	[0.14, 0.3994]	[0.11, 0.542]
	CFREQ	[0.1, 0.577]	[0.14, 0.4322]	[0.08, 0.652]	[-0.07, 0.6861]	[0.16, 0.3453]	[0.12, 0.4978]
	FREQD	[0.04, 0.8347]	[0.07, 0.6818]	[-0.02, 0.895]	[-0.09, 0.5935]	[-0.05, 0.7787]	[0.01, 0.9461]
ML	**RDIST**	[0.03, 0.8661]	[-0.23, 0.1804]	[0.09, 0.6032]	[0.07, 0.6724]	[-0.08, 0.6527]	[-0.01, 0.9461]
	MDIST	[-0.04, 0.8037]	[-0.24, 0.1546]	[0.01, 0.9697]	[0.05, 0.7834]	[-0.14, 0.4068]	[-0.08, 0.6357]
	TOTEX	[0.08, 0.6637]	[-0.04, 0.8329]	[0.11, 0.529]	[0.01, 0.9493]	[0.04, 0.8188]	[-0.04, 0.8393]
	MVELO	[0.08, 0.6637]	[-0.05, 0.7704]	[0.12, 0.5021]	[-0.02, 0.8981]	[0.02, 0.914]	[-0.01, 0.9461]
	MFREQ	[-0.03, 0.8686]	[0.14, 0.4176]	[0, 0.9908]	[-0.1, 0.563]	[0.11, 0.5213]	[0, 1]
	MEDFREQ	[0, 0.9799]	[0.09, 0.5842]	[0.03, 0.8729]	[-0.04, 0.8176]	[0.01, 0.938]	[0.04, 0.8393]
	CFREQ	[-0.13, 0.4379]	[0.13, 0.4661]	[-0.06, 0.7201]	[-0.27, 0.1134]	[-0.08, 0.6527]	[-0.04, 0.8393]
	FREQD	[-0.03, 0.8501]	[-0.13, 0.4396]	[-0.09, 0.5825]	[-0.06, 0.7282]	[-0.05, 0.7589]	[-0.06, 0.7353]

		Task 7		Task 8		Task 9	
COP-based Biomarkers		**Admission**	**Discharge**	**Admission**	**Discharge**	**Admission**	**Discharge**
RD	**RDIST**	[-0.25, 0.1489]	[-0.31, 0.0676]	[-0.09, 0.5925]	[-0.21, 0.2285]	[-0.03, 0.8757]	[-0.06, 0.7327]
	MDIST	[-0.31, 0.0653]	[-0.29, 0.0876]	[-0.14, 0.4059]	[-0.26, 0.1266]	[-0.12, 0.4708]	[-0.09, 0.5948]
	TOTEX	[-0.02, 0.9116]	[-0.21, 0.2258]	[0.15, 0.3905]	[-0.25, 0.1461]	[0.11, 0.5195]	[-0.08, 0.6486]
	MVELO	[-0.04, 0.8093]	[-0.2, 0.2535]	[0.1, 0.5687]	[-0.24, 0.153]	[0.09, 0.6155]	[-0.11, 0.5379]
	95% Conf. Ellipse	[0.03, 0.8411]	[-0.29, 0.0894]	[0.05, 0.7682]	[-0.16, 0.3616]	[0.08, 0.6371]	[0.03, 0.8735]
	Sway Area	[-0.12, 0.4714]	[-0.29, 0.0821]	[0.01, 0.9534]	[-0.31, 0.0626]	[0.05, 0.7837]	[-0.13, 0.4602]
	MFREQ	[0.16, 0.3471]	[0.09, 0.5984]	[0.16, 0.3629]	[-0.1, 0.5686]	[0.2, 0.2447]	[-0.04, 0.8377]
	MEDFREQ	**[0.33, 0.0465]**	[-0.04, 0.8366]	[0.28, 0.1002]	[0.07, 0.6736]	[0.24, 0.1593]	[0.12, 0.4791]
	CFREQ	[0.26, 0.1305]	[0.06, 0.7346]	[0.16, 0.3576]	[-0.16, 0.3446]	[0.25, 0.148]	[-0.17, 0.3283]
	FREQD	[-0.08, 0.6444]	[0.06, 0.7372]	[-0.29, 0.082]	[-0.15, 0.3942]	[-0.21, 0.2215]	[-0.24, 0.1544]
AP	**RDIST**	[-0.22, 0.2056]	[-0.26, 0.1259]	[0, 0.9987]	[-0.11, 0.5317]	[0.02, 0.8931]	[-0.01, 0.9637]
	MDIST	[-0.3, 0.0782]	[-0.26, 0.1216]	[-0.04, 0.812]	[-0.17, 0.3224]	[-0.09, 0.5846]	[-0.06, 0.7213]
	TOTEX	[0.07, 0.682]	[-0.22, 0.1976]	[0.17, 0.3098]	[-0.18, 0.2859]	[0.12, 0.4688]	[-0.04, 0.8082]
	MVELO	[0.01, 0.9668]	[-0.22, 0.2015]	[0.08, 0.6611]	[-0.19, 0.2601]	[0.1, 0.5627]	[-0.08, 0.6541]
	MFREQ	[0.22, 0.1919]	[-0.03, 0.8728]	[0.1, 0.5448]	[-0.13, 0.4488]	[0.16, 0.3651]	[-0.06, 0.727]
	MEDFREQ	[0.18, 0.2949]	[-0.18, 0.307]	[0.01, 0.9357]	[-0.11, 0.5078]	[0.08, 0.6289]	[0.06, 0.7156]
	CFREQ	[0.17, 0.3343]	[-0.08, 0.6406]	[0.04, 0.8376]	[-0.01, 0.9507]	[0.12, 0.4729]	[-0.27, 0.1097]
	FREQD	[-0.12, 0.4834]	[0, 0.9973]	[-0.04, 0.8376]	[0.06, 0.7359]	[-0.02, 0.9236]	[-0.13, 0.4556]
ML	**RDIST**	[-0.24, 0.1561]	[-0.3, 0.078]	[-0.19, 0.2658]	**[-0.38, 0.0221]**	[-0.15, 0.3853]	[-0.05, 0.7789]
	MDIST	[-0.31, 0.0674]	[-0.31, 0.065]	[-0.25, 0.1473]	**[-0.38, 0.0224]**	[-0.22, 0.2053]	[-0.05, 0.7557]
	TOTEX	[-0.12, 0.4699]	[-0.17, 0.3115]	[0.05, 0.7562]	**[-0.35, 0.0389]**	[0.08, 0.6465]	[-0.14, 0.4018]
	MVELO	[-0.15, 0.3971]	[-0.18, 0.2974]	[0.04, 0.8005]	**[-0.37, 0.025]**	[0.06, 0.7257]	[-0.19, 0.2774]
	MFREQ	[0.1, 0.5586]	[0.15, 0.3871]	[0.31, 0.0655]	[-0.08, 0.6295]	[0.28, 0.0993]	[-0.17, 0.336]
	MEDFREQ	[0.04, 0.8003]	[0.09, 0.606]	[0.1, 0.5642]	[-0.19, 0.2582]	[0.12, 0.4888]	[-0.05, 0.7789]
	CFREQ	[-0.06, 0.7378]	[0.01, 0.9479]	[0.09, 0.5931]	[-0.15, 0.3734]	[0.13, 0.4349]	[-0.13, 0.4509]
	FREQD	[-0.04, 0.7968]	[-0.15, 0.3815]	[-0.24, 0.1549]	[0.02, 0.9119]	[-0.13, 0.4552]	[0.01, 0.9396]

		Task 10		Task 11		Task 12	
COP-based Biomarkers		**Admission**	**Discharge**	**Admission**	**Discharge**	**Admission**	**Discharge**
RD	**RDIST**	[-0.06, 0.7419]	[-0.04, 0.8118]	[-0.03, 0.8471]	[-0.19, 0.2781]	[-0.04, 0.8372]	[-0.11, 0.5366]
	MDIST	[-0.1, 0.5741]	[-0.07, 0.6728]	[-0.13, 0.4451]	[-0.22, 0.1892]	[-0.09, 0.616]	[-0.14, 0.4278]
	TOTEX	[0.06, 0.7383]	[-0.05, 0.765]	[-0.12, 0.4806]	[-0.06, 0.7313]	[0.06, 0.7119]	[-0.16, 0.3402]
	MVELO	[0.04, 0.8025]	[-0.05, 0.7773]	[-0.14, 0.4202]	[-0.06, 0.7471]	[0.05, 0.7629]	[-0.16, 0.3536]
	95% Conf. Ellipse	[0.03, 0.8649]	[0.03, 0.8567]	[0.21, 0.2268]	[-0.02, 0.9136]	[0.16, 0.3435]	[0.03, 0.8663]
	Sway Area	[0.03, 0.8768]	[-0.09, 0.5996]	[-0.08, 0.6259]	[-0.18, 0.2803]	[0, 0.9876]	[-0.16, 0.3446]
	MFREQ	[0.17, 0.332]	[0.02, 0.9173]	[-0.12, 0.4895]	[0.11, 0.5381]	[0.12, 0.4679]	[-0.1, 0.5665]
	MEDFREQ	[0.24, 0.1646]	[0.13, 0.4403]	**[0.34, 0.0446]**	[0.23, 0.171]	[0.2, 0.2395]	[0.19, 0.2707]
	CFREQ	[0.21, 0.2252]	[-0.04, 0.8143]	[-0.03, 0.8605]	[-0.12, 0.4987]	[0.24, 0.164]	[-0.26, 0.1258]
	FREQD	[-0.14, 0.4005]	[-0.27, 0.1084]	[-0.11, 0.5339]	[-0.28, 0.1038]	[-0.15, 0.3926]	[-0.08, 0.6526]
AP	**RDIST**	[-0.07, 0.7023]	[0, 0.9924]	[-0.04, 0.8349]	[-0.08, 0.6383]	[-0.01, 0.9499]	[-0.02, 0.9076]
	MDIST	[-0.1, 0.5605]	[-0.01, 0.944]	[-0.15, 0.3812]	[-0.14, 0.4086]	[-0.08, 0.6593]	[-0.09, 0.6015]
	TOTEX	[0.03, 0.8731]	[-0.08, 0.6404]	[-0.03, 0.8838]	[-0.11, 0.5312]	[0.15, 0.3879]	[-0.15, 0.3806]
	MVELO	[0, 0.9975]	[-0.07, 0.667]	[-0.1, 0.5759]	[-0.11, 0.5312]	[0.08, 0.6392]	[-0.15, 0.3759]
	MFREQ	[0.12, 0.4876]	[-0.01, 0.9643]	[-0.05, 0.7521]	[0.02, 0.8894]	[0.19, 0.2569]	[-0.15, 0.3832]
	MEDFREQ	[0.12, 0.4871]	[0.16, 0.3596]	[0.08, 0.6359]	[0.1, 0.5597]	[0.21, 0.2252]	[-0.04, 0.8206]
	CFREQ	[0.1, 0.5513]	[-0.06, 0.7456]	[-0.09, 0.6028]	[-0.21, 0.2248]	[0.19, 0.2698]	[-0.25, 0.149]
	FREQD	[-0.02, 0.9192]	[-0.08, 0.6221]	[-0.05, 0.7747]	[-0.22, 0.2045]	[-0.08, 0.6275]	[-0.09, 0.6075]
ML	**RDIST**	[-0.03, 0.8429]	[-0.04, 0.8379]	[-0.02, 0.9047]	[-0.16, 0.354]	[-0.03, 0.8799]	[-0.08, 0.6447]
	MDIST	[-0.06, 0.7214]	[-0.08, 0.6438]	[-0.08, 0.6315]	[-0.23, 0.1742]	[-0.08, 0.6543]	[-0.12, 0.4909]
	TOTEX	[0.1, 0.5486]	[-0.06, 0.7298]	[-0.15, 0.3702]	[0.01, 0.9756]	[-0.01, 0.9734]	[-0.19, 0.2784]
	MVELO	[0.09, 0.6063]	[-0.07, 0.6717]	[-0.15, 0.389]	[-0.02, 0.913]	[-0.02, 0.8915]	[-0.21, 0.2205]
	MFREQ	[0.21, 0.2095]	[-0.11, 0.505]	[-0.2, 0.2504]	[0.11, 0.5381]	[0.06, 0.7137]	[-0.13, 0.4536]
	MEDFREQ	[0.17, 0.3113]	[-0.13, 0.4548]	[0.04, 0.8095]	[0.2, 0.2417]	[0.15, 0.3879]	[-0.06, 0.7303]
	CFREQ	[0.13, 0.4484]	[-0.1, 0.5807]	[-0.3, 0.0735]	[-0.07, 0.6869]	[-0.08, 0.6431]	[-0.26, 0.1307]
	FREQD	[-0.21, 0.2287]	[0.03, 0.8505]	[-0.01, 0.969]	**[-0.35, 0.0375]**	[-0.21, 0.2227]	[-0.09, 0.6163]

		Task 13		Task 14		Total Score	
COP-based Biomarkers		**Admission**	**Discharge**	**Admission**	**Discharge**	**Admission**	**Discharge**
RD	**RDIST**	[-0.22, 0.205]	[-0.02, 0.9039]	[-0.07, 0.6647]	[-0.19, 0.2659]	[-0.09, 0.5887]	[-0.22, 0.1885]
	MDIST	[-0.22, 0.2064]	[0.01, 0.9416]	[-0.11, 0.5403]	[-0.21, 0.2174]	[-0.18, 0.3064]	[-0.25, 0.1423]
	TOTEX	[-0.05, 0.7839]	[-0.11, 0.5222]	[0.11, 0.5414]	[-0.06, 0.7067]	[0.04, 0.8048]	[-0.25, 0.1466]
	MVELO	[-0.09, 0.5972]	[-0.11, 0.5108]	[0.08, 0.6475]	[-0.07, 0.6994]	[0, 0.9911]	[-0.24, 0.1526]
	95% Conf. Ellipse	[-0.22, 0.1916]	[-0.13, 0.4531]	[0.1, 0.5436]	[-0.14, 0.4023]	[0.18, 0.2908]	[-0.14, 0.4194]
	Sway Area	[-0.21, 0.2146]	[-0.14, 0.4188]	[0.03, 0.8408]	[-0.14, 0.4013]	[-0.04, 0.8037]	[-0.3, 0.0763]
	MFREQ	[0.08, 0.6347]	[0, 0.9807]	[0.09, 0.5843]	[0.08, 0.6399]	[0.1, 0.5585]	[-0.06, 0.7212]
	MEDFREQ	[-0.02, 0.8897]	[-0.05, 0.7923]	[0.26, 0.1269]	[0.11, 0.5334]	[0.32, 0.057]	[0.09, 0.5865]
	CFREQ	[0.16, 0.3399]	[-0.11, 0.5108]	[0.11, 0.5326]	[-0.03, 0.8467]	[0.22, 0.2004]	[-0.25, 0.1494]
	FREQD	[-0.24, 0.1536]	[0.02, 0.9072]	[-0.15, 0.3718]	[-0.12, 0.4774]	[-0.17, 0.3263]	[-0.13, 0.4456]
AP	**RDIST**	[-0.13, 0.433]	[0.02, 0.923]	[-0.05, 0.7703]	[-0.08, 0.6309]	[-0.06, 0.7166]	[-0.12, 0.4906]
	MDIST	[-0.13, 0.4368]	[0.02, 0.8973]	[-0.06, 0.7077]	[-0.08, 0.6547]	[-0.17, 0.3141]	[-0.17, 0.3195]
	TOTEX	[-0.02, 0.9113]	[-0.04, 0.833]	[0.12, 0.4958]	[-0.14, 0.4289]	[0.11, 0.5325]	[-0.25, 0.1401]
	MVELO	[-0.13, 0.446]	[-0.04, 0.7961]	[0.04, 0.7949]	[-0.14, 0.4183]	[0, 0.9833]	[-0.26, 0.1305]
	MFREQ	[-0.04, 0.8118]	[-0.05, 0.7923]	[0.06, 0.7285]	[-0.09, 0.6182]	[0.12, 0.4828]	[-0.12, 0.4973]
	MEDFREQ	[0, 0.9974]	[-0.31, 0.0663]	[0.08, 0.6392]	[-0.13, 0.4401]	[0.13, 0.4464]	[-0.06, 0.7392]
	CFREQ	[0.03, 0.8632]	[-0.02, 0.9204]	[0.02, 0.9197]	[-0.13, 0.458]	[0.11, 0.5149]	[-0.26, 0.1211]
	FREQD	[0.11, 0.5387]	[0.3, 0.0796]	[-0.07, 0.6761]	[-0.06, 0.7128]	[0, 0.9982]	[-0.08, 0.6425]
ML	**RDIST**	**[-0.4, 0.0159]**	[-0.17, 0.3348]	[0.01, 0.9686]	[-0.17, 0.317]	[-0.1, 0.558]	[-0.22, 0.2005]
	MDIST	**[-0.41, 0.0125]**	[-0.17, 0.3356]	[-0.03, 0.8498]	[-0.22, 0.2039]	[-0.18, 0.2992]	[-0.25, 0.1488]
	TOTEX	[-0.11, 0.517]	[-0.23, 0.1715]	[0.16, 0.3656]	[0.05, 0.7841]	[0, 0.9899]	[-0.26, 0.1317]
	MVELO	[-0.13, 0.4335]	[-0.24, 0.1552]	[0.15, 0.3936]	[0.01, 0.9472]	[-0.03, 0.8614]	[-0.29, 0.0904]
	MFREQ	**[0.35, 0.0359]**	[-0.1, 0.5471]	[0.09, 0.5826]	[0.18, 0.2861]	[0.09, 0.5877]	[-0.1, 0.5711]
	MEDFREQ	[0.3, 0.0791]	[-0.19, 0.2761]	[0.24, 0.1608]	[0.27, 0.1116]	[0.09, 0.6217]	[-0.04, 0.8173]
	CFREQ	[0.18, 0.2853]	[-0.15, 0.3708]	[-0.09, 0.5917]	[0.07, 0.7007]	[-0.08, 0.6255]	[-0.26, 0.1238]
	FREQD	**[-0.45, 0.0064]**	[0.02, 0.9164]	[-0.23, 0.1772]	**[-0.35, 0.0367]**	[-0.13, 0.4478]	[-0.14, 0.4295]

Supp Table 5. Spearman's correlation between each Berg Balance Scale (BBS) task score and center-of-mass (COM) acceleration balance biomarkers presented as [ρ, P] at both admission and discharge test sessions. Highlighted cells are significant values ($P < 0.05$).

		Task 1		Task 2		Task 3	
COM-based Biomarkers		**Admission**	**Discharge**	**Admission**	**Discharge**	**Admission**	**Discharge**
RD	**RDIST**	[0.26, 0.1239]	[0.21, 0.2192]	[-0.02, 0.8854]	[-0.25, 0.1378]	[NaN, NaN]	[NaN, NaN]
	MDIST	[0.26, 0.1324]	[0.24, 0.1517]	[-0.05, 0.7557]	[-0.25, 0.1378]	[NaN, NaN]	[NaN, NaN]
	TOTEX	[0.04, 0.8225]	**[0.36, 0.0295]**	[0.04, 0.7965]	[-0.27, 0.1134]	[NaN, NaN]	[NaN, NaN]
	MVELO	[-0.07, 0.6971]	**[0.36, 0.0295]**	[-0.16, 0.3599]	[-0.27, 0.1134]	[NaN, NaN]	[NaN, NaN]
	95% Conf. Ellipse	[0.15, 0.384]	[0.1, 0.5758]	[-0.09, 0.5948]	[-0.15, 0.368]	[NaN, NaN]	[NaN, NaN]
	Sway Area	[0.06, 0.7498]	[0.26, 0.1243]	[-0.2, 0.235]	[-0.22, 0.198]	[NaN, NaN]	[NaN, NaN]
	MFREQ	[-0.28, 0.0967]	[-0.07, 0.6932]	[-0.14, 0.4282]	[0.09, 0.6037]	[NaN, NaN]	[NaN, NaN]
	MEDFREQ	[-0.18, 0.2809]	[-0.11, 0.51]	[-0.07, 0.6763]	[-0.27, 0.1134]	[NaN, NaN]	[NaN, NaN]
	CFREQ	[-0.3, 0.0744]	[-0.12, 0.489]	[-0.02, 0.9094]	[0.24, 0.166]	[NaN, NaN]	[NaN, NaN]
	FREQD	[0.07, 0.6851]	[0.16, 0.3377]	[0.03, 0.8794]	[-0.04, 0.8138]	[NaN, NaN]	[NaN, NaN]
AP	**RDIST**	[0.21, 0.2198]	[0.2, 0.2457]	[-0.04, 0.8318]	[-0.25, 0.1378]	[NaN, NaN]	[NaN, NaN]
	MDIST	[0.22, 0.1891]	[0.23, 0.1833]	[-0.01, 0.9637]	[-0.25, 0.1378]	[NaN, NaN]	[NaN, NaN]
	TOTEX	[0.04, 0.8388]	[0.32, 0.059]	[0.13, 0.4509]	[-0.27, 0.1134]	[NaN, NaN]	[NaN, NaN]
	MVELO	[-0.08, 0.6399]	[0.31, 0.0692]	[-0.09, 0.6215]	[-0.27, 0.1134]	[NaN, NaN]	[NaN, NaN]
	MFREQ	[-0.16, 0.3525]	[-0.13, 0.4482]	[-0.03, 0.8615]	[0.09, 0.6037]	[NaN, NaN]	[NaN, NaN]
	MEDFREQ	[-0.21, 0.2236]	**[-0.35, 0.0354]**	[-0.18, 0.3022]	[0.22, 0.198]	[NaN, NaN]	[NaN, NaN]
	CFREQ	**[-0.39, 0.0196]**	[-0.07, 0.6932]	[-0.21, 0.2199]	[0.28, 0.0923]	[NaN, NaN]	[NaN, NaN]
	FREQD	[-0.01, 0.9743]	[0.07, 0.6691]	[-0.14, 0.4149]	[0.06, 0.7415]	[NaN, NaN]	[NaN, NaN]
ML	**RDIST**	[0.08, 0.6226]	[0.22, 0.1948]	[-0.09, 0.6001]	[0.14, 0.4212]	[NaN, NaN]	[NaN, NaN]
	MDIST	[0.09, 0.6043]	[0.26, 0.1243]	[-0.07, 0.6652]	[0.11, 0.5393]	[NaN, NaN]	[NaN, NaN]
	TOTEX	[-0.07, 0.6905]	**[0.35, 0.0354]**	[-0.06, 0.7442]	[-0.2, 0.2341]	[NaN, NaN]	[NaN, NaN]
	MVELO	[-0.14, 0.4294]	**[0.34, 0.0423]**	[-0.17, 0.3207]	[-0.2, 0.2341]	[NaN, NaN]	[NaN, NaN]
	MFREQ	[-0.26, 0.1216]	[-0.03, 0.8696]	[-0.19, 0.2638]	[-0.27, 0.1134]	[NaN, NaN]	[NaN, NaN]
	MEDFREQ	[-0.2, 0.2375]	[-0.01, 0.9476]	[-0.29, 0.0838]	[-0.27, 0.1134]	[NaN, NaN]	[NaN, NaN]
	CFREQ	**[-0.34, 0.0434]**	[-0.05, 0.7927]	[-0.15, 0.3805]	[-0.15, 0.368]	[NaN, NaN]	[NaN, NaN]
	FREQD	[0.22, 0.196]	[-0.11, 0.51]	[0.16, 0.3558]	[0.27, 0.1134]	[NaN, NaN]	[NaN, NaN]
ISway	**JERK**	[-0.04, 0.82]	[0.26, 0.1243]	[-0.07, 0.6763]	[-0.22, 0.198]	[NaN, NaN]	[NaN, NaN]
	RMS-ACC	[0.13, 0.4361]	[0.23, 0.1723]	[0.01, 0.9758]	[-0.24, 0.166]	[NaN, NaN]	[NaN, NaN]
	CF-ACC	**[-0.35, 0.0351]**	[-0.17, 0.3211]	[-0.13, 0.4463]	[0.27, 0.1134]	[NaN, NaN]	[NaN, NaN]

		Task 4		Task 5		Task 6	
COM-based Biomarkers		**Admission**	**Discharge**	**Admission**	**Discharge**	**Admission**	**Discharge**
RD	**RDIST**	[0.05, 0.7518]	[0.05, 0.7609]	[0.24, 0.1615]	[0.14, 0.4079]	[-0.05, 0.7556]	[-0.22, 0.1936]
	MDIST	[0.04, 0.8163]	[0.07, 0.6909]	[0.23, 0.1778]	[0.17, 0.3211]	[-0.06, 0.7164]	[-0.21, 0.2187]
	TOTEX	[0.19, 0.2699]	[0.11, 0.5215]	[0.2, 0.2404]	[0.2, 0.2498]	[0.17, 0.3341]	[-0.09, 0.588]
	MVELO	[0.04, 0.8144]	[0.1, 0.5757]	[0.06, 0.722]	[0.19, 0.2647]	[0.07, 0.7003]	[-0.08, 0.6357]
	95% Conf. Ellipse	[0.08, 0.6507]	[-0.08, 0.6636]	[0.23, 0.1707]	[0.07, 0.7037]	[-0.08, 0.6402]	[-0.07, 0.6848]
	Sway Area	[0.02, 0.9299]	[0.11, 0.5256]	[0.15, 0.3949]	[0.17, 0.3076]	[-0.05, 0.7688]	[-0.07, 0.6848]
	MFREQ	[-0.05, 0.7518]	[0.02, 0.8914]	[-0.21, 0.2205]	[-0.04, 0.8341]	[0.06, 0.7196]	[0.2, 0.2459]
	MEDFREQ	[-0.12, 0.4687]	[-0.12, 0.4816]	[-0.17, 0.3362]	[-0.23, 0.1781]	[-0.22, 0.2]	[-0.33, 0.0517]
	CFREQ	[-0.06, 0.7308]	[-0.08, 0.6367]	[-0.14, 0.4152]	[-0.24, 0.1606]	[0, 0.9931]	[0.3, 0.0719]
	FREQD	[-0.01, 0.9487]	[-0.02, 0.9111]	[0.03, 0.856]	[-0.02, 0.889]	[-0.02, 0.914]	[0.05, 0.7868]
AP	**RDIST**	[0.01, 0.9656]	[0.04, 0.8377]	[0.22, 0.1952]	[0.12, 0.4759]	[-0.09, 0.5853]	[-0.25, 0.1496]
	MDIST	[0.03, 0.8783]	[0.04, 0.8039]	[0.23, 0.1696]	[0.14, 0.4212]	[-0.1, 0.5646]	[-0.25, 0.1496]
	TOTEX	[0.11, 0.5374]	[0.04, 0.8135]	[0.18, 0.3058]	[0.14, 0.4187]	[0.16, 0.343]	[-0.2, 0.2459]
	MVELO	[-0.06, 0.7204]	[0.04, 0.8183]	[0.02, 0.9146]	[0.12, 0.4848]	[0.07, 0.7035]	[-0.13, 0.4555]
	MFREQ	[0.02, 0.9156]	[-0.05, 0.7515]	[-0.14, 0.4062]	[-0.11, 0.5369]	[0.17, 0.3254]	[0.16, 0.3409]
	MEDFREQ	[-0.19, 0.2652]	[-0.15, 0.3823]	[-0.22, 0.1926]	[-0.28, 0.1033]	[-0.05, 0.7787]	[0.2, 0.2459]
	CFREQ	[-0.32, 0.0546]	[0.1, 0.5757]	[-0.3, 0.0768]	[-0.11, 0.5108]	[-0.2, 0.2457]	**[0.4, 0.0165]**
	FREQD	[-0.1, 0.5703]	[0.15, 0.3823]	[-0.08, 0.6598]	[0.03, 0.8528]	[-0.18, 0.2897]	[0.16, 0.3409]
ML	**RDIST**	[0.01, 0.9422]	[-0.04, 0.8232]	[0.11, 0.5176]	[0.11, 0.5404]	[-0.08, 0.6402]	[0.29, 0.0842]
	MDIST	[0.01, 0.9461]	[-0.01, 0.9604]	[0.1, 0.574]	[0.14, 0.427]	[-0.08, 0.6621]	[0.27, 0.1133]
	TOTEX	[0.12, 0.4732]	[0.15, 0.3962]	[0.09, 0.6061]	[0.26, 0.1221]	[0, 0.9966]	[0.01, 0.9461]
	MVELO	[0.03, 0.8654]	[0.13, 0.4471]	[0, 0.9895]	[0.25, 0.1447]	[-0.06, 0.7196]	[0.01, 0.9461]
	MFREQ	[-0.06, 0.7197]	[0.08, 0.6411]	[-0.13, 0.4366]	[-0.01, 0.9739]	[-0.06, 0.7229]	**[-0.34, 0.0434]**
	MEDFREQ	[0, 0.9864]	[-0.14, 0.4176]	[0, 0.977]	[-0.01, 0.969]	[-0.09, 0.5913]	**[-0.36, 0.0301]**
	CFREQ	[-0.18, 0.2977]	[-0.03, 0.8816]	[-0.28, 0.098]	[-0.21, 0.2224]	[-0.1, 0.5734]	[-0.27, 0.1133]
	FREQD	[-0.03, 0.8437]	[-0.09, 0.6146]	[-0.03, 0.8696]	[-0.14, 0.4202]	[0.12, 0.4851]	**[0.35, 0.0363]**
ISway	**JERK**	[0.06, 0.7228]	[0.07, 0.6772]	[0.11, 0.5053]	[0.09, 0.6214]	[0.09, 0.6186]	[-0.07, 0.6848]
	RMS-ACC	[0, 0.9838]	[0.01, 0.9357]	[0.11, 0.54]	[0.06, 0.7416]	[-0.08, 0.6248]	[-0.22, 0.1936]
	CF-ACC	[-0.21, 0.2206]	[0.1, 0.5714]	[-0.25, 0.1446]	[-0.1, 0.5685]	[0.01, 0.9587]	**[0.4, 0.0165]**

		Task 7		Task 8		Task 9	
COM-based Biomarkers		**Admission**	**Discharge**	**Admission**	**Discharge**	**Admission**	**Discharge**
RD	**RDIST**	[-0.17, 0.3142]	**[-0.46, 0.0048]**	[-0.08, 0.6456]	[-0.15, 0.3687]	[0.03, 0.8492]	[-0.19, 0.2706]
	MDIST	[-0.23, 0.1727]	**[-0.45, 0.0061]**	[-0.09, 0.6145]	[-0.19, 0.2775]	[-0.01, 0.9582]	[-0.2, 0.2381]
	TOTEX	[-0.02, 0.9049]	[-0.15, 0.3871]	[0.18, 0.2913]	[-0.11, 0.5185]	[0.03, 0.8557]	[-0.19, 0.2774]
	MVELO	[-0.12, 0.4878]	[-0.13, 0.436]	[0.04, 0.8094]	[-0.15, 0.3869]	[0, 0.998]	[-0.23, 0.1761]
	95% Conf. Ellipse	[-0.08, 0.6344]	**[-0.44, 0.0075]**	[-0.09, 0.5954]	[-0.01, 0.9535]	[-0.01, 0.966]	[-0.15, 0.3889]
	Sway Area	[-0.23, 0.1755]	**[-0.34, 0.0436]**	[-0.1, 0.5806]	[-0.15, 0.3758]	[-0.02, 0.8892]	[-0.27, 0.1061]
	MFREQ	[0.07, 0.6911]	**[0.4, 0.016]**	[0.05, 0.7663]	[0.17, 0.3285]	[-0.06, 0.7207]	[0.1, 0.543]
	MEDFREQ	[0, 0.9957]	[-0.31, 0.0648]	[-0.07, 0.681]	[0.13, 0.443]	[-0.04, 0.8268]	[0.01, 0.9758]
	CFREQ	[0.05, 0.7896]	**[0.36, 0.0314]**	[0, 0.9928]	[0.16, 0.346]	[0.14, 0.3991]	[-0.1, 0.5532]
	FREQD	[-0.12, 0.4762]	[-0.02, 0.9026]	[-0.09, 0.6168]	**[-0.44, 0.0077]**	[0.26, 0.1253]	**[-0.4, 0.015]**
AP	**RDIST**	[-0.21, 0.2217]	**[-0.45, 0.006]**	[-0.08, 0.6332]	[-0.23, 0.1768]	[-0.04, 0.8313]	[-0.2, 0.254]
	MDIST	[-0.24, 0.1587]	**[-0.44, 0.0078]**	[-0.07, 0.6707]	[-0.26, 0.1245]	[-0.05, 0.7887]	[-0.2, 0.2381]
	TOTEX	[0, 0.9914]	[-0.3, 0.0804]	[0.21, 0.2294]	[-0.06, 0.7149]	[0.11, 0.5395]	[-0.12, 0.4886]
	MVELO	[-0.09, 0.6207]	[-0.28, 0.1026]	[0.05, 0.755]	[-0.11, 0.5066]	[0.07, 0.6733]	[-0.18, 0.2985]
	MFREQ	[0.15, 0.3867]	[0.28, 0.0962]	[0.1, 0.5811]	[0.25, 0.1379]	[0.03, 0.855]	[0.1, 0.5481]
	MEDFREQ	[-0.06, 0.7192]	[0.1, 0.5535]	[-0.07, 0.6986]	**[0.35, 0.0363]**	[-0.19, 0.2746]	[0.27, 0.1097]
	CFREQ	[-0.22, 0.2022]	[-0.03, 0.8517]	**[-0.38, 0.0225]**	[-0.07, 0.6883]	[-0.14, 0.4061]	[-0.23, 0.1736]
	FREQD	[-0.23, 0.1679]	[-0.15, 0.3759]	**[-0.34, 0.0451]**	**[-0.36, 0.0311]**	[-0.01, 0.9601]	**[-0.35, 0.0336]**
ML	**RDIST**	[-0.12, 0.4976]	[-0.3, 0.0707]	[-0.1, 0.552]	[-0.02, 0.8905]	[-0.08, 0.6436]	[-0.25, 0.1347]
	MDIST	[-0.14, 0.4059]	[-0.3, 0.0776]	[-0.09, 0.5851]	[-0.06, 0.7195]	[-0.08, 0.6465]	[-0.31, 0.069]
	TOTEX	[-0.13, 0.4675]	[0, 0.9793]	[0.04, 0.8107]	[-0.12, 0.4783]	[-0.03, 0.8666]	[-0.21, 0.2111]
	MVELO	[-0.17, 0.3207]	[0.02, 0.9272]	[-0.04, 0.8241]	[-0.13, 0.443]	[-0.05, 0.783]	[-0.23, 0.1787]
	MFREQ	[-0.07, 0.6662]	**[0.37, 0.0263]**	[-0.08, 0.6498]	[-0.06, 0.7438]	[-0.06, 0.7085]	[0.12, 0.5032]
	MEDFREQ	[-0.2, 0.2391]	[0.01, 0.9339]	[-0.09, 0.5908]	[-0.08, 0.6326]	[-0.2, 0.2326]	[0.09, 0.6001]
	CFREQ	[-0.06, 0.7169]	[0.15, 0.3773]	[-0.12, 0.4678]	[-0.07, 0.6736]	[-0.04, 0.8268]	[-0.17, 0.336]
	FREQD	[0.16, 0.3399]	[-0.23, 0.1817]	[0.02, 0.9161]	[0.06, 0.7273]	[0.18, 0.3028]	[-0.06, 0.7442]
ISway	**JERK**	[-0.06, 0.7332]	[-0.12, 0.4707]	[0.02, 0.9044]	[-0.06, 0.73]	[0.02, 0.8918]	[-0.18, 0.3022]
	RMS-ACC	[-0.13, 0.437]	**[-0.44, 0.007]**	[-0.15, 0.3881]	[-0.18, 0.2887]	[0.04, 0.8071]	[-0.32, 0.0596]
	CF-ACC	[-0.25, 0.1458]	[0.01, 0.9312]	[-0.28, 0.0986]	[-0.04, 0.8269]	[-0.15, 0.3695]	[0.15, 0.3805]

		Task 10		Task 11		Task 12	
COM-based Biomarkers		**Admission**	**Discharge**	**Admission**	**Discharge**	**Admission**	**Discharge**
RD	**RDIST**	[0.11, 0.5216]	[-0.02, 0.9021]	[0.17, 0.3325]	[-0.2, 0.2387]	[-0.01, 0.9555]	[-0.09, 0.5884]
	MDIST	[0.08, 0.6553]	[-0.02, 0.9021]	[0.15, 0.371]	[-0.21, 0.2179]	[-0.04, 0.8324]	[-0.1, 0.5522]
	TOTEX	[-0.01, 0.972]	[-0.06, 0.7119]	[-0.06, 0.7146]	[-0.02, 0.9009]	[0.04, 0.8101]	[-0.06, 0.728]
	MVELO	[-0.06, 0.748]	[-0.09, 0.594]	[-0.18, 0.307]	[-0.04, 0.8119]	[-0.06, 0.7212]	[-0.07, 0.6758]
	95% Conf. Ellipse	[0.11, 0.5294]	[0.08, 0.6496]	[0.22, 0.1957]	[-0.1, 0.5784]	[0.04, 0.8312]	[-0.04, 0.823]
	Sway Area	[0.01, 0.9357]	[0, 0.9898]	[0.03, 0.8471]	[-0.2, 0.2464]	[-0.02, 0.8909]	[-0.11, 0.5115]
	MFREQ	[-0.18, 0.2869]	[0.02, 0.9046]	**[-0.37, 0.0277]**	[0.18, 0.3056]	[-0.06, 0.7405]	[0.1, 0.5691]
	MEDFREQ	[0.19, 0.277]	[0.08, 0.6221]	[0.06, 0.7123]	[-0.12, 0.4879]	[-0.12, 0.4918]	[-0.05, 0.7778]
	CFREQ	[0.1, 0.5567]	[-0.03, 0.848]	[-0.26, 0.1294]	[0, 0.9897]	[-0.07, 0.6832]	[-0.04, 0.8012]
	FREQD	[0.28, 0.1034]	**[-0.4, 0.0148]**	[0.04, 0.8337]	[-0.31, 0.0623]	[-0.11, 0.5223]	[-0.25, 0.1419]
AP	**RDIST**	[-0.01, 0.9669]	[-0.05, 0.7675]	[0.17, 0.3177]	[-0.21, 0.2117]	[-0.01, 0.9413]	[-0.15, 0.3954]
	MDIST	[-0.02, 0.916]	[-0.06, 0.7083]	[0.19, 0.2715]	[-0.23, 0.1861]	[-0.05, 0.776]	[-0.16, 0.3661]
	TOTEX	[-0.03, 0.8461]	[0, 0.9987]	[-0.08, 0.6348]	[-0.07, 0.6928]	[-0.01, 0.9382]	[-0.08, 0.6582]
	MVELO	[-0.09, 0.6068]	[0.01, 0.9491]	[-0.19, 0.2625]	[-0.08, 0.6314]	[-0.12, 0.4713]	[-0.1, 0.5533]
	MFREQ	[-0.02, 0.9078]	[0.1, 0.5643]	**[-0.34, 0.0407]**	[0.18, 0.3067]	[0.02, 0.9099]	[0.07, 0.6758]
	MEDFREQ	[0.09, 0.6187]	[0.21, 0.2146]	[-0.28, 0.0966]	[0.22, 0.1998]	[-0.01, 0.9308]	[0.07, 0.6977]
	CFREQ	[-0.11, 0.508]	[-0.05, 0.7675]	**[-0.46, 0.0044]**	[-0.24, 0.1663]	[-0.12, 0.4713]	[-0.04, 0.7982]
	FREQD	[-0.12, 0.469]	[-0.24, 0.1659]	[-0.04, 0.8059]	[-0.33, 0.0523]	[-0.12, 0.4819]	[-0.13, 0.4631]
ML	**RDIST**	[0.11, 0.5111]	[0.19, 0.259]	[0.04, 0.8325]	[-0.01, 0.9532]	[-0.01, 0.9358]	[-0.05, 0.7934]
	MDIST	[0.13, 0.4567]	[0.15, 0.3751]	[0.01, 0.9393]	[-0.02, 0.8862]	[-0.04, 0.7962]	[-0.06, 0.7198]
	TOTEX	[-0.01, 0.9401]	[-0.03, 0.8743]	[-0.02, 0.922]	[-0.01, 0.9731]	[-0.05, 0.7552]	[0.02, 0.9008]
	MVELO	[-0.05, 0.7932]	[-0.04, 0.8007]	[-0.1, 0.5652]	[-0.02, 0.906]	[-0.11, 0.5233]	[0.01, 0.9627]
	MFREQ	[-0.29, 0.0908]	[-0.23, 0.1764]	[-0.19, 0.2584]	[-0.03, 0.8742]	[-0.12, 0.4742]	[-0.01, 0.9447]
	MEDFREQ	[-0.21, 0.2164]	[-0.12, 0.4856]	[-0.08, 0.646]	[-0.08, 0.647]	[0, 0.9876]	[-0.08, 0.6622]
	CFREQ	[-0.13, 0.4631]	[-0.2, 0.2474]	[-0.3, 0.073]	[-0.29, 0.0826]	[-0.16, 0.346]	[-0.24, 0.1527]
	FREQD	[0.31, 0.0695]	[0.06, 0.7238]	[-0.04, 0.7975]	[-0.03, 0.8812]	[0.08, 0.6236]	[-0.07, 0.6816]
ISway	**JERK**	[-0.03, 0.8429]	[-0.02, 0.9021]	[-0.08, 0.6304]	[-0.05, 0.7593]	[-0.05, 0.7611]	[-0.04, 0.8346]
	RMS-ACC	[0.04, 0.8311]	[-0.07, 0.6752]	[0.04, 0.8023]	**[-0.33, 0.0475]**	[-0.07, 0.6832]	[-0.15, 0.3729]
	CF-ACC	[-0.13, 0.4465]	[0.13, 0.4616]	**[-0.37, 0.0277]**	[-0.01, 0.95]	[-0.09, 0.5829]	[0, 0.9814]

COM-based Biomarkers		Task 13		Task 14		Total Score	
		Admission	Discharge	Admission	Discharge	Admission	Discharge
RD	RDIST	[-0.25, 0.138]	[-0.02, 0.9058]	[0.09, 0.5871]	**[-0.34, 0.0435]**	[0.04, 0.8205]	[-0.21, 0.2082]
	MDIST	[-0.22, 0.1882]	[-0.05, 0.7897]	[0.03, 0.8762]	[-0.32, 0.0572]	[0, 0.9839]	[-0.22, 0.2062]
	TOTEX	[-0.07, 0.7056]	[-0.12, 0.4862]	[0.17, 0.3197]	[0.05, 0.7608]	[0.02, 0.9221]	[-0.1, 0.5788]
	MVELO	[-0.2, 0.2529]	[-0.15, 0.3874]	[0.05, 0.7521]	[0.06, 0.739]	[-0.12, 0.4744]	[-0.11, 0.5079]
	95% Conf. Ellipse	**[-0.36, 0.0305]**	[-0.02, 0.9072]	[0.2, 0.2516]	[-0.18, 0.2878]	[0.05, 0.7749]	[-0.14, 0.4203]
	Sway Area	[-0.25, 0.1418]	[-0.06, 0.7125]	[0.07, 0.7052]	[-0.2, 0.2311]	[-0.08, 0.6372]	[-0.18, 0.297]
	MFREQ	[0.03, 0.8525]	[0.02, 0.9277]	[-0.12, 0.4751]	**[0.37, 0.0257]**	[-0.15, 0.3709]	[0.19, 0.2718]
	MEDFREQ	[-0.22, 0.2008]	[0.07, 0.7025]	[0.12, 0.472]	**[-0.36, 0.0336]**	[-0.07, 0.6872]	[-0.24, 0.1677]
	CFREQ	[0.25, 0.1479]	[-0.01, 0.9754]	[-0.02, 0.9262]	[0.19, 0.2662]	[-0.09, 0.5861]	[0.05, 0.7843]
	FREQD	[0.26, 0.1238]	[-0.25, 0.1334]	[-0.1, 0.5741]	[-0.21, 0.2129]	[0.02, 0.9245]	**[-0.35, 0.0377]**
AP	RDIST	[-0.2, 0.2444]	[-0.02, 0.8854]	[0.04, 0.8261]	**[-0.39, 0.0185]**	[-0.01, 0.9429]	[-0.26, 0.1327]
	MDIST	[-0.15, 0.3792]	[-0.02, 0.9058]	[-0.03, 0.873]	**[-0.38, 0.0229]**	[-0.03, 0.8808]	[-0.26, 0.1321]
	TOTEX	[0, 0.9942]	[-0.09, 0.6043]	[0.14, 0.4258]	[-0.07, 0.6763]	[0.02, 0.8961]	[-0.14, 0.403]
	MVELO	[-0.16, 0.3605]	[-0.13, 0.4475]	[0.04, 0.8292]	[-0.09, 0.6055]	[-0.12, 0.4795]	[-0.17, 0.3158]
	MFREQ	[0.11, 0.5197]	[0.01, 0.9767]	[-0.04, 0.8222]	**[0.34, 0.0452]**	[-0.01, 0.947]	[0.17, 0.3162]
	MEDFREQ	[-0.22, 0.1922]	[-0.02, 0.9177]	[0.08, 0.641]	[0.16, 0.3387]	[-0.14, 0.4051]	[0.11, 0.5147]
	CFREQ	[0.01, 0.9629]	[-0.01, 0.9356]	[-0.33, 0.0531]	[-0.25, 0.1354]	**[-0.39, 0.0194]**	[-0.18, 0.3067]
	FREQD	[0.01, 0.9323]	[-0.17, 0.328]	[-0.31, 0.0622]	**[-0.38, 0.0215]**	[-0.2, 0.2537]	[-0.29, 0.0833]
ML	RDIST	[-0.27, 0.1055]	[-0.09, 0.6183]	[0.23, 0.1704]	[-0.08, 0.6296]	[-0.02, 0.9032]	[-0.03, 0.8729]
	MDIST	[-0.23, 0.1789]	[-0.12, 0.4973]	[0.22, 0.1986]	[-0.08, 0.6239]	[-0.03, 0.8661]	[-0.05, 0.7889]
	TOTEX	[-0.11, 0.5329]	[-0.09, 0.613]	[0.07, 0.6864]	[0.17, 0.3286]	[-0.08, 0.6324]	[0.01, 0.944]
	MVELO	[-0.19, 0.2661]	[-0.1, 0.5799]	[0.02, 0.8911]	[0.16, 0.3382]	[-0.17, 0.3335]	[0, 0.997]
	MFREQ	[-0.03, 0.8714]	[0.1, 0.5708]	[-0.26, 0.1214]	[0.16, 0.3651]	[-0.21, 0.2101]	[0, 0.9851]
	MEDFREQ	[-0.32, 0.0605]	[-0.02, 0.8867]	[-0.23, 0.1756]	[0.03, 0.8748]	[-0.18, 0.2818]	[-0.15, 0.3941]
	CFREQ	[0.01, 0.9342]	[0.01, 0.9383]	**[-0.39, 0.0202]**	[-0.14, 0.4168]	[-0.27, 0.116]	[-0.23, 0.1777]
	FREQD	[0.2, 0.2417]	[-0.15, 0.3883]	[0.14, 0.4086]	[-0.23, 0.1759]	[0.17, 0.3144]	[-0.08, 0.6436]
ISway	JERK	[-0.19, 0.2577]	[-0.04, 0.8337]	[0.08, 0.6357]	[0.05, 0.7649]	[-0.07, 0.696]	[-0.08, 0.6582]
	RMS-ACC	[-0.1, 0.5532]	[-0.06, 0.7187]	[0.06, 0.7409]	**[-0.34, 0.0432]**	[-0.01, 0.9459]	[-0.28, 0.1031]
	CF-ACC	[-0.08, 0.6364]	[0.21, 0.2282]	**[-0.36, 0.0296]**	[-0.32, 0.0602]	**[-0.36, 0.0306]**	[-0.08, 0.655]

Supp Table 6. Spearman's correlation between each Berg Balance Scale (BBS) task score and inter-segment coordination balance biomarkers presented as [ρ, P] at both admission and discharge test sessions. Highlighted cells are significant values ($P < 0.05$).

	Task 1		Task 2		Task 3	
Inter-Segment Coordination	**Admission**	**Discharge**	**Admission**	**Discharge**	**Admission**	**Discharge**
Pelvis-Leg Coherence (f ≤ 1 Hz)	[-0.18, 0.2966]	[-0.08, 0.6334]	[0.09, 0.5842]	[0.06, 0.7414]	[NaN, NaN]	[NaN, NaN]
Trunk-Leg Coherence (f ≤ 1 Hz)	[-0.07, 0.6941]	[-0.08, 0.6452]	[0, 1]	[0.01, 0.9624]	[NaN, NaN]	[NaN, NaN]
Pelvis-Leg Coherence (f > 1 Hz)	[-0.25, 0.1335]	[0.11, 0.51]	**[-0.34, 0.0456]**	[-0.28, 0.0923]	[NaN, NaN]	[NaN, NaN]
Trunk-Leg Coherence (f > 1 Hz)	[-0.22, 0.1966]	[0, 1]	[-0.29, 0.0883]	[-0.28, 0.0923]	[NaN, NaN]	[NaN, NaN]

	Task 4		Task 5		Task 6	
Inter-Segment Coordination	**Admission**	**Discharge**	**Admission**	**Discharge**	**Admission**	**Discharge**
Pelvis-Leg Coherence (f ≤ 1 Hz)	[-0.1, 0.5664]	[0.01, 0.9728]	[-0.24, 0.1666]	[0, 0.9965]	[0, 0.9862]	[0.11, 0.5419]
Trunk-Leg Coherence (f ≤ 1 Hz)	[-0.06, 0.7246]	[0.07, 0.7001]	[-0.15, 0.3671]	[0.07, 0.7024]	[0.09, 0.5853]	[-0.05, 0.7868]
Pelvis-Leg Coherence (f > 1 Hz)	[-0.2, 0.2525]	[-0.17, 0.3265]	[-0.16, 0.356]	[0.06, 0.7189]	[-0.01, 0.969]	[-0.2, 0.2459]
Trunk-Leg Coherence (f > 1 Hz)	[-0.17, 0.3219]	[-0.27, 0.1082]	[-0.17, 0.3249]	[-0.11, 0.5056]	[0.05, 0.7887]	[-0.27, 0.1133]

	Task 7		Task 8		Task 9	
Inter-Segment Coordination	**Admission**	**Discharge**	**Admission**	**Discharge**	**Admission**	**Discharge**
Pelvis-Leg Coherence (f ≤ 1 Hz)	[-0.16, 0.34]	[0.08, 0.6596]	[-0.28, 0.0945]	[-0.05, 0.7663]	[0.03, 0.8406]	[0.03, 0.8526]
Trunk-Leg Coherence (f ≤ 1 Hz)	[-0.05, 0.7671]	[0.2, 0.2332]	[-0.11, 0.5278]	[0.17, 0.3298]	[0.06, 0.7226]	[0.24, 0.1591]
Pelvis-Leg Coherence (f > 1 Hz)	[-0.28, 0.094]	**[-0.45, 0.0056]**	[-0.27, 0.1127]	**[-0.4, 0.0147]**	[-0.03, 0.8473]	**[-0.38, 0.0213]**
Trunk-Leg Coherence (f > 1 Hz)	[-0.18, 0.288]	**[-0.37, 0.0264]**	[-0.16, 0.3386]	[-0.3, 0.075]	[-0.02, 0.9158]	**[-0.42, 0.0099]**

	Task 10		Task 11		Task 12	
Inter-Segment Coordination	**Admission**	**Discharge**	**Admission**	**Discharge**	**Admission**	**Discharge**
Pelvis-Leg Coherence (f ≤ 1 Hz)	[0, 0.9946]	[0.08, 0.6403]	[-0.17, 0.3088]	[-0.05, 0.7706]	[-0.32, 0.0546]	[-0.02, 0.9168]
Trunk-Leg Coherence (f ≤ 1 Hz)	[-0.19, 0.2695]	[0.16, 0.3461]	[-0.14, 0.4022]	[0.07, 0.7042]	[-0.14, 0.4216]	[0.21, 0.2273]
Pelvis-Leg Coherence (f > 1 Hz)	**[-0.45, 0.0059]**	[-0.3, 0.0766]	**[-0.43, 0.0097]**	**[-0.43, 0.0083]**	[-0.21, 0.2114]	**[-0.45, 0.0056]**
Trunk-Leg Coherence (f > 1 Hz)	**[-0.35, 0.0358]**	[-0.29, 0.0884]	[-0.3, 0.073]	**[-0.38, 0.0219]**	[-0.23, 0.1795]	**[-0.42, 0.0109]**

	Task 13		Task 14		Total Score	
Inter-Segment Coordination	**Admission**	**Discharge**	**Admission**	**Discharge**	**Admission**	**Discharge**
Pelvis-Leg Coherence (f ≤ 1 Hz)	[0.07, 0.6838]	[0.05, 0.7609]	**[-0.43, 0.0081]**	[-0.15, 0.3747]	[-0.2, 0.2344]	[-0.01, 0.9359]
Trunk-Leg Coherence (f ≤ 1 Hz)	[0.13, 0.4636]	[0.19, 0.2559]	[-0.29, 0.0876]	[0.11, 0.5169]	[-0.08, 0.6388]	[0.25, 0.1395]
Pelvis-Leg Coherence (f > 1 Hz)	[-0.12, 0.4943]	[-0.25, 0.1405]	[-0.32, 0.0566]	**[-0.43, 0.0087]**	**[-0.37, 0.0283]**	**[-0.55, 0.0005]**
Trunk-Leg Coherence (f > 1 Hz)	[-0.06, 0.7284]	[-0.26, 0.1241]	[-0.24, 0.1513]	**[-0.34, 0.0429]**	[-0.29, 0.0876]	**[-0.52, 0.001]**

Supp Table 7. Wilcoxon signed rank test effect sizes of balance biomarkers for senior adults between admission and discharge test sessions. Note that since the non-parametric Wilcoxon signed rank test was used in this study due to non-normal data, the effect sizes reported in this table are for the Wilcoxon signed rank test calculated according to [Cohen J. A power primer. Psychol Bull. 1992;112(1):155-159] as Effect size $= \frac{Z}{\sqrt{n_x+n_y}}$ where Z is the z-value from the Wilcoxon signed rank test, and n_x and n_y are population sizes.

	COP-based Biomarkers	Effect Size
RD	RDIST	0.07
	MDIST	0.06
	TOTEX	0.09
	MVELO	0.11
	95% Conf. Ellipse	0.12
	Sway Area	0.09
	MFREQ	0.16
	MEDFREQ	0.09
	CFREQ	0.09
	FREQD	0.07
AP	RDIST	0.04
	MDIST	0.01
	TOTEX	0.01
	MVELO	0.08
	MFREQ	0.21
	MEDFREQ	0.17
	CFREQ	0.16
	FREQD	0.05
ML	RDIST	0.11
	MDIST	0.10
	TOTEX	0.09
	MVELO	0.11
	MFREQ	0.06
	MEDFREQ	0.03
	CFREQ	0.09
	FREQD	0.01

	COM-based Biomarkers	Effect Size
RD	RDIST	0.03
	MDIST	0.01
	TOTEX	0.21
	MVELO	0.26
	95% Conf. Ellipse	0.11
	Sway Area	0.09
	MFREQ	0.20
	MEDFREQ	0.10
	CFREQ	0.14
	FREQD	0.04
AP	RDIST	0.05
	MDIST	0.11
	TOTEX	0.11
	MVELO	0.20
	MFREQ	0.22
	MEDFREQ	0.20
	CFREQ	0.12
	FREQD	0.18
ML	RDIST	0.25
	MDIST	0.26
	TOTEX	0.23
	MVELO	0.27
	MFREQ	0.09
	MEDFREQ	0.01
	CFREQ	0.07
	FREQD	0.10
ISway	JERK	0.19
	RMS-ACC	0.03
	CF-ACC	0.02

Inter-Segment Coordination	Effect Size
Pelvis-Leg Coherence (f ≤ 1 Hz)	0.06
Trunk-Leg Coherence (f ≤ 1 Hz)	0.10
Pelvis-Leg Coherence (f > 1 Hz)	0.06
Trunk-Leg Coherence (f > 1 Hz)	0.14